

https://dspace.org/

Effect of internal erosion on the mechanical behaviour of soils

MacRobert, Charles John

2017

https://hdl.handle.net/10539/24744

MacRobert, Charles John (2017) Effect of internal erosion on the mechanical behaviour of soils, University of the Witwatersrand, <https://hdl.handle.net/10539/24744>

Downloaded from a DSpace repository. https://dspace.org/

Effect of internal erosion on the mechanical behaviour of soils

Charles John MacRobert

A thesis submitted to the Faculty of Engineering and Built Environment, University of the Witwatersrand, Johannesburg, in fulfilment of the requirements for the Degree of Doctor of Philosophy.

Johannesburg, 2017

Candidate declaration

I declare that this thesis is my own unaided work. It is being submitted for the Degree of Doctor of Philosophy to the University of the Witwatersrand, Johannesburg. It has not been submitted before for any degree or examination to any other University.

…….

(Signature of Candidate)

…10…..day of……July…….year……2017……..

Abstract

The effect of internal erosion on the mechanical behaviour of soils was investigated experimentally, using sodium chloride grains as an analogue for erodible soil grains. With this technique, the loss of controlled quantities of finer particles could be simulated under more realistic hydro-mechanical conditions than in previous research, but within practical experimental time scales. Two experimental programs were undertaken. The first looked at general changes in volume and shear strength using a large diameter oedometer adapted to perform a punch test following salt dissolution. The second program investigated particular changes in volume and shear strength following salt dissolution using an adapted direct shear box

Previous studies have shown shear strength reductions following the loss of finer particles representing as little as 5 % of the total mass of the original soil. Findings here show shear strength can be largely unaffected if the erodible finer fraction (F) makes up less than a transition value (F_t) of approximately 10 – 15 % by mass of the original soil. This threshold represents F above which the coarser fabric is looser than at its minimum void ratio. As F increases further, finer particles increasingly hinder the coarser particles from achieving their densest packing, such that the coarser fabric remaining after finer particle loss is in a looser state than the original fabric, the remaining fabric reaching its maximum void ratio at a critical finer fraction (F_c) of approximately 25 – 35 %. For $F < F_c$, finer particle loss results in limited collapse of the coarser fabric and it was found that the state of this initial coarser fabric determines the shear behaviour of the soil following the loss of finer particles. The shear behaviour of initially dense specimens with $F < F_t$ remained similar to that of a dense soil following finer particle loss, whereas shear behaviour of initially dense specimens with $F_t < F < F_c$ approached that of a loose soil as F increased. Soils with higher internal filter ratios (D_{15c}/D_{85f}) were found to have higher values of F_t and F_c.

Soils with $F > F_c$, settled and weakened significantly following finer particle loss, reflecting the load-bearing role finer particles play in this case. This load bearing nature of the finer particles in soils with $F > F_c$ decreases the risk of internal erosion.

Dedication

Who has measured the waters in the hollow of his hand,
or with the breadth of his hand marked off the
heavens?
Who has held the dust of the earth in a basket,
or weighed the mountains on the scales
and the hills in a balance?

Isaiah 40:12

Acknowledgments

Whilst a PhD thesis can only have one name attached to it, the plain fact is that such a work cannot be completed without the assistance of many persons. In light of this, I would like to make the following acknowledgements.

I am grateful for the patient oversight provided by my supervisors Dr Irvin Luker, Dr Peter Day and Prof Chris James. Their positive criticism of this thesis has enhanced its scientific stature and improved its readability. Dr Luis Alberto Torres-Cruz helped tremendously both to verbalise and write down my ideas.

I am indebted to Edward Pretorius who adapted equipment to my needs based on rudimentary drawings and verbal explanations – a testament to his machining skills. I am grateful for the assistance of Tumelo Lamola, Samuel Mabote and Ralph Mulder.

Over a three-year period I was assisted by a number of undergraduate students who crushed salt, separated base material, experimented with determining reference state void ratios, carried out preliminary direct shear box experimentation and took readings over a number of days. In no particular order, they were Saddam Mbedzi, Skhulile Mashele, Ephraim Mashamaite, Kamogelo Segoe, Tshegofatso Tsitsi, Katlego Thakadu, Malebogo Esikang, Nonkululeko Mvelase and Vuyani Nyilika.

I am however, most thankful to my beautiful and gracious wife Jani. Without her continued love and affection, I would not have completed this work. Her continued support, despite my ramblings about soil, salt and suffusion speaks volumes of her long-suffering nature. The arrival of our son Eliot spurred me on during the last dash to completion.

Table of contents

Candidate declaration i
Abstract ii
Dedication iii
Acknowledgments iv
Table of contents v
List of figures vii
List of tables xii
Abbreviations and symbols xiii
List of published papers xviii
Chapter 1 General introduction 1
1.1 Background and justification of the research 1
1.2 Scope and objectives of the study 2
1.3 Structure of thesis 4
Chapter 2 Appraisal of internal erosion 5
2.1 Internal erosion and dam engineering 5
2.2 Material susceptibility to suffusion 10
2.3 Critical stress and hydraulic conditions leading to suffusion 13
2.4 Distinction between suffusion and suffosion 18
2.5 Summary 24
Chapter 3 Influence of fabric on internal erosion 26
3.1 Transition and critical finer fractions 26
3.1.1 Largest erodible particle 27
3.1.2 Maximum finer fraction 29
3.1.3 Packing behaviour of internally unstable soils 31
3.2 The role of finer particles in load transfer 40
3.3 The effect of finer particle loss on mechanical behaviour 43
3.3.1 $F < F_t$: Suffusion 44
3.3.2 $F_t < F < F_c$: Suffosion 44
3.3.3 Instability regions 46
3.4 Empirical evidence for a transition and critical finer fractions 49
3.5 Summary 52
Chapter 4 An analogue to internal erosion 54
4.1 The need for an analogue material 54
4.2 Experimental validation 56
4.2.1 Material properties 56
4.2.2 Description of suffusion oedometer and punch (SOAP) device 64
4.2.3 Test procedure 69
4.3 Results 72
4.3.1 Dissolution under one-dimensional loading 72
4.3.2 Punch test 73
4.4 Discussion of results 76
4.5 Proposed mechanical internal erosion criterion 84

Chapter 5 Development of the vertical axis restraint internal erosion direct shear box (variedSB) 87
5.1 Feasibility test work 87
5.2 Design of the variedSB 90
5.2.1 Description of the variedSB 90
5.2.2 Review of the literature on direct shear box testing 92
5.3 Calibration test work 102
5.3.1 Material used 103
5.3.2 Test procedure 105
5.3.3 Results 107
5.3.4 Comparison of results 112
5.4 Summary 120
Chapter 6 Soil-salt mixture preparation considerations 121
6.1 Measuring soil compactness 121
6.2 Proposed method for determining reference void ratios 123
6.3 Gravel-sand mixtures 124
6.4 Gravel-salt mixtures 127
6.5 Summary 132
Chapter 7 Internal erosion and mechanical behaviour 134
7.1 Experimental aim 134
7.2 Experimental method 135
7.2.1 Specimen preparation 135
7.2.2 Dissolution under one-dimensional loading 142
7.2.3 Shearing 144
7.3 Results 147
7.3.1 Dissolution under one-dimensional loading 147
7.3.2 Shearing 148
7.4 Discussion of results 155
7.4.1 Dissolution under one-dimensional loading 155
7.4.2 Shearing 166
7.5 Observed changes of mechanical behaviour compared to changes described in literature 172
7.6 Conceptual critical state framework for suffusion and suffosion 175
Chapter 8 Conclusions and recommendations 178
8.1 Conclusions 178
8.2 Recommendations for future work 183
References 184
Appendix A Distinguishing between “fines content” and “finer fraction” 193
Appendix B Raw data 196
Appendix C Phase relationship derivations 203
C.1 Derivation of Equation 3.1 (Wan and Fell, 2004) 203
C.2 Derivation of Equation C.2 204
C.3 Settlement potential derivations 205

List of figures

Figure 2.1: Venn diagram illustrating factors leading to the various mechanisms of internal erosion initiation, after Garner and Fannin (2010) and USBR-USACE (2015) 7
Figure 2.2: Filter criteria, after Cedergren (1977) 8
Figure 2.3: Conceptual framework for seepage-induced instability, after Fannin and Slangen (2014) 19
Figure 2.4: Stress states within an embankment, after Houlsby (1991) 22
Figure 3.1: Distinct finer and coarser fractions 26
Figure 3.2. Internally unstable particle size distributions, data from Chang and Zhang (2013) 28
Figure 3.3: Box-plot illustrating average diameter ratios (D_{50c}/D_{50f}) for 50 internally unstable soils reported by Chang and Zhang (2013) 29
Figure 3.4. Theoretical variation of void ratios for a binary mixture of spheres 30
Figure 3.5. Gradations investigated 32
Figure 3.6. Variations in a. minimum and b. maximum global void ratios 33
Figure 3.7: Variation of the void ratio of finer particles with increasing finer fraction 35
Figure 3.8. Simplified variation of void ratios for an internally unstable soil 36
Figure 3.9: Example of regression analysis carried out on Evans and Zhou (1995) data set; a. variation of global void ratios, b. variation of coarse void ratios and c. variation of relative density of coarser particles with finer fraction 38
Figure 3.10: Packing behaviour boundaries a. Transition finer fraction for global dense fabrics, b. Critical finer fraction for global dense fabrics, c. Critical finer fraction for global loose fabrics 39
Figure 3.11. Instability regions 47
Figure 3.12: Generalised instability regions (Meanings of A-A, B-B and C-C are given in the main text) 48
Figure 3.13: Finer fractions for various embankments, data from Rönnqvist and Viklander (2014) 50
Figure 3.14: Mass and volume changes due to seepage; a. internally stable soils and b. internally unstable soils, data from Rönnqvist (2015) 51
Figure 4.1: Digital photograph images of coarser particles 57
Figure 4.2: Light microscope and digital photograph images of salt particles 57
Figure 4.3: Particle size distributions: 1. Rounded pebbles; 2. Angular aggregate; 3. Very coarse salt; 4. Coarse salt; 5. Fine salt and 6. Very fine salt 58
Figure 4.4: Particle size distributions: 1. Rounded pebbles; 2. Angular aggregate; 3. Coarse silica sand; 4. Coarse salt; 5. Very fine salt; 6. Very fine silica sand 58
Figure 4.5: Comparison of PSD before and after Proctor compaction of angular coarse aggregate showing negligible crushing 59
Figure 4.6: Evidence of pebble crushing during Proctor compaction 59

Figure 4.7: Vibration setup showing mould with specimen on vibrating table, 2 kPa circular steel surcharge, rod used to flatten surface, scoop and spanner 60
Figure 4.8: Angular aggregate densities obtained by various methodologies 62
Figure 4.9: Rounded pebbles densities obtained by various methodologies 62
Figure 4.10: Impact of vibration on very coarse salt (VCS) and very fine salt (VFS) particles 63
Figure 4.11: Relative densities of aggregate-sand and pebble-sand mixtures (see Table 4.3 for nomenclature) 64
Figure 4.12: Developed SOAP device: 1. Bottom-drain; 2. PVC Cell; 3. Overflow-drain; 4. Holding nut; 5. Punch rod; 6. Loading yoke; 7. Ball bearing; 8. Top spacer; 9. Seepage inlet; 10. Bottom spacer; 11. Loading disk; 12. Specimen (143 mm diameter by 143 mm height) 65
Figure 4.13: Schematic of modelled SOAP device.....66
Figure 4.14: Variation in average vertical stress with height for: a. right-hand boundary fixed in X and Y direction; and b. right-hand boundary fixed in only X direction (see Table 4.4 for parameters assumed for each numbered scenario) 67
Figure 4.15: Calibration SOAP device: 1. Load cell; 2. Bottom load platen; 3. PVC cell; 4. Top load platen; 5. Specimen (143 mm diameter by 143 mm height); 6. Reaction frame. 67
Figure 4.16: Comparison of numerical and experimental results 68
Figure 4.17: Pre-flow relative densities of coarser particles for angular aggregate mixtures (see Table 4.6 for nomenclature) 71
Figure 4.18: Pre-flow relative densities of coarser particles for rounded pebble mixtures (see Table 4.6 for nomenclature) 71
Figure 4.19: Punch test results: a. Angular aggregate; b. Angular aggregate and very fine salt; c. Angular aggregate and fine salt; d. Angular aggregate and coarse salt; e. Angular aggregate and very coarse salt 74
Figure 4.20: Punch test results: a. Rounded pebbles; b. Rounded pebbles and very fine salt; c. Rounded pebbles and fine salt; d. Rounded pebbles and coarse salt.....75
Figure 4.21: Observed pebble crushing following punch testing 75
Figure 4.22: Punch test result comparison 76
Figure 4.23: SOAP test results for angular aggregate and very fine salt mixtures 77
Figure 4.24: SOAP test results for angular aggregate and fine salt mixtures 78
Figure 4.25: SOAP test results for angular aggregate and coarse salt mixtures 79
Figure 4.26: SOAP test results for angular aggregate and very coarse salt mixtures ..80
Figure 4.27: SOAP test results for rounded pebbles and very fine salt mixtures 81
Figure 4.28: SOAP test results for rounded pebbles and fine salt mixtures 82
Figure 4.29: SOAP test results for rounded pebbles and coarse salt mixtures 83
Figure 4.30: Mechanical internal erosion criterion 85
Figure 5.1: Conventional direct shear box: 1. Screw drive; 2. Top-half; 3. Bottom-half; 4. Bath; 5. Top platen; 6. Swan neck; 7. Vertical dial gauge; 8. Horizontal dial gauge; 9. Proving ring; 10. Tailstock 88
Figure 5.2: Conventional direct shear box equipment 90

Figure 5.3: Developed variedSB: 1. Screw drive; 2. Shear load cell; 3. Top-half; 4. Vertical restraining frame; 5. Top-half fixing rods; 6. Vertical LVDT; 7. Loading frame; 8. Vertically restrained loading shaft; 9. Linear bearing; 10. Vertical load cell; 11. Top platen; 12. Horizontal LVDT; 13. Bath; 14. Bottom-half 91
Figure 5.4: Details of seepage provisions: 1. Drainage collection channels; 2. Connection to outlet; 3. Drainage outlet; 4. Perforated top platen. 91
Figure 5.5: Laboratory set-up.....92
Figure 5.6: Calibration soils gradations 103
Figure 5.7: Light microscope images of silica sand particles 104
Figure 5.8: Digital photograph images of gravel particles.....104
Figure 5.9: Behaviour of dense silica sand with different methods of lubrication (average σ_{yy} is indicated) 108
Figure 5.10: Behaviour of loose silica sand with different methods of lubrication (average σ_{yy} is indicated) 108
Figure 5.11: Change in vertical force during shear for a. dense and b. loose silica sand specimens 109
Figure 5.12: Behaviour of dense gravel with different specimen heights (average σ_{yy} is indicated).....111
Figure 5.13: Behaviour of loose gravel with different specimen heights (average σ_{yy} is indicated).....111
Figure 5.14: Change in vertical force during shear for a. dense and b. loose gravel specimens 112
Figure 5.15: Influence of increase in the vertical force on variedSB results for silica specimens 113
Figure 5.16: Influence of the increase in vertical force on variedSB results for gravel specimens 114
Figure 5.17: Influence of wall lubrication on variedSB results for silica sand.....115
Figure 5.18: Influence of wall lubrication on measured ϕ_p and ψ values for silica sand specimens at 150 kPa 116
Figure 5.19: Influence of specimen height on variedSB results for gravel specimens 117
Figure 5.20: Influence of specimen height on variedSB results for gravel specimens 118
Figure 5.21: Influence of specimen height on measured ϕ_p and ψ values for gravel specimens at 150 kPa 119
Figure 5.22: Influence of specimen height on measured ϕ_p and ψ values for gravel specimens at 75 kPa 119
Figure 6.1: Gradations investigated 125
Figure 6.2: Gravel-sand void ratios 126
Figure 6.3: Light microscope images of fine sand and salt particles 127
Figure 6.4: Impact of specimen preparation on sand particle sizes 129
Figure 6.5: Impact of specimen preparation on salt particle sizes 129
Figure 6.6: Coarse void ratios for dense mixtures prepared by volume 130
Figure 6.7: Coarse void ratios for dense mixtures prepared by mass 131

Figure 6.8: Coarse void ratios for loose mixtures prepared by volume 131
Figure 6.9: Coarse void ratios for loose mixtures prepared by mass 132
Figure 7.1: Gradations investigated 136
Figure 7.2: Initial coarse void ratio in relation to reference states 139
Figure 7.3: Coarse void ratio error due to resolution of volume and mass measurements 141
Figure 7.4: Illustration of dissolution process: 1. Specimen; 2. Water supply; 3. Top platen with shallow recess and numerous perforations to facilitate vertical flow into specimen; 4. Bath; 5. Drainage outlet 142
Figure 7.5: Dissolution of all-salt-fines specimens: a. F = 6% and b. F = 34 % 143
Figure 7.6: Relationship between salt mass concentration and conductivity at 15.4 °C 143
Figure 7.7: Typical frozen specimen showing latex membranes (Specimen No. S1G-F30-D-150-50_50-1) 144
Figure 7.8: Typical frozen specimen showing sheared halves (Specimen No. S1G-F25-D-150-25_75-1) 145
Figure 7.9: Fines migration: a. half-salt-fines specimens, b. quarter-salt fines specimens 145
Figure 7.10: Behaviour of dense specimens under an applied vertical stress of 150 kPa: a. small finer fractions, b. intermediate finer fractions, c. large finer fractions and d. intermediate finer fractions with half and quarter finer particle loss 148
Figure 7.11: Behaviour of dense specimens under an applied vertical stress of 75 kPa: a. small finer fractions and b. intermediate finer fractions 149
Figure 7.12: Behaviour of loose specimens under an applied vertical stress of 150 kPa: a. small finer fractions and b. large finer fractions 150
Figure 7.13: Behaviour of loose specimens under an applied vertical stress of 75 kPa: a. small finer fractions and b. large finer fractions 150
Figure 7.14: Absolute difference between values determined from paired tests 153
Figure 7.15: Influence of finer fraction on constant volume friction angle 154
Figure 7.16: Influence of specimen density and finer fraction on flow rules 155
Figure 7.17: Changes in void ratios for dense specimens under 150 kPa vertical stress, a. all-sand-fines, b. all-salt-fines, c. half-salt-fines and d. quarter-salt-fines. 157
Figure 7.18: Changes in void ratios for dense specimens under 75 kPa vertical stress, a. all-sand-fines and b. all-salt-fines 159
Figure 7.19: Changes in void ratios for loose specimens under 150 kPa vertical stress, a. all-sand-fines and b. all-salt-fines 160
Figure 7.20: Changes in void ratios for loose specimens under 75 kPa vertical stress, a. all-sand-fines and b. all-salt-fines 161
Figure 7.21: Settlement envelopes of internally unstable soils 162
Figure 7.22: Change in coarse void ratios due to finer particle loss: a. Dense specimens at 150 kPa; b. Dense specimens at 75 kPa; and c. All loose specimens ..163
Figure 7.23: Summary of settlement behaviour for different percentages of finer particle loss, a. Dense specimens at 150 kPa vertical stress, b. Dense specimens at 75

kPa vertical stress, c. Loose specimens at 150 kPa vertical stress and c. Loose specimens at 75 kPa 165
Figure 7.24: Shear behaviour of dense specimens under an initial vertical stress of 150 kPa with different finer fractions and finer particle loss.....166
Figure 7.25: Shear behaviour of dense specimens under an initial vertical stress of 75 kPa with different finer fractions and finer particle loss.....167
Figure 7.26: Shear behaviour of loose specimens under an initial vertical stress of 150 kPa with different finer fractions and finer particle loss.....168
Figure 7.27: Shear behaviour of loose specimens under an initial vertical stress of 75 kPa with different finer fractions and finer particle loss.....169
Figure 7.28: Shear behaviour of dense specimens under an initial vertical stress of 150 kPa in relation to coarse void ratio.....170
Figure 7.29: Shear behaviour of dense specimens under an initial vertical stress of 75 kPa in relation to coarse void ratio.....170
Figure 7.30: Shear behaviour of dense specimens under an initial vertical stress of 150 kPa in relation to global relative density.....171
Figure 7.31: Shear behaviour of dense specimens under an initial vertical stress of 75 kPa in relation to global relative density.....172
Figure 7.32: Conceptual framework for strength behaviour during internal erosion (relative positions are exaggerated for clarity) 176

List of tables

Table 2.1: Summary of internal stability criteria, after Chang and Zhang (2013b).....11
Table 3.1: Properties of component materials 32
Table 3.2. Instability criteria 32
Table 3.3: Properties of sand-silt and gravel-sand mixtures and their references 37
Table 4.1: Summary of methodologies and obtained densities for angular aggregate 61
Table 4.2: Summary of methodologies and obtained densities for rounded pebbles ..61
Table 4.3: Aggregate-sand and pebble-sand mixtures 63
Table 4.4: Assumed elastic-plastic parameters of the loaded specimen 66
Table 4.5: Details for preparing specimens in their densest state 70
Table 4.6: Summary of SOAP specimens.....70
Table 4.7: Post flooding and dissolution relative densities of coarser particle.....72
Table 4.8: Summary of settlement potential values.....73
Table 5.1: Direct shear box designs, adapted from Shibuya et al. (1997), Lings and Dietz (2004) 93
Table 5.2: Proposed gap sizes 96
Table 5.3: Proposed shear rates.....96
Table 5.4: Calibration soils characteristics 104
Table 5.5: Summary of silica sand testing program.....105
Table 5.6: Summary of gravel testing program 107
Table 5.7: variedSB results on silica sand 109
Table 5.8: variedSB results on gravel 112
Table 5.9: Statistical parameters describing influence of the increase in vertical force on variedSB results on silica specimens 113
Table 5.10: Statistical parameters describing influence of the increase in vertical force on variedSB results on gravel specimens.....114
Table 5.11: Statistical parameters describing influence of specimen height on variedSB results 116
Table 6.1: Dimensions of special mould.....123
Table 6.2: Particle sizes of base material used to form gravel and sand gradations..125
Table 6.3: Gravel-sand particle specific gravities.....125
Table 6.4: Gravel-sand soils dry density and void ratio errors 126
Table 6.5: Particle sizes of base material used to form sand-sized salt gradations....127
Table 7.1: Particle sizes of base material 136
Table 7.2: Summary of internal erosion test specimens 138
Table 7.3: Vertical strain during vertical loading 141
Table 7.4: Post flooding and dissolution coarse void ratios 147
Table 7.5: Summary of peak and constant volume friction angles 151
Table 7.6: Summary of dilation angles 152

Abbreviations and symbols

ASTM	American Society for Testing and Materials	organisation that develops and publishes testing standards
BC	before Christ	events that took place before the birth of Christ
BS	British Standards	organisation that develops and publishes testing standards
C	conductivity	measure of a solution's ability to conduct electricity
cm	centimetre	one hundredth of a meter. **See m**
CSL	critical state line	locus of points at which indefinite shearing can occur at constant stress and constant volume
C_u	coefficient of uniformity	ratio of D_{60}/D_{10}. **See D**
D	particle size	size of a given particle in mm Subscripts: 5, 15, 10, 20, 60, 90, 85 - corresponding percentage finer on the PSD. **See PSD** b PSD of base material fi PSD of filter material c PSD of coarser part of an internally unstable soil f PSD of finer part of an internally unstable soil max maximum particle size
D_r	relative density	ratio of the difference between e_{max} and any given e of a cohesionless, free draining soil; to the difference between e_{max} and e_{min}. **See e, e_{max} and e_{min}**
$D_{r,ec}$	relative density of the coarser particles	equivalent relative density of the coarser particles making up a soil
$D_{r,ec,0}$	initial relative density of the coarser particles	equivalent relative density of the coarser particles making up a soil following specimen preparation
$D_{r,ec,d}$	dissolved relative density of the coarser particles	equivalent relative density of the coarser particles making up a soil following flooding or dissolution
DEM	discrete element modelling	computer method to simulate the interaction of small particles
e	global void ratio	ratio of voids volume to solids volume in a unit total volume of soil
e_c	coarse void ratio	ratio of voids volume and finer solids volume to coarser solids volume in a unit total volume of soil

$e_{c,0}$	initial coarse void ratio	coarse void ratio of specimen following specimen preparation
$e_{c,d}$	dissolved coarse void ratio	coarse void ratio of specimen following flooding or dissolution
e_f	finer void ratio	ratio of voids volume to finer solids volume in a unit total volume of soil
e_{max}	maximum void ratio	void ratio of a soil at its loosest packing
e_{min}	minimum void ratio	void ratio of a soil at its densest packing
F	finer fraction	percentage of erodible or suffusive particles in a soil
F_c	critical finer fraction	maximum finer fraction at which the coarser particles are at their loosest packing
FC	fines content	percentage of particles smaller than 0.075 mm
F_D	percentage passing	percentage passing at D. **See D**
F_t	transition finer fraction	maximum finer fraction at which the coarser particles remain at their densest packing.
G	gravel	residual granite gravel used in thesis
g	gram	one thousandth of a kilogram. **See kg**
G_r	gap ratio	ratio of the maximum to minimum particle size of the deficient portion of a PSD. **See PSD**
G_s	particle specific gravity	ratio of the weight in air of a given volume of solids to the weight in air of an equal volume of distilled water at 4 °C
H	mass fraction	mass fraction between particle sizes D and 4D. **See D**
H	specimen height	height of specimen in direct shear box
h	shear displacement	measure of horizontal movement during shear
i	hydraulic gradient	change in total head per unit distance in the direction of flow
i_c	critical hydraulic gradient	hydraulic gradient at which internal erosion initiates. **See i**
k	hydraulic conductivity	the rate of discharge of water under laminar flow conditions through a unit total cross-sectional area of porous media under a unit hydraulic gradient and standard temperature condition (20 °C)
kg	kilogram	système international d'unités measure of mass
kPa	kilopascal	a thousand Pa. **see Pa**

L	specimen length	length of specimen in direct shear box
LVDT	linearly varying displacement transducer	electronic device that measures displacement
M	mass of solids	a measure of the quantity of matter in an object
m	meter	système international d'unités measure of length
min	minute	sixty seconds. **See s**
mL	millilitre	one millionth of a m^3. **See m**
n	porosity	ratio of voids volume to total soil mass volume
P	percentage fines	percentage finer than 0.063 mm
Pa	pascal	système international d'unités measure of pressure or stress
P_r	percentage finer particles remaining	portion of erodible particles remaining after internal erosion
PSD	particle size distribution	the proportion by mass of various particle sizes
S	siemen	Measured of conductivity
S	sand	residual granite sand used in thesis
s	second	système international d'unités measure of time
S_{ey}	standard error in y	measure of scatter about a regression line
SI	strength index	measure of strength determined from a SOAP test. **See SOAP**
SOAP	suffusion oedometer and punch	device used to determine mechanical effects of internal erosion
SP	settlement potential	measure of strain during particle loss
T	time	measure of event duration
u	pore pressure	stress transmitted through water filling the voids of a soil
v	discharge velocity	the rate of discharge of seepage water through a porous medium per unit of total area perpendicular to the direction of flow
v	vertical displacement	measure of vertical movement during shear
variedSB	vertical axis restrained internal erosion direct shear box	device to observe the mechanical consequences of particle loss

V_c	coarser volume	volume occupied by coarser particles
V_F	vertical force	vertical force measured in the variedSB. **See variedSB**
V_f	finer volume	volume occupied by finer particles Subscripts: f,r finer particles remaining after internal erosion
V_t	total volume	volume occupied by solids and voids
V_v	voids volume	volume occupied by voids
α	reduction factor	factor used to determine the fraction of i_c, which results in zero effective stress, that causes suffusion
γ	shear strain	change in shape, expressed by the relative change of the right angles at the corner of what was in the undeformed state an infinitesimally small rectangle or cube
γ'	effective unit weight	that unit weight of a soil which, when multiplied by the height of the overlying column of soil, yields the effective pressure due to the weight of the overburden
γ_w	unit weight of water	the weight per unit volume of water
δh	incremental horizontal displacement	measure of incremental movement in horizontal direction during shear
ΔH	change in height	measure of specimen settlement
Δz	specimen thickness	measure of the height of a specimen
δv	incremental vertical displacement	measure of incremental movement in vertical direction during shear
ε	strain	change in length per unit length in a given direction Subscripts: 3 minor principal strain 1 major principal strain
$\rho_{c,0}$	initial coarser particle dry density	mass of dry coarser particles per unit volume following specimen preparation
$\rho_{c,d}$	dissolved coarser particle dry density	mass of dry coarser particles per unit volume following flooding or dissolution
ρ_d	dry density	mass of dry soil per unit volume
$\rho_{d,max}$	maximum dry density	dry density of a soil at its densest packing

$\rho_{d,min}$	minimum dry density	dry density a soil at its loosest packing
ρ_i	salt mass concentration	mass of dry salt per unit volume of water
σ	total stress	resultant force perpendicular to a plane of unit total area within a soil Subscript: yy stress on a plane perpendicular to y (vertical) in direction y (vertical)
σ'	effective stress	resultant of forces per unit total area of a plane transmitted from grain to grain within a soil mass Subscripts: 3 minor principal stress 1 major principal stress
τ	shear stress	resultant force parallel to a plane in a material per unit total area of that plane Subscripts: yx shear stress on a plane perpendicular to y (vertical) acting in direction x (horizontal)
ν	Poisson's ratio	the ratio of strains in the longitudinal or axial direction and strains in the lateral or radial direction
υ	specific volume	total volume of soil which contains unit volume of solids (1 + e). **See e**
$\widehat{\upsilon_p}$	maximum specific volume	specific volume corresponding to $e_{max.}$ **See e_{max}**
$\widecheck{\upsilon_p}$	minimum specific volume	specific volume corresponding to $e_{min.}$ **See e_{min}**
ϕ	friction angle	angle whose tangent is the ratio of shear stress to vertical stress on a plane in the soil Subscripts: crit critical friction angle cv constant volume friction angle ds direct shear friction angle p peak or maximum friction angle ps plane strain friction angle u angle of friction for grain-to-grain contact
ψ	dilation angle	measure of the expansion of a cohesionless soil when subjected to shearing deformation. The maximum inverse tangent of $\delta v/\delta h$. **See δv, δh**
°C	degree Celsius	système international d'unités measure of temperature

where relevant definitions are as per ASTM D653

List of published papers

The following conference papers are based on work contained in this thesis:

MacRobert, C.J. & Day, P.W. (2016). *Considerations for using soil-salt mixtures to model soil fabric changes.* Paper presented at the 1st South African Geotechnical Conference, Sun City, South Africa

MacRobert, C.J. & Torres-Cruz, L.A. (2016). *Evaluation of methods to determine reference void ratios.* Paper presented at the 1st South African Geotechnical Conference, Sun City, South Africa

MacRobert, C.J. (2016). *A theoretical framework to understand the mechanical consequences of internal erosion*. Paper presented at the 84th ICOLD Annual Meeting, Johannesburg, South Africa

MacRobert, C.J. (2015). *Appraisal of seepage-induced erosion of earth dams*. Paper presented at the 2015 SANCOLD Annual Meeting, Cape Town, South Africa

Chapter 1 General introduction

1.1 Background and justification of the research

Geotechnical engineering has focused traditionally on design of structures placed upon, within or made from soil and rock. Very little attention has been paid to the possibility that the properties of the soil or rock may change over time. Ageing infrastructure and requirements for long design lives require that attention. This is especially relevant for earth embankment dams. A statistical study of embankment failures showed that 2 % of failures resulted from earthquakes, 4 % from sliding, 48 % from overtopping and 46 % from particle erosion due to seepage (Foster et al., 2000a). Whilst earthquakes, sliding and overtopping are significant risks at any stage of a dam's life, seepage through dams most often influences long-term performance. Uncontrolled seepage can result in failure by either erosion of particles or build-up of excessive seepage pressures resulting in sliding failures (Cedergren, 1977). Although understanding the effects of seepage through earth embankments has received much research attention for over a century, design approaches are still predominantly empirical (ICOLD, 2014).

Of particular relevance to this study is suffusion, the mechanism of internal erosion where finer particles from a soil mass are removed under the action of seepage. In earth dams suffusion often presents as a sinkhole after varying lengths of time or in some cases decades into operation (Rönnqvist, 2009). Soils susceptible to suffusion are generally widely or gap graded such that the finer particles are able to flow out from between the coarser particles even under relatively low hydraulic gradients. Design approaches, therefore, predominantly consider the particle size distribution (PSD) of the soil used to build the dam. Materials are deemed suitable or unsuitable based on an evaluation of their PSD using various empirical criteria developed from permeameter tests. These approaches do not take into account the actual change in mechanical behaviour caused by suffusion and simply answer the question of whether finer particles could migrate.

Consequently, these approaches are often conservative. Materials may be deemed unstable simply because a loss of finer particles can take place, even when the impact of such loss on compressibility and strength is negligible. This can result in unwarranted use of costly materials for new dams, or expensive repairs on old dams without sufficient reason. This research, therefore, is intended to add to the body of knowledge of how suffusion affects mechanical behaviour.

1.2 Scope and objectives of the study

Due to the importance of screening PSDs for susceptibility to suffusion, much research has been conducted into establishing filter criteria using permeameters (Istomina, 1957, Blight, 1958, Kezdi, 1969, de Mello, 1975, Sherard, 1979, Kenney and Lau, 1985, 1986, Li and Fannin, 2008, Wan and Fell, 2008, Chang and Zhang, 2013, Rönnqvist and Viklander, 2014). Theoretical approaches to establishing filter criteria have used stochastic grain and pore structures models (Åberg, 1993, Indraratna et al., 2011) and more recently discrete element modelling (DEM) to determine constriction sizes and probabilities of particle loss (Shire and O'Sullivan, 2016, To et al., 2016). An extension to permeameter research has been to establish critical stress and hydraulic conditions (hydromechanical conditions) required to initiate suffusion (Skempton and Brogan, 1994, Moffat and Fannin, 2011, Moffat et al., 2011, Chang and Zhang, 2012, Li and Fannin, 2012, Zou et al., 2013, Moffat and Herrera, 2014). Although these studies are informative, their applicability is limited by scale effects (Bezuijen and Steedman, 2010, Marot et al., 2012, van Beek et al., 2014) and the long time over which suffusion often takes place in reality (Fell et al., 2003, Rönnqvist, 2009). Consequently, more recent studies have used DEM to investigate these hydromechanical conditions (Shire et al., 2014, Langroudi et al., 2015).

The mechanical consequences of internal erosion have received less research attention. Sterpi (2003) suggested soil strength could increase following suffusion, based on tests of reconstituted specimens. Ke and Takahashi (2012), using a miniature cone penetrometer, showed that a specimen subject to suffusion in a permeameter

reduced in strength. Subjecting specimens to suffusion in triaxial cells has shown a reduction in strength (Shwiyhat and Xiao, 2010, Chang et al., 2014). Difficulties in modelling fabric changes by reconstituting specimens and unrealistic hydromechanical conditions limit the usefulness of the approaches above. Continuum and DEM modelling (Muir Wood et al., 2010, Scholtès et al., 2010, Hicher, 2013) have had some success, showing that the loss of finer particles results in an increase in global void ratio, causing initially dilative soils to become contractive. Although informative in establishing a theoretical framework to the mechanical consequences of internal erosion, these models are limited and experimentally untested. It is apparent that an improved method to investigate experimentally the mechanical consequences of finer particle loss is required. An experimental method utilising sodium chloride salt grains as an analogue for the eroded particles was therefore developed. Similar studies have been taken place during the same time period of this study; exploring settlement behaviour (McDougall et al., 2013) and shear behaviour (Chen et al., 2016) following particle loss. These two studies add credence to using sodium chloride as an analogue for investigating experimentally the mechanical consequences of finer particle loss.

The original contribution of this work is to extend the use of sodium chloride salt grains (as an analogue for finer erodible particles) to establish the effect of internal erosion on the mechanical behaviour of soils. Using this novel approach, fabric changes likely to occur in the field can be recreated under more realistic hydromechanical conditions within realistic time scales. Key questions that will be addressed are what volume and shear strength changes take place during complete and partial loss of finer particles. The investigation also seeks to establish how finer erodible particles (finer fabric) contribute to load transfer as they fill the void space between the coarser non-erodible particles (coarser fabric) in the soil mass and the effect which this has on their susceptibility to removal by seepage. Tentative design considerations are also presented to guide engineers in assessing whether the loss of finer particles will have a significant effect on mechanical behaviour based on soil's gradation and percentage of finer particles.

1.3 Structure of thesis

This thesis is divided into eight chapters. Chapter 1 sets out the background, justification, objectives and scope of the study. Chapter 2 outlines existing knowledge of seepage risks associated with dams. A critical review of research into material susceptibility, critical stress and hydraulic conditions, and effects of suffusion is presented.

Chapter 3 discusses the mechanical effects of suffusion by observing how the initial fabric, prior to suffusion, changes as the quantity of potentially erodible finer particles increases. Based on these initial fabrics, a theoretical framework of the mechanical effects of finer particle loss is presented.

The use of soil-salt mixtures as an experimental analogue to investigate the mechanical effects of internal erosion is outlined in Chapter 4. A simple Suffusion Oedometer and Punch (SOAP) device is developed to explore the analogue and establish a generalised understanding of how finer particle loss changes soil strength.

Chapter 5 outlines the development of the vertical axis restrained internal erosion direct shear box (variedSB) used to explore the mechanical consequences of finer particle loss with greater rigour. Due to the novel nature of the equipment, results of calibration testing are presented. Chapter 6 explores the effects of differences in particle shape, hardness and particle specific gravity on packing behaviour between gravel-sand and gravel-salt mixtures. This established a more accurate method of using salt as an analogue for the finer fabric. Chapter 7 then presents results from tests using the variedSB, which investigated the changes in soil fabric during internal erosion and the effect of these on mechanical behaviour.

Chapter 8 summarises the main conclusions of the study and offers recommendations for future study.

Chapter 2 Appraisal of internal erosion

This chapter starts with a broad discussion of dam engineering and the four mechanisms of internal erosion: (i) concentrated leak erosion; (ii) backward erosion; (iii) contact erosion; and (iv) suffusion (ICOLD, 2014). Focus then shifts to suffusion: discussing material susceptibility and the stress and hydraulic conditions that lead to suffusion. The chapter ends by distinguishing between suffusion and suffosion.

2.1 Internal erosion and dam engineering

Earth, as a dam construction material, has a worse safety record than masonry or concrete. The failure of the Sadd el-Kafara dam, c2850 BC, attributed to both erosion through and over the structure (Smith, 1971), exemplifies the main risks to earth dams. In the modern era, these two modes account for roughly 48 % and 46 % of failures, respectively, with the remainder due to slides and earthquakes (Foster et al., 2000a). Although flow over dams causing surface erosion is a large risk, this topic will not be discussed here. The low incidence of sliding failures can be credited to Terzaghi's principle of effective stress and refinement by others (Smith, 1971). However, as Victor de Mello pointed out, "Water has an unfortunate habit of seeping through every theory" (Burland, 2008). The problem is that seepage can erode particles from within the soil fabric when susceptible material is subject to critical stress and hydraulic loads (Garner and Fannin, 2010).

The continued use of masonry and mortar dams built by the Romans in the 1st or 2nd century in Merida, Spain, illustrates an empirical understanding of the forces at play from antiquity. By the beginning of the 20th century design of masonry dams was well advanced, utilising mathematical calculations for safety based on water pressures (Jansen, 1988). Modern physical and computer modelling along with an improved understanding of material science has led to some elegant concrete structures impounding vast volumes of water. However, such dams require sites with competent foundations and abutments. Where competent geology is not present or where there are wide valleys, earth dams are favoured (Armstrong, 1977). Although some of the

largest dams are earth dams, their design, especially against internal erosion, is still largely empirical. The ICOLD Bulletin 164 (ICOLD, 2014) advocates a quantitative risk approach to assessing dam safety against internal erosion. These methods are based on statistical studies of dam failure records, such as by Foster et al. (2000a).

Given enough energy and time, water can erode any material. Soils are not made up of single sized particles but rather a range of particle sizes quantified by the particle size distribution (PSD) curve. This curve's shape dictates a soil's susceptibility to erosion. Generally, non-plastic soils such as silts, sands and gravels are more susceptible than plastic soils, with smaller particles eroding at lower energies. Surrounding grains in many cases then rearrange and clog flow paths. Plastic soils, with a higher proportion of clay-sized particles, require higher energies to erode, but can sustain cracks. Certain clays, if dispersive, can de-flocculate in water with low salt concentrations and are eroded at far lower energies (ICOLD, 2014). Of the nine Southern African incidents reported by Foster et al. (2000a), five occurred due to the erosion of dispersive clays.

Load applied to the soil skeleton can reduce the tendency for individual particles to be removed by erosion. However, critical conditions can be reached when the imposed stresses become lower than necessary to retain particles. This can happen due to soil arching and differential settlement: (i) around conduits, (ii) adjacent to steep foundation sections, (iii) across valleys and (iv) between zones of different stiffness. In some cases, these critical conditions can lead to cracking. Poor compaction can worsen the situation due to poor particle interlock. In some soils, large particles can carry the majority of load on the soil, resulting in finer particles being unloaded and mobile. When critical hydraulic conditions are reached, typically expressed in terms of discharge velocity or hydraulic gradient, sufficient energy is available to transport particles. In some cases, even where there is no flow, pore pressure can exceed the minor principal stress and soil tensile strength, resulting in cracking termed hydraulic fracturing. The term "critical hydromechanical conditions" is often used to refer to the combination of stress and hydraulic load required to initiate internal erosion.

Literature describes various mechanisms of internal erosion. ICOLD (2014) summarises these as: (i) concentrated leak erosion; (ii) backward erosion; (iii) contact erosion; and (iv) suffusion. Concentrated leak erosion initiates due to low stress conditions, resulting in erosion of materials that would otherwise not be susceptible. As flow tends to concentrate in these areas, flow velocity increases. This type of internal erosion is the cause of almost half of all internal erosion failures (Foster et al., 2000b). Backward erosion initiates where flow exits from the downstream face of a dam or at a transition into a more permeable zone. The hydraulic gradient in the material upstream of these interfaces can be high, initiating erosion, and the flow velocity downstream of these interfaces can be high, initiating erosion. As material is removed, these critical conditions move upstream resulting in backward propagation of the eroded area. Contact erosion occurs where a finer soil is in contact with a coarser soil. Flow parallel to the contact zone can erode finer particles into the coarser material. The loss of finer particles from within a soil is termed suffusion and is due primarily to material susceptibility. Susceptible soils have PSD that contain a significant portion of finer particles which are mobile at low hydraulic gradients due to the loads on the soil being carried predominantly by the larger particles. Suffusion is therefore also referred to as internal instability (USBR-USACE, 2015). Figure 2.1 below attempts to summarise the contribution of material susceptibility, critical hydraulic loads and critical stress conditions to the initiation of the four main mechanisms of internal erosion.

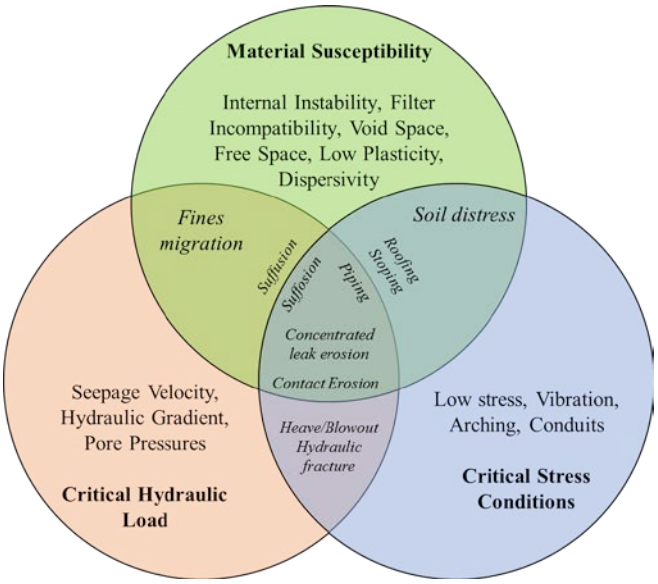


Figure 2.1: Venn diagram illustrating factors leading to the various mechanisms of internal erosion initiation, after Garner and Fannin (2010) and USBR-USACE (2015)

It is likely that in many cases, some internal erosion takes place, but the passage of particles ceases due to local grain structure collapses. However, if the conditions are such that internal erosion progresses, erosion channels with a loose assembly of soil particles or erosion pipes devoid of any soil particles can develop. In some cases, the process is slow enough that it is possible to detect that erosion is taking place by the emergence of muddy leakage or when minor sinkholes form as imposed stresses are no longer sustained. In other cases, gross enlargement of the erosion pipe or collapse occurs, resulting in a loss of freeboard and overtopping, with the majority of failures taking place within 12 hours of detection (Foster et al., 2000a). In cases where the process is slow enough, eroding forces can be reduced, stopping particle loss. This can be done by lowering the water level in the reservoir, thereby reducing the hydraulic load on the dam.

The most efficient way to stop erosion is with filters. These are successive downstream zones of larger particles designed to stop migration of finer particles and reduce hydraulic gradients. The larger particles, therefore, need to be both bigger and smaller than certain limiting criterion; the earliest proposed (Fannin, 2008) being the Terzaghi criterion:

$$4D_{85b} > D_{15fi} > 4D_{15b} \qquad \text{Equation 2.1}$$

where D is particle size, the numerical subscripts denote the corresponding percentage passing from the particle size distribution curve (PSD), subscript b refers to the base or retained material and subscript fi refers to the filter (Figure 2.2).

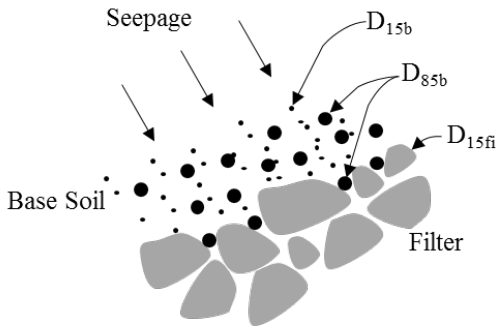


Figure 2.2: Filter criteria, after Cedergren (1977)

Foster et al. (2000b) indicate that dams with well-designed and constructed filters are virtually at no risk of internal erosion. The design of new embankment dams, therefore, centres predominantly on preventing conditions that will initiate internal erosion and ensuring correct filters are present to prevent progressive deterioration. Further, research by Foster and Fell (2001) showed that many dams with filters that do not meet modern criteria, such as proposed by Sherard and Dunnigan (1989), still provide protection, although a degree of particle migration takes place.

Richards and Reddy (2007) outline how, at the beginning of the last century, phenomena associated with backward erosion and concentrated leak erosion started to receive scientific attention, mainly to prevent internal erosion beneath masonry and concrete structures. A more empirical approach was taken by Clibborn (c1902), Bligh (c1910) and Lane (c1934) and a more theoretical approach by Terzaghi (c1922). Initial research into contact erosion is attributed to Dutch researchers, assessing dikes of fine material on coarse foundations (Cyril et al., 2009). Further research has been carried out into these three mechanisms of internal erosion but will not be covered in this review.

Sinkholes in the Balderhead dam, England, 1967, focused attention on the effects of suffusion. This interest was fuelled by the formation of two sinkholes in the crest of the WAC Bennet dam, British Columbia, in 1996 after 28 years of service (Fannin and Slangen, 2014). Suffusion has also been of interest in natural systems. Following the eruption of Mount St. Helens, Washington State, 1980, a debris avalanche created a landslide dam consisting of material that was judged marginally susceptible to suffusion (Meyer et al., 1994). Research has also been driven by settlement of areas surrounding Milano, Italy, that has been attributed to suffusion caused by ground water level lowering (Sterpi, 2003). The remainder of this chapter will focus on suffusion, with topics arranged by the progression of research, which initially centred on determining material susceptibility, then on critical stress and hydraulic conditions and more recently on the mechanical behaviour with the differentiation between suffusion and suffosion.

2.2 Material susceptibility to suffusion

In soils which are widely graded (large range of particle sizes) or gap-graded (large and small particles with a deficiency of intermediate sizes) the smaller particles can erode from the interstices between the larger/coarser particles. Particles with a potential to move are referred to as "finer", although not necessarily silt or clay sized (see Appendix A page 193). Various empirically derived criteria have been proposed and these are summarised in Table 2.1. To avoid grammatical complications, a set of rules is referred to as a criterion.

Istomina (1957) proposed an early criterion using the coefficient of uniformity (C_u) to differentiate stable, transitional and unstable soils. This is termed the "I criterion" in this thesis. Kezdi (1969), de Mello (1975) and Sherard (1979) independently proposed very similar criteria. In these, the PSD is divided into coarser and finer fractions, at increasing grain sizes, and the Terzaghi filter criterion applied to the two fractions. This is termed the "K criterion" in this thesis.

Kenney and Lau (1985) carried out permeameter tests on widely graded sandy gravels, and stated that internally stable soils have $H/F_D \geq 1.3$, where F_D is the percentage of total mass passing at any particle size D and H is the mass fraction between D and 4D. The reasoning was that particles of size D were found to be capable of passing through the constrictions formed by particles of size 4D. The Kenney and Lau (1985) criterion was criticised by Milligan (1986) and Sherard and Dunnigan (1986) for being conservative due to hydromechanical conditions in their tests being unrepresentative of field conditions. This criterion was therefore revised to $H/F_D \geq 1.0$ (Kenney and Lau, 1986), this is termed the "KL criterion" in this thesis.

Li and Fannin (2008) assessed the K and KL criterion using a larger database of tests, including gap-graded materials. They concluded that the K criterion is better for gap-graded soils and the KL criterion better for widely graded soils. They proposed that the K criterion should be applied for F below 15 % and the KL criterion above 15 %. This is termed the "LF criterion".

Table 2.1: Summary of internal stability criteria, after Chang and Zhang (2013b)

Reference	Material description	Geometric criteria to determine material susceptibility	Abbreviation
Istomina (1957)	Sandy gravel	$C_u \leq 10$: internally stable. $10 \leq C_u \leq 20$: transitional. $C_u \geq 20$: unstable.	I criterion
Kezdi (1969), de Mello (1975), Sherard (1979)	None specified	Terzaghi criteria at increasing grain size: $(D_{15c}/D_{85f})_{max} \leq 4$ to 5: internally stable (Kezdi (1969) specified 4).	K criterion
Kenney and Lau (1985, 1986)	Granular soils	At increasing grain size: $(H/F_D)_{min} \geq 1.0$: internally stable. Applied between $F_D = 0 – 20$ %, for widely graded coarser fractions ($C_u > 3$); and between $F_D = 0 – 30$ %, for narrowly graded coarser fractions ($C_u < 3$).	KL criterion
Wan and Fell (2008)	Widely graded soils	$30/\log(D_{90}/D_{60})$, or $30/\log(D_{90}/D_{60})$ and $15/\log(D_{20}/D_5) > 22$: internally stable.	WF2 criterion
Li and Fannin (2008)	Granular soils	For $F < 15$, $(H/F)_{min} \geq 1.0$: internally stable. For $F > 15$, $H \geq 15$: internally stable.	LF criterion
Chang and Zhang (2013)	Widely graded soils	$P < 5$, $(H/F)_{min} > 1.0$: internally stable. $5 \leq P \leq 20$, $(H/F)_{min} > -(1/15)P + 4/3$: internally stable for low plasticity soils $P > 20$: stable	CZ1 criterion
	Gap-graded soils	$P < 10$, $G_r < 3.0$: internally stable. $10 \leq P \leq 35$, $G_r < 0.3P$: internally stable for medium plasticity soils. $P > 35$: stable	CZ2 criterion
C_u = coefficient of uniformity; F_D = percentage mass passing at any grain size D; H = mass fraction between particle sizes D and 4D; D_{15c} = diameter of the 15 % mass passing in the coarse part; D_{85f} = diameter of the 85 % mass passing in the fine part; D_{90}, D_{60}, D_{20}, D_5 = diameter of the 90 %, 20 %, 15 % and 5 % mass passing respectively; P = percentage finer than 0.063 mm; G_r = ratio of the maximum to minimum particle sizes of the deficient portion of the PSD.			

Wan and Fell (2008) carried out permeameter tests on silty sandy gravels and clayey silty sandy gravels. They concluded that the KL and K criteria are conservative and developed new criteria, which included results from published tests. The first criterion, termed the “WF1 criterion”, uses logistic regression, based on a model proposed by Burenkova (1993), to determine the probability of internal instability based on D_{90}/D_{60} and D_{90}/D_{15} of the whole PSD. Applying this criterion led to a

second, simpler chart criterion, termed the “WF2 criterion”, which identifies unstable, transition and stable materials based on D_{20}/D_5 and D_{90}/D_{60}.

Chang and Zhang (2013) analysing the I, K and KL criteria against 131 experimental datasets from literature, concluded they are conservative and do not reflect the enhanced erosion resistance of particles smaller than 0.063 mm. Two criteria were proposed for widely graded and gap-graded soils. The first criterion for widely graded soils, termed the “CZ1 criterion”, was based on the KL criterion and percentage finer than 0.063 mm. The second criterion for gap-graded soils, termed the “CZ2 criterion”, was based on the gap ratio (G_r) and percentage finer than 0.063 mm.

Based on the application of the LF criterion to the as-built PSD curves for the WAC Bennet dam, Li et al. (2009) suggest that the LF criterion should be applied between F = 0 – 41 %, as the original KL criterion boundaries were judged too narrow. A similar assessment of 78 dams, 21 of which had experienced suffusion episodes, was undertaken by Rönnqvist et al. (2014). The KL criterion was found to be the most accurate, followed by the WF1 criterion (based on a 5 % probability of internal instability) and then the LF criterion. The WF2 criterion assessed a number of PSD curves to be stable where these had been found unstable in practice. Thus, although these criteria may have been criticised for being based on tests with unrepresentative hydromechanical conditions, they appear adequate for suffusion screening. ICOLD (2014) advocates using the KL and WF1 criteria or permeameter tests if the risk is deemed high enough.

Åberg (1993) proposed a method to assess internal stability based on a stochastic grain and pore structure model rather than on empirical analysis of permeameter tests. Although this purports to predict the extent of washout and volume change, very little validation of the method is apparent in literature, possibly because it could only be verified under extreme hydromechanical conditions. Indraratna et al. (2011) developed a method based on the same stochastic grain and pore structure model to divide a PSD into coarser and finer parts. The ratio of D_{35c}/D_{85f} (where subscripts c

and f refer to the coarser and finer parts) is used to differentiate stable (< 0.73), transitional (0.73 - 0.82) and unstable (> 0.82) soils. The method is found to perform adequately against various published data sets. A criticism of both methods is that assumptions regarding the relative density of the coarser fraction are required, which is often unknown and can lead to a large variation in results.

Glacial tills are particularly prone to internal instability. Alluvial deposits of large rivers and the colluvium in the bed of rivers in mountainous areas can also be internally unstable (ICOLD, 2014). None of the Southern African incidents reported in Foster et al. (2000a) were directly attributed to suffusion although it is suspected to have taken place in the Bloemhoek dam.

2.3 Critical stress and hydraulic conditions leading to suffusion

Initial experimental work to define material susceptibility paid little attention to the stress and hydraulic conditions necessary to initiate suffusion. The first scientific work into soil seepage is attributed to Darcy (c1856) who determined a linear relationship between hydraulic gradient (i) and discharge velocity (v) (Freeze, 1994). Fannin (2008) reports similar tests carried out by Terzaghi (1925) showing that when the hydraulic gradient reaches a critical value (i_c), v suddenly increases and the specimen heaves. This i_c could be determined as it corresponded to the upward water pressure resulting in zero effective stress, and is close to unity (Terzaghi, 1925):

$$i_c = (1 - n)(1 - G_s) = {\gamma'}/{\gamma_w} \qquad \text{Equation 2.2}$$

where n is the global porosity of the material, G_s is the particle specific gravity, γ' is the effective unit weight and γ_w is the unit weight of water.

Skempton and Brogan (1994) carried out permeameter tests on internally unstable soils at increasing i under low confining stress. A similar increase in v accompanied

by a discharge of finer particles was observed, but at i_c less than that required to reduce the effective stress to zero. This was attributed to a bimodal load distribution, such that the load on the finer particles was a fraction of that on the entire mass, such that the finer particles could be eroded at lower hydraulic gradients. Skempton and Brogan (1994) suggested that i_c for suffusion could be obtained by multiplying Equation 2.2 by a reduction factor (α):

$$i_c = \alpha \, {\gamma'}/{\gamma_w} \qquad \text{Equation 2.3}$$

where α = 1 for heaving and becomes increasingly smaller as less load is carried by the finer particles.

Moffat et al. (2011) carried out seepage tests in a permeameter adapted to apply a vertical force to the soil, which showed a localised and episodic loss of finer particles at varying locations. This was associated initially with a local increase in hydraulic conductivity and no volume change, but as the hydraulic gradient increased, this was accompanied by volume changes. Moffat and Fannin (2011) demonstrated that failure follows a particular path in stress and hydraulic gradient space terminating along a unique envelope that depends on material susceptibility. Li and Fannin (2012) proposed a theoretical equation to define this envelope based on the hydraulic gradient, which results in zero effective stress and α:

$$i_c = \alpha \left(\bar{\sigma}'_{vm0} + 0.5 \, {\gamma'}/{\gamma_w} \right) \qquad \text{Equation 2.4}$$

where $\bar{\sigma}'_{vm0} = \sigma'_{vm0}/\gamma_w \Delta z$ is the normalised mean vertical effective stress, σ'_{vm0} is the initial mean vertical stress and Δz is the specimen thickness. With α set to unity, the equation reduces to that of heaving of an internally stable material as reported by Terzaghi (1925). Discrete element modelling (DEM) by Shire et al. (2014) suggested that α is dependent on D_{15c}/D_{85f}, finer fraction and density. When the finer particles are considerably smaller than the voids between coarser particles, α increases from

close to zero to unity as the finer fraction fills the voids. When the voids are close to being full, dense specimens had higher α values than loose specimens. Finer particles that are similar in size to the coarser particles had α values close to unity. Langroudi et al. (2015) carried out a similar DEM study on a smaller number of PSD curves, broadly confirming these conclusions.

In an effort to better control the stresses that act on a specimen, investigations into suffusion have been carried out in triaxial cells adapted to allow seepage and collection of finer particles (Bendahmane et al., 2006, Bendahmane et al., 2008, Shwiyhat and Xiao, 2010). Due to the diameter of triaxial specimens restricting particle size, these experiments used mixtures of sand and plastic kaolin clay. To initiate suffusion uncharacteristically large hydraulic gradients, atypical for dams, were required and clogging of triaxial apparatus was reported in some experiments. Nevertheless, results showed that the critical hydraulic gradient was dependent on the percentage of clay and that increasing confinement reduced the rate of erosion.

Chang and Zhang (2012) developed a larger triaxial cell and carried out tests to determine critical hydraulic gradients, on a gravel-sand mixture, at different stress ratios (deviatoric stress/mean effective stress). They showed that critical hydraulic gradients initially increase as the shear stress ratio increases, but then decrease as the soil approaches failure. This behaviour was attributed, by the authors, to an initial decrease in porosity as the stress ratio increased and then the formation of locally elongated pores in the direction of the major principal stress close to failure. These elongated pores are assumed to form because particle force chains form in the direction of the major principal stress. As flow was also in the direction of the major principal stress, the resulting increase in hydraulic conductivity was assumed to cause the observed decrease in critical hydraulic gradient. Zou et al. (2013) also demonstrated this phenomenon under plane-strain conditions with the critical hydraulic gradient initially increasing as pores are compressed and then decreasing as ongoing deformation aligns grains and pore spaces. An alternative explanation for this decrease in critical hydraulic gradient is that large shear strain destabilises the grains,

causing increased internal erosion, with both the erosion and the shear induced dilation increasing hydraulic conductivity (Luker, personal communication).

A criticism of using permeameter tests to determine critical hydraulic gradients is that scale effects are often not adequately addressed. A theoretical assessment of scaling in the internal erosion process was undertaken by Bezuijen and Steedman (2010) illustrating that the hydraulic gradient needs to reach a certain threshold over a given number of grains to initiate erosion. Marot et al. (2012) developed a triaxial system placed in a geotechnical centrifuge to investigate scale effects. They found that doubling the specimen length nearly halved the critical hydraulic gradient and doubled the erosion rate. Marot et al. (2012) did not give a rigorous explanation for this, simply attributing it to the probability either for a detached particle to be filtered or not along the seepage path. However, these authors show that the expended power of the flow to cause internal erosion was unaffected by scale effects. A study by van Beek et al. (2014) showed that for backward erosion under small, large and full-scale models, the critical hydraulic gradient decreased with increasing model size. This was attributed to the critical hydraulic gradient over the grains undergoing erosion staying more or less the same but the average hydraulic gradient (which is the parameter being measured) across the structure decreasing.

Although experimentally determined critical hydraulic gradient values may not realistically represent field conditions, it is possible to compare them to those in actual dams to assess the potential for suffusion. Chang and Zhang (2013) compiled a list of critical hydraulic gradient values for suffusion from 24 experimental studies reported in literature. In eleven of these studies, the critical hydraulic gradient was less than unity, eighteen were below 10, twenty-two below 25, with the highest reported as 140. Tests resulting in extremely high critical hydraulic gradients were on soils containing bentonite and kaolin clays. Tests resulting in critical hydraulic gradients above unity were either on soils under stressed conditions or occurred in tests used to determine material susceptibility where the high hydraulic gradients were created to ensure particle loss.

Fenton and Griffiths (1997) carried out a statistical study to estimate extreme hydraulic gradients in dams. They considered an embankment of a single material with a varying hydraulic conductivity (Coefficient of variation = 50 %), drained by a horizontal drain extending into the dam from the toe. This analysis showed that extreme hydraulic gradients occurred where flow transitioned into the drain, and were generally between 1 and 2 but did not exceed 3.5. It is acknowledged that hydraulic gradients in dams can be as high as 20 and exceed 100 but this is usually at seepage cut-offs which are thin impermeable elements (Brown and Bruggemann, 2002). It is clear that some of the experimental critical hydraulic gradients reported by Chang and Zhang (2013) exceed the extreme hydraulic gradients suggested by Fenton and Griffiths (1997). For a horizontal drain at the base of a dam as considered by Fenton and Griffiths (1997), it is realistic to assume soil particles would be stressed, even if the stresses are lower than may be predicted by self-weight (Zhang and Du, 1997). Data presented by Chang and Zhang (2013) suggests that under these stresses the critical hydraulic gradient required would be higher than the maximum of 3.5 suggested to occur by Fenton and Griffiths (1996). This brings into question whether stress and hydraulic gradients can be used to screen internal erosion.

This criticism of trying to predict suffusion from stress and hydraulic gradients is reinforced by case histories. Considering the failure of the Gouhou dam in China, Zhang and Chen (2006) showed it unlikely that hydraulic gradients exceeded 1.6 at a depth of 16 m during the event. A review of case studies by Foster et al. (2002) showed that average hydraulic gradients across cores at failure were generally between 0.1 and 1.0 although some were between 2 and 4.2. In the failure of the Gouhou dam, a preferential flow path was suspected to have developed due to particle segregation during construction. In the case studies reviewed by Foster et al. (2002), preferential flow paths were suspected to have developed in zones with low stress due to foundation irregularities. Foster et al. (2002) concluded that average hydraulic gradients are not as important as other factors that can lead to the formation of continuous seepage paths. These factors are primarily influenced by anomalies caused by stress conditions or construction defects. If cracking occurs along these continuous seepage paths, the head drop across intact sections can result in large hydraulic gradients (Kakuturu and Reddi, 2006). Data presented by Rönnqvist et al. (2014)

suggests that suffusion incidents develop on average 10 years after first filling, although this ranges from first filling to 52 years later. Suffusion can therefore, be a very slow process taking place at hydraulic gradients much lower than used to bring about suffusion in laboratory experiments within realistic time scales.

Porous media theory has been used to model the hydromechanical conditions under which finer particles are lost. Although micro-scale models can be developed in which individual flow paths are considered, such as by Indraratna and Radampola (2002), the gross simplifications required for the pore network leads to macro-scale models being preferred. In macro-scale models, the soil skeleton and pore constituents of air, water and eroded particles are defined as phases. The interaction of these phases is governed by mass and momentum balance equations, with the erosion of particles governed by empirically based erosion laws. Such a model was developed by Cividini and Gioda (2004) to assess settlement caused by finer particle loss during ground water lowering. Fujisawa et al. (2010) developed a model incorporating changes in porosity, PSD, concentration of eroded particles and distribution of pore pressures. The model was validated using published experimental data. Fujisawa et al. (2010) predicted that suffusion in a homogenous embankment would propagate downstream from the surface of the impounded water, along the phreatic surface within the embankment and horizontally upstream from a horizontal toe drain. Bonelli and Marot (2011) presented a model based on the view that internal erosion can be viewed as a micro-scale clay/water erosional process. Although these models based on porous media theory are promising, they require further validation and do not incorporate the important process of redeposition and clogging or the mechanical effects of particle loss.

2.4 Distinction between suffusion and suffosion

The two terms most commonly associated with studies on the loss of finer particles from internally unstable soils are suffusion and suffosion. Fannin and Slangen (2014), considered the historical use of the terms, and suggested they should be used to identify distinct phenomena, although this has not always been the case. Suffusion is

defined as, “the phenomenon whereby fine particles are transported by seepage flow and the soil structure remains intact … quantified by a mass loss, no change in volume and an increase in hydraulic conductivity.” Suffosion is defined as, “[the] phenomenon in which the transport of fine particles by seepage flow is accompanied by a collapse of the soil structure … quantified by a mass loss, a volumetric contraction and a change in hydraulic conductivity”. Figure 2.3 summarises these two definitions.

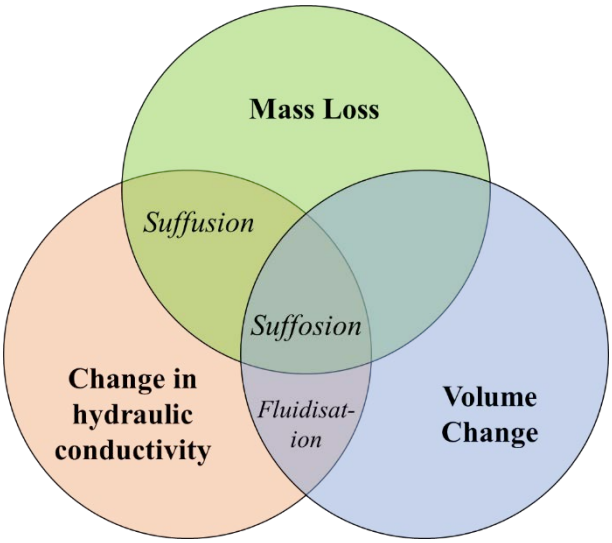


Figure 2.3: Conceptual framework for seepage-induced instability, after Fannin and Slangen (2014)

Suffosion is therefore used to describe situations where finer particle loss results in collapse of the soil structure, and suffusion instances where finer particle loss is not accompanied by collapse. Whilst suffusion may not result in soil structure collapse, ICOLD (2014) highlights that an increase in hydraulic conductivity results in greater seepage velocities, which potentially increases upstream hydraulic gradients, and the rate of erosion. Further, a loss of finer particles from filters renders them coarser and less effective at protecting cores from erosion.

Moffat et al. (2011) suggested that initially at low hydraulic gradients, suffusion takes place developing into suffosion as the hydraulic gradient increases. However, it is unlikely that hydraulic gradients increase as rapidly in embankment dams as occurred in their experiments. Skempton and Brogan (1994) suggested that a key factor to

understanding internal instability is the manner in which the finer fraction fits into the void space between the coarser fraction. In a soil comprising a mixture of coarser and finer particles, an increase in the finer fraction does not change the porosity of the coarser fraction until the void spaces between the coarser particles are filled. The addition of further finer particles after this point increases porosity of the coarser fraction. Skempton and Brogan (1994) proposed that this porosity increase theoretically takes place at finer fractions of between 29 - 24 % depending on global packing. However, they suggested that it is more likely lower: between 20 - 15 %. They also pointed out that if the finer fraction exceeds 35 % then the coarser particles will be floating in a matrix of finer particles. A subsequent synthesis of nine studies by Rönnqvist and Viklander (2014) suggests that these ranges are realistic. Understanding the interaction of the finer and coarser fabrics during internal erosion is therefore necessary to understand the changes in mechanical behaviour.

The contribution of various particles sizes to soil strength is an important field of geotechnical research. Lade et al. (1998) illustrated that for finer particles to be completely contained in the void spaces of coarser particles, they need to be considerably smaller than the coarser particles. This is because as the ratio between the diameters of the coarser to finer particles decreases, there is an increasing misfit in the void spaces. For binary packings of spheres, a diameter ratio below 6.5 results in significant misfit. This ratio represents the boundary at which small particles can fit through the constrictions of densely packed large spheres. They point out that for natural soils friction, adhesion, particle angularity and bridging can cause misfit at higher diameter ratios. For sand-silt mixtures with diameter ratios between 7.1 and 30 the packing was fairly close to the theoretical relationship for fines contents (particles smaller than 0.075 mm) less than 15 % but showed an increased amount of misfit above this. For diameter ratios below 7.1, there was significant misfit and the porosity of the coarser fraction increased as soon as fines were added. Although simplistic, the coefficient of uniformity can be viewed as the diameter ratio between coarser and finer fractions of a PSD. The I criterion, which suggests that soils with C_u values above 10 are potentially unstable, illustrates that internally unstable soils are those with sufficiently small finer particles to fit within the voids of the coarser fraction.

Studies by Vallejo and Mawby (2000) and Vallejo (2001) broadly confirmed the packing behaviour reported by Lade et al. (1998), although it is shown that less misfit occurs at larger stresses. These studies also show that for fines contents less than ~ 30 % the coarser particles control shear strength. A transition then occurs with lower strength fines completely controlling shear strength at fines contents above ~ 60 %. This transition is more pronounced for non-plastic materials. Thevanayagam et al. (2002) show that for fines contents less than ~ 25 % the porosity of the coarser fraction controls shear strength. They suggested that when the porosity of the coarser fraction is high and fines occupy void spaces between coarser particles, the fines could provide resistance to the collapse of coarser particles, termed a "cushioning effect", thereby increasing strength. However, if some of these fines separate coarse grains, a fragile metastable fabric results. Three fabric types were suggested by Thevanayagam et al. (2002): (i) fines confined in the voids of the coarse structure; (ii) fines partially supporting the coarse structure; and (iii) fines partially separating the coarse structure. Shire et al. (2014) suggested that the first case would result in suffusion, the second case suffosion, and the third suffusion as the erosion of the finer particles between coarser grains is unlikely to take place.

Numerical modelling has been used to study the effects of the actual loss of finer particles on mechanical behaviour. Muir Wood et al. (2010) used both discrete element modelling (DEM) and continuum modelling (this term is also used to refer to analytical micromechanical or constitutive modelling in this thesis) to demonstrate that finer particle loss can have a weakening effect. They showed that, as finer particles are lost some compression takes place, but the global porosity increases, potentially causing an initially dilative soil to become contractive. If the loss takes place from specimens with large imposed shear stresses, significant distortions can result. They suggest that the narrowing of the PSD curve raises the critical state line, potentially compensating for the increase in porosity. Consequently, the shear behaviour may not change significantly due to finer particle loss.

Scholtès et al. (2010) also used DEM and continuum modelling to investigate this mechanical response to particle loss. Their findings broadly agree with those of Muir

Wood et al. (2010). They suggest that overall stability will depend on the shear strength that can be mobilised at the critical state. Using a continuum model, Hicher (2013) showed that at low mobilised stresses, although finer particle loss does not result in significant deformations, the resulting fabric is very fragile. This fabric is shown to collapse if pore pressures increase or is subjected to rapid loads from shocks or vibrations. While formative on soil mechanical response to particle loss, in the opinion of the current author, the numerical studies highlighted here were based on relatively narrow PSD curves and so the finer particles potentially have a greater role in mechanical behaviour than may be the case for soils with wider PSD actually used in practice.

Within an embankment dam, soil elements will be at different stress states. This results in soil elements along a slip circle having different mobilised stresses as illustrated by Figure 2.4 (τ is shear stress and γ is shear strain). The numerical modelling reported above suggests that a consequence of particle loss is a reduction in strength from that associated with a dilatant state, having a peak strength, to a contractant state, having the critical state strength. Considering the graph in Figure 2.4, point B at which the peak strength is mobilised, loss of finer particles would have a significant destabilising effect; at point A the loss of finer particles would not have a significant effect, as the mobilised strength is lower than the critical state strength. However, the available peak strength will be reduced. Such zones would then be at an increased risk of collapse due to sudden loads.

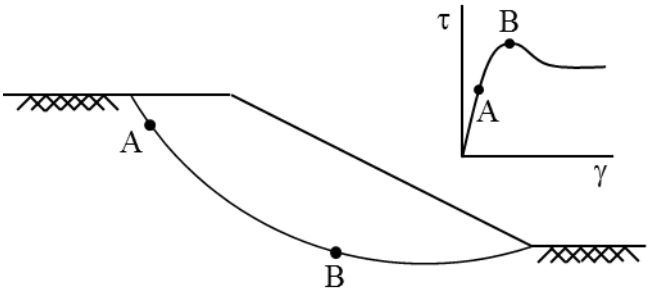


Figure 2.4: Stress states within an embankment, after Houlsby (1991)

Some attempts have been made to model the effect on soil mechanical properties of finer particle loss experimentally. Sterpi (2003) theorised that during erosion, the volume can remain unchanged (i.e. coarser fabric carries all load), or reduce (i.e. finer fabric carries some load). Two assumptions were proposed to determine the volume reduction, namely (i) the volume of voids remains constant (that is the coarser fabric collapses to take up space occupied by lost finer particles) or (ii) global void ratio remains constant (that is the coarser fabric collapses to take up space occupied by lost finer particles and void spaces between finer particles). No attempt was made to justify these assumptions, with the assumption that the global void ratio remains constant being adopted, as it results in the largest volumetric strain. Tests on specimens, reconstituted to a void ratio consistent with assuming global void ratio remained constant, showed that strength and stiffness increase as finer particles are eroded, in contradiction to most studies.

Shwiyhat and Xiao (2010) attempted to use a modified triaxial setup to erode finer particles and then test mechanical behaviour. However, in the words of the authors: "triaxial test results do not offer, with certainty, an explanation of the performances of the post-suffusion soil specimens." Chang et al. (2014) using a triaxial set up with a specimen containing gravel and sand in a 65:35 mix, succeeded in showing that finer particle loss results in a change from dilative to contractive behaviour. Peak friction angle was reported to reduce by 1.1 – 5.9 ° following a loss of 2.5 – 6.8 % of finer particles. Ke and Takahashi (2012) showed that mechanical resistance reduced following internal erosion by using a miniature cone penetration test on an internally unstable material following upward flow.

It is evident that experimental studies using reconstituted specimens (Sterpi, 2003), triaxial tests on internally unstable soils (Shwiyhat and Xiao, 2010, Chang et al., 2014) or permeameter tests (Ke and Takahashi, 2012) have been unable to adequately investigate the mechanical response of a soil to internal erosion. This is because the mechanical response is dependent on the actual fabric changes that take place during internal erosion (Muir Wood et al., 2010).

No studies appear to be have been carried out specifically on how hydraulic conductivity changes as erosion takes place. A study by Kenney et al. (1984) demonstrated that regardless of PSD curve shape, hydraulic conductivity is controlled by the size of particles making up the finest 5 % of the PSD. Thus, even the loss of a small portion of finer particles is likely to result in a significant increase in hydraulic conductivity. Few studies have been carried out on whether all the potentially erodible finer particles or a fraction thereof are eroded, Wan and Fell (2008) tentatively suggest 50 % can be assumed to be eroded.

2.5 Summary

Seepage-induced erosion of dams is an area of dam safety that still relies to a significant degree on empirically derived methods of assessing the potential for internal erosion. These involve identifying mechanisms in which internal erosion can initiate, continue, progress, and potentially breach a dam. The use of filters designed to modern criteria have been shown to remove almost completely the risk of internal erosion. However, as incidents continue to occur, research has continued to understand the phenomenon better. This chapter has outlined the state of knowledge of one particular mode of internal erosion caused by internal instability, which results in the two phenomena of suffusion and suffosion.

Criteria to assess material susceptibility to internal instability, continue to be refined, with over ten criteria proposed to date. Recent emphasis has been on assessing soils containing significant portions of silt and clay due to their potential stabilising effect. If there is a bimodal structure, in which finer particles are mobile within the coarser skeleton, critical hydraulic gradients required to initiate suffusion are lower than required to erode the entire PSD. Imposed stress can increase the hydraulic gradients required to initiate erosion due to increased confinement. However, if the imposed stresses result in large shear stresses, the hydraulic gradients required to initiate erosion can decrease, possibly due an alignment of pore spaces. It is most likely that suffusion develops due to stress anomalies or construction defects concentrating flow

in particular zones. This combination of stress and hydraulic conditions most often leads to a slow erosion of finer particles, but in extreme cases, this can be rapid.

The effects of suffusion are an increase in porosity, which increases permeability and, in some cases, decreases volume, the latter referred to as suffosion. Literature suggests that if the finer fraction is below ~ 15 %, suffusion will dominate because the finer particles would initially fit within the coarser fraction and their removal would have no effect on the coarser fabric. As shear strength is dominated by the coarser fraction, the loss of finer particles may go unnoticed for a significant period. As the finer fraction increases, the misfit between sizes increases, with finer particles contributing to overall strength. Some finer particles may become sufficiently loaded by coarser particles not to be at risk of erosion. It is at these finer fractions that suffosion is likely to dominate. If the finer fraction increases above ~ 30 % the finer particles completely fill the voids between coarser fraction and the coarser particles play a diminishing role. At this point, all the finer particles are likely to be sufficiently loaded by surrounding coarser particles to prevent their erosion. The literature suggests that the increasing porosity that results from both suffusion and suffosion may be very destabilising in highly stressed zones, and in less stressed zones, the resulting fragility would be at risk of pore pressure increases or sudden loads.

Chapter 3 Influence of fabric on internal erosion

This chapter develops a fabric-based explanation for internal erosion by investigating how the finer and coarser fractions of an internally unstable soil pack together. As internally unstable soils are typically granular (or cohesionless), fabrics are discussed largely by considering density relationships. Although density relationships are not always a good indicator of fabric (Holtz and Kovacs, 1981), subsequent chapters will show they adequately reflect observed engineering behaviour. When the finer fraction is small, suffusion dominates as finer particles are contained in a dense stable coarser skeleton. However, as the finer fraction increases suffosion dominates as finer particles are contained in a loose unstable coarser skeleton.

3.1 Transition and critical finer fractions

For a soil to be susceptible to suffusion, Skempton and Brogan (1994) proposed that two criteria need to be met. The first criterion is that the finer fraction of the soil must be smaller than the constrictions on flow paths between the coarser particles. This implies that for an internally unstable soil there exists a largest erodible particle size (D) that divides a soil's particle size distribution (PSD) into a finer and coarser fraction (Figure 3.1). The second criterion is that the finer particles must only partially fill the voids between the coarser particles, leaving the finer particles relatively unloaded. A maximum finer fraction (F) can therefore be defined above which overburden loads become more uniformly distributed throughout all particle sizes.

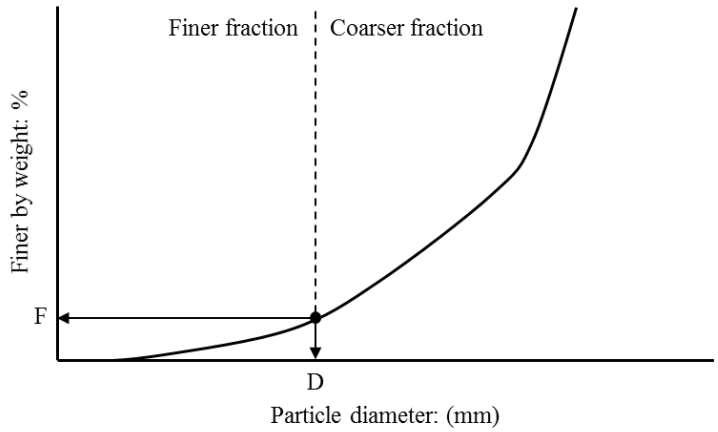


Figure 3.1: Distinct finer and coarser fractions

3.1.1 Largest erodible particle

Theoretically, for a binary mixture of spheres, if the ratio of diameters is greater than 6.5, the smaller spheres can pass through the constrictions between the larger spheres at their densest packing (Lade et al., 1998). The division between finer and coarser fractions is not as clear-cut for soils that have a more continuous range of sizes. The division is not arbitrary either, such as dividing the PSD at 0.075 mm (Casagrande, 1948), used to classify fines in studies on the role of fines in the liquefaction potential of sands (e.g. Thevanayagam et al. (2002); Rahman and Lo (2008)). Empirical criteria based on a soil's PSD are commonly used to assess the constriction size of a soil. Kezdi (1969), considering an ideal arrangement of spheres, concluded that the constriction size ranges between $0.25D_{15}$ and $0.2D_{15}$. Kenney and Lau (1985), using granular filters, concluded that particles of size D passed through the constrictions of particles of size 4D and larger. Recent discrete element modelling (DEM) has shown that these empirical criteria have a sound basis (Shire and O'Sullivan, 2016).

These empirical criteria can be used to divide a soil's PSD into finer and coarser fractions. Using the Kezdi (1969) criterion the division occurs at the largest particle size where a given PSD, separated into a coarser and finer fraction, does not fulfil $D_{15c}/D_{85f} < 4$. Alternatively, based on the Kenney and Lau (1985, 1986) criterion, this is the particle size D for a given PSD, at which the ratio H/F_D is a minimum, where F_D is the percentage passing at D and H is the difference in percentages passing D and 4D. Chapius (1992) showed that the Kezdi (1969) and Kenney and Lau (1985, 1986) criteria are mathematically similar and rely on determining the minimum value of the secant slope of a given PSD. If this secant slope is lower than 24.9 % per log cycle it fails the Kezdi (1969) criterion and if the secant slope is lower than $1.66F_D$ it fails the Kenney and Lau (1985, 1986) criterion. As this minimum slope will occur at the same particle size for both criterion, the division between coarser and finer fraction will be similar by either method. Wan and Fell (2004) compared the finer and coarser fractions proposed by the Kenney and Lau (1985, 1986) criterion to the PSDs before and after suffusion finding the criterion predicted the division within 1.5 log cycle of the respective particle size. ICOLD (2014) suggests that the division between finer and coarser fractions can be based on the point of inflection of an internally unstable soil's PSD or the position of the gap for gap-graded soils. Rönnqvist (2015) found

these simpler ICOLD (2014) criteria provided a satisfactory estimate of the division between finer and coarser fractions.

To illustrate typical PSDs associated with suffusion, relevant grading parameters (D_5, D_{10}, D_{20}, D_{60} and D_{90}), compiled by Chang and Zhang (2013) from published research, are plotted in Figure 3.2. For each grading parameter, a box plot indicates the interquartile range and median. This shows that the coarser particles (D_{60}, D_{90}) are typically gravel sized, whereas the finer particles (D_5, D_{10}) are fine sand sized. Chang and Zhang (2013) point out that the finer particles are typically non-plastic, although small percentages of low to medium plastic fines may be susceptible to suffusion. Each grading reported by Chang and Zhang (2013) has been divided into a coarser and finer fraction using the Kezdi (1969) criterion. The average D_{50c}/D_{50f} was 290, although the values range between 10 and 6750 and were left skewed with a median of 80 (Figure 3.3). This illustrates that the particles making up the finer fraction are significantly smaller than the particles making up the coarser fraction.

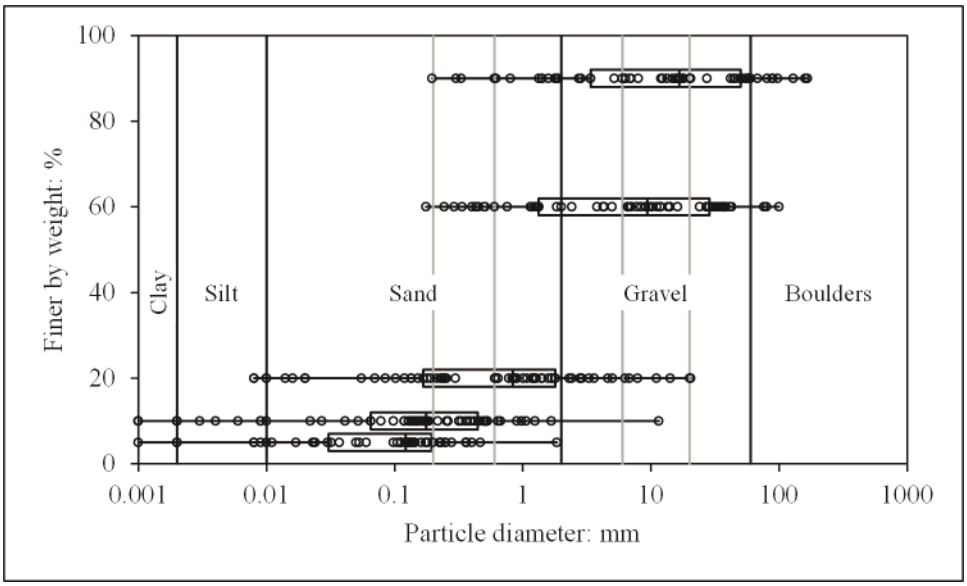


Figure 3.2. Internally unstable particle size distributions, data from Chang and Zhang (2013)

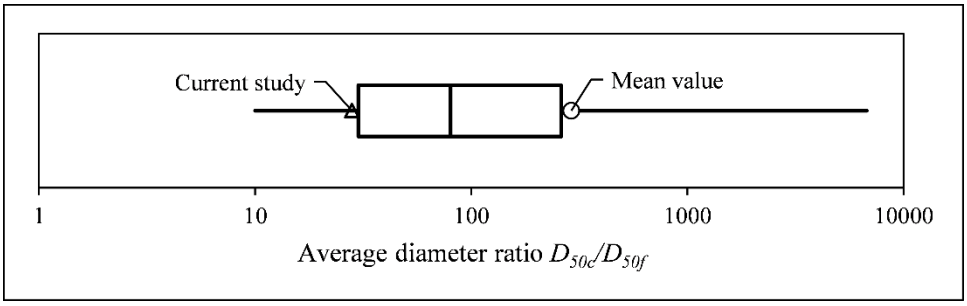


Figure 3.3: Box-plot illustrating average diameter ratios (D_{50c}/D_{50f}) for 50 internally unstable soils reported by Chang and Zhang (2013)

3.1.2 Maximum finer fraction

As mentioned before, the second criterion for a soil to be susceptible to suffusion, proposed by Skempton and Brogan (1994), is that the voids between the coarser fraction are only partially filled. The maximum finer fraction where the voids between the coarser fraction are only partially filled is the critical finer fraction (F_c). To determine F_c various researchers (Kenney and Lau, 1985, Skempton and Brogan, 1994, Wan and Fell, 2004) have proposed the following equation (although each expresses it in a different form) based on the phase relationships between the coarser and finer particles (see derivation in Appendix C.1 page 203):

$$F_c = \frac{e_c}{1 + e_c + e_f} \qquad \text{Equation 3.1}$$

where e_c is the void ratio of the coarser fraction alone ($e_c = (V_t - V_c) / V_c$, where V_t is the total soil volume and V_c is the volume occupied by coarser particles) and e_f is the void ratio of the finer fraction ($e_f = (V_t - V_c - V_f) / V_f$, where V_f is the volume occupied by finer particles). e_c is equivalent to the skeletal void ratio proposed by various authors (Thevanayagam et al., 2002, Rahman and Lo, 2008) in the study of the susceptibility of sands containing fines to liquefaction. In these studies, fines are considered particles smaller than 0.075 mm (ASTM D2487) or alternatively 0.063 mm (BS 1377-2). Whilst there is considerable debate about using the skeletal void ratio in liquefaction studies of silty sands (Yang et al., 2015) it is perhaps more applicable to studies of internally unstable soils. Reasons for this are twofold. Firstly, the division of a soil into a finer and coarser fraction is based on rational criteria for internally unstable soils, rather than an arbitrary delineation at 0.075 mm or 0.063 mm

(Casagrande, 1948). Secondly, as the finer fraction is considerably smaller than the coarser fraction (Figure 3.3), finer particles are more likely to be contained within void spaces between coarser particles.

Prior to considering an actual soil, attention will be given to the derivation of Equation 3.1. This equation assumes that the packing of the coarser particles remains at e_c up to the point at which the finer particles completely fill the voids between the coarser particles. This is shown by line AB in Figure 3.4. Initially as the finer particles are added, they will be dispersed between the coarser particles at a high void ratio (assuming they are evenly distributed throughout the void space between coarser particles), but as the finer fraction increases and the voids between the coarser fraction become filled up, e_f decreases (line DE). Once the voids between the coarser fraction are filled with finer particles, the coarser particles will become separated by the finer particles and the void ratio of the coarser fabric will increase along line BC. The global void ratio (e) begins at e_c and decreases as voids between coarser particles are filled, after which it increases to e_f when the soil has become 100 % finer particles.

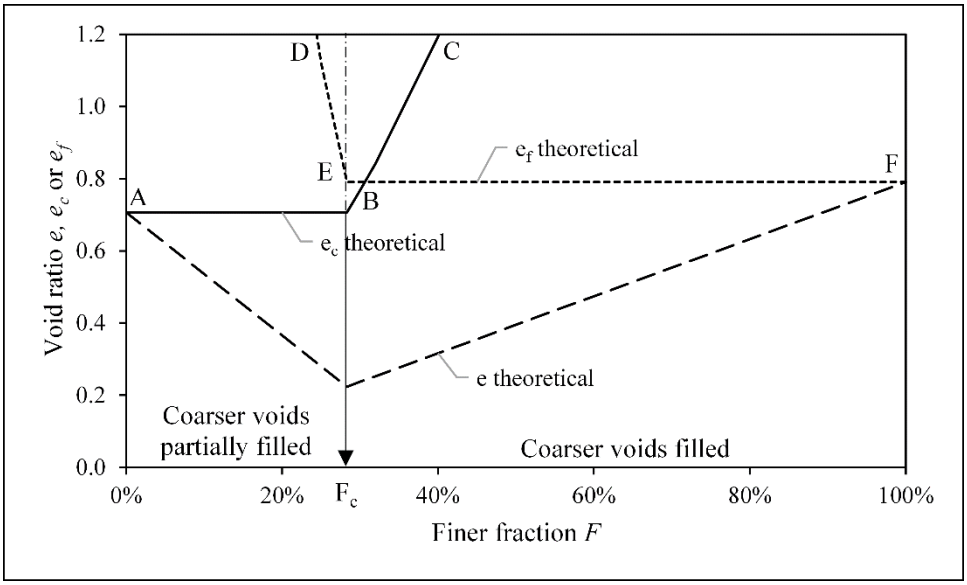


Figure 3.4. Theoretical variation of void ratios for a binary mixture of spheres

Based on this bimodal fabric and values of e_c and e_f, chosen in different ways by the different authors, Kenney and Lau (1985) suggested F_c was between 20 and 30 %, Skempton and Brogan (1994) suggested it could be as high as 35 % but likely between 24 and 29 % and Wan and Fell (2004) suggested the upper limit was 40 %.

Lade et al. (1998) showed that for actual binary mixtures of spheres the changes are not as sharp cornered as shown in Figure 3.4, although the behaviour is close for ratios of diameters greater than 7. Real soil particles are obviously non-spherical and are subject to attractive and repulsive static forces such that packing behaviour deviates substantially from that depicted in Figure 3.4 (Lade et al., 1998). This brings into question the suitability of Equation 3.1 to define F_c.

3.1.3 Packing behaviour of internally unstable soils

Although numerous studies on soil packing behaviour have been carried out, the author is not aware of any well-documented experiential studies on the packing behaviour of soils whose gradations have been shown to be internally unstable. Therefore, to investigate this, increasing quantities of a fine sand (S) were added to a fine gravel (G). The particle size distributions of components S and G were chosen so as to form a gradation found to be internally unstable in tests by Skempton and Brogan (1994); Li (2008) and Shire et al. (2014). Figure 3.5 illustrates S and G and shows an example of a gradation with a finer fraction (F) of 15 %. The material used was a non-plastic, residual granite with sub-angular particles of moderate sphericity (Cho et al. (2006) Sphericity values between 0.5 and 0.7, and Roundness values between 0.5 and 0.7). Further details about this material are given in Chapter 6. Grading properties of the components (Table 3.1) show that they do not meet the internal filter ratio criterion (Kezdi, 1969) and so, by that criterion, are potentially unstable. The diameter ratio of 28 is towards the lower end of the typical range for internally unstable soils, based on the review of data presented by Chang and Zhang (2013) (Figure 3.3). All the composite gradations considered (Table 3.2) also fail the Kenney and Lau (1985, 1986) criterion with $(H/F_D)_{min}$ less than unity, although these authors suggested their criterion should only be applied for $F < 30$ %. Only gradations with $F > 15$ % are classified as unstable ($C_u > 20$) by the Istomina (1957) criterion.

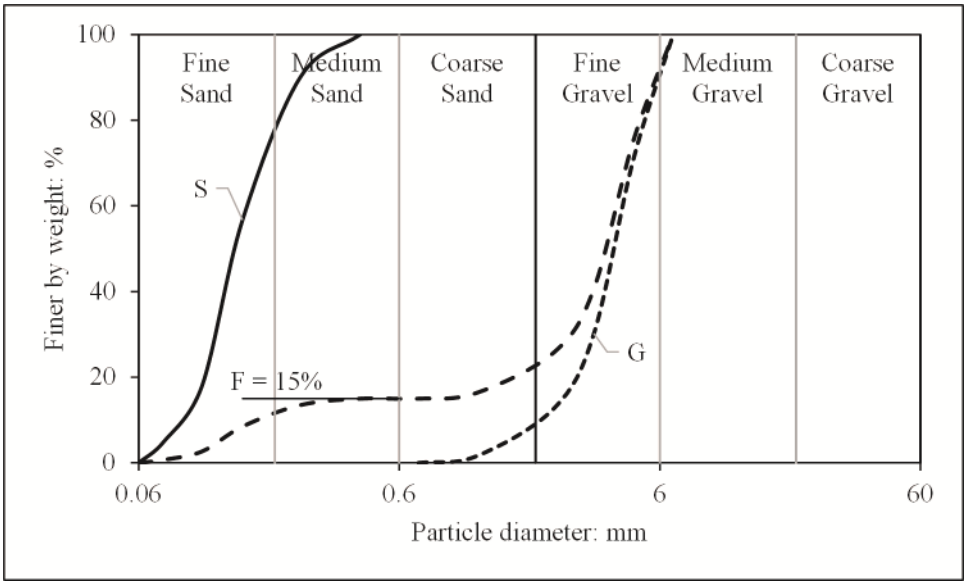


Figure 3.5. Gradations investigated

Table 3.1: Properties of component materials

Parameter	S	G
D_{85}: mm	0.23	5.6
D_{50}: mm	0.14	4.0
D_{15}: mm	0.10	2.5
Coefficient of uniformity, C_u (=D_{60}/D_{10})	1.9	2.2
Minimum void ratio, e_{min}	0.79	0.71
Maximum void ratio, e_{max}	1.23	0.96
Internal filter ratio (D_{15c}/D_{85f})	11	
Ratio of diameters (D_{50c}/D_{50f})	28	

Table 3.2. Instability criteria

Finer fraction, F	5	10	15	20	25	30	35
Stability index $(H/F_D)_{min}$	0.38	0.22	0.17	0.14	0.12	0.11	0.10
Coefficient of uniformity, C_u (=D_{60}/D_{10})	2.9	9.6	23	28	30	31	31

It is widely accepted that for a given soil there exist two limiting fabrics, a dense packing and a loose packing. Minimum and maximum global void ratios can be used to define these limiting fabrics, although they are arbitrary as they are dependent on the methodology used to obtain the limiting packings. No standard methodologies are available for gravel materials and an effort was made to develop a repeatable method that minimised particle breakage and segregation. (Described in detail in Chapter 6). The maximum global void ratio was determined using a method adapted from the ASTM D4254 funnel method and the minimum global void ratio by pouring small

increments of material into a standard mould which was successively tapped with a rubber mallet (similar to Lade et al. (1998) and Cubrinovski and Ishihara (2002)).

Results from these tests (Figure 3.6) show that the changes in void ratio are clearly different to the theoretical propositions. Considering the densest packings (i.e. minimum global void ratios), close theoretical behaviour is observed up to F = 15 % after which the global minimum void ratio, e_{min} remains essentially constant and e_c increases. The loosest packings (i.e. maximum global void ratios) are similar, although global maximum void ratio, e_{max} reduces slightly between F = 15 % to 30 % and then increases slightly.

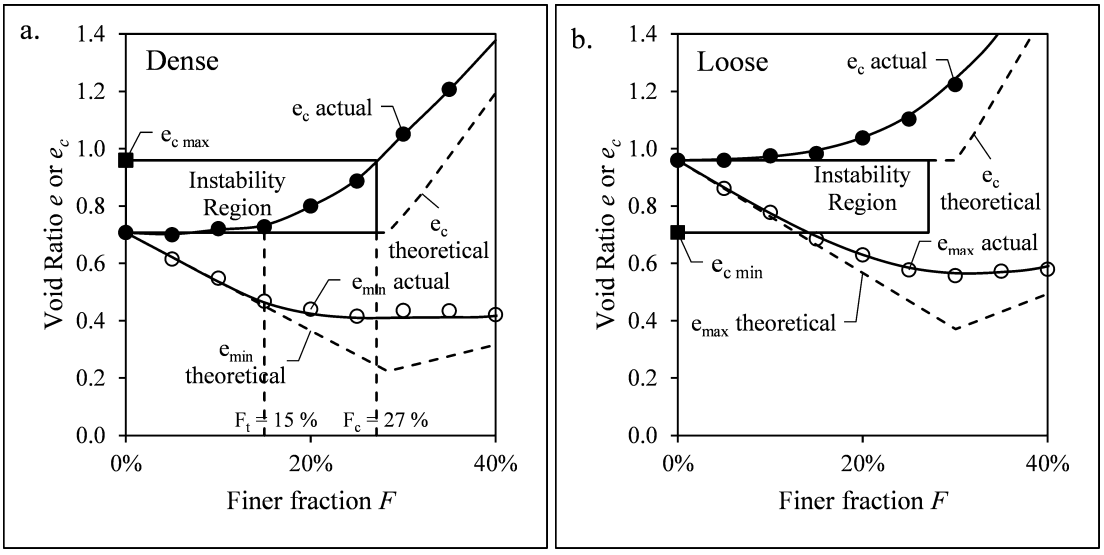


Figure 3.6. Variations in a. minimum and b. maximum global void ratios

Lade et al. (1998) and Cubrinovski and Ishihara (2002) studied global void ratios for various composite gradations. For composite gradations with D_{50c}/D_{50f} between 7 and 325, observed behaviour was similar to that observed in this study and shown in Figure 3.6. Granting their gradations were not indicated as being internally unstable, they show that increasing the diameter ratio does not increase packing efficiency. Thus although the diameter ratio of the components used in this study is 28, it is unlikely that the behaviour would vary considerably for larger diameter ratios typical of other internally unstable soils. It can be concluded, therefore, that it is only up to approximately F = 15 %, that the finer particles would be contained within the voids of an unchanging coarser fabric, be it dense or loose. This transition is significantly

lower than the range of F_c values of 20 – 30 % suggested by Kenney and Lau (1985); < 35 % proposed by Skempton and Brogan (1994) and < 40 % proposed by Wan and Fell (2004). A more rigorous assessment of the packing between the finer and coarser particles is now presented.

If we first consider the dense packings (Figure 3.6a), above F = 15 % the coarser fabric becomes progressively less dense as e_c increases. Finer particles are therefore hindering the coarser particles from moving into a denser arrangement. At F = 0% on Figure 3.6a, the loosest stable fabric for the coarser particles is indicated as $e_{c\,max} = 0.96$. Whilst e_c remains below $e_{c\,max}$, the coarser particles are in a stable arrangement regardless of whether finer particles are present or not. The coarser particles are therefore unlikely to collapse significantly if all finer particles were suddenly removed. It is only when e_c exceeds $e_{c\,max}$ that the coarser particles would no longer be in a stable arrangement if all finer particles were suddenly removed. Above this $e_{c\,max}$ threshold, it is therefore unlikely that suffusion would take place as the finer particles no longer only partially fill void spaces, but rather support the coarser particles and carry load. It is proposed, therefore, that the finer fraction at which the coarser particles reach their loosest stable fabric is the critical finer fraction (F_c). Using this definition, F_c for the gradations investigated was approximately 27 % (Figure 3.6).

A similar assessment of the loose packings (Figure 3.6b) shows that above F = 15 % the coarser particles are at a packing that is looser than their loosest stable fabric, which can only be possible if finer particles are carrying load. For the finer particles alone, the void ratio at its loosest stable packing was 1.23. However, the void ratio of the finer fraction was higher than this and it was only at F > 60 % that the finer fraction void ratio became smaller than this (Figure 3.7, dense global void ratio mixtures included for comparison). Thus, for F lower than 60 %, the finer particles are unlikely to fill all the void spaces, but rather sit between coarser particles, resulting in a very loose honeycomb structure (Lade et al., 1998).

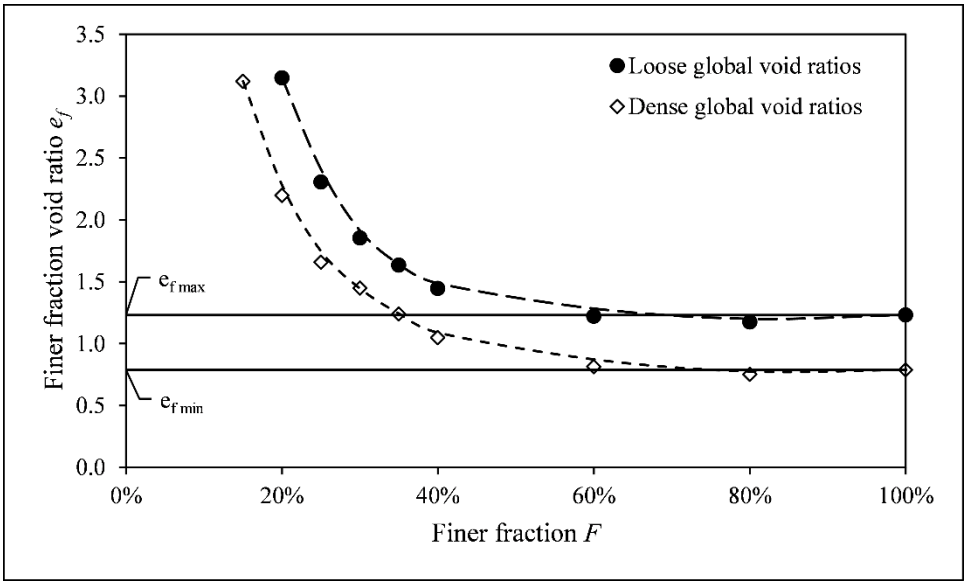


Figure 3.7: Variation of the void ratio of finer particles with increasing finer fraction

To estimate the range of F_c values for other internally unstable soils, a theoretical variation of global void ratio with increasing F is proposed for dense packings. A discussion of loose packings is not presented, as no engineer would specify such low densities for the construction of embankment dams. Based on the research presented here (Figure 3.6), it is assumed that the global minimum void ratio, $e_{min,}$ follows the theoretical trend for binary mixtures (Figure 3.8) up to a transition finer fraction (F_t) and then remains constant. The coarser fraction void ratio (e_c) can then be determined, based on this variation of e_{min} with F, using the following equation (Thevanayagam et al., 2002):

$$\boldsymbol{e_c = \frac{F + e_{min}}{1 - F}} \qquad \text{Equation 3.2}$$

Various assumptions regarding the densest and loosest packing of the coarser particles are necessary to estimate F_c. The densest packing of the coarser particles (i.e. e_{min} at F = 0 %) is required as this defines the initial point of the proposed relationship of e_{min} with F (Figure 3.8). The loosest packing of the coarser particles (i.e. e_{max} at F = 0 %) is required as this defines the limiting value of e_c above which it is impossible for finer particles to only partially fill coarser fraction voids and therefore must become load bearing. For a soil of coarser particles only (i.e. F = 0 %), it is realistic to assume that e_{min} ranges between 0.4 and 1.0, and the difference between e_{max} and e_{min} ranges

between 0.2 and 0.3 (Cubrinovski and Ishihara, 2002). By assuming F_t ranges between 10 and 20 % and that all variables have a uniform distribution within their given range, a Monte Carlo simulation (Ang and Tang, 2007), was used to estimate F_c. Based on 10^6 iterations it was found that on average F_c is 26 %, with a standard uncertainty of ±3 % and a maximum uncertainty of ±8 %. This range of F_c values is in line with the range suggested by Kenney and Lau (1985) and Skempton and Brogan (1994), but still slightly lower than proposed by Wan and Fell (2004).

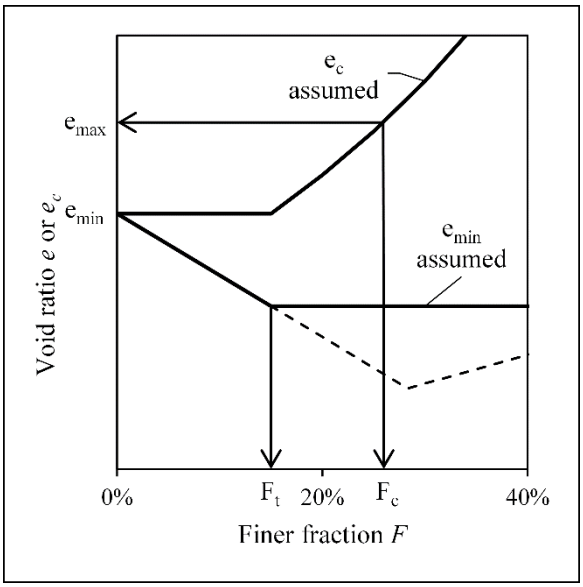


Figure 3.8. Simplified variation of void ratios for an internally unstable soil

In order to assess whether the range of F_t and F_c values determined above are realistic a data set of previous studies in which minimum and maximum global void ratios were determined for mixtures of two soils was compiled (Table 3.3). A number of such studies have been made with sand-silt mixtures for the purposes of assessing the role of silt in the liquefaction of sand. Fewer studies have been made looking at gravel-sand mixtures, which are more typical of internally unstable soils. Whilst these studies were not specifically looking at internal stability, it is apparent from the D_{15c}/D_{85f} ratios (Table 3.3) that a number of the mixtures would potentially be internally unstable. No other internal stability criteria were applied, as insufficient gradation data was available.

Table 3.3: Properties of sand-silt and gravel-sand mixtures and their references

Reference	Coarser component			Finer component			Internal filter ratio D_{15c}/D_{85f}	Ratio of diameters D_{50c}/D_{50f}
	D_{15}	D_{50}	D_{85}	D_{15}	D_{50}	D_{85}		
R1	0.10	0.14	0.21	0.02	0.04	0.05	2.2	3.9
R2	0.17	0.22	0.33	0.002	0.01	0.03	5.6	21
R3	0.20	0.25	0.28	0.03	0.05	0.07	3.0	5.0
R4	1.0	1.1	1.1	0.15	0.17	0.18	5.8	6.5
	1.0	1.1	1.1	0.13	0.14	0.16	6.3	7.9
	1.0	1.1	1.1	0.08	0.10	0.15	6.9	11
	1.0	1.1	1.1	0.13	0.14	0.15	7.0	7.9
	1.0	1.1	1.1	0.08	0.10	0.13	7.7	11
	1.0	1.1	1.1	0.08	0.10	0.11	8.9	11
	1.0	1.1	1.1	0.04	0.06	0.07	15	19
	1.0	1.1	1.1	0.33	0.40	0.52	2.0	2.7
	1.0	1.1	1.1	0.28	0.42	0.54	1.9	2.6
	1.0	1.1	1.1	0.21	0.26	0.29	3.6	4.1
R5	1.2	1.5	1.8	0.03	0.05	0.07	18	30
R6	0.25	0.45	0.75	0.03	0.03	0.06	3.9	13
R7	0.30	0.38	0.54	0.00	0.02	0.05	5.9	13
R8	10	11	12	0.21	0.27	0.39	25	40
	20	22	24	0.21	0.27	0.39	51	81
R9	5.1	6.5	8.5	0.19	0.40	0.66	7.7	16
R10	5.6	7.6	10	1.3	1.5	1.9	3.0	4.9
Current	2.5	4.0	5.6	0.10	0.14	0.23	11	28

R1 - Yamamuro and Covert (2001), R2 - Thevanayagam et al. (2002), R3 - Lade and Yamamuro (1997), R4 - Yilmaz (2009), R5 - Lade et al. (1998), R6 - Yang et al. (2006), R7 - Salgado et al. (2000), R8 - Hamidi et al. (2009), R9 - Evans and Zhou (1995), R10 - Kumara and Hayano (2013)

For each data set (Table 3.3) values of e_{max} and e_{min}, were plotted against values of finer fraction and third-degree polynomials were plotted through the points (Figure 3.9a). Here finer fraction was simply the percentage of the finer component as a proportion of the sum of the finer and coarser components in each study. The lowest R^2 value for all regressions was 0.96 and the average was 0.99. In view of the variety of ways in which e_{max} and e_{min} can be determined, the smoothness of fit is good. The coarser fraction void ratio was then calculated using Equation 3.2 and plotted against finer fraction (Figure 3.9b). As e_{max} and e_{min} of the coarser fabric were known, the relative density of the coarser fabric ($D_{r,ec}$) could be calculated (Figure 3.9c). F_t was estimated by assuming that the coarser fabric remains at essentially its densest packing up to $D_{r,ec}$ = 90 %. F_c was estimated both for global loose and dense fabrics by assuming the coarser fabric reached its loosest packing at $D_{r,ec}$ = -10 %. The choice

of $D_{r,ec}$ = -10 % over $D_{r,ec}$ = 0 % was because of the variability in relative density measurements (Tavenas and La Rochelle, 1972). Using $D_{r,ec}$ = -10 % ensures that the coarser particles are in an unstable arrangement in the absence of finer particles.

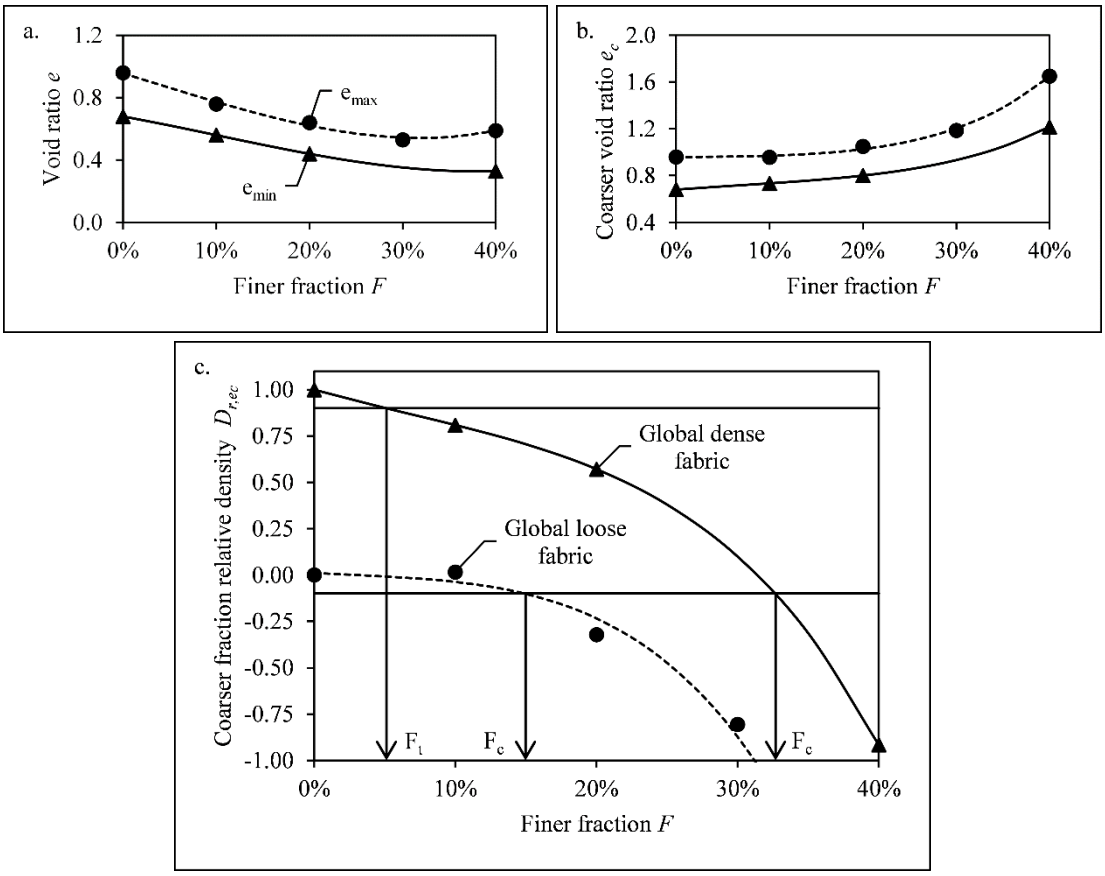


Figure 3.9: Example of regression analysis carried out on Evans and Zhou (1995) data set; a. variation of global void ratios, b. variation of coarse void ratios and c. variation of relative density of coarser particles with finer fraction

F_t and F_c boundaries for each mixture (Table 3.3), determined as described in the preceding paragraph, were plotted (Figure 3.10) against respective D_{15c}/D_{85f}. On each graph in Figure 3.10 the D_{15c}/D_{85f} < 4 criterion (Kezdi, 1969) is indicated with a vertical line that shows that all mixtures to the right are gradations that would be considered internally unstable by this criterion. It is clear that F_t and F_c are dependent on D_{15c}/D_{85f}, with a greater portion of finer particles filling the coarser fraction voids as D_{15c}/D_{85f} increases.

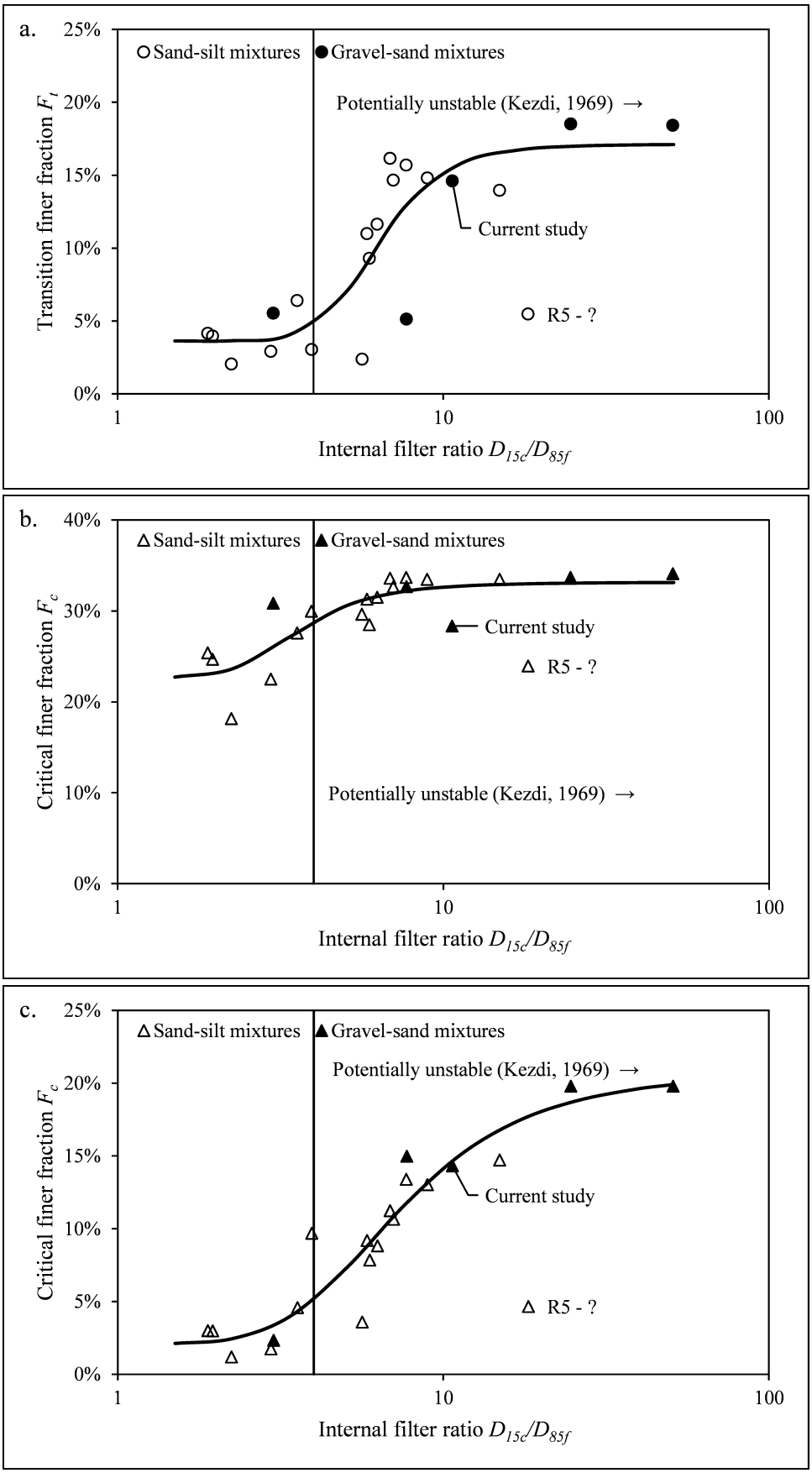


Figure 3.10: Packing behaviour boundaries a. Transition finer fraction for global dense fabrics, b. Critical finer fraction for global dense fabrics, c. Critical finer fraction for global loose fabrics

Figure 3.10a shows that for overall dense gradations with $D_{15c}/D_{85f} > 4$, the proportion of finer particles that can remain within the voids of a dense coarser fabric increases substantially from $F \approx 5$ % to $F \approx 17$ %. Except for the one Lade et al. (1998) data set (R5), sand-silt mixtures behaved similarly to gravel-sand mixtures, suggesting packing behaviour is more dependent on diameter ratio than actual particle size.

Figure 3.10b shows that the finer fraction at which the coarser fabric reaches its loosest packing (whilst the global fabric is still dense) increases marginally for $D_{15c}/D_{85f} > 4$, reaching a maximum value of approximately 33 %. These boundaries ($F_t \approx 17$ % and $F_c \approx 33$ %) are in line with the boundaries suggested by the Monte Carlo simulation based on an assumed variation in void ratios ($F_t = 10 – 20$ % and $F_c = 26 \pm 8$ %).

Although, as highlighted earlier loose global fabrics have little practical relevance, Figure 3.10c shows that the finer fraction at which the coarser particles move into an arrangement looser than their limiting arrangement (i.e. unstable in a gravitational field) varies in a similar fashion to the transition finer fraction for dense global fabrics.

3.2 The role of finer particles in load transfer

Based on the preceding discussion three general fabrics are proposed for global fabrics at their densest packing. For $F < F_t$ the global fabric is made up of coarser particles at essentially their densest packing with finer particles loosely occupying coarser fraction voids. For $F_t < F < F_c$ the global fabric is still predominantly made up of coarser particles, although they are in an increasingly loose arrangement, with finer particles partially filling coarser fraction voids to maintain a global dense fabric. For $F > F_c$ the finer particles completely fill the voids with the coarser particles playing a diminishing role in the global fabric as F increases.

The stress state in soil can be conveniently considered as being composed of an isotropic component, which causes volumetric changes, and a deviatoric component, which causes distortion. As the difference between the principal stresses increases, the deviatoric component increases, and greater shear stresses are imposed. On the other hand the closer the principal stresses are, the closer to isotropic the stresses will be. Considerations of how loads are carried in the three general fabrics identified above under states in which either isotropic or deviatoric stresses dominate are now presented.

Shire et al. (2014) used DEM to investigate fabric interactions between finer and coarser particles in internally unstable soils under isotropic stress. Their study showed that for $F < 24$ % the finer particles carry very little load, whereas for $F > 35$ % load is equally carried between coarser and finer particles. For 24 % $< F <$ 35 % a sharp transition was observed, with load carried by finer particles increasing substantially in denser global fabrics. Within this range (24 % $< F <$ 35 %), the transition occurred at a higher F for loose specimens and for specimen gradations with higher internal filter ratios (i.e. greater potential of internal instability). This suggests that for both $F < F_t$ and $F_t < F < F_c$ finer particles will carry little load under predominantly isotropic stress, even with the coarser particles being in an increasingly loose arrangement in the latter case. It is only for $F > F_c$ that finer particles become significantly loaded under isotropic stress.

The author is not aware of any well-documented studies on how finer particles, in internally unstable soils, carry load under deviatoric stress. However, inferences can be made from various studies of soil shear strength. Shear strength of granular materials is dependent on their physical nature and state. Grain-size, particle characteristics and mineralogy define physical nature, whereas the degree of compactness and stress define the state. For a given soil, i.e. for a given physical nature, the shear stress-strain behaviour can increase monotonically to a limiting value or peak and then soften to a critical state or constant volume shear stress. This peak is due to dilation, which is additional work needed to overcome particle interlock beyond that required to overcome particle sliding (Taylor, 1948). Bolton (1986)

showed that this peak is most pronounced when a soil is at its densest fabric and non-existent at its loosest fabric. However, at very high confining stresses, dense fabrics behave as loose fabrics, because dilation is suppressed and particles can crush. Soil strength can be quantified by a friction angle, and for these two conditions, they are called the peak friction angle (ϕ_p) and the constant volume friction angle (ϕ_{cv}).

Studies of gravel-sand mixtures (Vasil'eva et al., 1971, Vallejo, 2001) have shown that for dense mixtures, ϕ_p remains essentially constant for F < 30 % being identical to that of the coarser particles alone. For 30 % < F < 60 % finer particles start to dominate shear behaviour with floating coarser particles providing diminishing reinforcement. For F > 60 %, ϕ_p remains essentially constant and was identical to that of the finer particles. This suggests that for $F < F_t$ the loose finer particles within the dense coarser fraction voids do not contribute to resisting load under deviatoric stress. However, for $F_t < F < F_c$ the continued development of a constant peak strength, despite the coarser particles being in a looser arrangement, must entail a contribution by the finer particles. Under deviatoric stress, the distortion of the skeleton of coarser particles, which are no longer at their densest packing, forces the coarser particles to mobilise finer particles to resist the imposed loads, and dilation still takes place. Thus, as the finer fraction increases from F_t to F_c, coarser particles still dominate load transfer but finer particles play an increasing role in resisting deviatoric stress. For $F > F_c$ finer particles play a dominant role in resisting deviatoric stress with coarser particles providing a diminishing contribution (Simoni and Houlsby, 2006).

As deviatoric stress increases, large distortions of the fabric will take place and force chains between larger particles will develop and then collapse. This leads to a reduction in available shear strength until a steady state develops in which force chains continuously develop and collapse in a relatively loose arrangement of particles (Rechenmacher et al., 2010). As mentioned earlier, the strength at this stage is defined by the constant volume friction angle (ϕ_{cv}). Although a small finer fraction (F < 15%) may increase ϕ_{cv} (Murthy et al., 2007), the effect is minor, especially if the finer and coarser particles have similar particle shapes (Cho et al., 2006). Further, at the steady state, loads may be preferentially carried by certain grain sizes (Poulos,

1971) making it difficult to determine how particles of different size carry load. It is suggested however, that for $F < F_c$ coarser particles will dominate load transfer and finer particles will be very loosely held within the locally enlarged coarse voids. For $F > F_c$, as the fabric is made up predominantly of finer particles, they will dictate $\phi_{cv,}$ although the coarser particles can still provide some resistance (Simoni and Houlsby, 2006).

Rahman and Lo (2014) investigated the behaviour of silty sands during isotropic consolidation and shearing. They found that metastable fabrics could be formed that were relatively stable under isotropic loading but underwent significant volume changes during shearing. It is likely that similar metastable fabrics can develop due to suffusion, which although stable, can distort significantly when sudden loads cause shearing.

3.3 The effect of finer particle loss on mechanical behaviour

In light of the above discussions on packing behaviour and the role of finer particles in load transfer, the effect of finer particle loss on mechanical behaviour is now discussed. Two terms most used when referring to the consequences of finer particle loss on mechanical behaviour are suffusion and suffosion. Considering the historical use of the two terms, Fannin and Slangen (2014) proposed that suffusion should be used to describe non-destructive soil responses to finer particle loss (i.e. no volume changes occur) and suffosion should be used when finer particle loss is accompanied by collapse of the soil structure (i.e. a volume change). Within the context of mechanical behaviour, suffusion would therefore describe situations where no change in strength takes place and no change in volume, and suffosion describing situations where a reduction of strength takes place, precipitating large volume changes during shear distortion.

3.3.1 $F < F_t$: Suffusion

For internally unstable soils with $F < F_t$, it is unlikely that finer particle loss will have a significant impact on mechanical behaviour. The reasoning for this is that the coarser particles remain at their densest packing and the finer particles are loosely contained within the voids. Thus in regions of the dam were both small and large shear distortions have occurred, finer particles are unlikely part of the load carrying fabric. These finer particles can therefore be lost with no detrimental impact on available shear strength. Nevertheless, permeability will increase, as even a small change in the finer fraction impacts hydraulic conductivity (Kenney et al., 1984). In addition, if this material were used as a filter, its continued function would be jeopardised as the gradation changes as finer particles are lost, potentially leading to additional mechanisms of internal erosion (Rönnqvist, personal communication). Using the definitions proposed by Fannin and Slangen (2014) this behaviour would be suffusion.

3.3.2 $F_t < F < F_c$: Suffosion

For internally unstable soils with $F_t < F < F_c$, finer particle loss will have an increasing impact on mechanical behaviour as F increases to F_c. From the discussion on packing behaviour it was shown that for internally unstable soils with $F_t < F < F_c$ the coarser fabric is becoming looser as F increases. Therefore, the loss of finer particles will leave behind a fabric predominantly made up of coarser particles that are further from their densest packing as F increases. Using the definitions proposed by Fannin and Slangen (2014) this behaviour would be suffosion. However, it is suggested that both the loss of finer particles and the impact of the loss may be dependent on stress state.

During the loading of an embankment dam by filling, the distribution of shear distortions will not be uniform throughout. Whilst the distribution of shear distortions will vary from structure to structure due to stress redistribution between zones of different stiffness and foundation irregularities (ICOLD, 1986), in general larger shear distortions are likely to take place towards the base and flanks of embankments (Griffiths and Lane, 1999).

Recall that for dense soils with $F_t < F < F_c$ a peak of shear strength develops throughout the range of F despite the coarser particles being in an increasingly loose arrangement, even up to $F \geq F_c$ when the coarser particles are held apart (Vasil'eva et al., 1971, Vallejo, 2001). Consequently, in zones in which shear distortion is such that a peak of shear strength is mobilised, in the range $F_t < F < F_c$ finer particles must be increasingly incorporated into the load bearing fabric as F increases. It is presently postulated that for a finer particle to be bearing load, it must be touching other particles and so less susceptible to being carried away by water drag forces.

However, in zones in which shear distortions are such that the peak shear strength has been passed and the critical state reached, dilation will have resulted in locally enlarged voids and coarser particles orientating themselves to the major (compressive) principal stress direction (Chang and Zhang, 2012), reducing the load on finer particles. At the other extreme, zones in which very little shear distortion has taken place (i.e. stresses are predominantly isotropic) distortion of the coarser voids has not taken place and so fewer finer particles are likely to be part of the load bearing fabric (Shire et al., 2014). In both these cases, finer particles would be more susceptible to being carried away by water drag forces.

Experimental work by both Chang and Zhang (2012) and Zou et al. (2013) has shown that the hydraulic gradient required to induce internal erosion increases initially as shearing takes place, but then reduces as shearing continues. (Chang and Zhang (2012) carried out their work in a triaxial cell, whereas Zou et al. (2013) carried out their experiments under plane-strain.) This experimental work adds some support to the suggestion that initially shear distortion loads finer particles (which then require larger hydraulic gradients to be removed), but as further shear distortion causes dilation of the coarser particles fabric, fewer finer particles are part of the load carrying fabric (which then require lower hydraulic gradients to be removed). However, it is unlikely that such a bimodal load carrying fabric results when the isotropic component of overall stress is high enough to suppress dilation as shear behaviour is independent of initial fabric in such cases (Poulos, 1971). It has been noted that suffosion often takes place in small structures or within the upper 10 m of

dams, suggesting an upper limit of 200 kPa normal stress to suffosion (Bridle, personal communication).

The loss of finer particles ($F_t < F < F_c$) from zones in which different shear distortions have taken place is likely to impact available shear strength in different ways. Zones in which negligible shear distortion has taken place are likely left with metastable fabrics following particle loss. Finer particles, which would be required to develop peak strengths, would no longer be available. In these zones, a progressively larger zone of loose coarser particles may develop, until either the in-situ stresses can no longer be resisted, or an external trigger causes failure. As the material will contract, as no finer particles are available to cushion the loose coarser particles, failure will be associated with large deformations (Poulos, 1971), resulting in sinkholes or settlement. The fact that incidents associated with suffosion often occur over long time periods or are externally triggered (Rönnqvist, 2009), supports the hypothesis that collapse does not occur immediately as particles are lost but that loose zones develop slowly as more and more particles are eroded. In zones in which shear distortion is such that finer particles are part of the load bearing fabric, their loss would result in immediate localised failure, although being loaded they are less likely to be lost.

3.3.3 Instability regions

For the internally unstable gradation formed by S and G, investigated in this study, three instability regions are proposed (Figure 3.11) based on the effect of particle loss on mechanical behaviour. Namely, a suffusion region for $F < F_t$, a suffosion region for $F_t < F < F_c$ and an internally stable region for $F > F_c$ where $F_t = 15$ % and $F_c = 27$ %.

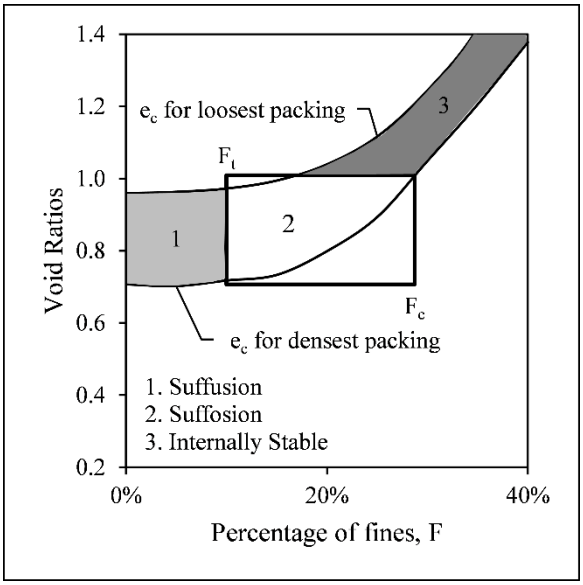


Figure 3.11. Instability regions

Based on the review of data presented in Figure 3.10, more generalised instability regions are proposed in Figure 3.12. In this figure line A-A represents the upper boundary of where the voids of coarser particles are only partially filled with finer particles. For F above A-A, e_c is greater than the loosest stable packing of the coarser particles. Line B-B represents the upper boundary of F, where the coarser particles remain at their densest fabric. Between F = 0 % and B-B it can be expected that finer particle loss would result in a minor change to the strength of the soil (i.e. suffusion). However, as F increases between B-B and A-A finer particle loss will leave behind an increasingly loose coarser fabric. The available shear strength would therefore reflect this change from a dense overall fabric to a loose coarser fabric as finer particles are lost (causing volume reduction during shear distortion i.e. suffosion).

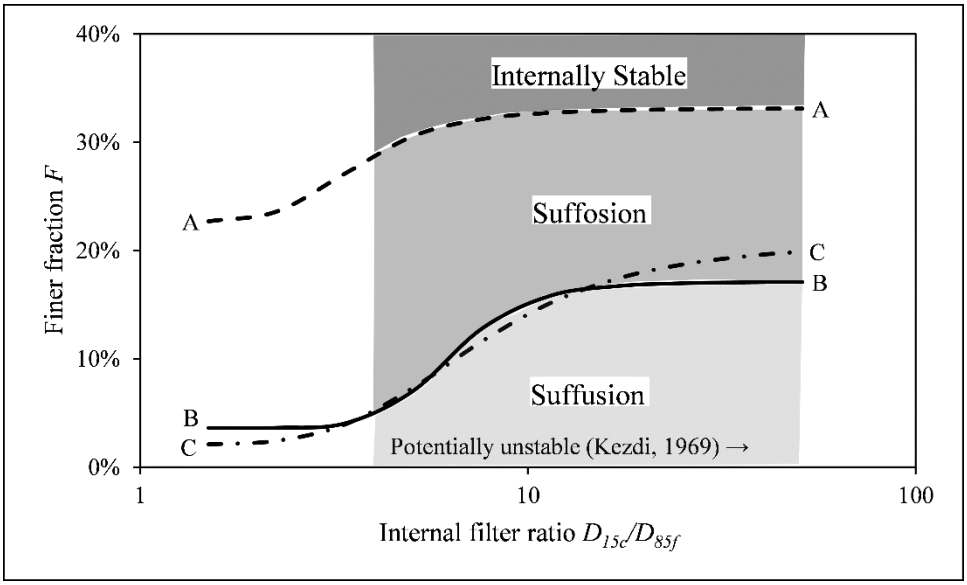


Figure 3.12: Generalised instability regions (Meanings of A-A, B-B and C-C are given in the main text)

Considering global fabrics at their loosest packing, line C-C represents the maximum finer fraction at which the coarser fabric is still in a stable arrangement. For practical purposes line C-C is coincident with line B-B. Between F = 0 % and C-C the loss of finer particles will result in some contraction of the coarser fabric but it will still be loose. This would also be suffusion as no significant change in strength is likely, as the loose global fabric becomes a loose coarser particle fabric. In effect, as the global fabric moves from its densest packing to its loosest packing, line A-A moves down to position C-C, reducing the suffosion region. However, a metastable fabric is likely to develop which may be stable under predominantly isotropic loading but would collapse if loading changes suddenly.

3.4 Empirical evidence for a transition and critical finer fractions

Rönnqvist and Viklander (2014) compiled a database of glacial till soils used for the core of embankment dams. Of particular interest in their study was whether any physical distress of the structures was observed due to internal erosion. Based on the available gradation envelopes for each dam, the internal stability of the soils was assessed by the Kenney and Lau (1985, 1986) criteria and found to be unstable in all cases where distress was noted. The maximum and minimum finer fractions were also determined for the gradation envelopes based on the point of inflection of the PSDs (ICOLD, 2014). This range of finer fractions for dams with physical distress are plotted in Figure 3.13. The proposed F_t (= 15 %) and F_c (= 35 %) boundaries are also shown. The type of physical distress is indicated. The term "Erosion channels" is used to define various forms of physical distress including loose zones, zones deficient of finer particles, piping and cavities that did not form sinkholes.

It is clear that either the entire range of finer fractions, or the majority thereof for most of the soils, falls within the proposed F_t and F_c boundaries (Figure 3.13). This supports the suggestion that there exist upper and lower boundaries outside which internal erosion does not result in physical distress. Such physical distress would be a consequence of a change in mechanical behaviour, induced by the erosion of finer particles. Of the three cases that lie entirely above the F_c boundary, incident reports suggest other internal erosion mechanisms may have been at play. For Dam 1 a pipe developed alongside the concrete nib of the spillway, for Dam 2 concentrated leakage along cracks was suspected and for Dam 3 an under-compacted coarse material in a ditch within the foundation layer was suspected of concentrating flow. Therefore, suffusion/suffosion of the core material may not have been the main cause of distress in these three cases.

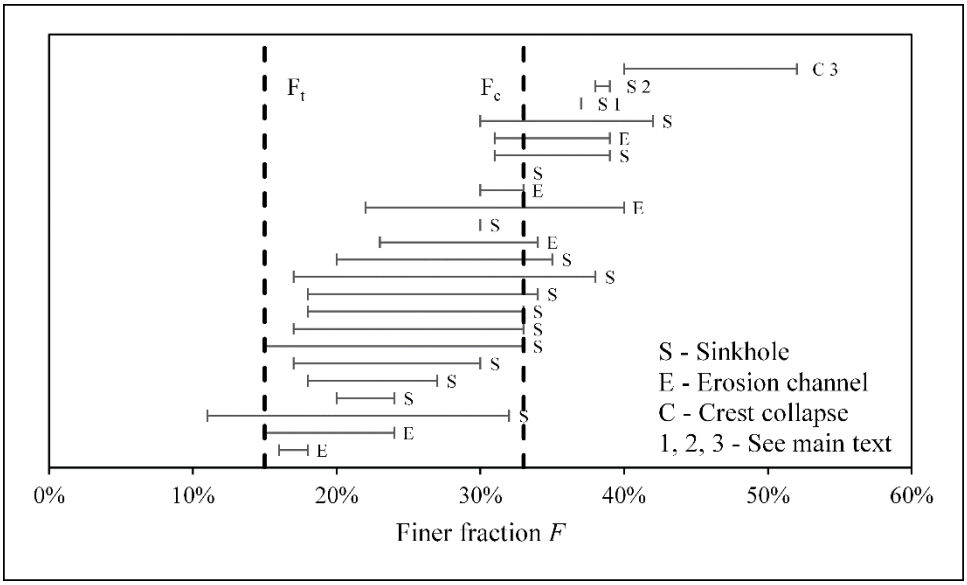


Figure 3.13: Finer fractions for various embankments, data from Rönnqvist and Viklander (2014)

Rönnqvist (2015) carried out large diameter permeameter tests on natural, non-plastic till soils from borrow areas or cores of existing earth dams. Twelve widely or gap-graded soils were subjected to seepage over durations ranging from 5 hours to 77 days. Internal stability of the material was assessed based on whether particle erosion was evident from gradations before and after seepage. Following flow through the soils in the permeameter, relative mass loss and relative displacement of the top surface were determined. Data from soils found to be internally stable, based on no changes in gradation during seepage, are plotted in Figure 3.14a. Data from soils found to be internally unstable, based on changes in gradation during seepage, are plotted in Figure 3.14b. The finer fraction (F) was determined by dividing the soil at either the point of inflection, for widely graded soils, or the location of the gap, for gap-graded soils.

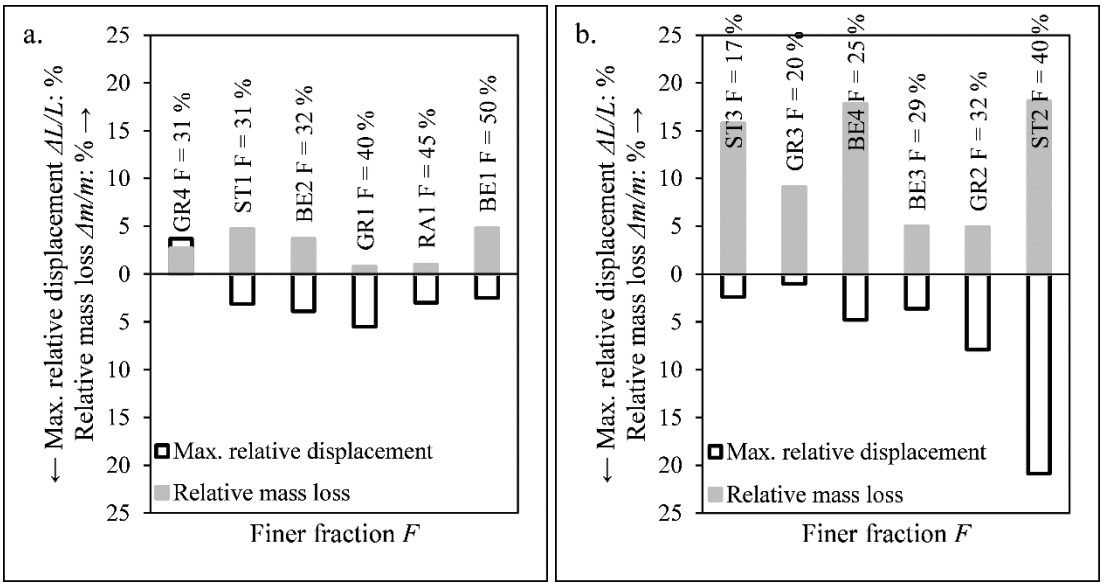


Figure 3.14: Mass and volume changes due to seepage; a. internally stable soils and b. internally unstable soils, data from Rönnqvist (2015)

In general, Figure 3.14 shows that greater mass loss was recorded from internally unstable soils. However, as soils ST1, BE2 and BE1 (stable) recorded similar mass losses to BE3 and GR2 (unstable) mass losses could have also occurred due to experimental error or from filter materials placed on the downstream side of specimens. Volume changes did not appear directly related to mass losses, as for instance GR1 showed the least mass loss but the largest volume change for stable soils. GR4 appeared to increase in volume. These discrepancies highlight the difficulty of using permeameter tests to establish mechanical behaviour. The relative displacement of the top surface of the specimen may also not be a good indication of volume changes. Granting this, it is evident that for unstable soils, with low finer fractions (ST3, GR3 and BE4), although large mass losses occurred, smaller volume changes occurred than soils with high F. This is further evidence that adverse volume changes only occur for F > Ft (≈ 15 %) and become worse as F increases.

3.5 Summary

Soils susceptible to suffusion contain finer particles that sit relatively unloaded within the voids of the coarser fraction and as a result can be easily eroded. The following theoretical framework, which is the subject of subsequent experimental investigation, is proposed to understand the impact of finer particle loss on mechanical behaviour.

For low finer fractions ($F < F_t$, F_t approximately 10 – 15 %), coarser particles remain at essentially the same void ratio during finer particle loss, and dominate strength and compressibility of the material. Consequently, finer particles can be lost with little impact on mechanical behaviour, but hydraulic conductivity will increase. This behaviour is defined as suffusion.

For intermediate finer fractions ($F_t < F < F_c$, F_c approximately 25 – 35 %), finer particles hinder coarser particles from moving into their densest arrangement. Although the coarser particles are in a looser arrangement, they would remain in a relatively stable arrangement if all finer particles were suddenly removed as e_c remains below $e_{c\,max}$. Coarser particles, despite being in an increasingly looser arrangement, dominate load transfer leaving finer particles free to be eroded. Erosion of finer particles will leave behind a loose metastable fabric of coarser particles. Zones undergoing erosion are likely to grow until the in-situ stresses can no longer be resisted or an external trigger occurs, resulting in a sinkhole. This behaviour is defined as suffosion, not suffusion, as finer particle loss impacts mechanical behaviour.

Prior to particle erosion, soils throughout the range $F_t < F < F_c$ behave as dense soils (i.e. shearing to a peak strength), despite the coarser particles being in an increasingly loose arrangement as F increases. This implies that when the global fabric is distorted the finer particles form part of the load carrying fabric. These finer particles carrying load would become less susceptible to loss and if lost would result in immediate localised collapse of the coarser fabric, possibly restricting further finer particle loss. Conversely, shear distortions can cause dilation of the coarser particles fabric, removing load from finer particles within voids. This would result in finer particles

being more susceptible to erosion. However, their loss may have a negligible impact on future mechanical strength as coarser particles are dominating load transfer. Where the isotropic component of overall stress is so high that dilation is suppressed, finer and coarser particles are likely both heavily isotropically loaded, preventing any particle loss.

For high finer fractions ($F > F_c$) finer particles completely fill the voids between coarser particles, dispersing them as F further increases. Loads will be carried, therefore, equally by both finer and coarser particles resulting in internal stability.

The remainder of this thesis will outline experimental work exploring the changes in mechanical behaviour due to finer particle loss for $F < F_t$, $F_t < F < F_c$ and $F > F_c$. Prior research based on permeameter tests has had limited success. This is due to unrealistic hydraulic conditions required to erode particles in reasonable periods using permeameters (Sterpi, 2003, Shwiyhat and Xiao, 2010, Chang and Zhang, 2012, Ke and Takahashi, 2012). Continuum and DEM modelling (Muir Wood et al., 2010, Scholtès et al., 2010, Hicher, 2013) have had some success, showing that finer particle loss results in an increase in global void ratio, causing initially dilative soils to become contractive. Although in agreement with the framework outlined here, these models are limited. Firstly, continuum models do not take into account the actual size of particles lost and secondly, in the opinion of the current author, the DEM models are based on PSDs that are too narrow. The effect of these narrow PSDs is that following the loss of small quantities of finer particles (5 %) significant strength deterioration is predicted.

Chapter 4 An analogue to internal erosion

4.1 The need for an analogue material

The preceding chapters have shown a considerable body of knowledge on criteria to assess a material's susceptibility to internal erosion. The effect of this erosion on mechanical behaviour is, however, still a developing field. The most promising research has used discrete element modelling and continuum modelling (Muir Wood et al., 2010, Scholtès et al., 2010, Hicher, 2013). Experimental approaches to date (Sterpi, 2003, Shwiyhat and Xiao, 2010, Chang and Zhang, 2012, Ke and Takahashi, 2012) have relied on reconstituted specimens, modified triaxial tests in which suffusion is initiated under high seepage velocities, and cone penetration tests on an internally unstable material in a permeameter subject to upward flow. As shown in earlier chapters, these studies are limited (e.g. narrow PSDs and high seepage velocities) and are thus somewhat inconclusive providing only a general, superficial understanding of the behaviour. It is clear that a better method is needed to investigate the consequences of finer particle loss on mechanical behaviour.

Using seepage alone to erode finer particles from a soil is fraught with difficulties. Firstly, the loss of finer particles can take place over an extended period as is often the case with embankment dams (Fell et al., 2003). Secondly, scaling erosional processes is difficult (Bezuijen and Steedman, 2010) as the scaled specimen needs to be capable of reproducing single grain erosion processes (Marot et al., 2012). As such, modelling the process within realistic time scales and under representative hydromechanical conditions is difficult in a laboratory setting.

One alternative considered by the current author was to place a material with an internally unstable PSD in a hydraulic flume (900 mm wide, 800 mm high and 7200 mm long) and subject it to long-term flow. Deformations at the boundary could possibly be tracked using particle image velocimetry (White et al., 2003) and deformations within the soil mass tracked using fibre optic cables (Vorster et al., 2006). The practicalities involved and questions about whether any quantifiable data

on the mechanical behaviour would be obtained, precluded further development of this idea.

X-ray computed tomography (CT scanning) is another non-destructive method of observing the interior of physical systems and is increasingly finding application in geotechnical research. The development of ice lenses has been investigated by Torrance et al. (2008), development of shear zones in triaxial testing by Hall et al. (2010) and soil arching by Eskişar et al. (2012). The possibility of using CT scanning was considered to track developing strains in a soil system undergoing internal erosion, from which changes in mechanical behaviour could be inferred. The difficulties involved in conveying water through a specimen in an environment with sensitive electronic equipment were considered prohibitive. It was proposed that suitably crushed and sized solid carbon dioxide (dry ice) and chilled soil particles could respectively form the finer and coarser particles of an unstable material. This material formed around a thin heating element, which is then slowly heated within a CT scanning unit, could shed light on the mechanical processes taking place. Practicalities around handling dry ice at temperatures of -78 °C, and uncertainty whether any quantifiable data would be produced precluded further development of this idea.

The concept of replacing the erodible finer particles with an analogue material that could be eroded in shorter periods and under realistic hydraulic conditions was pursued further. Recently, sodium chloride salt was used as an analogue material to explore the change in earth pressure coefficients during soil diagenesis (Shin and Santamarina, 2009), settlement behaviour during particle loss by degradation or erosion (McDougall et al., 2013) and changes in shear behaviour during internal erosion (Chen et al., 2016). Using sodium chloride salt allows controlled quantities of finer particles to be lost by dissolving them by flooding under atmospheric pressure, precluding the need for high seepage velocities and resulting high pore pressures. Sodium chloride was therefore used as an analogue material to investigate the effect of internal erosion on the mechanical behaviour of soils in this study.

4.2 Experimental validation

In order to investigate the practicalities and limitations of using salt as an analogue material for the erodible finer particles, a simple experimental procedure was devised. Changes in the coarser fabric as finer particles were lost were determined by dissolving salt particles in an oedometer large enough to accommodate coarse particles. A punch test, similar to the California Bearing Ratio test, was used as an index to assess the strength of the resulting fabric. The developed device was referred to as the suffusion oedometer and punch (SOAP) device.

The main experimental aim was to investigate how the transition finer fraction (F_t) and critical finer fraction (F_c) vary for different soils. The two main variables were particle shape of the coarser particles and internal filter ratio (D_{15c}/D_{85f}). The results were used to develop a generalised understanding of the effect on mechanical behaviour of finer particle loss. From this, a preliminary criterion is suggested to assess the potential mechanical consequences of internal erosion for a given soil.

4.2.1 Material properties

Two materials were used as the coarser particles: angular crushed rock aggregate commonly used for concrete in Johannesburg and rounded riverbed pebbles. The crushed rock has Sphericity values between 0.7 and 0.9, and Roundness values between 0.1 and 0.3 based on the chart suggested by Cho et al. (2006). The pebbles have Sphericity values between 0.7 and 0.9, and Roundness values between 0.7 and 0.9 based on the chart suggested by Cho et al. (2006). Digital photograph images of these two materials are shown in Figure 4.1. Four different salt sizes were separated from fine and coarse table salt (sodium chloride). Light microscope and digital photograph images of these salt sizes are shown in Figure 4.2. Particle size distributions (PSD) of these various materials are given in Figure 4.3. Two crushed silica sands with PSDs similar to two of the salt sizes were also used (Figure 4.4).

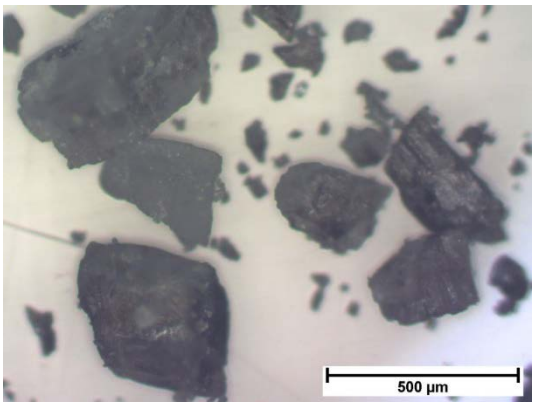


Angular aggregate

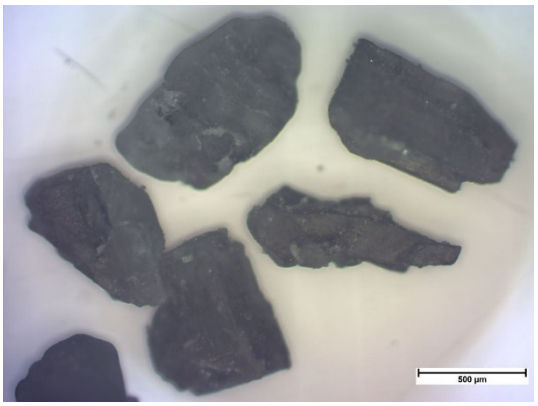


Rounded pebbles

Figure 4.1: Digital photograph images of coarser particles



Very fine salt



Fine salt



Coarse salt



Very coarse salt

Figure 4.2: Light microscope and digital photograph images of salt particles

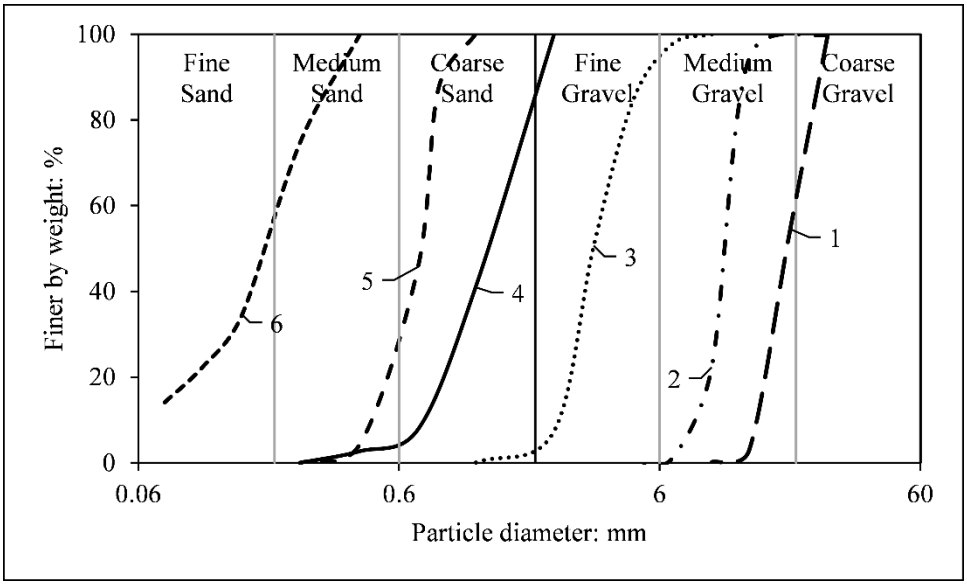


Figure 4.3: Particle size distributions: 1. Rounded pebbles; 2. Angular aggregate; 3. Very coarse salt; 4. Coarse salt; 5. Fine salt and 6. Very fine salt

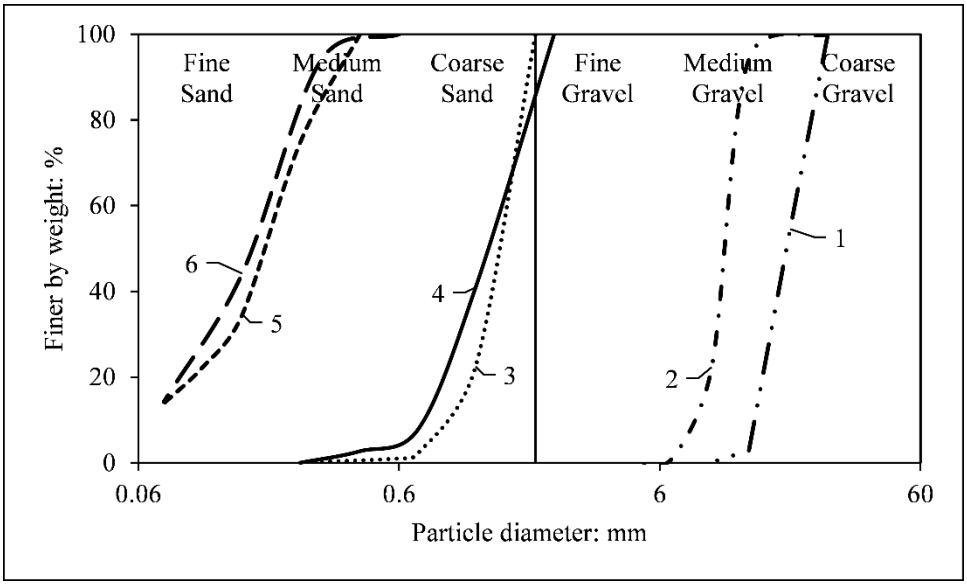


Figure 4.4: Particle size distributions: 1. Rounded pebbles; 2. Angular aggregate; 3. Coarse silica sand; 4. Coarse salt; 5. Very fine salt; 6. Very fine silica sand

Due to the coarse nature of the material, the effectiveness of various methodologies to define the limiting dense and loose fabrics of the test materials were assessed (i.e. maximum and minimum dry densities respectively). These included: (i) SANS 5845:2008 used in concrete material studies to determine bulk densities of concrete aggregates; (ii) standard Proctor compaction (ASTM D698); and (iii) a vibrating table method. SANS 5845:2008 outlines a methodology to determine an uncompacted density whereby aggregate is carefully placed into a 9022 cm^3 mould with a scoop, whilst the compacted density is determined by rodding 3 successive layers with 20

strokes with a 16 mm diameter rod. Standard Proctor compaction (ASTM D698) was carried out in a 6-inch mould (2753 cm^3); as the material was free draining the test was carried out dry. This compactive effort was used as it represents the compactive effort most used in embankment dam construction. No evidence of angular aggregate breakage was observed during the test (Figure 4.5). However, extensive rounded pebble crushing was observed (Figure 4.6) excluding this methodology from further consideration.

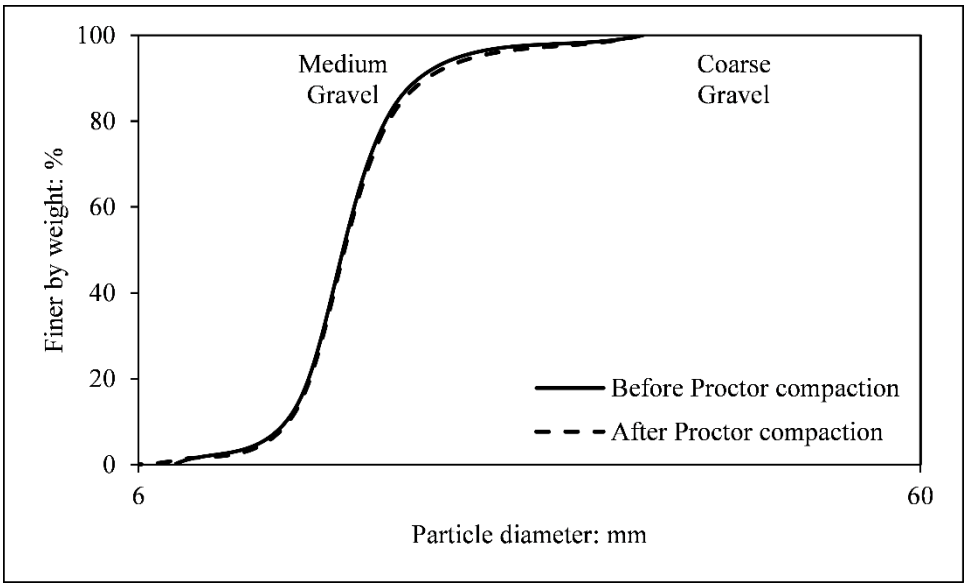


Figure 4.5: Comparison of PSD before and after Proctor compaction of angular coarse aggregate showing negligible crushing



Figure 4.6: Evidence of pebble crushing during Proctor compaction

A PVC mould was fabricated (Nominal inside diameter and height = 144 mm) that could be secured on to a small vibrating table (Figure 4.7). The volume was 2383 cm^3, determined by water filling. Different filling layer thickness and vibration times were investigated to obtain the maximum density possible and to produce densities similar to those achieved with standard Proctor compaction. Details of these combinations and results obtained are given in Table 4.1 for angular aggregate and Table 4.2 for rounded pebbles. Densities obtained by all methodologies are shown in Figure 4.8 for angular aggregate and in Figure 4.9 for rounded pebbles. Filling the mould in four lifts with 10 s of vibration with a 2 kPa surcharge in place resulted in similar densities to those obtained by standard Proctor compaction for angular aggregate. For the rounded pebbles, the methodology was varied to produce a similar relative density as obtained for the angular aggregate. This was because the Proctor density of the rounded pebbles was anomalous due to the particle crushing. Filling the mould in two lifts with 10 s of vibration with the 2 kPa surcharge in place for the rounded pebbles resulted in a similar relative density to the angular aggregate.



Figure 4.7: Vibration setup showing mould with specimen on vibrating table, 2 kPa circular steel surcharge, rod used to flatten surface, scoop and spanner

Table 4.1: Summary of methodologies and obtained densities for angular aggregate

Methodology	Number of tests	Average density (kg/m^3)	Standard deviation (kg/m^3)
SANS 5845:2008 Uncompacted density	4	1470	5
SANS 5845:2008 Compacted density	4	1616	4
ASTM D698 Standard Proctor	2	1698	-
Mould filled in 4 lifts with 5 s of vibration with 2 kPa surcharge in place	3	1687	3
Mould filled in 4 lifts with 10 s of vibration with 2 kPa surcharge in place	5	1696	5
Mould filled in 4 lifts with 15 s of vibration with 2 kPa surcharge in place	5	1707	6
Mould filled in 4 lifts with 30 s of vibration with 2 kPa surcharge in place	3	1721	8
Mould filled in 8 lifts with 30 s of vibration with 2 kPa surcharge in place	3	1728	13
Mould filled in 16 lifts with 30 s of vibration with 2 kPa surcharge in place	3	1746	10

Table 4.2: Summary of methodologies and obtained densities for rounded pebbles

Methodology	Number of tests	Average density (kg/m^3)	Standard deviation (kg/m^3)
ASTM D698 Standard Proctor	1	1746	-
Mould filled gently with a scoop and no vibration.	5	1466	17
Mould filled in 16 lifts with 30 s of vibration with 2 kPa surcharge in place	3	1771	7
Mould filled in 4 lifts with 5 s of vibration with 2 kPa surcharge in place	3	1732	9
Mould filled in 2 lifts with 10 s of vibration with 2 kPa surcharge in place	3	1715	2

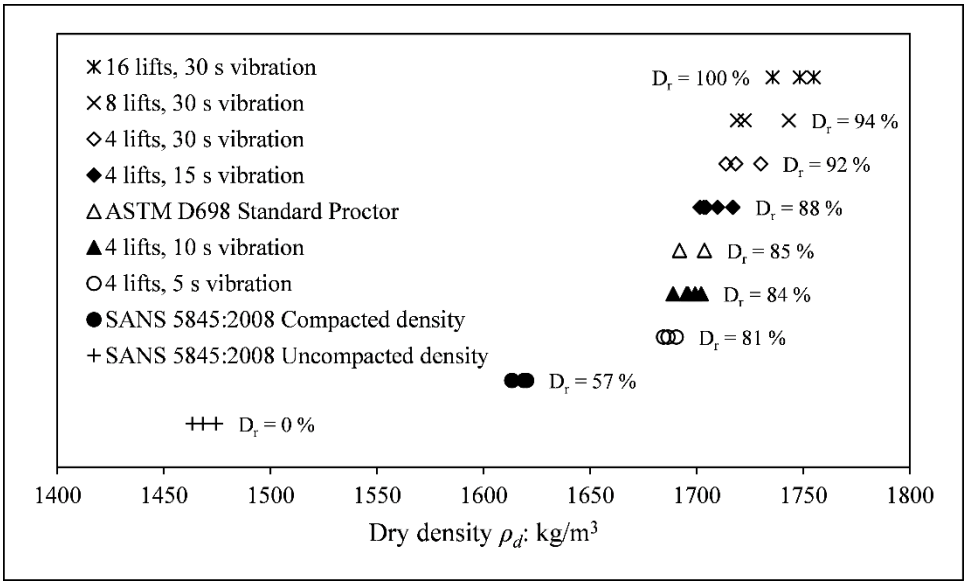


Figure 4.8: Angular aggregate densities obtained by various methodologies

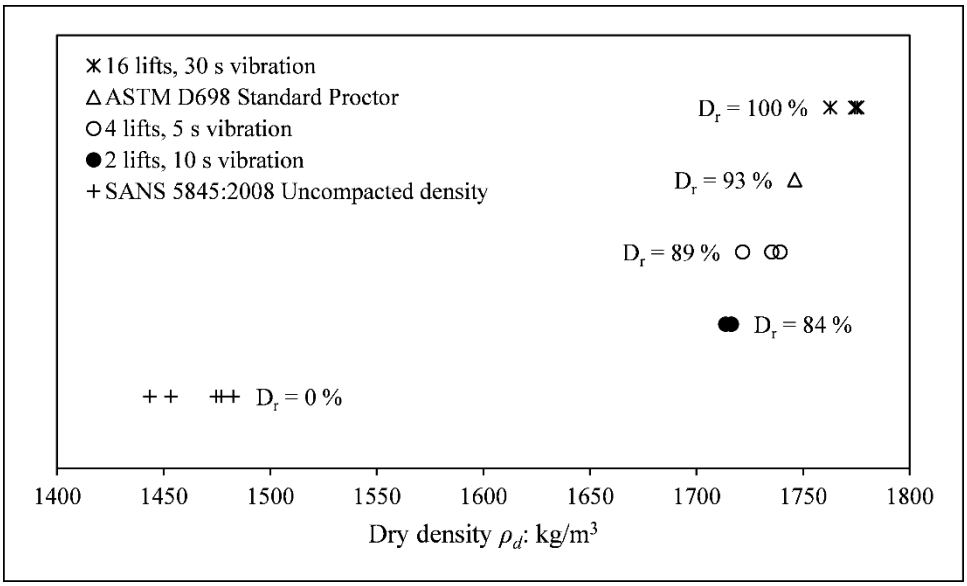


Figure 4.9: Rounded pebbles densities obtained by various methodologies

To investigate the extent of salt crushing, two specimens: one with angular aggregate and very fine salt and another with angular aggregate and very coarse salt were vibrated in the mould for 1 min. As shown in Figure 4.10 negligible salt crushing was observed.

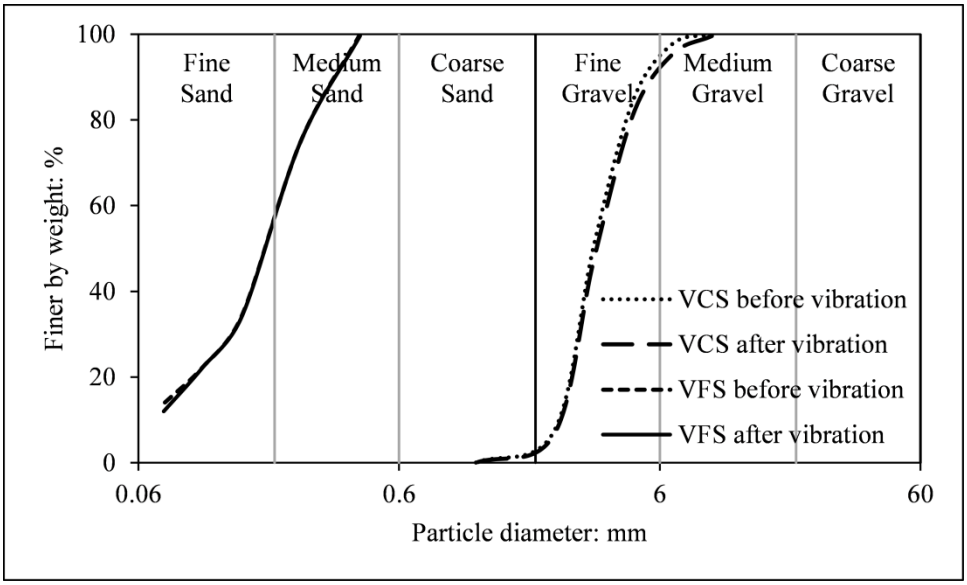


Figure 4.10: Impact of vibration on very coarse salt (VCS) and very fine salt (VFS) particles

Aggregate-sand and pebble-sand mixtures

Packing behaviours of the angular aggregate and rounded pebbles were investigated using the two crushed silica sands (Table 4.3). Based on the vibration procedures for the angular aggregate and rounded pebbles identified above, densities for mixtures with increasing finer fraction were determined. These densities are expressed (Figure 4.11) as relative densities of the coarser particles ($D_{r,ec}$). Whilst there is some difference in the packing behaviour at lower internal filter ratios (D_{15c}/D_{85f}), there is less difference at higher internal filter ratios. This suggests there is a maximum packing efficiency that can be achieved such that making the finer particles smaller (making D_{15c}/D_{85f} bigger) does not result in a significant change in the relative density of the coarser particles (Lade et al., 1998).

Table 4.3: Aggregate-sand and pebble-sand mixtures

Coarser particles	Finer particles	Internal filter ratio, D_{15c}/D_{85f}	Short name[†]
Angular aggregate	Very fine silica sand	32	A:S 32
	Coarse silica sand	4.7	A:S 4.7
Rounded pebbles	Very fine silica sand	54	P:S 54
	Coarse silica sand	8.0	P:S 8.0

[†] Short name identifies mixture components (A – angular aggregate, P – rounded pebbles, S – Sand) and states the internal filter ratio.

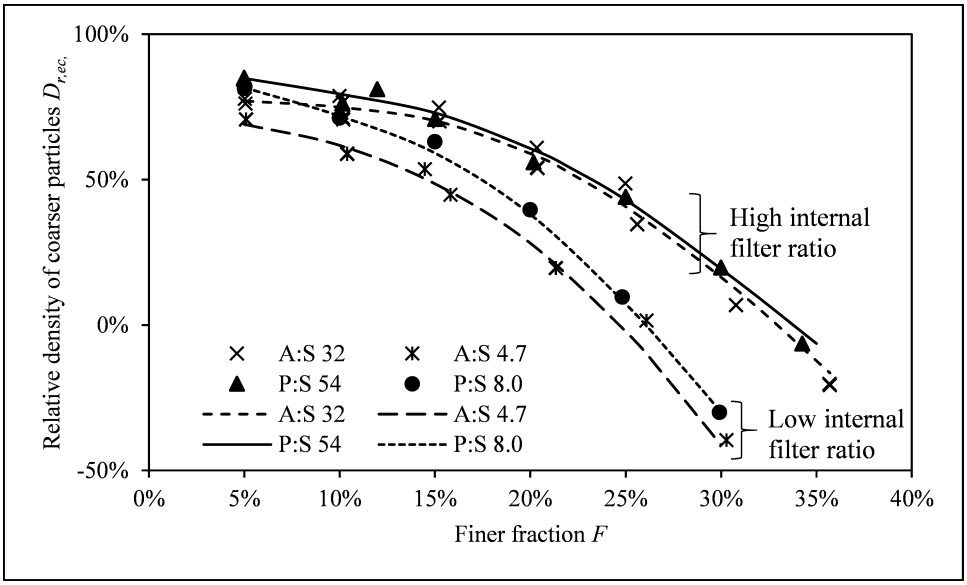
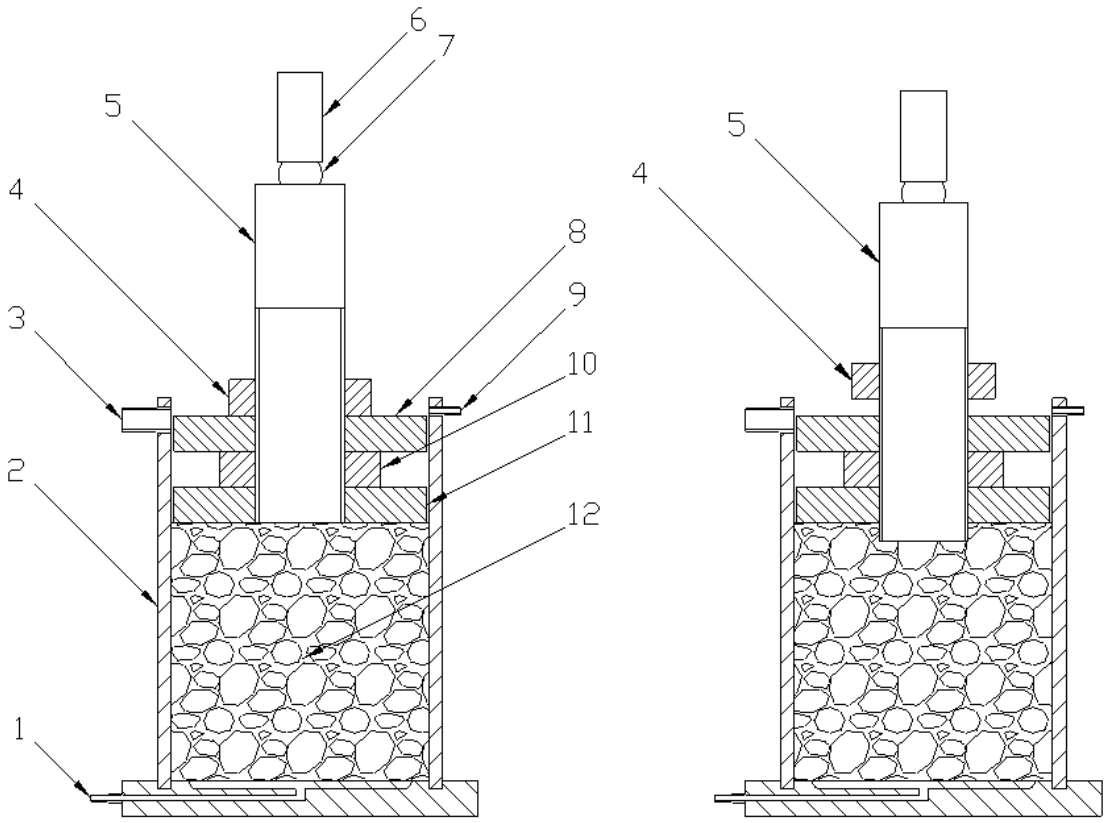


Figure 4.11: Relative densities of aggregate-sand and pebble-sand mixtures (see Table 4.3 for nomenclature)

4.2.2 Description of suffusion oedometer and punch (SOAP) device

Figure 4.12 is a schematic of the suffusion oedometer and punch (SOAP) device developed during this research at the University of the Witwatersrand. The cell was made from extruded PVC pipe with a nominal internal diameter of 143 mm fixed to a PVC base machined to collect and discharge seepage. At the top of the cell, water was supplied on one side and an overflow-drain placed on the other side to maintain a constant head of water through the specimen. A perforated galvanised steel sheet was placed below the specimen. The loading setup, made from aluminium, consisted of a 142 mm diameter circular bottom disk and two elongated circle spacer disks. As the cell was not perfectly circular, the diameter of the disks was made slightly smaller than that of the cell. A 50 mm diameter clean cut hole through the centres of the three disks held the aluminium punch rod. A screw thread on the punching rod allowed the position of the holding nut to be changed, thereby moving load from the disks to the punch rod. Between the specimen and the loading setup, a 1 mm thick HDPE breaker layer consisting of two disks was placed. One disk was the diameter of the cell with a 50 mm hole into which the second disk fitted. For the initial stage, during which salt dissolution took place under constant load over the entire surface, the nut was secured so that the bottom disk and punching rod were flush. Water could easily flow through the annulus between the loading disk and cell wall, and between the disks and punch rod. In the second, punch test stage, the nut was unscrewed transferring all load to the punching rod.



Entire surface loaded Punch rod loaded

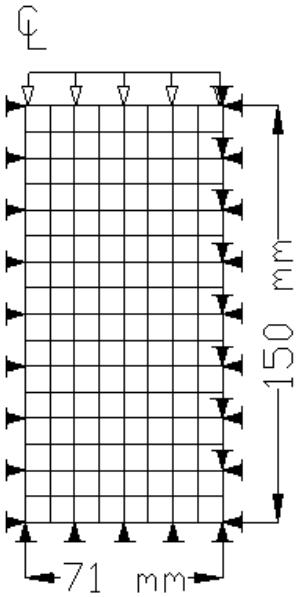
Figure 4.12: Developed SOAP device: 1. Bottom-drain; 2. PVC Cell; 3. Overflow-drain; 4. Holding nut; 5. Punch rod; 6. Loading yoke; 7. Ball bearing; 8. Top spacer; 9. Seepage inlet; 10. Bottom spacer; 11. Loading disk; 12. Specimen (143 mm diameter by 143 mm height)

Side friction

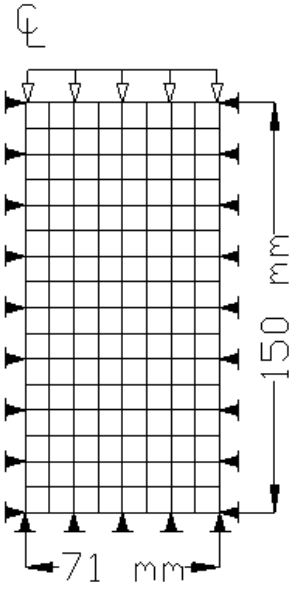
To limit the effect of side friction standard oedometer test methods (BS 1377: Part 5) limit the specimen height to less than 0.4 times the internal diameter of the oedometer ring. However, for the punch test a greater height was necessary. Although the California Bearing Ratio test has a height to diameter ratio of 0.8 (BS 1377: Part 4, ASTM D1883), a height to diameter ratio of 1.0 was used for the SOAP device. Consequently, the effect of side friction was investigated numerically and experimentally. A numerical sensitivity study was carried out using SIGMA/W (GEO-SLOPE, 2007) in which various elastic-plastic parameters were assumed for the specimen (Table 4.4). A schematic of the axisymmetric numerical model is given in Figure 4.13. To keep the variables to a minimum, the two extreme boundary conditions between which actual behaviour would fall were modelled. These boundaries were: (i) right hand boundary fixed in both the X and Y direction; and (ii) the right hand boundary fixed in the X direction only.

Table 4.4: Assumed elastic-plastic parameters of the loaded specimen

Scenario	Young's Modulus (MPa)	Unit weight (kN/m^3)	Friction angle (°)	Poisson's ratio
1	50	17	25	0.2
2	30	17	25	0.2
3	50	14	25	0.2
4	50	17	35	0.2
5	50	17	25	0.3
6	50	17	35	0.3
7	50	17	35	0.4
8	50	17	25	0.4



Righ-hand boundary fixed in X and Y direction



Righ-hand boundary fixed in X direction

Figure 4.13: Schematic of modelled SOAP device

Fixing the right hand boundary in both the X and Y direction implies zero slippage (high frictional resistance) between the specimen and the cell walls. As expected, this resulted in a non-uniform stress distribution within the cell (Figure 4.14a). Varying the Young's modulus, unit weight and friction angle had a negligible effect on the stress distribution for Poisson's ratios (ν) between 0.2 and 0.3. However, for ν = 0.4 the side friction increased reducing the stress transferred to the base. For this case (ν = 0.4) the higher friction angle (ϕ = 35 °) resulted in the least stress transferred to the base. Fixing the right boundary in only the X direction implies frictionless slippage between the specimen and the cell walls. As expected, this resulted in a uniform stress distribution within the cell for all elastic parameters analysed (Figure 4.14b)

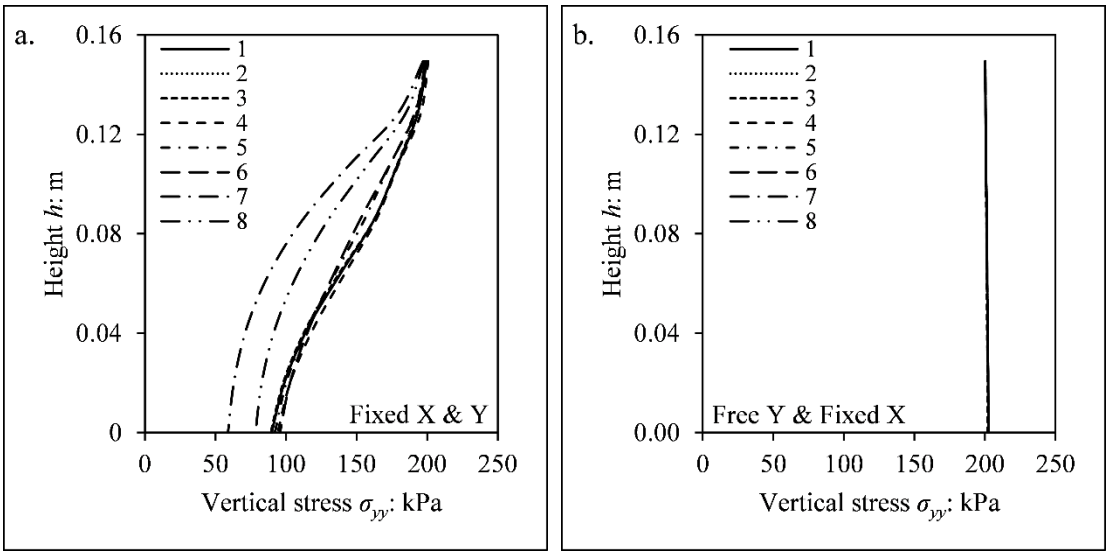


Figure 4.14: Variation in average vertical stress with height for: a. right-hand boundary fixed in X and Y direction; and b. right-hand boundary fixed in only X direction (see Table 4.4 for parameters assumed for each numbered scenario)

In order to compare the numerical results to experimental results, a modified device in which the force transferred to the base could be measured was fabricated (Figure 4.15). For comparisons purposes, the measured force was converted to an average stress on the base of the specimen. Two specimens of angular aggregate were loaded in the device and the force at the bottom measured. One specimen was prepared at a relative density of 90 % and the other at a relative density of 0 %.

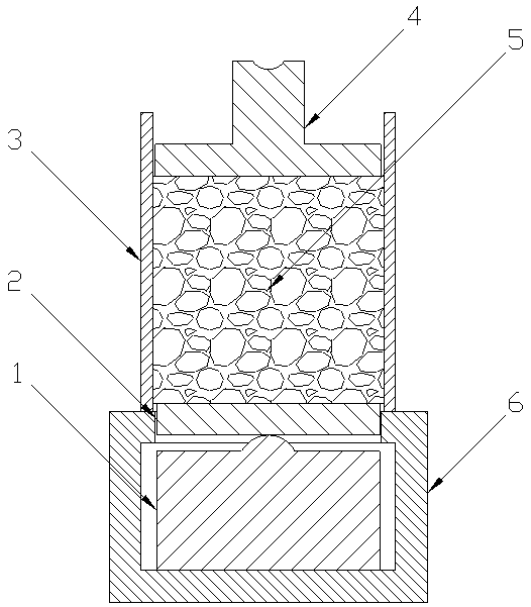


Figure 4.15: Calibration SOAP device: 1. Load cell; 2. Bottom load platen; 3. PVC cell; 4. Top load platen; 5. Specimen (143 mm diameter by 143 mm height); 6. Reaction frame.

Experimental results were bounded by the two boundary conditions numerically modelled (Figure 4.16). For the dense specimen, the average stress measured at the bottom of the specimen (measured force divided by area) was not significantly lower than the average stress applied to the top for average top stresses less than 100 kPa but at 200 kPa, the average stress at the bottom was 80 % of that at the top. For the loose specimen the average stress measured at the bottom was consistently less than that applied at the top approaching the values determined from the numerical model with the right-hand boundary fixed in both the X and Y direction.

This behaviour (Figure 4.16) agrees with the numerical model. The loose specimen having a lower friction angle will have a larger coefficient of earth pressure at rest (since $K_0 = 1 - \sin\phi$, Jaky (c1944) see Powrie (2014)) and consequently a larger ν (since $K_0 = \nu/(1- \nu)$). Conversely, a dense specimen with a higher ϕ will have a lower K_0 and a lower ν. Greater side friction would therefore be generated for a loose specimen (e.g. scenario 9 in Figure 4.14) than for a dense specimen (e.g. scenario 6 in Figure 4.14). As no attempts were made to reduce the side friction, this non-uniformity of stress is highlighted as a limitation of the device.

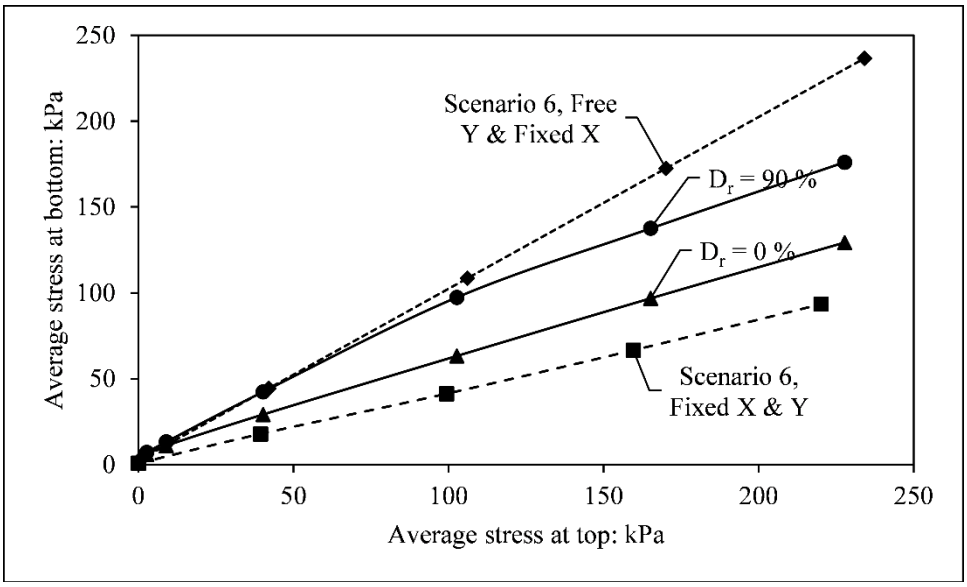


Figure 4.16: Comparison of numerical and experimental results

4.2.3 Test procedure

The following procedure was followed for all tests:

1. Specimens with different finer fractions were prepared, with the amount of salt added on a mass basis. Specimens were sequentially placed into the cell ensuring an even distribution of coarser and finer particles. After each lift, the 2 kPa surcharge was placed and the cell vibrated. Details of the number of lifts and vibration period are given in Table 4.5. Once all the lifts were placed, the surface was levelled by tamping. The HDPE breaker layer, loading disk, spacer disks and punch rod were placed into the cell. A load equivalent to an average vertical stress of 200 kPa was imposed in steps (16, 44, 75, 140 and finally 200 kPa) over the entire surface using a lever arm load frame, and settlement monitored with a dial gauge. A stress of 200 kPa was used as this represents the highest stress at which suffusion is realistically expected to occur (Moffat and Fannin, 2011) and would result in the largest settlement during salt dissolution. Table 4.6 details prepared specimens.
2. The specimen was then flooded and flow initiated. Salt dissolution was monitored by measuring the electrical conductivity (C) of the seepage with Jenway 430 Portable pH/Conductivity meter. Flow was continued over night or until the electrical conductivity (C) of the seepage was down to 250 µS (this was the conductivity of the municipal water used). Settlement was measured throughout this process. For specimens with no salt, the cell was kept flooded for at least 30 min as negligible settlement took place after this. The specimen was then unloaded and rebound measured.
3. With only the yoke load (approximately 12 N) acting, the holding nut was unscrewed transferring all load to the punch rod (The average dial gauge movement during this process was 0.17 mm). The punch rod was then loaded incrementally (Cumulative punch stress: 22, 73, 200, 455, 966, 1476, 1986, 2496, 3006, 3517 kPa). Following each load step, punching settlement was recorded for 15 min, as negligible settlement was observed to occur for longer durations. Loading was continued until the apparatus's load capacity was reached. The specimen was then unloaded and rebound measured. The cell was removed from the loading frame and readied for the next test.

Table 4.5: Details for preparing specimens in their densest state

Coarser particles	Number of lifts	Vibration period per lift
Angular aggregate	4	10 s
Rounded pebbles	2	10 s

Table 4.6: Summary of SOAP specimens

Coarser particles	Finer particles	Internal filter ratio, D_{15c}/D_{85f}	Short name†	Finer fraction F (%) and initial coarser particles relative density, $D_{r,ec,0}$ (%) ‡	
Angular aggregate	Very fine salt	27	A:N 27	F:	5, **10**, 15, **20**, 25, **30** and 35
				$D_{r,ec,0}$:	86, **89**, 76, **66**, 51, **13** and -46
	Fine salt	11	A:N 11	F:	5, **10**, 15, **20**, 25 and **30**
				$D_{r,ec,0}$:	89, **82**, 79, **62**, 29 and **-18**
	Coarse salt	4.3	A:N 4.3	F:	5, **10**, 15, **20**, 25 and **30**
				$D_{r,ec,0}$:	76, **72**, 55, **40**, 8 and **-32**
	Very coarse salt	1.8	A:N 1.8	F:	5, **10**, 15 and **20**
				$D_{r,ec,0}$:	76, **59**, 17 and **-36**
	No salt	-	A	F:	0, **0**, 0 and **0**
				$D_{r,ec,0}$:	89, **89**, 101 and **92**
Rounded pebbles	Very fine salt	46	P:N 46	F:	5, **10,** 15, **2**0, 25 and **30**
				$D_{r,ec,0}$:	80, **83**, 71, **65**, 38 and **-11**
	Fine salt	18	P:N 18	F:	5, **10**, 15, **20**, 25 and **30**
				$D_{r,ec,0}$:	86, **83**, 71, **52**, 17, **-28**
	Coarse salt	7.3	P:N 7.3	F:	5, **10**, 15, **20**, 25 and **30**
				$D_{r,ec,0}$:	86, **77**, 62, **45**, 9, **-15**
	No salt	-	P	F:	0, **0**, 0, **0** and 0
				$D_{r,ec,0}$:	91, **89**, 86, **80** and 83

† Short name identifies mixture components (A – angular aggregate, P – rounded pebbles, N – Salt) and states the internal filter ratio.
‡ Bold typeface for ease of reference only

Initial relative densities of coarser particles obtained with aggregate-salt and aggregate-sand mixtures are compared in Figure 4.17. Similar $D_{r,ec,0}$ were obtained for the two comparable aggregate-salt and aggregate-sand mixtures. This similarity was better for lower F but deviated at higher F. At high F, $D_{r,ec,0}$ decreases rapidly with small changes in F, making it harder to create similar coarser fabrics. Overall, similar coarser fabrics were created with the salt. Similar conclusions can be drawn for the pebble-salt and pebble-sand mixtures (Figure 4.18). Although $D_{r,ec,0}$ decreases with increasing F for all these mixtures, all specimens were prepared so that the overall fabric would be in its densest state.

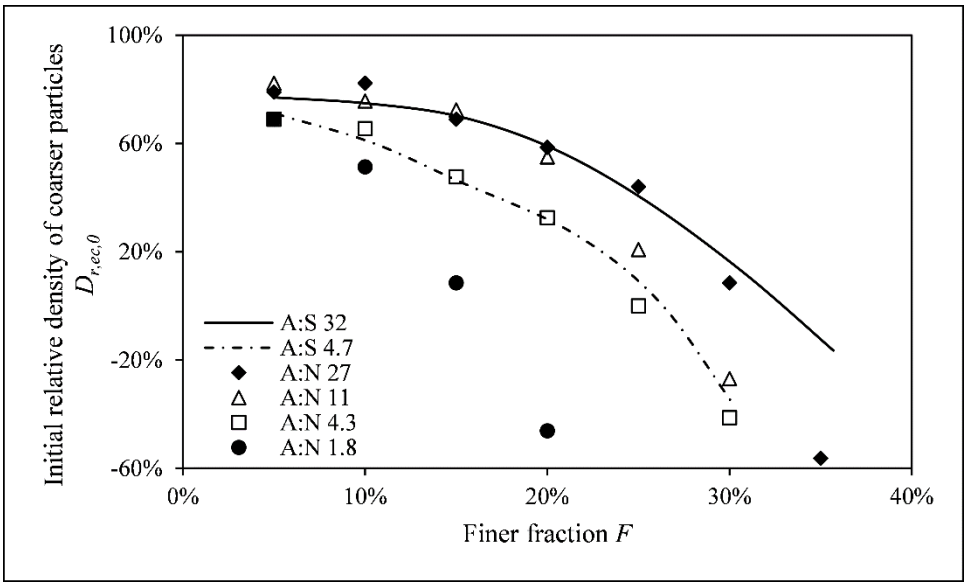


Figure 4.17: Pre-flow relative densities of coarser particles for angular aggregate mixtures (see Table 4.6 for nomenclature)

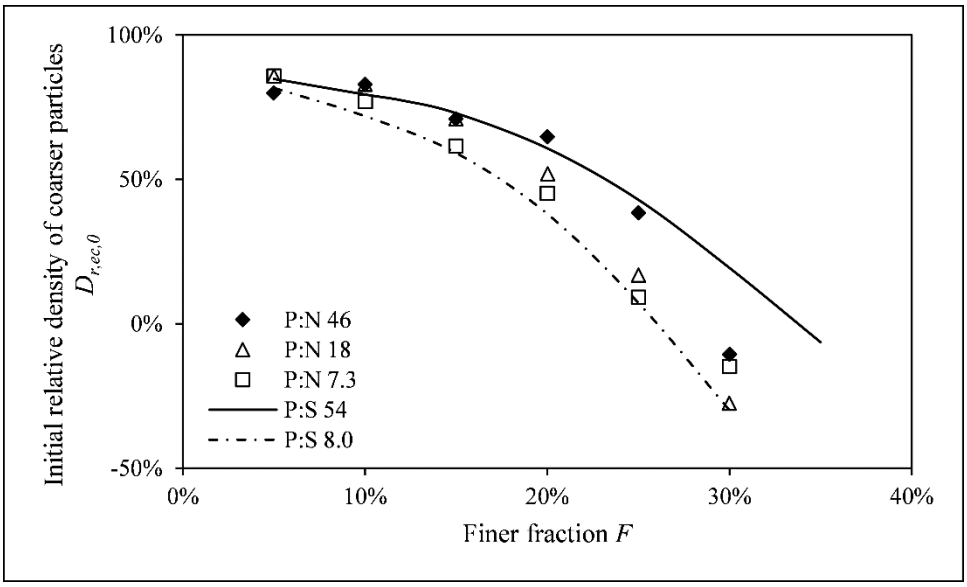


Figure 4.18: Pre-flow relative densities of coarser particles for rounded pebble mixtures (see Table 4.6 for nomenclature)

4.3 Results

4.3.1 Dissolution under one-dimensional loading

Table 4.7 presents dissolved or flooded relative densities of coarser particles ($D_{r,ec,d}$) following either flooding or dissolution. All raw data is provided in companion files (see Appendix B for details).

Table 4.7: Post flooding and dissolution relative densities of coarser particle

Coarser particles	Finer particles	Internal filter ratio, D_{15c}/D_{85f}	Short name	Finer fraction F (%) and dissolved relative densities of coarser particle $D_{r,ec}$ (%) ‡	
Angular aggregate	Very fine salt	27	A:N 27	F:	5, **10**, 15, **20**, 25, **30** and 35
				$D_{r,ec,d}$:	82, **89**, 79, **69**, 59, **33** and 4
	Fine salt	11	A:N 11	F:	5, **10**, 15, **20**, 25 and **30**
				$D_{r,ec,d}$:	89, **86**, 82, **72**, 59 and **36**
	Coarse salt	4.3	A:N 4.3	F:	5, **10**, 15, **20**, 25 and **30**
				$D_{r,ec,d}$:	72, **76,** 69, **59**, 40 and **33**
	Very coarse salt	1.8	A:N 1.8	F:	5, **10**, 15 and **20**
				$D_{r,ec,d}$:	72, **55**, 25 and **-9**
	No salt	-	A	F:	0, **0**, 0 and **0**
				$D_{r,ec,d}$:	82, **82**, 95and **86**
Rounded pebbles	Very fine salt	46	P:N 46	F:	5, **10,** 15, **2**0, 25 and **30**
				$D_{r,ec,d}$:	83, **86**, 77, **71**, 52 and **35**
	Fine salt	18	P:N 18	F:	5, **10**, 15, **20**, 25 and **30**
				$D_{r,ec,d}$:	86, **89**, 80, **71**, 52, **38**
	Coarse salt	7.3	P:N 7.3	F:	5, **10**, 15, **20**, 25 and **30**
				$D_{r,ec,d}$:	91, **83**, 74, **71**, 55, **62**
	No salt	-	P	F:	0, **0**, 0, **0** and 0
				$D_{r,ec,d}$:	91, **91**, 86, **83** and 83
‡ Bold typeface for ease of reference only					

Table 4.8 gives the settlement potential (SP) calculated during dissolution or flooding. Settlement potential was calculated using:

$$SP = \frac{\Delta H}{H_0} \qquad \text{Equation 4.1}$$

where ΔH is the settlement recorded during dissolution or flooding and H_0 is the initial height.

Table 4.8: Summary of settlement potential values

Coarser particles	Finer particles	Internal filter ratio, D_{15c}/D_{85f}	Short name	Finer fraction F (%) and settlement potential SP (%) ‡	
Angular aggregate	Very fine salt	27	A:N 27	F:	5, **10**, 15, **20**, 25, **30** and 35
				SP:	0.3, **1.4**, 1.4, **1.7**, 2.6, **4.1** and 9.1
	Fine salt	11	A:N 11	F:	5, **10**, 15, **20**, 25 and **30**
				SP:	1.1, **1.4**, 2.0, **3.1**, 6.5 and **9.6**
	Coarse salt	4.3	A:N 4.3	F:	5, **10**, 15, **20**, 25 and **30**
				SP:	1.0, **1.9**, 3.2, **4.5**, 6.1 and **10.8**
	Very coarse salt	1.8	A:N 1.8	F:	5, **10**, 15 and **20**
				SP:	0.2, **0.7**, 2.3 and **5.3**
	No salt	-		F:	0, **0**, 0 and **0**
				SP:	0.1, **0.1**, 0.1 and **0.1**
Rounded pebbles	Very fine salt	46	P:N 46	F:	5, **10,** 15, **2**0, 25 and **30**
				$D_{r,ec,d}$:	0.2, **0.7**, 1.2, **1.3**, 2.4 and **7.6**
	Fine salt	18	P:N 18	F:	5, **10**, 15, **20**, 25 and **30**
				$D_{r,ec,d}$:	0.2, **1.1**, 1.9, **3.5**, 6.1, **11.1**
	Coarse salt	7.3	P:N 7.3	F:	5, **10**, 15, **20**, 25 and **30**
				$D_{r,ec,d}$:	0.9, **1.0**, 2.1, **4.7**, 7.9, **12.5**
	No salt	-	P	F:	0, **0**, 0, **0** and 0
				$D_{r,ec,d}$:	0.1, **0.1**, 0.0, **0.0** and 0.0
‡ Bold typeface for ease of reference only					

4.3.2 Punch test

Punch test results from the angular aggregate test series are shown in Figure 4.19. A clear reduction in strength is observed with increasing F and internal filter ratio. A second-degree polynomial was fitted to results from each punch test. Punch test results for the rounded pebbles test series are similarly presented in Figure 4.20. Whilst there is a similar trend to the angular aggregate test series (Figure 4.19), punch tests results showed greater variability for rounded pebbles (Figure 4.20). This is clearly illustrated in Figure 4.20a, where most tests followed a similar trend but one test resulted in significantly more settlement for comparative punch stresses. The reason for this behaviour was that as rounded particles had fewer contacts between particles, much larger point loads were transferred between particles, resulting in greater particle crushing (Figure 4.21).

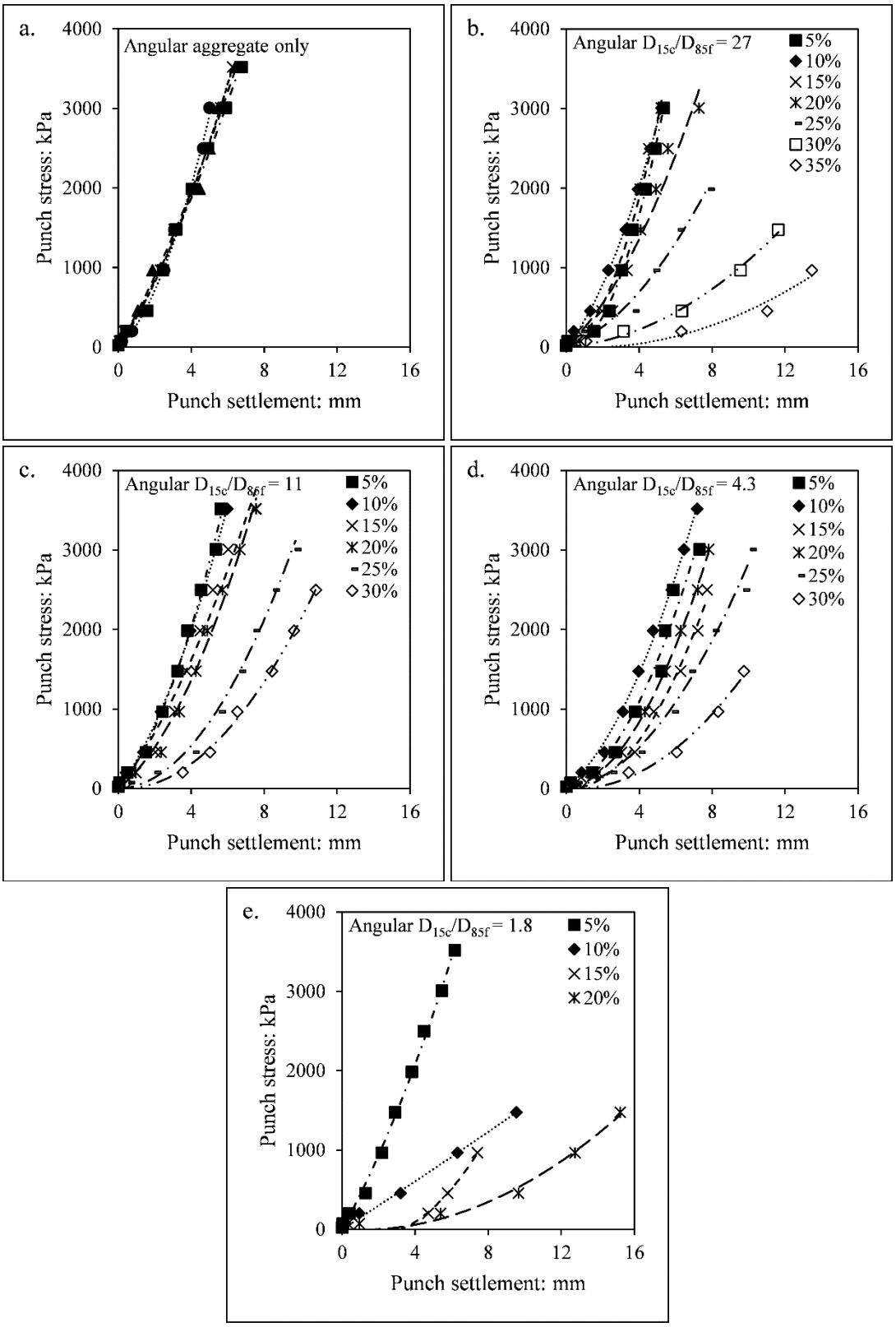


Figure 4.19: Punch test results: a. Angular aggregate; b. Angular aggregate and very fine salt; c. Angular aggregate and fine salt; d. Angular aggregate and coarse salt; e. Angular aggregate and very coarse salt

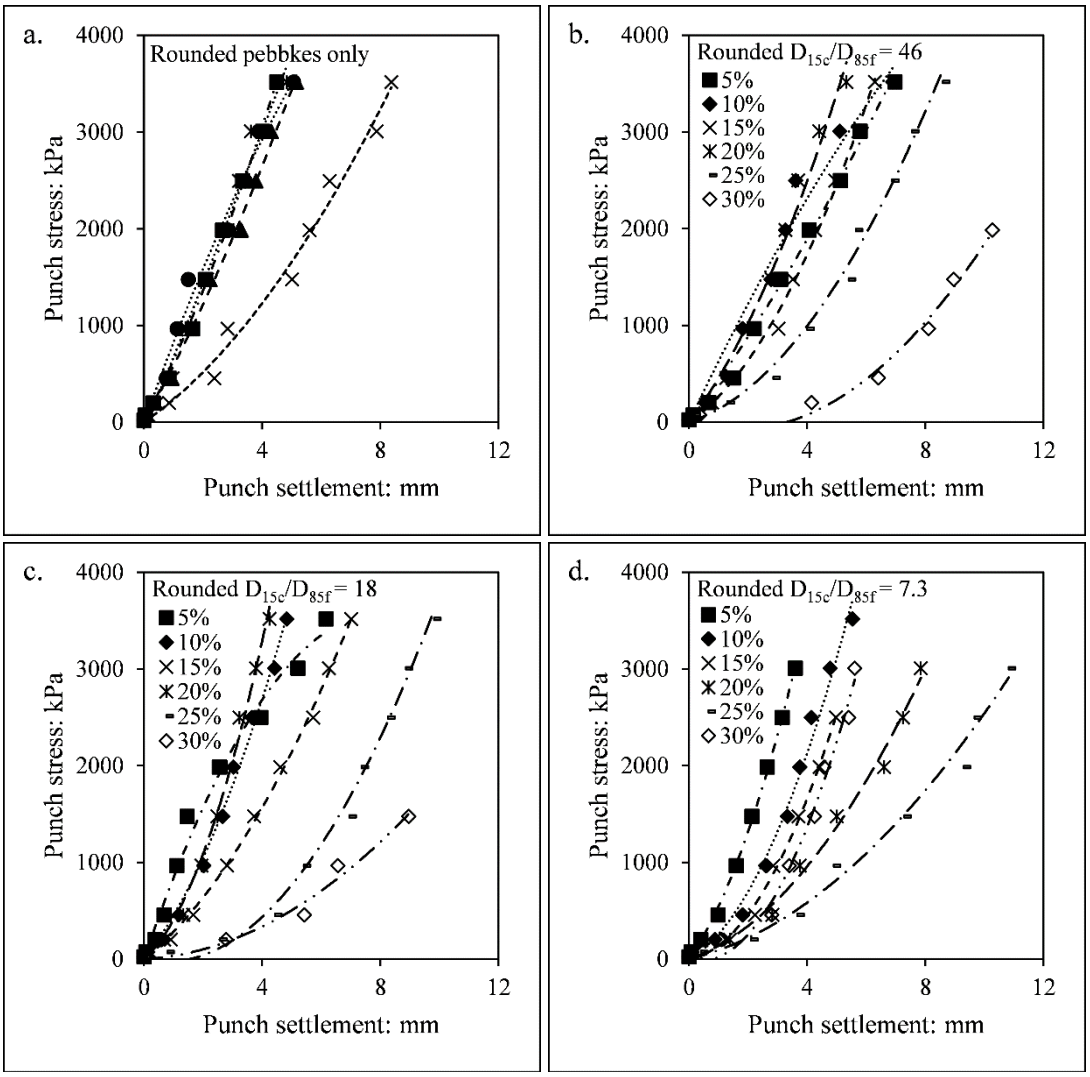


Figure 4.20: Punch test results: a. Rounded pebbles; b. Rounded pebbles and very fine salt; c. Rounded pebbles and fine salt; d. Rounded pebbles and coarse salt



Figure 4.21: Observed pebble crushing following punch testing

In order to compare punch test results, an index of strength was sought (i.e. a single number to represent the resistance to the whole punch test). As strength is proportional to relative density, the punch stress that correlated best with relative density was sought. For all angular aggregate and rounded pebble tests, the linear correlation between punch settlement and $D_{r,ec,d}$ was determined at each cumulative punch stress (22, 73, 200, 455, 966, 1476, 1986, 2496, 3006 and 3517 kPa). The Pearson correlation coefficients (Figure 4.22a) showed that for angular aggregate a strong linear correlation existed at all punch stresses and was highest at a punch stress of 966 kPa. However, for rounded pebbles the correlation decreased substantially after a punch stress of 966 kPa, possibly as particle crushing became pronounced at these higher punch stresses. Consequently, the punch settlement at 966 kPa was used as an index of strength. Figure 4.22b illustrates the linear relationship between punch settlements at 966 kPa and $D_{r,ec,d}$ for the two series.

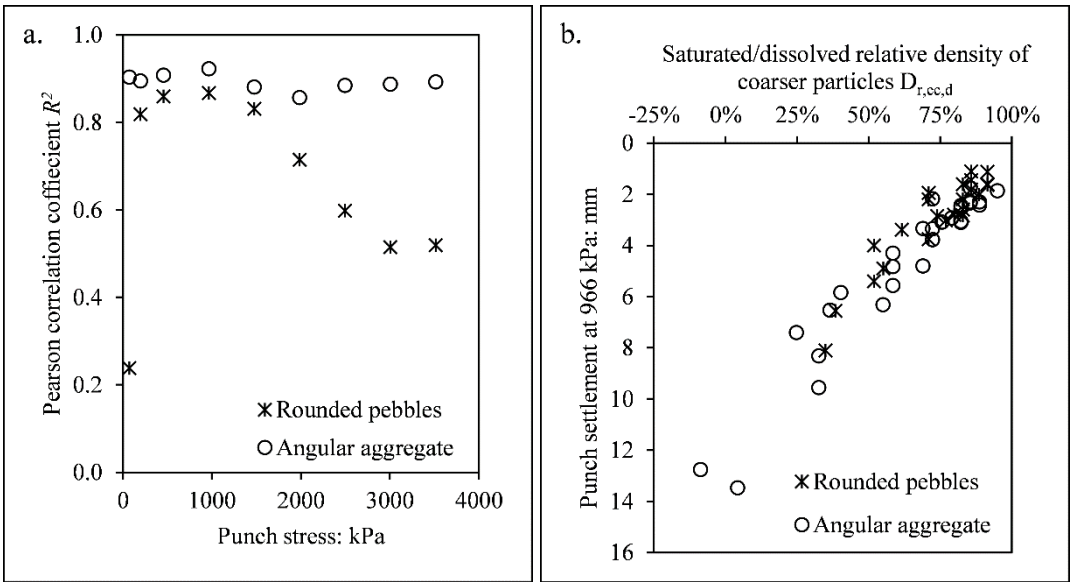


Figure 4.22: Punch test result comparison

4.4 Discussion of results

Results from the SOAP device tests are depicted with co-axial graphs, an example of which is Figure 4.23. In this figure, angular aggregate and very fine salt data are shown with black symbols and for comparison, all other angular aggregate data are included as grey symbols. In the top left-hand quadrant, ordinates are the initial relative density of the coarser particles ($D_{r,ec,0}$) and abscissae are the finer fraction (F).

It is clear that the coarser particles are in an increasingly looser arrangement as F increases. Comparative curves for aggregate-sand mixtures show similar packing behaviour at low F but at high F, aggregate-sand mixtures pack more efficiently than aggregate-salt mixtures. The top right-hand quadrant illustrates results following dissolution or flooding with abscissae giving the resulting relative density of the coarser particles ($D_{r,ec,d}$). If no settlement took place during dissolution $D_{r,ec,d}$ would fall along the 0 % settlement potential (SP) line. However, some settlement did occur and the amount of settlement increased with F. The bottom right-hand quadrant illustrates punch test results with ordinates being the punch settlement at 966 kPa. A clear reduction in strength with decreasing $D_{r,ec,d}$ is evident.

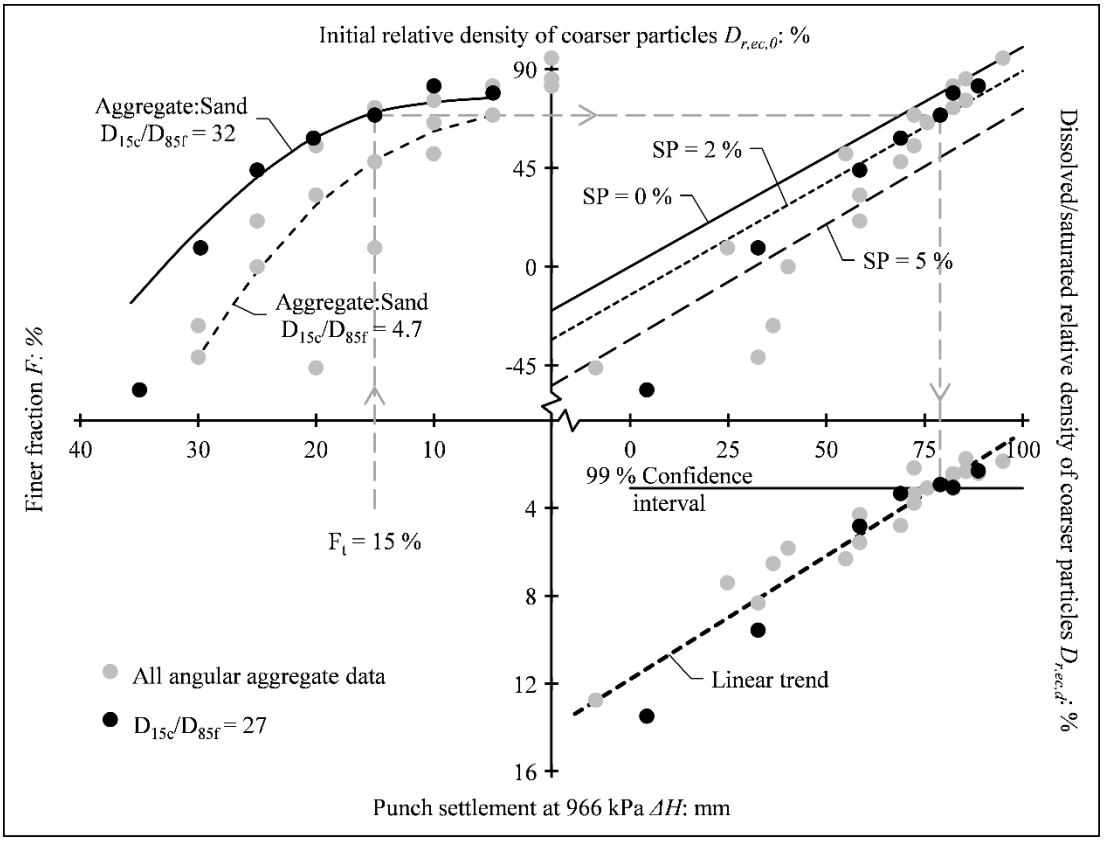


Figure 4.23: SOAP test results for angular aggregate and very fine salt mixtures

Figure 4.23 shows that for the angular aggregate and very fine salt (D_{15c}/D_{85f} = 27) tests for F < 15 % very little settlement took place (SP < 2 %). For F < 15 % the punch settlement at 966 kPa was 2.9 mm, which did not differ significantly from that of the coarser particles only, which had an average punch settlement of 2.2 mm with a standard deviation of 0.34 mm and therefore a 99 % confidence interval of 3.1 mm. However, for F > 15 % increasing settlement took place and strength decreased

reflecting the loose coarser fabric left behind. Chapter 3 proposed that mechanical behaviour could be largely unaffected following particle loss if the finer fraction is below a transition value (F_t). To determine the F_t boundary, F at which SP < 2 % and the punch settlement at 966 kPa was within the 99 % confidence interval of the coarser particles only was sought. From Figure 4.23, it can be concluded then that for a soil with D_{15c}/D_{85f} = 27, the transition finer fraction (F_t) is 15 %. Chapter 3 also proposed that at a higher critical finer fraction, finer particles would dominate mechanical behaviour and their loss would result in significant settlement and strength loss. It is harder to define F_c as $D_{r,ec,0}$ changes significantly at high F (Figure 4.23). However, it is clear that for $D_{r,ec,0}$ < 0 significant settlement took place and the resulting fabric was very loose. This highlights the greater role finer particles play in mechanical behaviour as F increases. F_c likely lies between 30 and 35 % for an internal filter ratio of 27 (Figure 4.23).

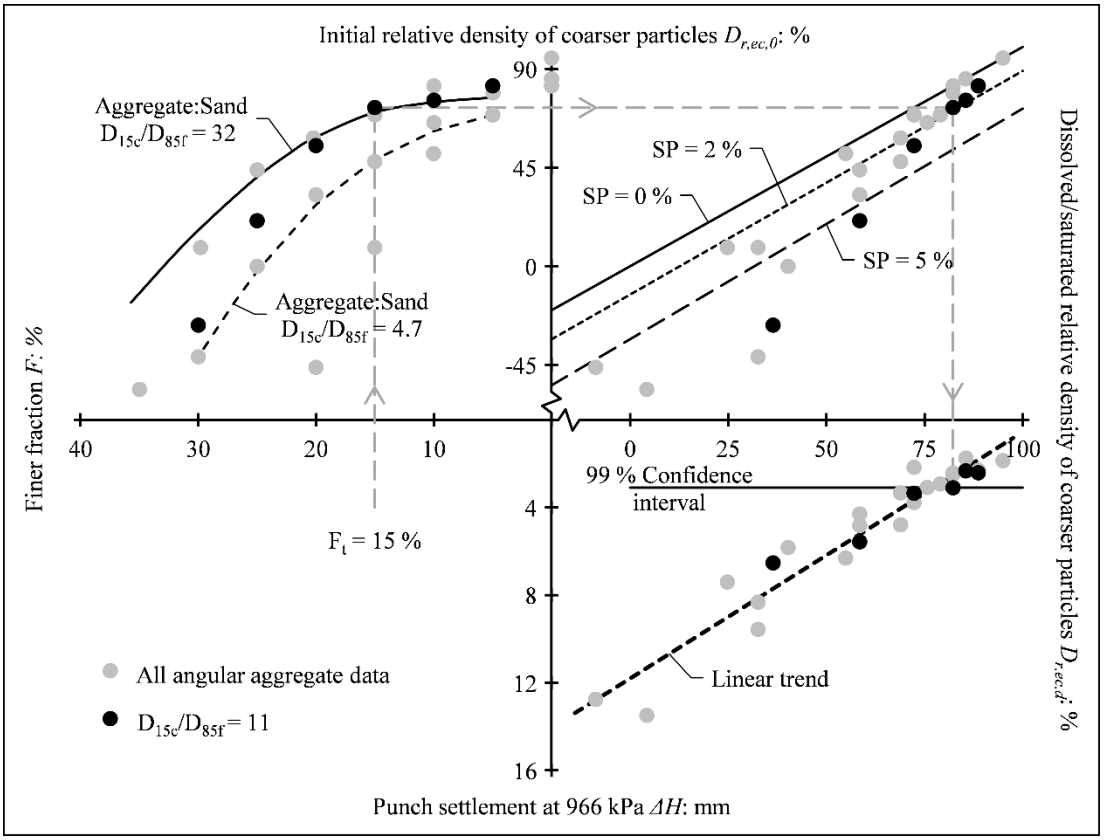


Figure 4.24: SOAP test results for angular aggregate and fine salt mixtures

Figure 4.24 shows results for angular aggregate and fine salt (D_{15c}/D_{85f} = 11) tests. They are similar to those described above for very fine salt, although $D_{r,ec,0}$ decreased faster with F. Based on similar reasoning outlined above, it is evident that that for a soil with an internal filter ratio of 11, F_t = 15 % and F_c lies between 25 and 30 %.

Figure 4.25 shows results for angular aggregate and coarse salt (D_{15c}/D_{85f} = 4.3) tests were similar to those described above for fine salt, although $D_{r,ec,0}$ values were lower for all F. Such a soil would be on the boundary between being internally stable and unstable, as its internal filter ratio is marginally above 4 (Kezdi, 1969). Based on similar reasoning outlined above, it is evident that that for a soil with an internal filter ratio of 4.3, F_t = 10 % and F_c lies between 25 and 30 %.

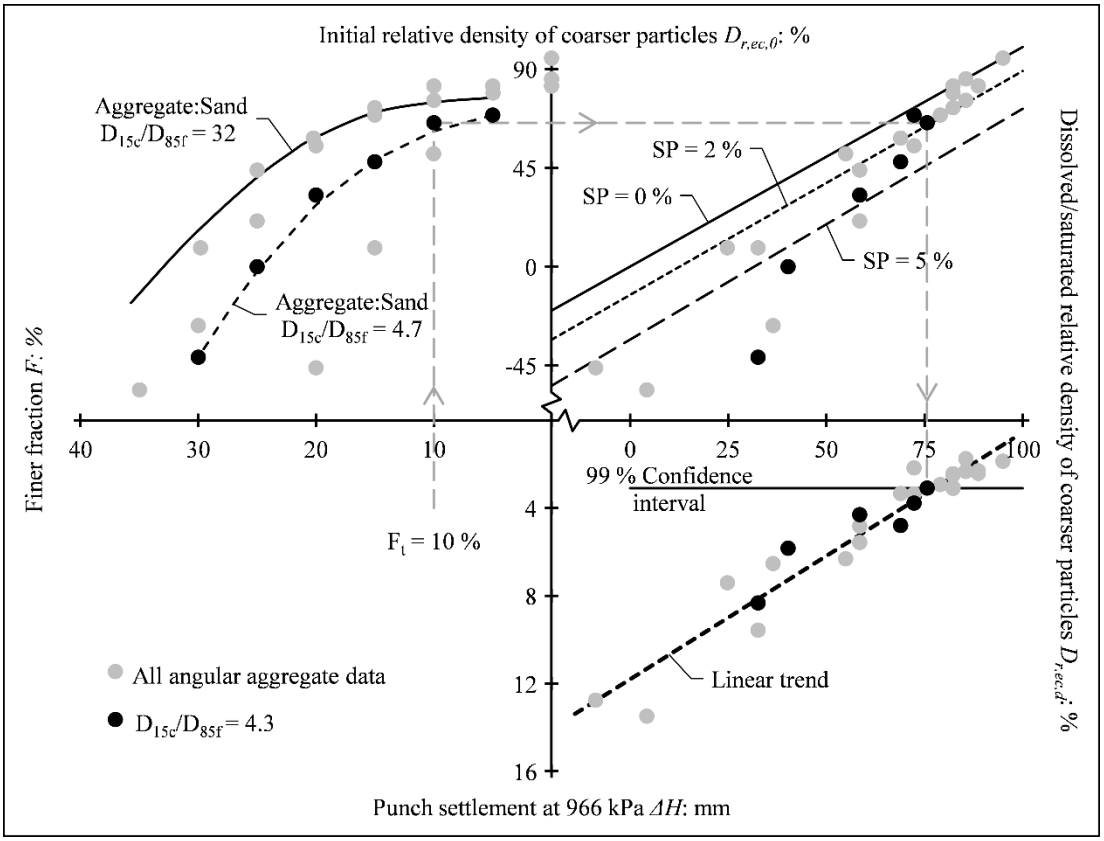


Figure 4.25: SOAP test results for angular aggregate and coarse salt mixtures

Results from the angular aggregate and very coarse salt tests (Figure 4.26) illustrate how $D_{r,ec,0}$ decreases rapidly with F when the internal filter ratio is lower than 4 (D_{15c}/D_{85f} = 1.8 in this case). Although this is the case, the observed settlement was lower than cases with similar $D_{r,ec,0}$ but higher F. This is presumably because the finer particles make up a smaller portion of the soil, meaning a smaller volume is lost during finer particle loss. Defining F_t and F_c is purely academic for such a soil, as such finer particles are too large to be lost due to seepage. However, based on similar reasoning outlined above, for a soil with an internal filter ratio of 1.8, F_t = 5 % and F_c lies between 15 and 20 %.

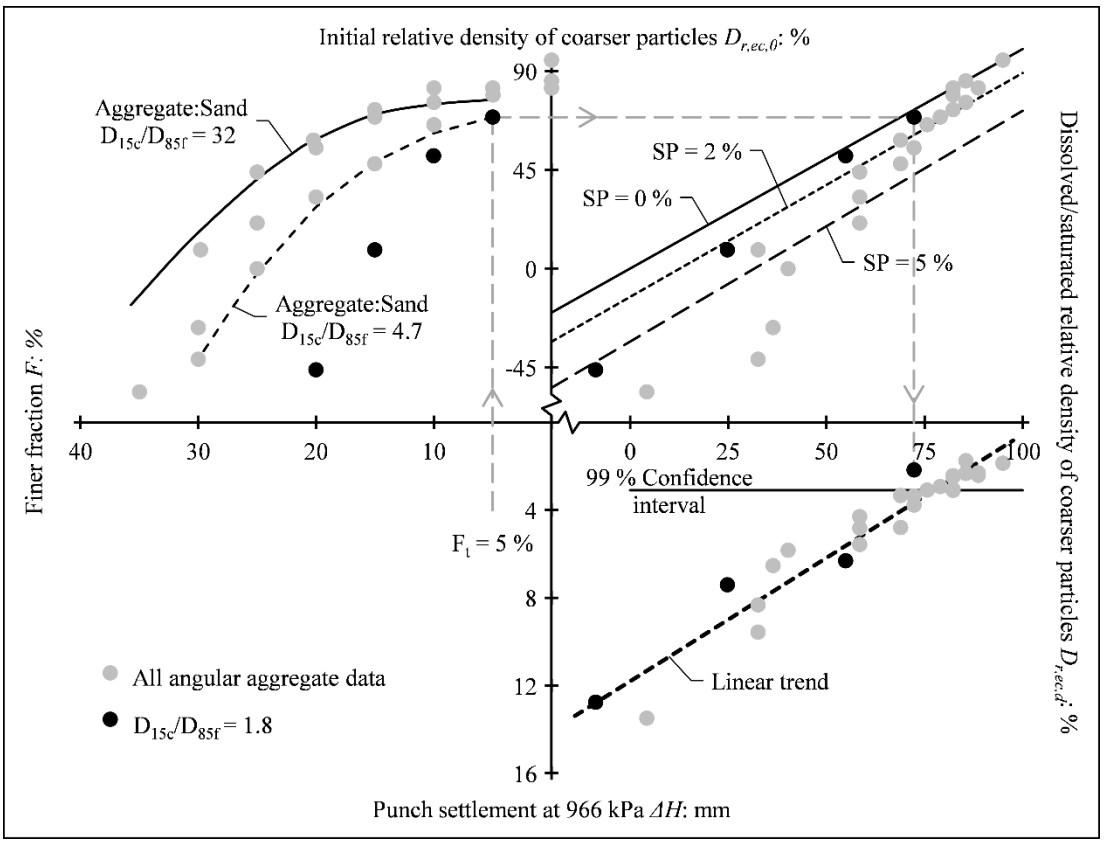


Figure 4.26: SOAP test results for angular aggregate and very coarse salt mixtures

Figure 4.27 shows that results from rounded pebbles and very fine salt (D_{15c}/D_{85f} = 46) tests are very similar to those for angular aggregate and very fine salt tests (Figure 4.23) suggesting particle shape does not play a major role. The influence of mineralogy was not considered. Although packing is such that $D_{r,ec,0}$ was marginally larger for F < 20 %, but lower for F = 30 %. These results suggest that for a soil with an internal filter ratio of 46 the finer fraction above which mechanical behaviour is impacted by finer particle loss (F_t) is 20 %. F_t is as before, F for which SP < 2 % and punch settlement at 966 kPa is within 99 % confidence interval of coarser particles only (For pebbles only, the average punch settlement at 966 kPa was 1.7 mm with a standard deviation of 0.65 mm and therefore a 99 % confidence interval of 3.4 mm). Based on a similar argument as outlined above for angular aggregate (i.e. large settlements and strength loss at $D_{r,ec}$ > 0), the finer fraction above which finer particles dominate mechanical behaviour (F_c) lies between 25 and 30 % for pebbles with D_{15c}/D_{85f} = 46.

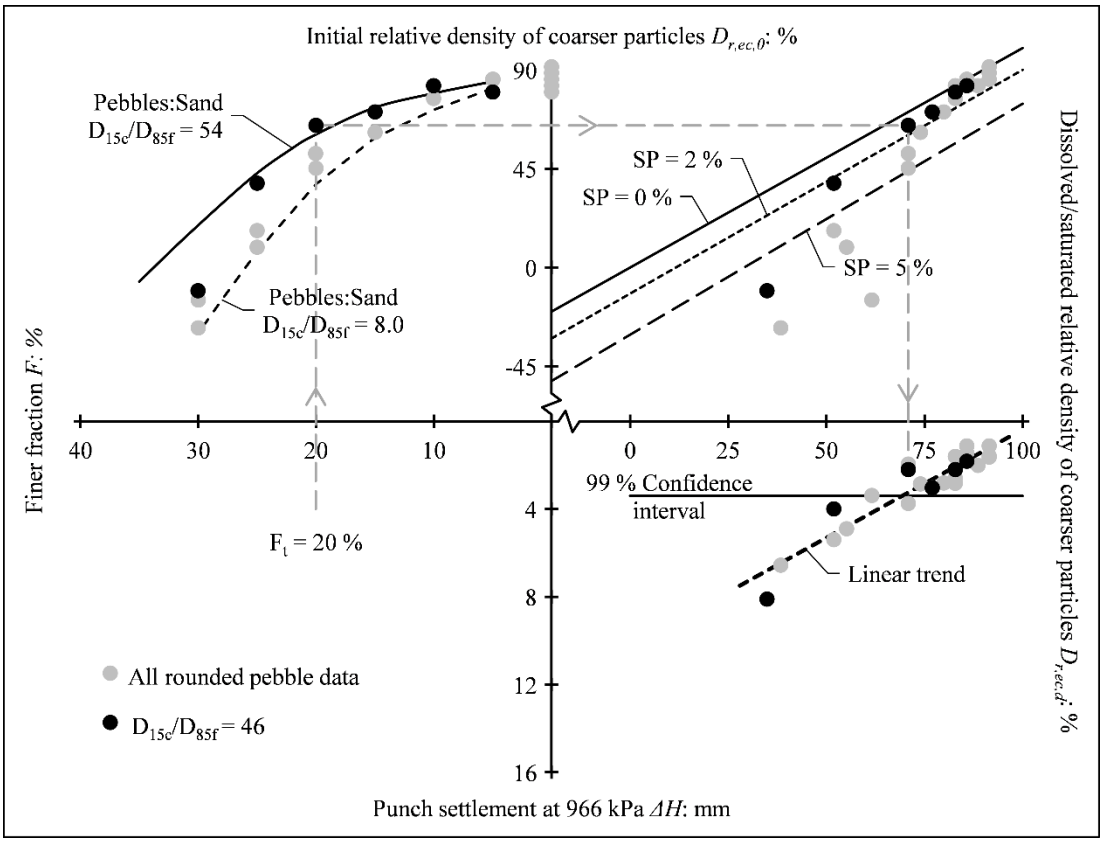


Figure 4.27: SOAP test results for rounded pebbles and very fine salt mixtures

Results from the rounded pebbles and fine salt tests (Figure 4.28) suggest for a soil with D_{15c}/D_{85f} = 18, F_t = 15 % and F_c lies between 25 and 30 %. As these are the same values suggested for angular aggregate mixtures with D_{15c}/D_{85f} = 11, particle shape does not appear to play a major role.

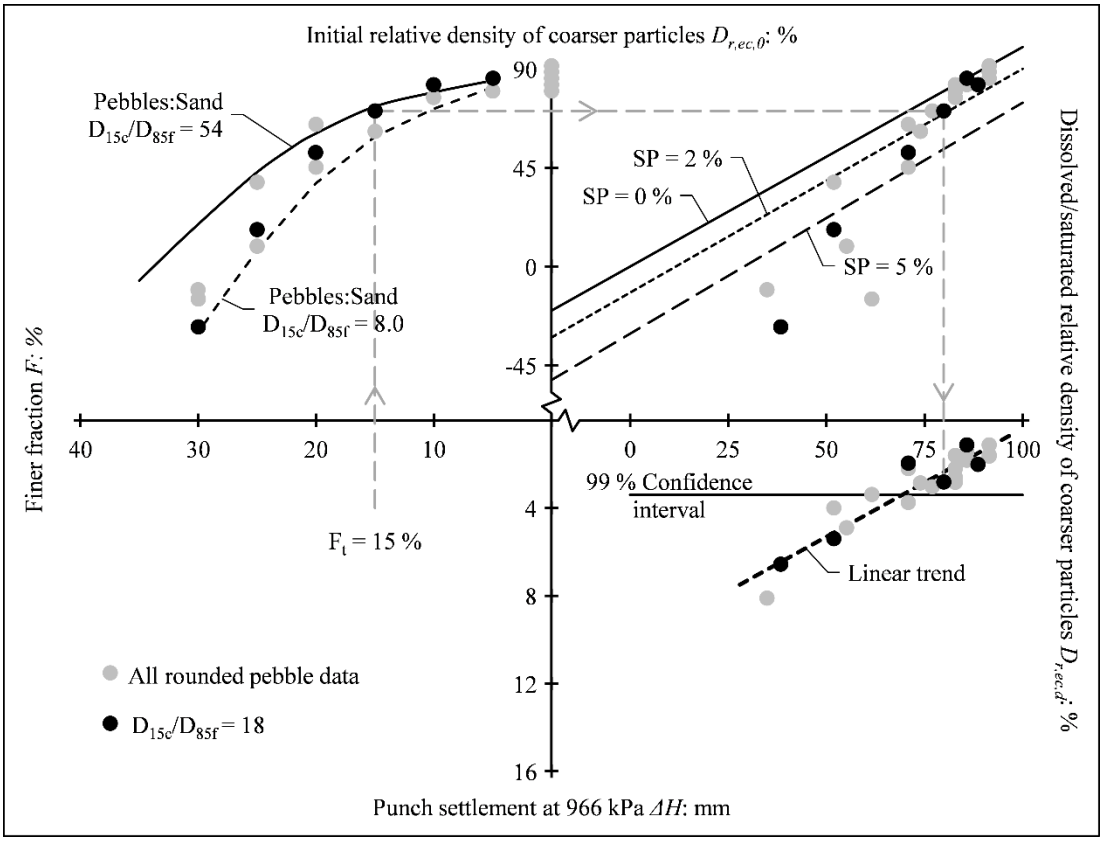


Figure 4.28: SOAP test results for rounded pebbles and fine salt mixtures

Figure 4.29 shows results from rounded pebbles and coarse salt (D_{15c}/D_{85f} = 7.3) tests. These results suggest that for a D_{15c}/D_{85f} = 7.3, F_t = 10 % and F_c lies between 25 and 30 %. This is further evidence that particle shape does not play a major role, as the same boundaries were suggested from angular aggregate and coarse salt tests with D_{15c}/D_{85f} = 4.3.

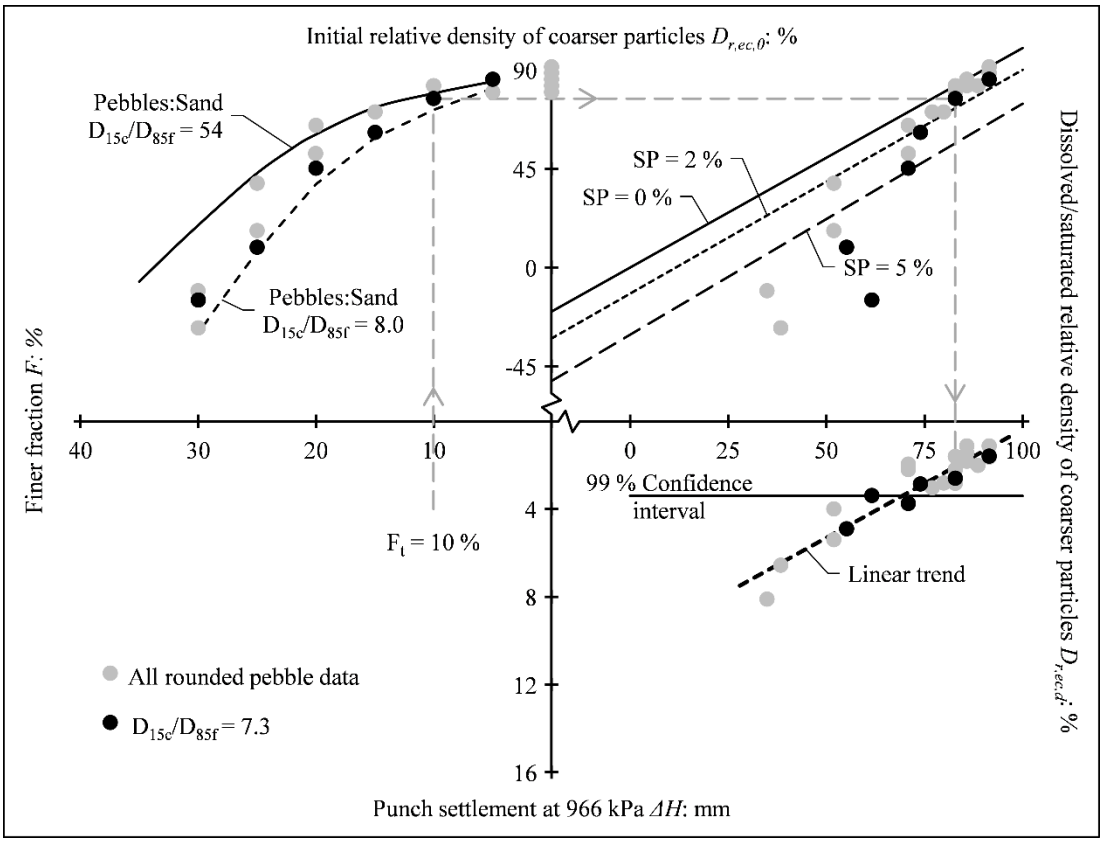


Figure 4.29: SOAP test results for rounded pebbles and coarse salt mixtures

4.5 Proposed mechanical internal erosion criterion

From a practical standpoint, tentative suggestions for design can be made, concerning changes to soil mechanical behaviour during internal erosion. Results from all SOAP device tests are plotted in a co-axial plot in Figure 4.30. It is evident from the top left-hand quadrant that packing behaviour is not very sensitive to the coarser component particle shape. There is some difficulty in comparing settlement potentials (SP) in the top right-hand quadrant as the points are plotted by relative density of the coarser components. It can be shown (see Appendix C.3 page 205) that the equation of the straight line that defines the relationship between $D_{r,ec,d}$ and $D_{r,ec,0}$ at a given SP is:

$$D_{r,ec,d} = D_{r,ec,0}(1 - SP) + \frac{SP\rho_{d,max}}{\rho_{d,max} - \rho_{d,min}} \qquad \text{Equation 4.2}$$

where, $\rho_{d,min}$ is the minimum dry density and $\rho_{d,max}$ is the maximum dry density of the coarser component. Therefore, whilst the slope is independent of the reference densities, the intercept is dependent on these densities. As the reference densities varied slightly for the angular aggregate and rounded pebbles, the average of the angular aggregate and rounded pebble SP contours are plotted in Figure 4.30. The error in doing this was found to be negligible (see Appendix C.3 page 205). The bottom right-hand quadrant (Figure 4.30) shows that punch settlements at 966 kPa were similar for both angular aggregate and rounded pebble tests justifying the use of a single trend line.

On average Figure 4.30 shows that for all internally unstable gradations (i.e. $D_{15c}/D_{85f} > 4.0$) when F < 15 % the loss of finer particles (by salt dissolution) resulted in small settlements and negligible changes in strength. An estimate of the F_t boundary for the range of internally unstable soils considered is therefore 15 ± 5 %, being lower for D_{15c}/D_{85f} = 4.0 and higher for rounded particles when D_{15c}/D_{85f} is higher. For soils with unstable gradations with $F < F_t$, the loss of finer particles would have a negligible effect on mechanical behaviour. Such soils do not pose a significant risk to structural integrity. However, if such material is used as a critical filter, its continued ability to retain base material could be jeopardised as it becomes coarser.

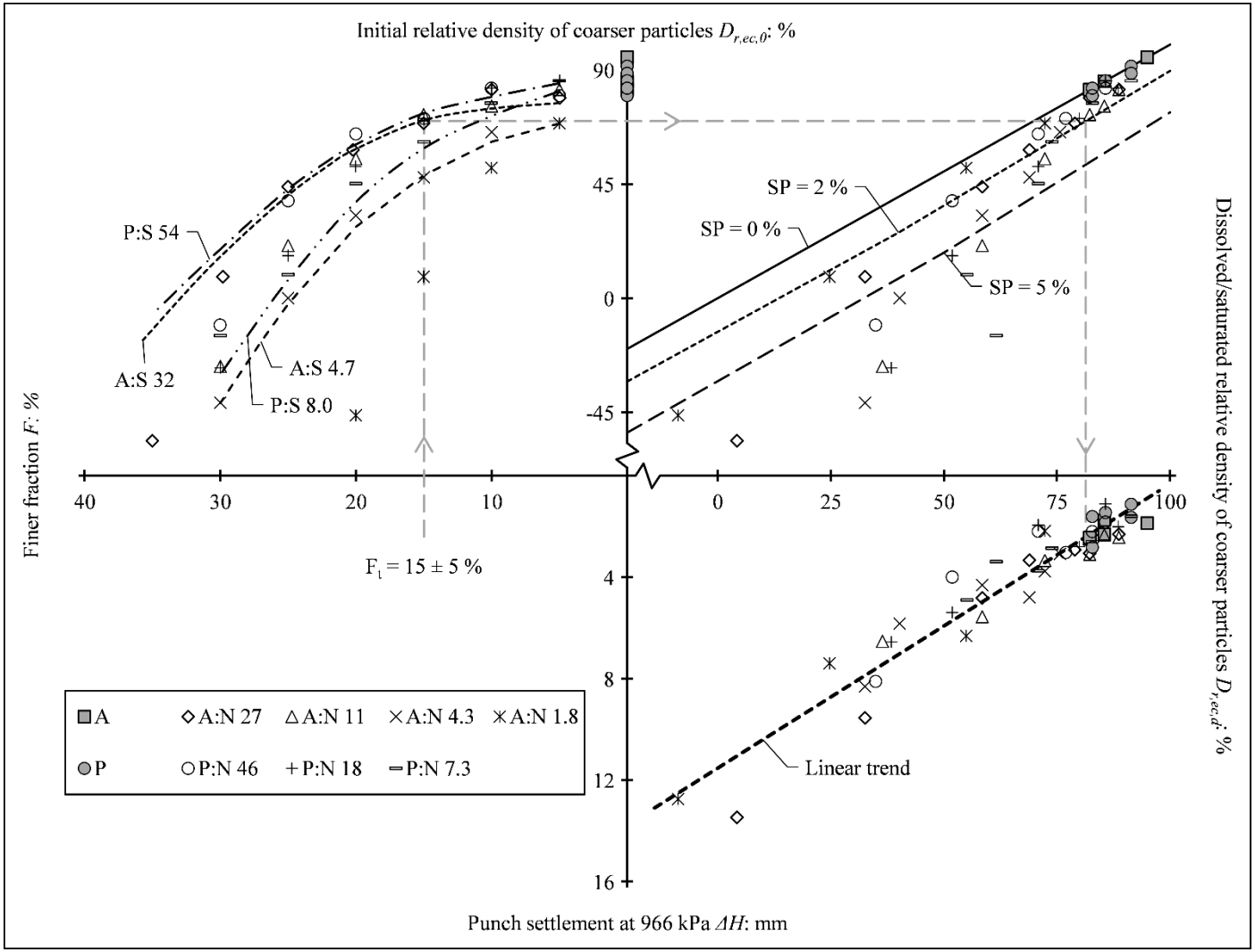


Figure 4.30: Mechanical internal erosion criterion

It is clear from Figure 4.30 that for all soils considered when $D_{r,ec} < 0$ significant settlement and strength loss occurred. This reflects the fact that the coarser particles are no longer in a stable arrangement without the presence of finer particles. The finer fraction at which this occurs is then the critical finer fraction (F_c). Above F_c finer particles are significantly load bearing preventing their loss by water drag forces. For the soils considered in Figure 4.30, F_c ranged between 25 and 30 %. However, at such high F, finer particles are on the cusp of being fully loaded within a loose coarser fabric, with regions of the overall fabric having erodible finer particles within a loose coarser fabric and others with fully loaded finer particles. Salt dissolution will result in collapse in both these regions. This makes it difficult to define an upper limit above which internal erosion is unlikely to occur. An upper value of 35 % is suggested

Soils with unstable gradations with $F_t < F < F_c$ are at a greater risk of suffosion (that is mechanical behaviour being impacted), with the loss of shear strength increasing with increase in finer fraction. Soils with $F > F_c$ are less likely to be at risk of either suffusion or suffosion as finer particles are integral to load transfer and are not easily lost. This does not rule out other forms of internal erosion that may arise due to extreme hydromechanical conditions developing.

Skempton and Brogan (1994) introduced the terms clast-supported (i.e. loads are predominantly carried by coarser particles) and matrix-supported (i.e. loads are predominantly carried by finer particles) for use with internally unstable gradations. Internally unstable gradations with $F < F_t$ can be considered to be fully clast-supported and gradations with F > Fc can be considered to be fully matrix-supported, with a transition between the two fabrics for $F_t < F < F_c$.

Chapter 5 Development of the vertical axis restraint internal erosion direct shear box (variedSB)

Preceding chapters developed a generalised understanding of how the overall fabric changes as finer particles are lost and the impact of this on mechanical behaviour. It was shown that this impact on mechanical behaviour depends on the coarser fabric, which changes as F increases. A transition finer fraction (F_t) below which mechanical behaviour was not significantly impacted following finer particle loss was identified. A critical finer fraction (F_c) was also identified above which finer particles dominate mechanical behaviour resulting in internal stability. Experimental work described in Chapter 4 illustrated these changes, but the indicators of performance used (settlement potential in a cell with side friction resulting in a non-uniform stress distribution and a punch test) are not fundamental parameters. Furthermore, the role of the finer fraction in resisting shear distortion was not investigated.

Traditionally, triaxial-type or direct shear box-type equipment is used to determine changes in fundamental soil strength parameters under different loading conditions. To explore the effects of the change in fabric due to internal erosion and the consequential impact on mechanical behaviour either of the two types of equipment could be suitably adapted to achieve this. Both of these types of equipment would need to be adapted so that a specimen could be placed and collapse of the soil fabric monitored as dissolution took place. Then, once all salt had dissolved, shearing of the specimen would be required to determine whether the loss of finer particles had any effect on the shear behaviour. For practical reasons, direct shear box-type equipment was used in which the specimen could be loaded and collapse monitored, and the specimen subsequently sheared.

5.1 Feasibility test work

A precursor to the direct shear box (DSB) test was used by Collin (c1846) to quantify the strength of clay (Skempton, 1949). However, due to dominant theories in soil mechanics at the time relying on judgment, it was only following Terzaghi's work in

the early 1920's that significant advances in quantifying soil strength began (Mayne, 2013). Early shear boxes were disadvantaged by being stress controlled, with strain control being later developed by Gilboy at MIT in 1936, enabling post peak strength of soil to be investigated (Matthews, 1988).

The modern DSB depicted in Figure 5.1, which can be found in most soils laboratories, comprises a rigid metal box consisting of two halves containing a specimen square or round in plan. The bottom-half is submerged in a bath flooding the specimen and forced to slide at a constant rate relative to the top-half. A constant vertical load is transferred to the top of the specimen through a rigid plate (top platen) by means of suspended weights or pneumatics. Varying rates of displacement of the bottom-half are achieved by gearing and, more recently, variable speed motors. Vertical displacements of the top platen are measured to quantify dilation or contraction. The developing shear force is measured by measuring the reaction force required to keep the top-half stationary via a swan neck over the edge of the bath. Displacements are measured with dial gauges and forces with proving rings, although these are being replaced by linearly varying differential transformers (LVDTs) and load cells. Although, as will be shown, Jewell (1989), Shibuya et al. (1997) and Lings and Dietz (2004) have proposed various adaptations, the current DSB, used in most laboratories, is virtually unchanged from the device developed in the 1930's, albeit with modern means of data capture added.

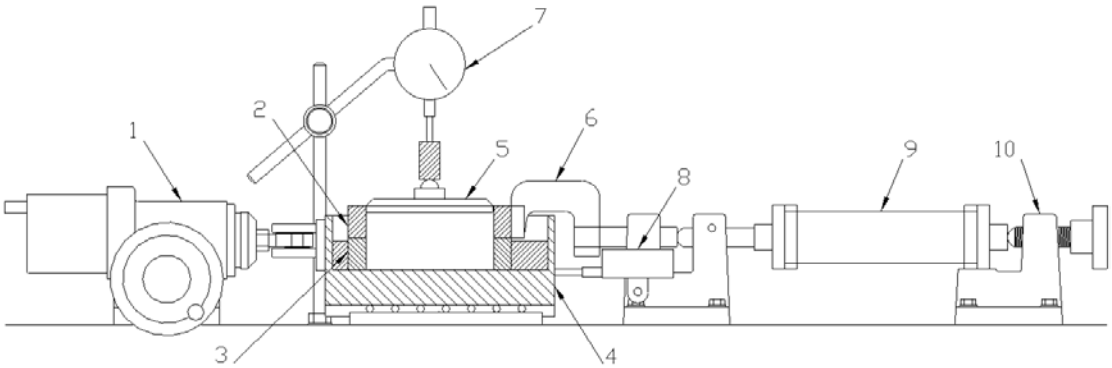


Figure 5.1: Conventional direct shear box: 1. Screw drive; 2. Top-half; 3. Bottom-half; 4. Bath; 5. Top platen; 6. Swan neck; 7. Vertical dial gauge; 8. Horizontal dial gauge; 9. Proving ring; 10. Tailstock

All soil laboratory tests result in non-uniform stresses (Verveckaite et al., 2007) although they are probably least uniform in the DSB test. Despite this, studies on the stress distribution within the specimen have shown that the overall stress ratio on the central plane is close to uniform with little progressive failure (Jewell and Wroth, 1987, Potts et al., 1987). These studies, procedural simplicity, the wide spectrum of materials that can be tested, and the applicability of results to failures involving lateral displacement (e.g. slopes) have resulted in the DSB remaining in use.

An existing conventional 100 × 100 mm DSB, manufactured by Farnell Testing Equipment, see Figure 5.2, was used to determine the feasibility of the proposed soil-salt experimental method. Over twenty tests were conducted, showing the concept to be feasible, however the following modifications were deemed essential to obtaining useable data:

- For the majority of tests the quantity of salt within the specimen precludes relying on conventional flooding in the apparatus' bath to dissolve the salt. The reason being that a super-saturated solution would develop within the voids as no circulation could take place. Adaptations to enable water circulation through the specimen and collection of seepage were therefore necessary.
- With the conventional top platen arrangement, where it is free to rotate, excessive rotation occurred during dissolution. The reason for this is that the rate of dissolution was not uniform throughout the specimen. This rotation was particularly pronounced for specimens with large salt quantities. To counter this, it was evident that the top platen would need to be prevented from rotating. Such rotation induces a non-uniform stress distribution.

Extensive modification of the equipment was undertaken to permit percolation of water and prevent rotation of the top platen.

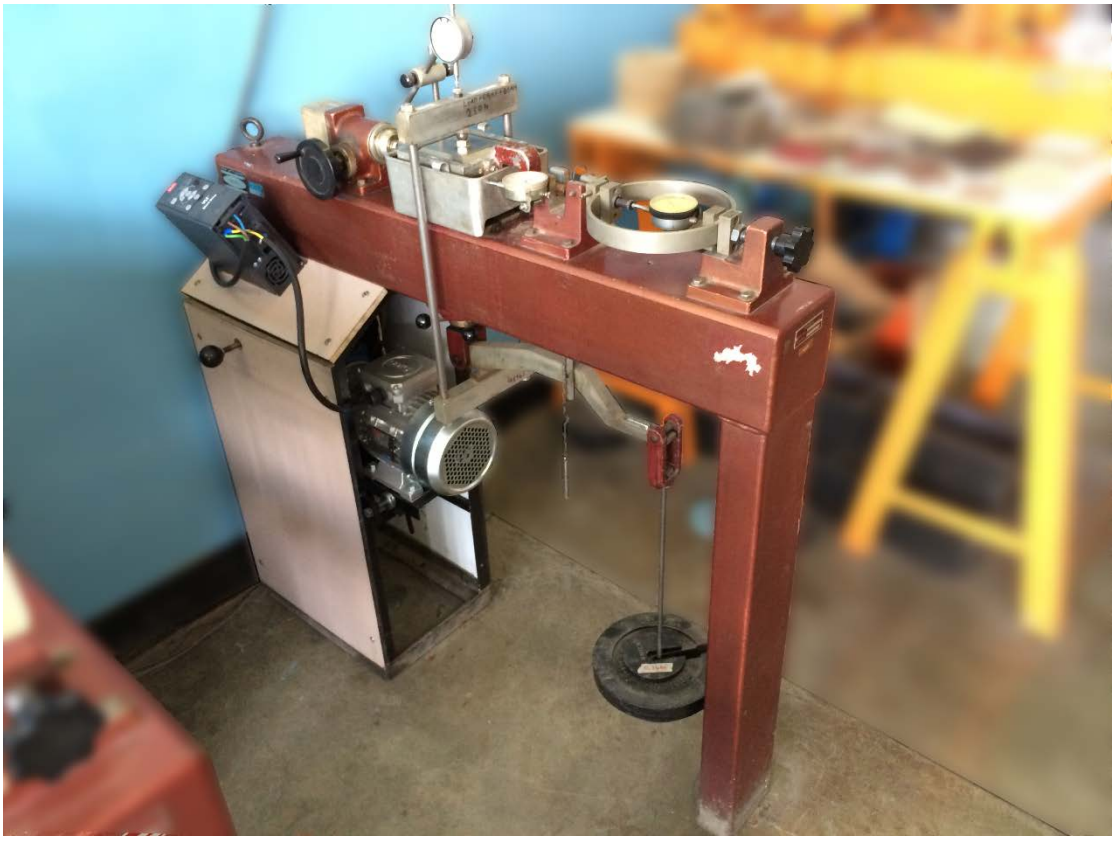


Figure 5.2: Conventional direct shear box equipment

5.2 Design of the variedSB

5.2.1 Description of the variedSB

The vertical axis restrained internal erosion direct shear box (variedSB) was developed during this research at the University of the Witwatersrand, by modifying an existing 100 × 100 mm Farnell Testing Equipment DSB. Figure 5.3 is a schematic of the developed variedSB. To prevent rotation of the top platen, the top platen was rigidly connected to a shaft that was restrained to move along the vertical axis by a linear bearing secured in a rigid frame. This frame was also used to restrain fully the top-half of the shear box against vertical and horizontal movements and rotation. The vertical load was applied using the existing load frame and suspended weights. Dissolution (finer particle loss) by seepage was therefore under 1-Dimensional loading. This set-up also enforced rotational restraint on the top platen during shear. An S-type load cell was used to measure the vertical load directly above the top platen. Vertical displacements were measured with a LVDT. A screw drive, driven by a servomotor forced the bath and bottom-half to slide at a constant rate. Developing

shear load was measured with an S-type load cell and horizontal displacement with a LVDT.

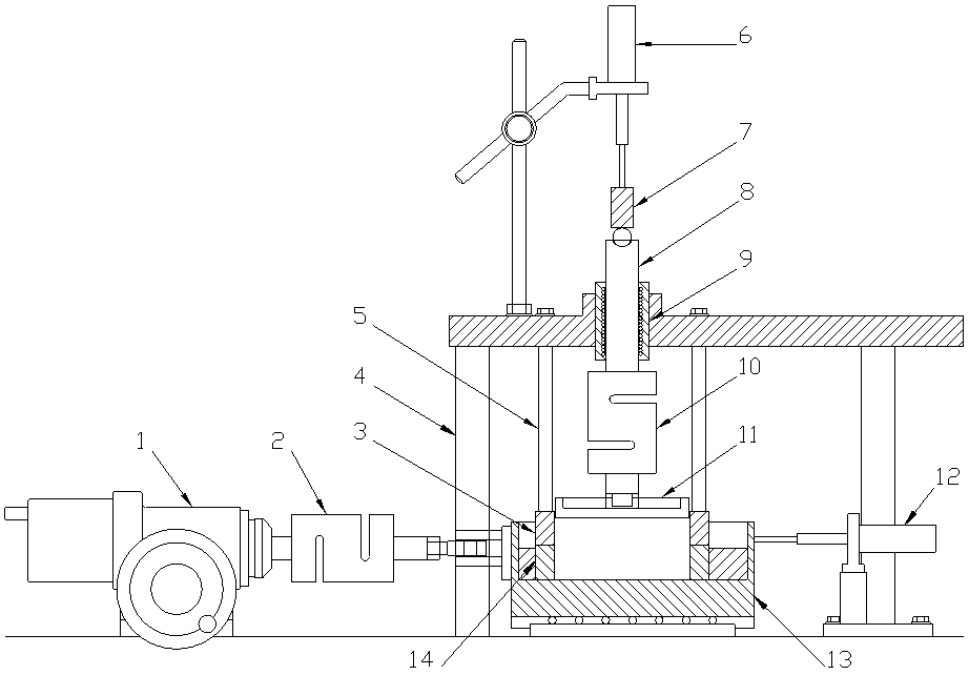
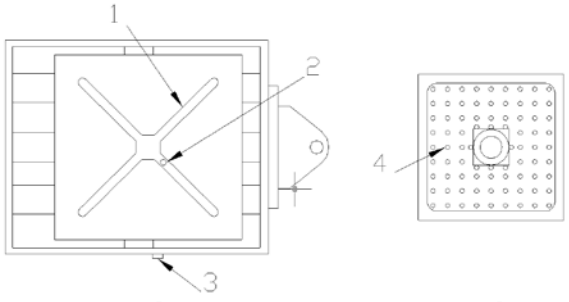


Figure 5.3: Developed variedSB: 1. Screw drive; 2. Shear load cell; 3. Top-half; 4. Vertical restraining frame; 5. Top-half fixing rods; 6. Vertical LVDT; 7. Loading frame; 8. Vertically restrained loading shaft; 9. Linear bearing; 10. Vertical load cell; 11. Top platen; 12. Horizontal LVDT; 13. Bath; 14. Bottom-half

To facilitate seepage through the specimen, a shallow bath was cut into the top platen, feeding many 1 mm diameter holes. Seepage collection channels were recessed into the bottom of the bath and connected to the outside of the bath. These details are shown in Figure 5.4. A perforated grid plate was placed above the drainage channels to prevent loss of soil grains. A similar plate was also placed between the top platen and specimen.



Bath Top platen

Figure 5.4: Details of seepage provisions: 1. Drainage collection channels; 2. Connection to outlet; 3. Drainage outlet; 4. Perforated top platen.

Figure 5.5 shows the variedSB, along with the seepage supply tank, collection pipe and overflow bucket, power supplies and the Agilent 34972A data acquisition unit attached to a HP ProBook 450 personal computer for data capture.

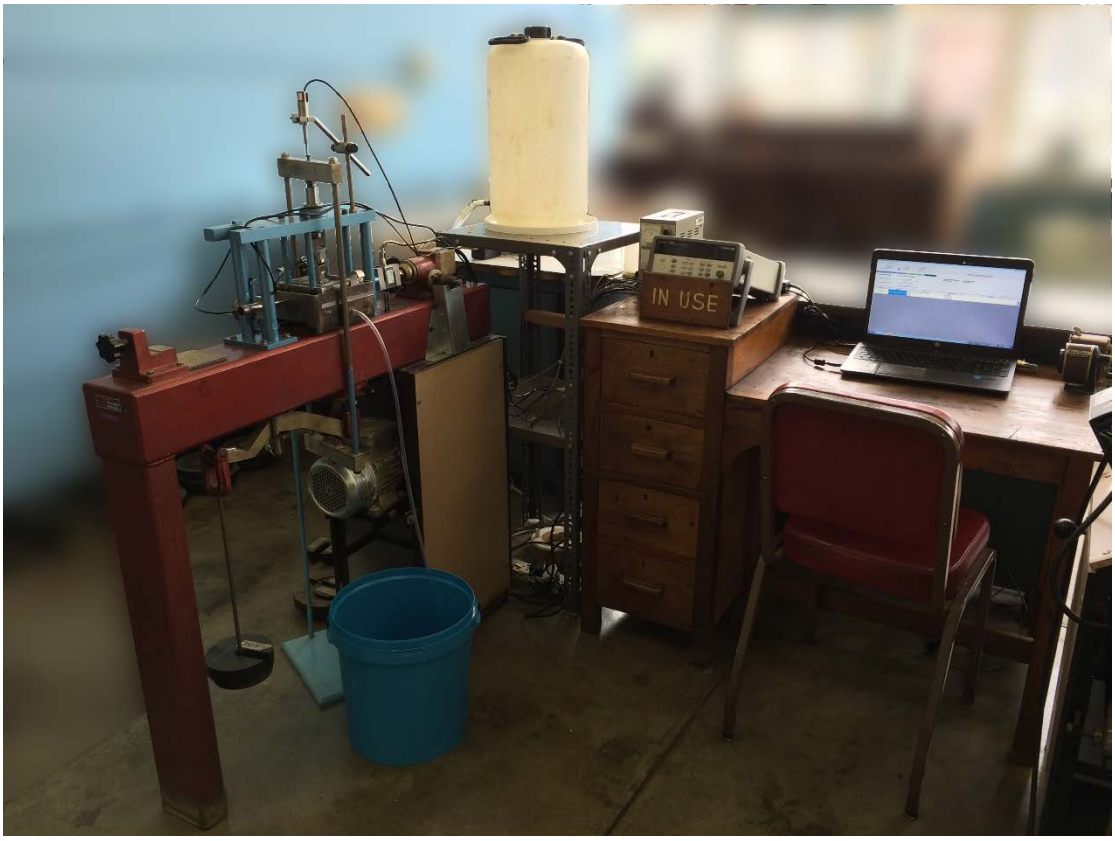


Figure 5.5: Laboratory set-up

In view of the changes in boundary conditions necessitated to facilitate seepage in the variedSB, relevant literature is now reviewed to ascertain how these changes will influence testing and the interpretation of results.

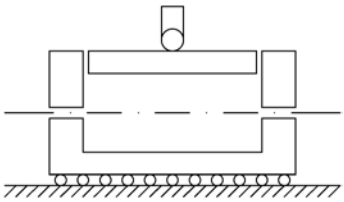
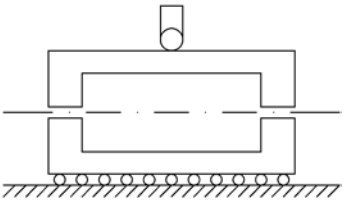
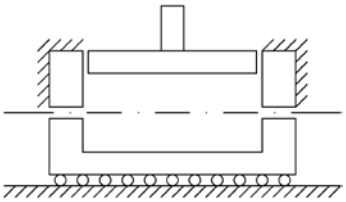
5.2.2 Review of the literature on direct shear box testing

Influence of test equipment and procedure

Jewell (1989) and Shibuya et al. (1997) presented experimental work indicating that shear force transfer takes place through the end-walls, with little transfer through the top and bottom of the box. Consequently, the top-half of the box and specimen are subject to an equal and opposite couple, causing rotation of the top-half. Theoretical work by Potts et al. (1987) suggested this has little effect on results, however,

experimental work presented by Jewell (1989) showed this resulted in the stress ratio (shear stress (τ_{yx}) / vertical stress (σ_{yy})) being overestimated. Shibuya et al. (1997) highlighted that rotation results in an undesirable variation in density and showed that progressive failure was more likely. Most adaptations have been to address this concern. Lings and Dietz (2004) classified these (Table 5.1) as either "enforced" or "induced", that is either physically restraining rotation or increasing rigidity so that rotational uniformity is improved.

Table 5.1: Direct shear box designs, adapted from Shibuya et al. (1997), Lings and Dietz (2004)

Free	Induced	Enforced
		
Top platen and top-half of box can move vertically or rotate independently.	Top platen is fixed to top-half and moves vertically or rotates as a unit.	The top-half is fixed and the top platen is restricted to move vertically.

Jewell and Wroth (1987) proposed that more uniform deformation was possible with induced rotational restraint by securing the top platen to the top-half of the box after load application, creating a single top unit. Lings and Dietz (2004) refined this methodology by optimising the manner in which the shear force is measured. Conventionally this is done through a swan neck, which, due to its weight, applies a further moment to the top-half. More recently, a shaft through the bath sealed with an O-ring has been adopted although this results in some frictional resistance. Lings and Dietz (2004), therefore, proposed an elaborate adaptation, using "wings" attached to the sides of the top-half. The arms that measure the shear load are maintained central and horizontal by being attached via ball races to the wings. A criticism of such devices is that the gap between the two boxes varies during testing, and can cause metal-to-metal friction should the specimen contract. This mechanical friction can result in errors when testing, especially at vertical stresses below 20 kPa (Lehane and Liu, 2013).

Lehane and Liu (2013) used principles of statics to investigate the effects of the presence and absence of a gap on the analysis of such results. They showed that for low stresses and at post peak, the weight of the top-half needs to be included when calculating the vertical force. For peak shear loads the same applied; however, at very low applied stresses the gap cannot be maintained, as the internal friction cannot support the weight of the top-half. They estimated that the maximum force generated by the internal friction in their device was about 10 ± 1 % of the applied load. Thus, if the weight of the top-half is greater than this, the gap is not maintained and friction develops. This then needs to be taken into account when calculating the shear resistance of the soil. A Polytetrafluoroethylene (Teflon) shear box was advocated due to the material's lightweight and low frictional resistance.

Shibuya et al. (1997) proposed that greater uniformity could be achieved using enforced rotational restraint. This was accomplished by fixing the top-half of the box to a frame, and fixing the top platen to a shaft running through a linear bearing. The shear load is then measured with a load cell in the load ram. The main criticism of enforced rotational restraint is that as the soil dilates it generates friction as it moves up against the top-half. This friction is equivalent to the friction highlighted by Lehane and Liu (2013), although in this case, as the top-half is fixed, this increases the vertical force on the shearing plane. The vertical force, ideally, needs to be measured below the shear plane, i.e. immediately below the bottom-half of the shear box. DEM and experimental work by Liu et al. (2005) confirmed the need to measure the vertical force at the bottom of the shear box, however, the presented results suggest that vertical displacements are not greatly affected.

In order to counter the friction against the top-half during dilation Thermann et al. (2006) suggested using a device in which the top-half runs in a bearing race. This prevents rotation but allows vertical movements, and was reported to result in better reproducibility. Alternatively, the inside of the shear box can be lubricated to reduce the friction (Shibuya et al., 1997). Further criticism of the Shibuya et al. (1997) device is that, due to the potential for lateral loads in the loading arms, stiff load cells are required (Lings and Dietz, 2004). An advantage of the arrangement is that it is

possible to maintain the same gap between the two halves during testing preventing mechanical friction, which is not possible in the other methods.

During shearing, shear bands propagate from either side of the artificially induced failure plane between the two boxes. The size of the box relative to the soil grains can influence the measured shear force depending on whether developing shear bands are impeded. ASTM D3080 requires a minimum specimen thickness, H of six times the maximum particle size (D_{max}), a minimum specimen length, L of 10 times D_{max} and a minimum aspect ratio (i.e. L/H) of two. A DEM study by Wang and Gutierrez (2010) into this scale effect found that large specimen lengths resulted in greater strain at the ends than in the middle, reducing the measured peak strength. Smaller specimen thickness prevented full shear band development, due to interference from the upper and lower boundaries, reducing the measured peak strength. A close examination of the Wang and Gutierrez (2010) data suggests that, although the peak strength was influenced by scale effects, the peak rate of dilation was less influenced. Wang and Gutierrez (2010) recommend a minimum value of 60 for L/D_{max}, a minimum value of 40 for H/D_{max} and a range of 1.5 to 2 for L/H. Although their minimum width and height suggestions are in line with research by others (Jewell and Wroth, 1987, Cerato and Lutenegger, 2006), most of their simulations were done with an aspect ratio greater than their suggested range.

Various gap sizes have been proposed in literature, as detailed in Table 5.2. Lings and Dietz (2004) and Shibuya et al. (1997) showed that small gaps below 1 mm resulted in large friction angles, suggesting significant gaps should be adopted. To prevent specimen loss through the gaps they proposed using edging. However, as Simoni and Houlsby (2006) pointed out, the proposed gaps can be very large when testing large particle sizes, leading to impractical edging arrangements. A closer examination of the data presented by Lings and Dietz (2004) and Shibuya et al. (1997) suggests that a gap of 2 mm should be adequate in most instances.

Table 5.2: Proposed gap sizes

Gap Size	Reference
0.63 mm and higher for granular material	ASTM D3080
Not exceed 1 mm	BS 1377-7:1990
Initial gap of 1 mm	Simoni and Houlsby (2006)
4 mm or $5D_{50}$	Lings and Dietz (2004)
$10\text{-}20D_{50}$	Shibuya et al. (1997)

As pore pressures cannot be measured in the DSB, it is important that no shear induced pore pressures develop. This is achieved by matching the shear rate to the material's permeability as shown by its rate of consolidation (Germaine and Germaine, 2009). ASTM D3080 requires that the time to failure be 50 times the time required for the specimen to achieve 50 % consolidation under the specified vertical stress. Shearing normally consolidated clays too fast results in reduced strengths, but for over-consolidated clays the measured strength will be too high (Germaine and Germaine, 2009). Estimating consolidation times for granular materials is difficult as they often compress immediately. This reflects the fact that under most conventional loading scenarios excess pore pressures do not develop in granular soils. Shear rates reported in literature for sands are given in Table 5.3.

Table 5.3: Proposed shear rates

Shear rate (mm/min)	Reference
0.25	Shibuya et al. (1997)
1.0	Guo (2008)
1.2	Lings and Dietz (2004)

Interpretation of results

A major disadvantage of the DSB is that only stresses on the horizontal plane are measured with no way of quantifying stresses on the vertical plane. Consequently only one point on a Mohr diagram can be plotted through which a multitude of potential circles can be drawn. The conventional approach of interpretation is to assume that plane strain/simple shear deformation occurs, with the failure plane coincident to the horizontal plane formed between the two halves of the box. Under these assumptions the direct shear angle of friction (ϕ_{ds}) is equal to the plane strain angle of friction (ϕ_{ps}), the angle that defines the Mohr-Coulomb failure envelope (Matthews, 1988). With ϕ_{ds} obtained from the average boundary measurements of

horizontal shear stress (τ_{yx}) and vertical stress (σ_{yy}) using (Skempton and Bishop, 1950):

$$\tan \phi_{ds} = \frac{\tau_{yx}}{\sigma_{yy}} \qquad \text{Equation 5.1}$$

The angle of dilation (ψ) is obtained from the incremental vertical displacement (δv), expansion taken as positive and incremental horizontal displacement (δh) using:

$$\tan \psi = \frac{\delta v}{\delta h} \qquad \text{Equation 5.2}$$

During testing, principal stress direction rotation occurs continuously until the peak stress is reached, potentially causing the failure plane to deviate from horizontal. By assuming the failure plane is inclined at $45\ ^\circ - \psi/2$ from the horizontal, the relationship between ϕ_{ds} and ϕ_{ps} is given by (Davis, 1968):

$$\tan \phi_{ds} = \frac{\sin \phi_{ps} \cos \psi}{1 - \sin \phi_{ps} \sin \psi} \qquad \text{Equation 5.3}$$

The conventional approach tends to underestimate ϕ_{ps} and the second approach tends to overestimate ϕ_{ps}. To quantify how much the value is overestimated Matthews (1988) advocates the use of stress-dilatancy relationships (or flow rules). Jewell (1989) highlights the inherent conservatism of using flow rules, especially if ψ is underestimated due to boundary measurements and if principal axes of stress and incremental strain do not coincide during testing.

Fundamentally, an accurate assessment of which approach should be used requires accurate plane strain data from simple shear devices to be compared with corresponding direct shear data (Arthur and Dunstan, 1988). Such an approach also

needs to take into account anisotropy, as the strength of granular materials depends on the orientation of bedding planes relative to the shear plane. Shearing along bedding planes results in the minimum friction angle, and the friction angle can be 25 % higher when shearing is perpendicular to the bedding planes (Jewell, 1989).

With induced rotational restraint, Jewell and Wroth (1987) and Lings and Dietz (2004) advocated that Equation 5.3 is best suited to interpreting results. Arthur and Dunstan (1988) suggested an interpretation based on Equation 5.1 should still be used. For enforced rotational restraint, Shibuya et al. (1997) showed results interpreted with Equation 5.1 compared well with flow rules and torsional simple shear, although Equation 5.3 is used with some success to take into account anisotropy in comparison with simple shear.

Flow rules

The frictional strength of soil is made up of sliding, rolling and interlocking friction. Rolling friction is usually ignored, as it is difficult to separate from the phenomenon associated with particles riding over each other as the interlocking is released (Yong and Warkentin, 1975). Taylor (1948) proposed that the resistance due to sliding and interlocking could be differentiated by energy considerations. Firstly, the total dissipated work in shearing is determined. Then the work dissipated in volume increase, which is associated with interlock release or dilation, is determined. The difference gives the dissipated work in sliding. Jewell (1989) cites experimental work by Stroud (c1971) as confirming this hypothesis and Houlsby (1991) showed that this relationship could be expressed mathematically, using the conventional interpretation, i.e. Equation 5.1 and Equation 5.2, as:

$$\tan \phi_{ds} = \tan \phi_{cv} + \tan \psi \qquad \text{Equation 5.4}$$

where ϕ_{cv} is the plane strain friction angle associated with shearing at constant volume ($\psi = 0$) and is equal to the friction angle at the critical state (ϕ_{crit}) (Sadrekarimi and Olson, 2011). Alternatively using the second approach, i.e. Equation 5.3, as:

$$\tan \phi_{ds} = \sin \phi_{cv} + \tan \psi \qquad \text{Equation 5.5}$$

Rowe (1962) developed a stress-dilatancy theory based on assemblies of spheres and obtained an expression relating the stress ratio (σ'_1/σ'_3), strain rate ratio ($-d\varepsilon_3/d\varepsilon_1$) and the fundamental angle of friction for grain-to-grain contact (ϕ_u):

$$\frac{\sigma_1'}{\sigma_3'} = \tan^2\left(\frac{\pi}{4} + \frac{\phi_u}{2}\right)\left(\frac{-d\epsilon_3}{d\epsilon_1}\right) \qquad \text{Equation 5.6}$$

Using experimental work Houlsby (1991) suggested that ϕ_u could be replaced with ϕ_{cv}. Lings and Dietz (2004), therefore, replaced ϕ_u with ϕ_{cv} and derived the following equation:

$$\sin \phi_{ps} = \frac{\sin \phi_{cv} + \sin \psi}{1 + \sin \phi_{cv} \sin \psi} \qquad \text{Equation 5.7}$$

Bolton (1986) adopted an empirical approach and suggested the following equation:

$$\phi_{ps} = \phi_{cv} + 0.8\psi \qquad \text{Equation 5.8}$$

Equation 5.8 was developed by relating peak friction angles and maximum dilation rates from various plain strain and triaxial tests assuming similarity in results. This assumption was questioned by Houlsby (1991). Lehane and Liu (2013) suggested that the constant in Equation 5.8 decreases with reducing stress level and is closer to 0.71 - 0.75 for direct shear. It can be shown that Taylor's and Bolton's flow rules in Equation 5.5 and Equation 5.8 respectively closely bound that proposed by Rowe in Equation 5.6 (Jewell, 1989).

It is important to note at this point that dilation is related to the density of the specimen and inversely related to vertical stress, although only slightly (Bolton, 1986, Houlsby, 1991). A comprehensive discussion on this relationship requires introducing concepts of critical state soil mechanics. Central to this is the critical void ratio, which is the void ratio at which the critical friction angle is mobilised. It is not possible to track changes in void ratio within the direct shear box and, therefore, applying critical state soil mechanics directly to the results is not possible.

The accuracy of individual tests can be ascertained by plotting the tangent of the mobilised friction angle ($\tan \phi_{ds} = \tau_{yx}/\sigma_{yy}$) against the current dilation rate ($\tan \psi = \delta v/\delta h$) as the test progresses. This relationship can then be compared to the various flow rules. Multiple tests can be assessed by plotting the peak friction angles against the maximum dilation rates and comparing these to the flow rules (Jewell, 1989).

Key to using flow rules is choosing an appropriate value for ϕ_{cv} as this appears in all the flow rules. The critical friction angle, ϕ_{cv} depends on factors such as mineralogy, particle shape, interparticle friction, particle size distribution, particle damage during shear and mode of shear (Sadrekarimi and Olson, 2011). Bolton (1986) observed that ϕ_{cv} rarely falls outside a range between 32.0 and 37.0 °. Lower values are typically obtained for quartz sands and higher values for feldspathic sands and increasing particle angularity. For angular particles, ϕ_{cv} can be as high as 40 °. Methods to measure ϕ_{cv} include:

- Simple shear tests on loose specimens (Bolton, 1986),
- Triaxial tests (Bolton, 1986, Sadrekarimi and Olson, 2011),
- Direct ring shear tests (Sadrekarimi and Olson, 2011),
- Dry angle of repose subject to toe excavation (Bolton, 1986, Jewell, 1989, Sadrekarimi and Olson, 2011),
- Saturated angle of repose obtained by tilting a specimen in a volumetric cylinder (Santamarina and Cho, 2001) and

- The angle of a continuously failing slope in a rotating cylinder (Atkinson, 2007)
- Or, simply mineralogy (Bolton, 1986, Jewell, 1989).

Schanz and Vermeer (1996) suggest that ϕ_{cv} is generally independent of experimental method. Santamarina and Cho (2001) report that the coefficient of variation for values of ϕ_{cv} determined by the saturated angle of repose obtained in a tilted cylinder is less than 5 % suggesting the standard deviation is less than 1.5 °. The saturated method can result in lower values in silty sands due to liquefaction, which is avoided when the tests are carried out dry. Sadrekarimi and Olson (2011) suggest the direct ring shear is preferable to triaxial testing for determining ϕ_{cv}, with the coefficient of variation ranging between 1 and 3 %. The angle of repose values reported by these authors fell within this range. Lings and Dietz (2004) report that ϕ_{cv} values, determined by the angle of repose, are on average within 0.6 ° of values obtained from simple shear tests. Although simple shear, triaxial and direct ring shear tests may give better results, values obtained from angle of repose tests appear adequate for most purposes.

Flow rules can also be used to obtain values of ϕ_{cv} from multiple direct shear tests (Simoni and Houlsby, 2006). This is done by plotting measured peak ϕ_{ds} against peak ψ and using linear regression to determine ϕ_{cv}, which is the intercept value based on Equation 5.8.

5.3 Calibration test work

From the review of research into DSB testing, it is apparent that there are some potential sources of error due to the necessary boundary conditions adopted for facilitating seepage in the variedSB. The following two sources were deemed sufficiently significant to investigate.

- The effect of measuring the vertical force above the failure plane and the possibility of using lubrication to reduce in-box friction, given that the top-half is fully restrained.
- The effect of particle size and aspect ratio on the measured shear response. This is important as soils tested included gravel sized particles and the specimen height reduced during salt dissolution.

The following aspects, which may influence results, were not investigated, as it was not anticipated that they would introduce significant error.

- Lings and Dietz (2004) suggest that loads cells used should be unaffected by side loading. However, the S-Type load cells used, although stiffer than most commercially available load cells, are not designed purposefully for side loading.
- A constant gap size of 2 mm was used for all tests.
- A shear rate of 0.50 mm/min was used for all tests apart from some initial tests where a shear rate of 0.43 mm/min was used.

This calibration testing, along with the review of research on interpreting DSB test results, provided the basis for interpreting the data obtained.

5.3.1 Material used

Two materials were used for calibration testing: a commercially crushed silica sand (99.8 % silica) and a non-plastic residual granite gravel. Particle size distributions (PSD) for the materials are shown in Figure 5.6. The silica sand is a poorly graded coarse sand, whereas the gravel is a poorly graded fine gravel. Light microscope images of the silica sand particles (Figure 5.7) show that the particles are angular to sub-angular (Cho et al. (2006) Sphericity values between 0.7 and 0.9, and Roundness values between 0.1 and 0.3). Digital photograph images of the gravel particles (Figure 5.8) show that and the particles are sub-angular with moderate sphericity (Cho et al. (2006) Sphericity values between 0.5 and 0.7, and Roundness values between 0.5 and 0.7). Key characteristics of the soils are given in Table 5.4. The small pyknometer method in accordance with clause 8.3 of BS1377: Part 2: 1990 was used to determine G_s. Maximum void ratio was determined using the ASTM D4254 funnel method and minimum void ratio by pouring small increments of material into a standard mould which was successively tapped with a rubber mallet (Lade et al., 1998, Cubrinovski and Ishihara, 2002).

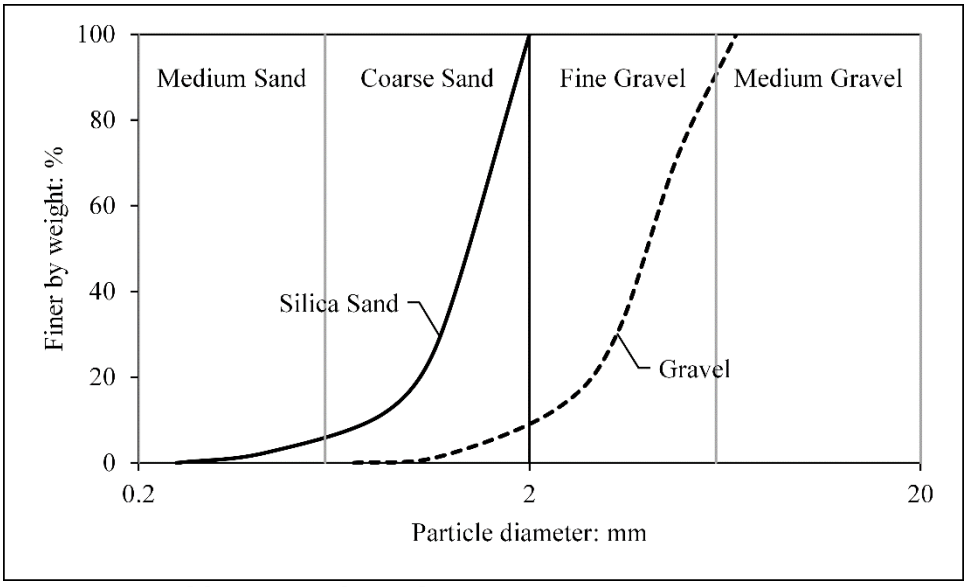


Figure 5.6: Calibration soils gradations

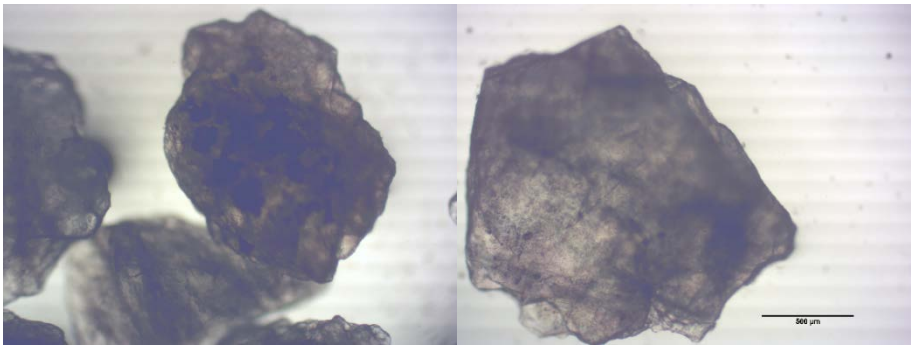
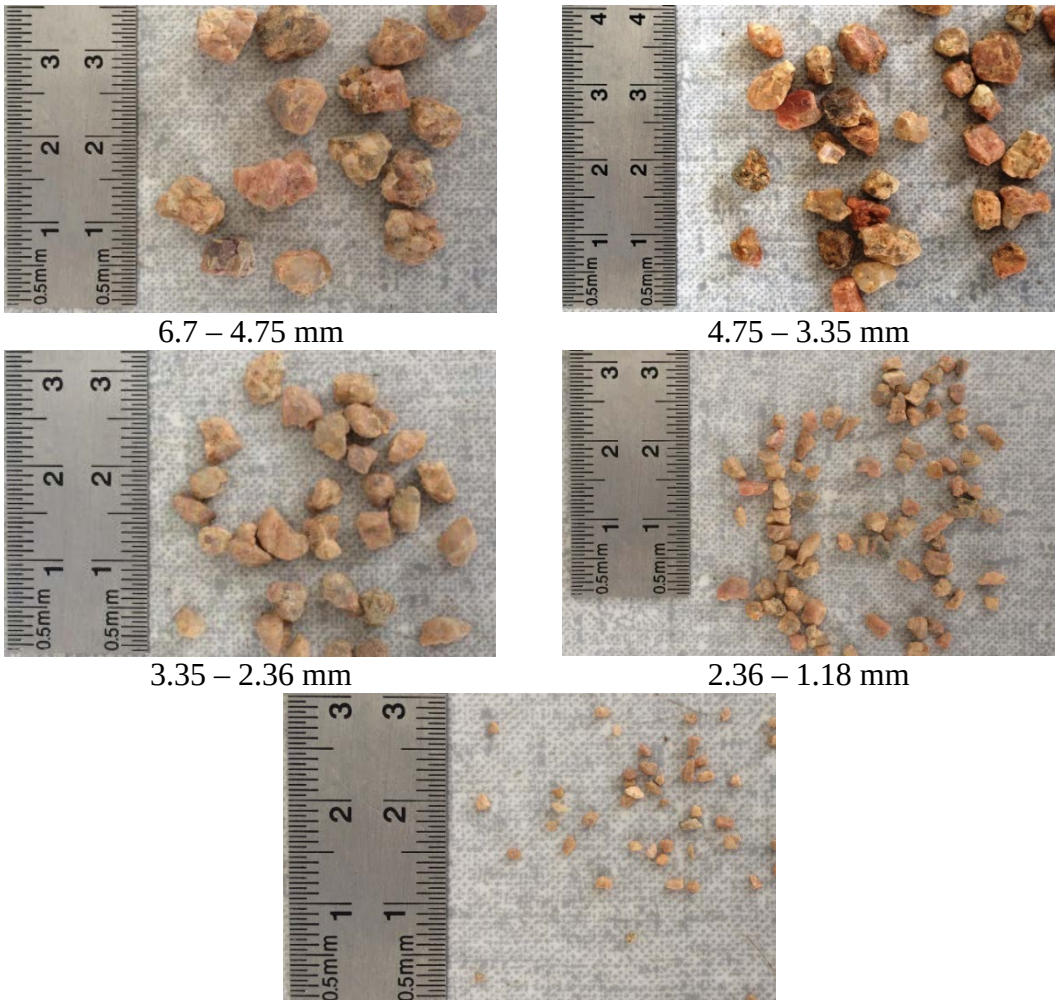


Figure 5.7: Light microscope images of silica sand particles



6.7 – 4.75 mm

4.75 – 3.35 mm

3.35 – 2.36 mm

2.36 – 1.18 mm

1.18 – 0.710 mm

Figure 5.8: Digital photograph images of gravel particles

Table 5.4: Calibration soils characteristics

Parameter	Material	
	Silica Sand	Gravel
Particle specific gravity, G_s	2.66	2.66
Maximum void ratio, e_{max}	0.98	0.96
Minimum void ratio, e_{min}	0.70	0.71
Median particle size, D_{50} (mm)	1.5	4.2
Maximum particle size, D_{max} (mm)	2.0	6.7

5.3.2 Test procedure

In-box friction

The first set of tests investigated whether measuring the vertical force above the failure plane would significantly affect results and whether lubricating the inner walls of the shear box could alleviate the frictional effects. Two means of lubricating the inner wall were investigated: using petroleum jelly only and using silicone grease with a latex membrane. Testing was carried out on dense and loose specimens.

Air-dried silica sand was rained through a height of 300 mm to produce dense specimens and loose specimens were prepared by pouring the sand through a funnel as proposed by Germaine and Germaine (2009). After the specimen was placed, the top was flattened and the top platen placed. The shear box was carefully transferred to the frame and secured. Thereafter, the bath was flooded and a vertical stress (σ_{yy}) of 149 ± 1.5 kPa applied in a single step (these are referred to as tests at 150 kPa). The initial void ratio (e) was then determined. The relative density after application of the vertical load (D_r) was 95 – 99 % for the dense specimens and 38 – 49 % for the loose specimens. Following consolidation, which was immediate, shearing was initiated at a rate of 0.43 mm/min. Testing was continued until the vertical displacement became constant, roughly after 14 mm of horizontal displacement. A summary of the calibration-testing program using the silica sand is given in Table 5.5.

Table 5.5: Summary of silica sand testing program

Test identification	Initial e	D_r (%)	Wall lubrication	Initial σ_{yy} (kPa)
C-V-D-150-1	0.70	99	Petroleum jelly	149
C-V-D-150-2	0.70	99		151
C-V-L-150-1	0.85	45		149
C-V-L-150-2	0.87	38		149
C-SL-D-150-1	0.71	95	Latex and silicone grease	148
C-SL-D-150-2	0.70	99		149
C-SL-D-150-3	0.70	99		146
C-SL-L-150-1	0.84	49		151
C-SL-L-150-2	0.86	41		151
C-SL-L-150-3	0.85	45		150

Specimen height and particle size

The second set of tests investigated the impact of particle size and aspect ratio (L/H). For the silica sand, L/D_{max}, H/D_{max} and L/H were 50, 21 and 2.4 respectively. While these values adequately meet the requirements of ASTM D3080, it is only L/D_{max} that meets the more stringent requirements suggested by Wang and Gutierrez (2010). However, the material used in the main testing program (reported in Chapter 7) is substantially coarser than the silica sand. Furthermore, during salt dissolution, the specimen height decreased.

To investigate the effect of changing specimen height and particle size, gravel specimens with various specimen heights were tested. The width of the box could not be varied with L/D_{max} remaining 15, meeting the ASTM D3080 requirements but not the Wang and Gutierrez (2010) requirements. H/D_{max} was varied between 6.7 and 4.9, the lower values not meeting the ASTM D3080 requirements, and no specimens meeting the Wang and Gutierrez (2010) requirements. Further, it should be noted that the specimen height above the shear plane was varied, as this reflected settlement during salt dissolution. The aspect ratio (L/H) for all tests met the ASTM D3080 requirements but fell outside the range suggested by Wang and Gutierrez (2010).

The specimens were prepared as either dense or loose, in a similar manner as used for the silica sand, and latex membranes and silicone grease were used to lubricate the walls in all tests. Testing was carried out at an initial vertical stress of either 73 ± 0.9 kPa or 147 ± 2.1 kPa (referred to as tests at 75 and 150 kPa respectively). Due to the large particles, it was more difficult to determine an accurate specimen height, as the surface was more undulated. This affected the accuracy with which the initial void ratio could be determined. Following consolidation, which was immediate, shearing was initiated at a rate of 0.50 mm/min. Testing was continued until the vertical displacement became constant, roughly after 16 mm of horizontal displacement. A summary of the calibration-testing program using the gravel is given in Table 5.6.

Table 5.6: Summary of gravel testing program

Test identification	L/D_{max}	H/D_{max}	L/H	Initial e	D_r, %	Initial σ_{yy} (kPa)
G-D-150-1	15	6.6	2.3	0.69	100	145
G-D-150-2		6.7	2.2	0.71	98	147
G-D-150-7		5.9	2.5	0.70	100	147
G-D-150-4		5.9	2.5	0.70	100	146
G-D-150-6		4.9	3.0	0.69	100	151
G-D-150-3		5.1	2.9	0.72	95	147
G-L-150-1		6.6	2.3	0.92	16	144
G-L-150-4		6.5	2.3	0.91	18	144
G-L-150-5		5.7	2.6	0.90	23	146
G-L-150-3		5.7	2.6	0.91	21	147
G-L-150-2		4.9	3.1	0.93	11	144
G-L-150-6		4.9	3.1	0.94	6	151
G-D-75-1		6.6	2.2	0.70	100	73
G-D-75-3		6.6	2.2	0.70	100	74
G-D-75-4		5.9	2.5	0.74	89	74
G-D-75-5		5.8	2.6	0.69	100	73
G-L-75-1		6.7	2.2	0.95	4	73
G-L-75-3		6.6	2.3	0.93	10	74
G-L-75-4		5.2	2.9	0.96	0	71
G-L-75-2		5.1	2.9	0.98	0	72

5.3.3 Results

Figure 5.9 shows the results of two tests on dense silica sand. In one test, the inside of the shear box was lubricated with petroleum jelly and in the other with latex membranes and silicone grease. It can be seen that larger shear resistance is recorded throughout the test when petroleum jelly is used. However, the recorded vertical displacement is essentially the same for both methods of lubrication. A similar trend is observed for the loose silica sand (Figure 5.10).

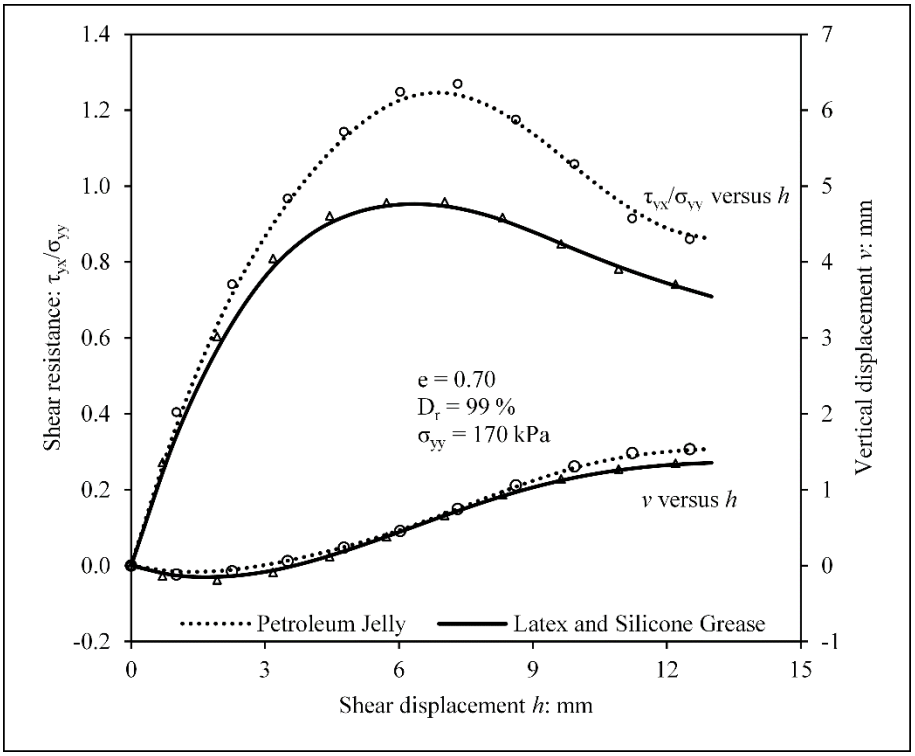


Figure 5.9: Behaviour of dense silica sand with different methods of lubrication (average σ_{yy} is indicated)

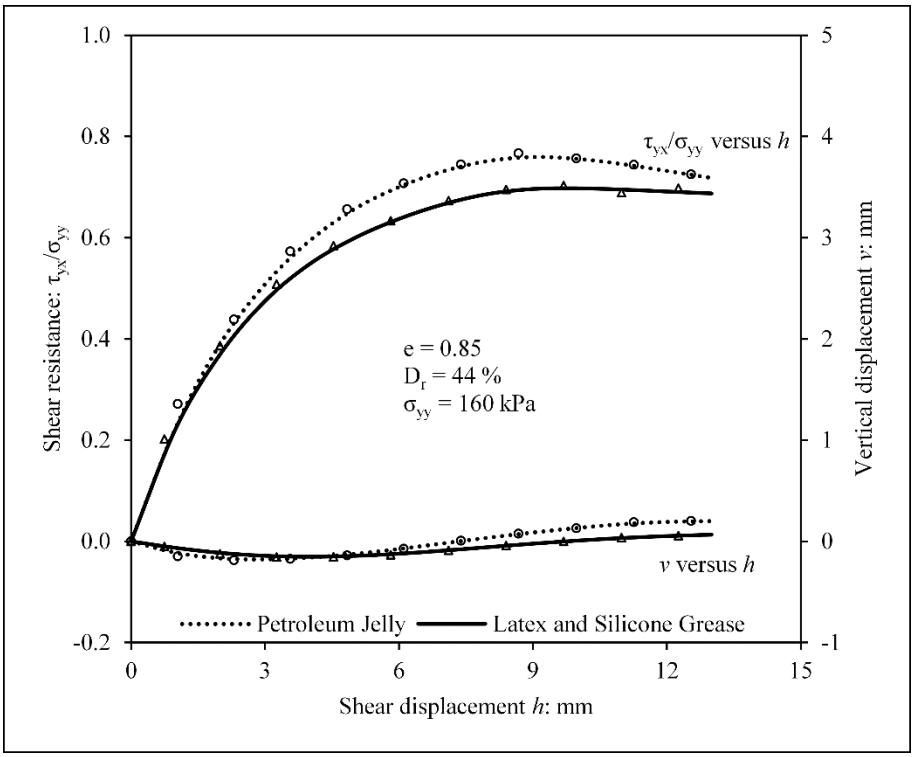


Figure 5.10: Behaviour of loose silica sand with different methods of lubrication (average σ_{yy} is indicated)

A smoothed line was fitted through the raw data (Figure 5.9 and Figure 5.10) using a spline function algorithm (Klasson, 2008). The peak value of τ_{yx}/σ_{yy} was used to obtain values of peak friction angle (ϕ_p) using Equation 5.1. The spline function algorithm (Klasson, 2008) enables one to calculate the derivatives of the fitted spline. This was used to determine the maximum value of $\delta v/\delta h$ from which ψ was calculated using Equation 5.2. A summary of ϕ_p and ψ obtained for all the silica sand tests is given in Table 5.7.

Table 5.7: variedSB results on silica sand

Test identification	Consistency†	Wall lubrication	ϕ_p (°)	ψ (°)	Increase in V_F	Average σ_{yy} (kPa)
C-V-D-150-1	Dense	Petroleum jelly	47.7	10.9	15 %	174
C-V-D-150-2			51.2	12.7	12 %	176
C-V-L-150-1	Loose		39.4	3.6	3 %	164
C-V-L-150-2			37.2	3.3	3 %	162
C-SL-D-150-1	Dense	Latex and silicone grease	43.5	11.8	14 %	174
C-SL-D-150-2			43.6	12.0	11 %	172
C-SL-D-150-3			45.3	13.3	15 %	172
C-SL-L-150-1	Loose		35.2	2.6	1 %	169
C-SL-L-150-2			34.9	2.0	10 %	169
C-SL-L-150-3			35.0	2.1	1 %	164
† Consistency is a descriptor of a specimen's state of compactness						

Figure 5.11 shows that the measured vertical force (V_F) increased during shear, which is attributed to the effect of dilation and friction in the linear bearing. The difference between the maximum V_F and the initial V_F for each test is indicated in Table 5.7 as a percentage of the initial V_F. The average vertical stress (σ_{yy}) for each test, also given in Table 5.7, was calculated from the average V_F and average sheared surface area.

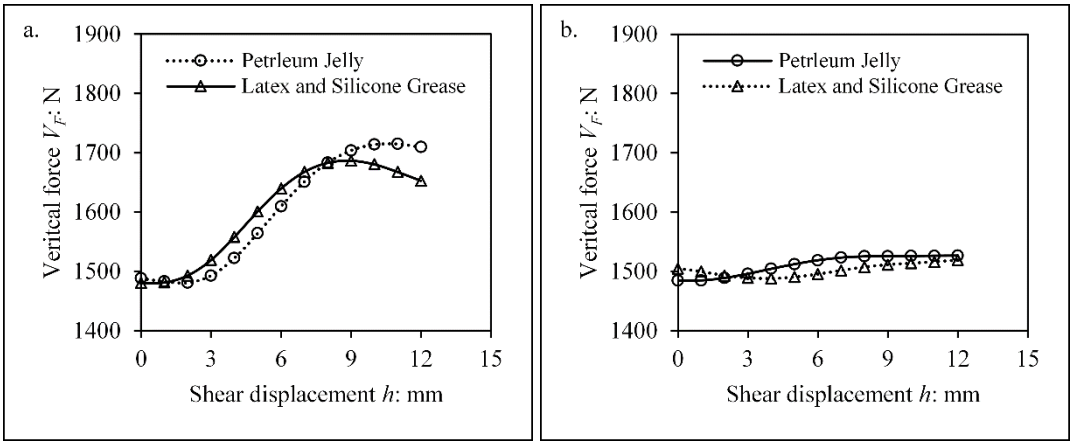


Figure 5.11: Change in vertical force during shear for a. dense and b. loose silica sand specimens

Figure 5.12 shows the results of two tests on dense gravel, with different specimen heights. It can be seen that the shear resistance recorded throughout the test is lower for the smaller specimen height. However, the recorded vertical displacement is essentially the same for both specimen heights. The shear resistance curves obtained for the gravel specimens are not as smooth as obtained for the silica sand, because of the larger particles. For the loose gravel, there is less distinction between the shear resistance and vertical displacements for the different specimen heights (Figure 5.13). Values of ϕ_p and ψ, obtained in the same manner as for the silica sand, are summarised in Table 5.8. Figure 5.14 illustrates the effect of dilation and friction in the linear bearing on the measured vertical force (V_F). The difference between the maximum V_F and the initial V_F for each test is indicated in Table 5.8 as a percentage of the initial V_F. The average vertical stress (σ_{yy}) for each test, also given in Table 5.8, was calculated from the average V_F and average sheared surface area.

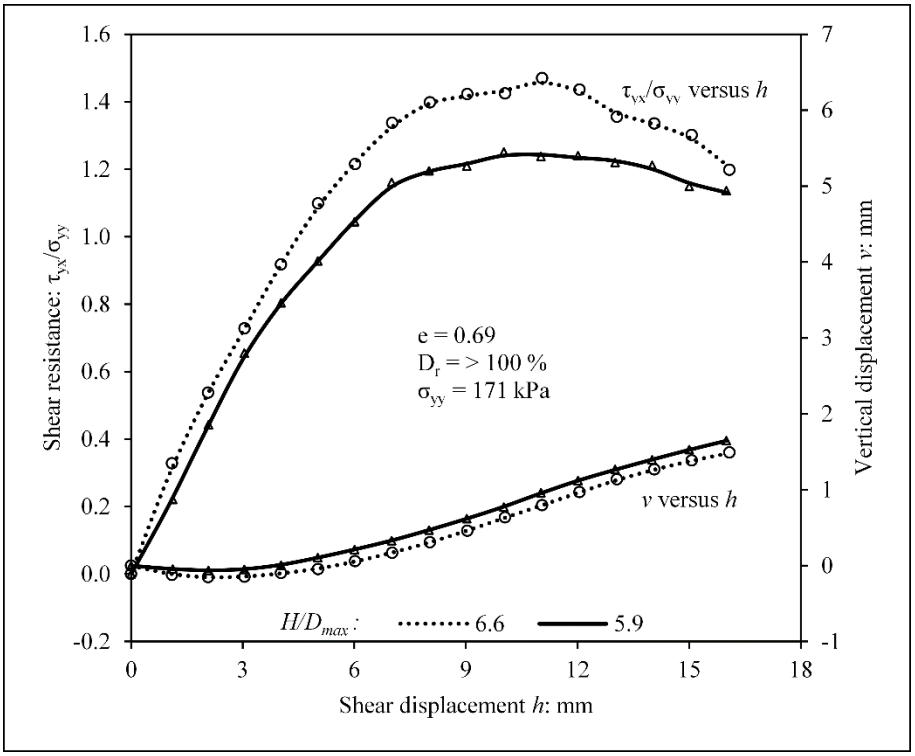


Figure 5.12: Behaviour of dense gravel with different specimen heights (average σ_{yy} is indicated)

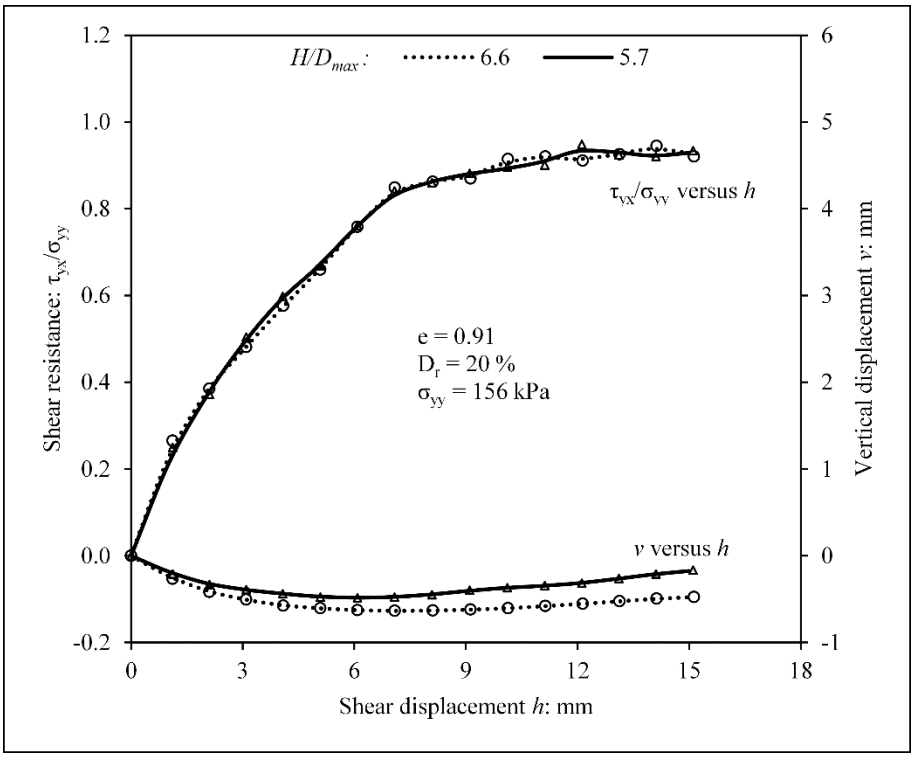


Figure 5.13: Behaviour of loose gravel with different specimen heights (average σ_{yy} is indicated)

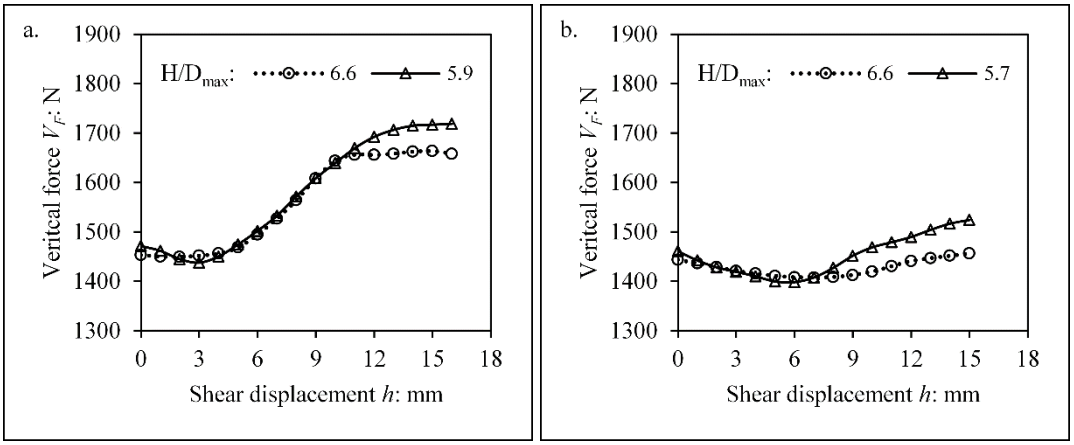


Figure 5.14: Change in vertical force during shear for a. dense and b. loose gravel specimens

Table 5.8: variedSB results on gravel

Test identification	Consistency	H/D_{max}	ϕ_p (°)	ψ (°)	Increase in V_F	Average σ_{yy} (kPa)
G-D-150-1	Dense	6.6	55.5	9.6	14 %	170
G-D-150-2		6.7	55.3	10.6	8 %	166
G-D-150-7		5.9	51.2	10.0	17 %	171
G-D-150-4		5.9	50.0	11.2	12 %	169
G-D-150-6		4.9	47.1	10.1	10 %	175
G-D-150-3		5.1	44.8	10.2	5 %	165
G-L-150-1	Loose	6.6	43.2	1.7	1 %	154
G-L-150-4		6.5	42.5	1.6	0 %	153
G-L-150-5		5.7	43.0	3.1	4 %	157
G-L-150-3		5.7	42.9	3.2	6 %	159
G-L-150-2		4.9	36.6	2.5	4 %	159
G-L-150-6		4.9	38.0	1.5	0 %	161
G-D-75-1	Dense	6.6	59.2	16.0	4 %	80
G-D-75-3		6.6	55.8	16.4	5 %	82
G-D-75-4		5.9	53.4	16.3	10 %	82
G-D-75-5		5.8	53.3	17.6	7 %	81
G-L-75-1	Loose	6.7	45.7	3.8	0 %	78
G-L-75-3		6.6	49.6	6.5	3 %	81
G-L-75-4		5.2	42.2	5.7	3 %	78
G-L-75-2		5.1	39.4	4.1	1 %	78

5.3.4 Comparison of results

Increase in vertical force

It was not possible to control the increase in vertical force during testing, therefore the effect of this on results is now considered. Results from all tests on silica sand are plotted against the observed increase in vertical force during testing in Figure 5.15. No differentiation is made between whether petroleum jelly or latex and silicone

grease was used to lubricate the box. As explained later, this accounts for the greater variability in ϕ_p compared to ψ values. Relevant statistical parameters for the plotted linear relationships are given in Table 5.9. All measured ϕ_p and ψ values showed very weak correlation with the observed increase in vertical force. This suggests the increasing vertical force does not have a controlling influence on results.

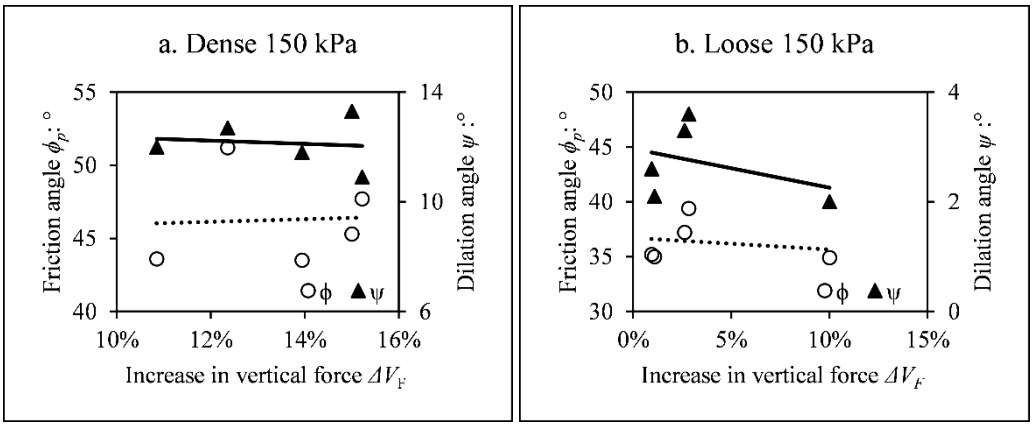


Figure 5.15: Influence of increase in the vertical force on variedSB results for silica specimens

Table 5.9: Statistical parameters describing influence of the increase in vertical force on variedSB results on silica specimens

Test Series	Correlation coefficients	
	ϕ_p vs. ΔV_F	ψ vs. ΔV_F
Dense 150 kPa	0.05	-0.21
Loose 150 kPa	-0.12	-0.37

Results from all tests on gravel are plotted against the observed increase in vertical force during testing in Figure 5.16. No differentiation is made between specimen heights. Relevant statistical parameters for the plotted linear relationships are given in Table 5.9. Most measured ϕ_p and ψ values showed very weak correlation with the observed increase in vertical force. However, ϕ_p values showed strong negative correlation with the increase in vertical force for tests done on dense specimens at 75 kPa. Whilst this suggests that, the increase in vertical force had an effect, H/D_{max} was also changing and this will be shown to have a more consistent effect. Dilation angles for tests on loose specimens showed strong positive correlation with the observed increase in vertical force. However, the dilation angles did not increase substantially, with the range of dilation angles being similar to those from tests on dense specimens.

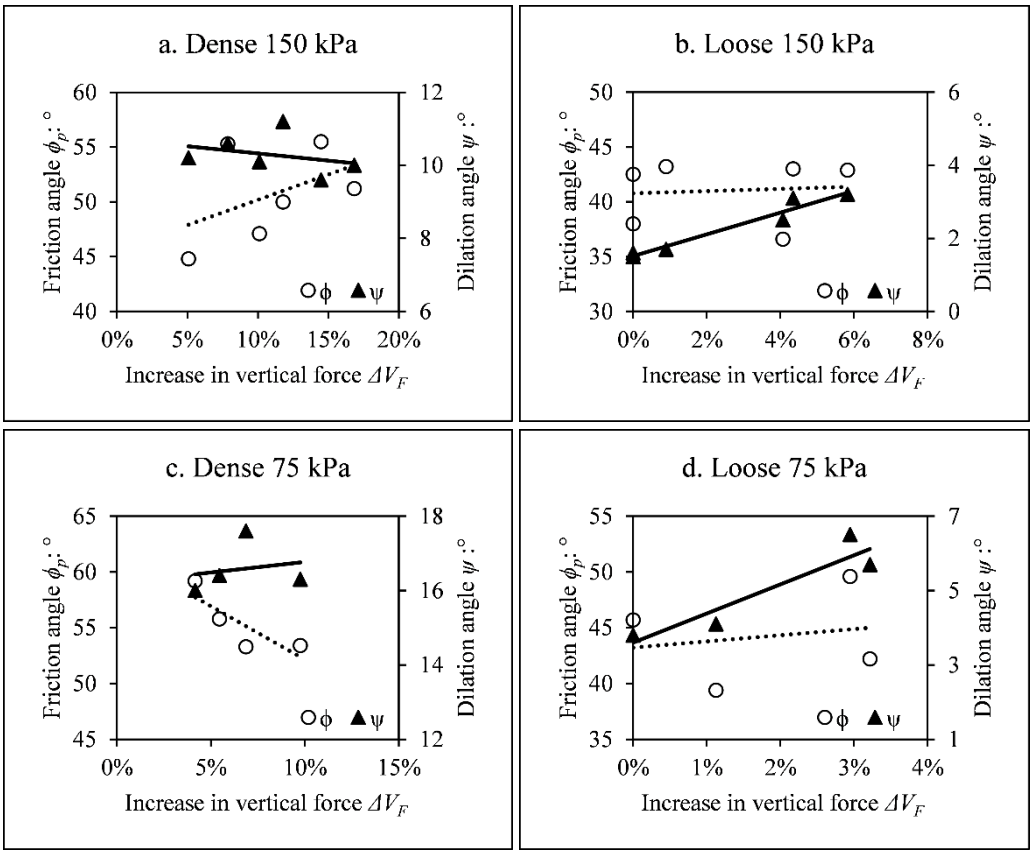


Figure 5.16: Influence of the increase in vertical force on variedSB results for gravel specimens

Table 5.10: Statistical parameters describing influence of the increase in vertical force on variedSB results on gravel specimens

Test Series	Correlation coefficients	
	ϕ_p vs. ΔV_F	ψ vs. ΔV_F
Dense 150 kPa	0.32	-0.09
Loose 150 kPa	0.09	0.97
Dense 75 kPa	-0.83	0.20
Loose 75 kPa	0.19	0.93

In-box friction

Results from the silica sand tests are compared to various flow rules (Figure 5.17) assuming ϕ_{cv} equals 34 °. This value of ϕ_{cv} was estimated from the angle of a continuously failing slope in a rotating cylinder (Atkinson, 2007). The final recorded friction angles (approaching constant volume conditions) for loose silica specimens (Figure 5.10) were on average 34 °. This is consistent with the estimated ϕ_{cv} value. It is apparent that tests using latex membranes and silicone grease resulted in values of ϕ_p and ψ closer to those anticipated by flow rules. This suggests that sufficient lubrication can be achieved by using latex membranes and silicone grease. Tests on

dense specimens with petroleum jelly resulted in high values of ϕ_p. In this case, petroleum jelly did not provide sufficient lubrication to prevent additional vertical stress being applied to the shear plane by in-box friction. The influence of lubrication, although similar for the loose specimens, was not so pronounced. A key observation from this comparison is that although the measured value ϕ_p may be high, depending on the method of lubrication, the values of ψ appear largely unaffected.

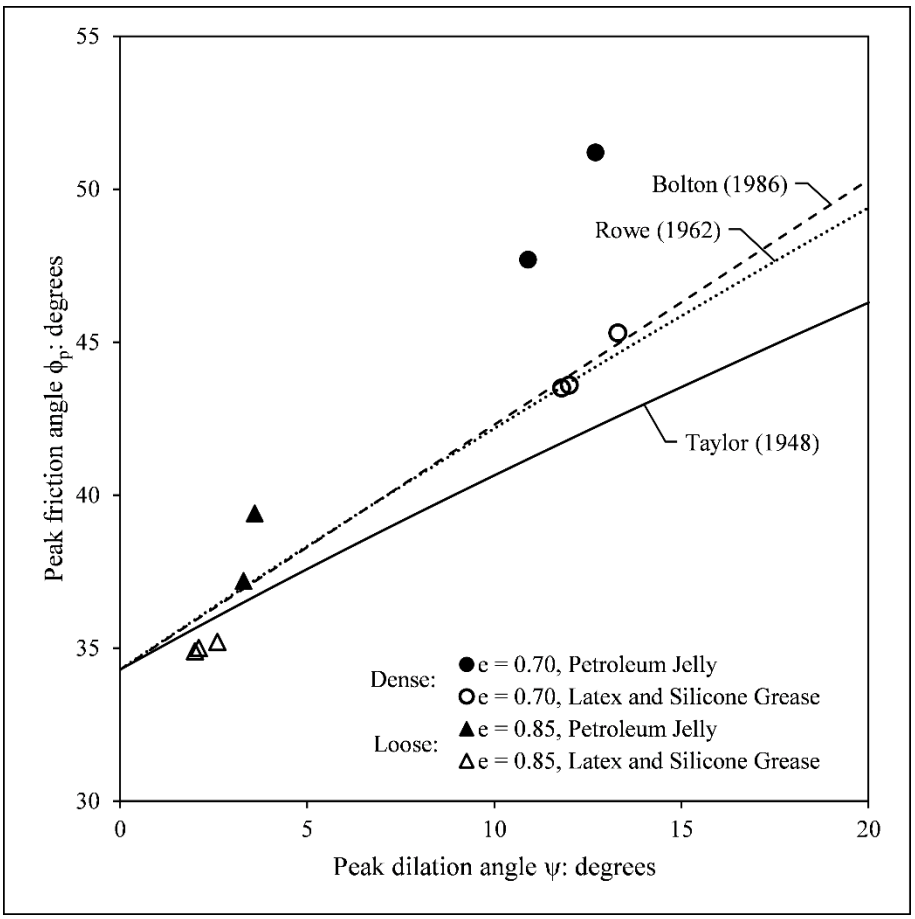


Figure 5.17: Influence of wall lubrication on variedSB results for silica sand

Tornado plots illustrating the variability due to wall lubrication are shown in Figure 5.18. The variability indicated in these plots is the range between the maximum and minimum value for each respective series. Inherent variability was calculated from tests done using only silicone grease with latex membranes for lubrication. Lubrication variability was calculated from tests done with both petroleum jelly and silicone grease with latex membranes. Comparing Figure 5.18a and Figure 5.18c, with Figure 5.18b and Figure 5.18d, it is evident that the measured values of ϕ_p showed greater sensitivity to lubrication compared to measured values of ψ.

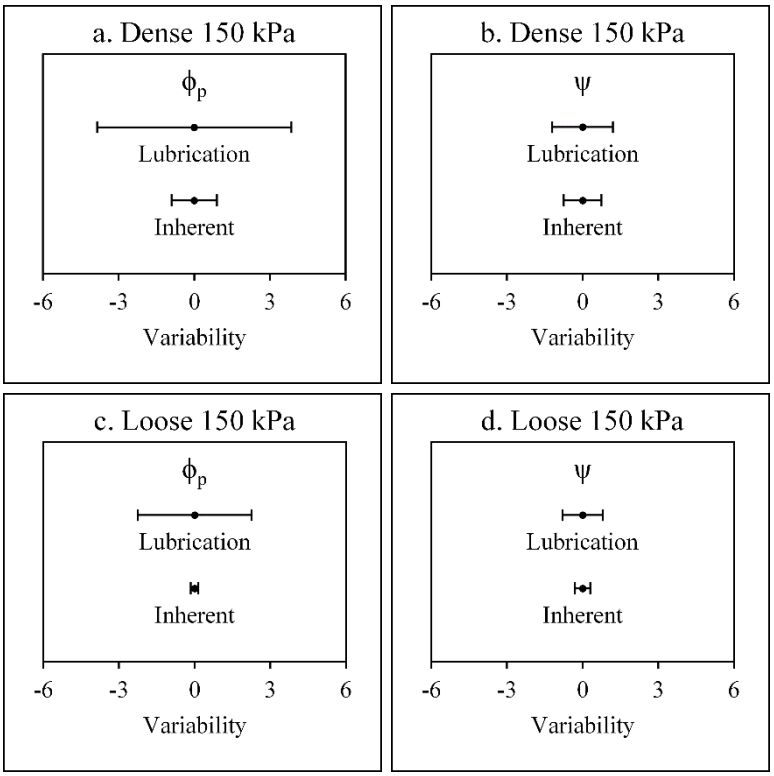


Figure 5.18: Influence of wall lubrication on measured ϕ_p and ψ values for silica sand specimens at 150 kPa

Specimen height and particle size

Results from the various tests on the influence of specimen height are compared in Figure 5.19. In each graph, ϕ_p and ψ are plotted against H/D_{max} and relevant statistical parameters for the plotted linear relationships are given in Table 5.11. All measured values of ϕ_p showed a strong positive correlation with specimen height. On the other hand, measured values of ψ, showed very weak correlation with specimen height.

Table 5.11: Statistical parameters describing influence of specimen height on variedSB results

Test Series	Correlation coefficients	
	ϕ_p vs. H/D_{max}	ψ vs. H/D_{max}
Dense 150 kPa	0.96	0.01
Loose 150 kPa	0.84	-0.22
Dense 75 kPa	0.86	-0.68
Loose 75 kPa	0.89	0.10

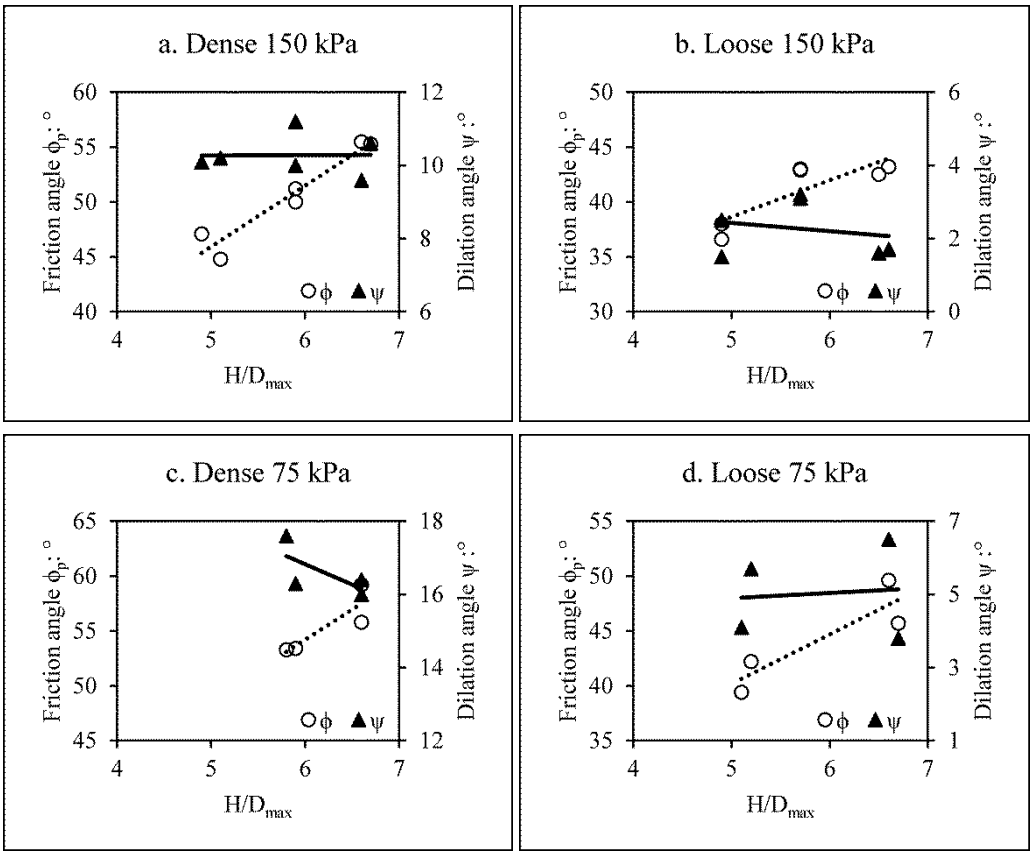


Figure 5.19: Influence of specimen height on variedSB results for gravel specimens

To explore the influence of specimen height further, values of ϕ_p and ψ, grouped according to specimen height, are plotted in Figure 5.20. For each grouping a flow rule according to Equation 5.8 (Bolton, 1986) is plotted through the data. As Equation 5.8 is a straight line, the value of ϕ_{cv} could be calculated to give the best fit to the data. It is apparent that the predicted value of ϕ_{cv} increases with specimen height. The value of ϕ_{cv} was estimated to be approximately 39 ° from the angle of a continuously failing slope in a rotating cylinder (Atkinson, 2007). Thicker specimens, therefore, resulted in higher measured values of ϕ_{cv}, whereas the thinner specimens resulted in a lower measured value. A possible explanation is that for thicker specimens, latex membranes and silicone grease did not provide sufficient lubrication, resulting in an underestimation of the vertical stress on the shear plane. Whereas, for the thinner specimens, the shear zone could not develop completely, resulting in an underestimation of shear stress.

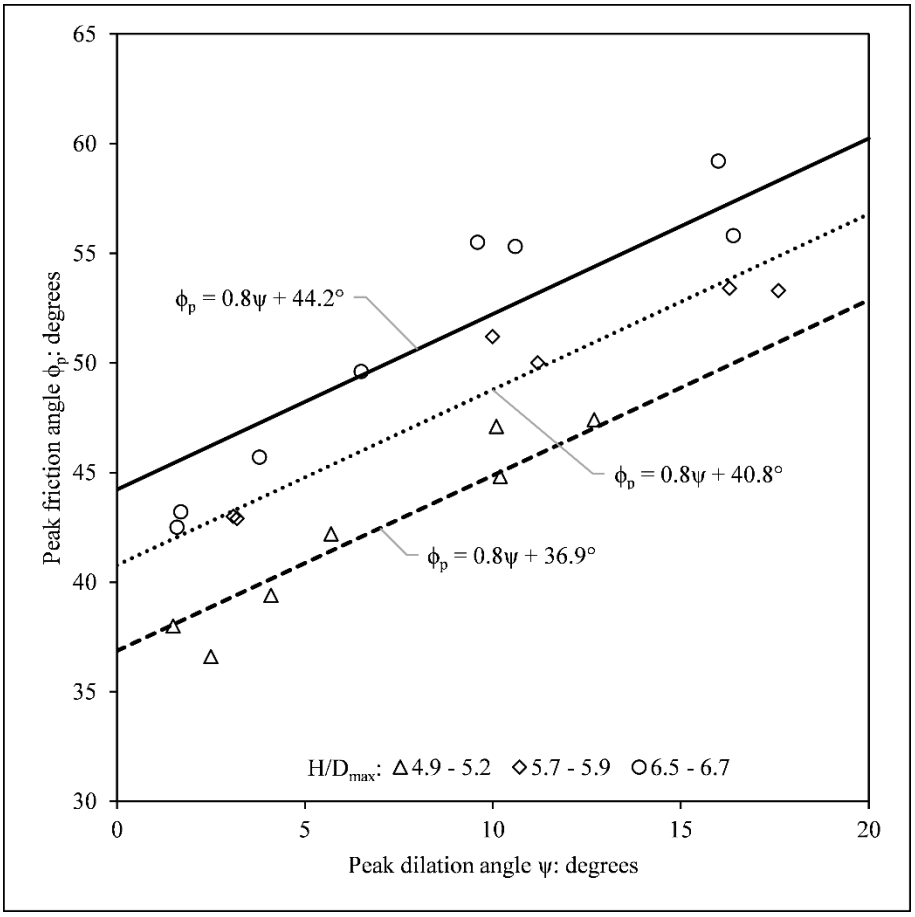


Figure 5.20: Influence of specimen height on variedSB results for gravel specimens

Tornado plots illustrating the variability due to specimen height are shown in Figure 5.21 for gravel specimens at 150 kPa. The variability indicated in these plots is the absolute difference between the maximum and minimum value for each respective series. Inherent variability was calculated from the paired tests done for H/D_{max} between 6.5 and 6.7. Specimen height variability was calculated from the full range of H/D_{max}. The inherent variability of ψ and ϕ_p is very low with the average range between extreme values being 0.25 °. Tornado plots illustrate (Figure 5.22) similar variability due to specimen height for gravel specimens at 75 kPa, although the inherent variability is greater. It is clear that at both applied stresses specimen height introduces considerably more variability to measured values of ϕ_p compared to measured values of ψ. A key observation is that, as with the silica sand, measured values of ψ appear largely independent of specimen height. This is important, as specimen height could not be controlled, as it was dependent on dissolution of the salt which represented eroded finer particles.

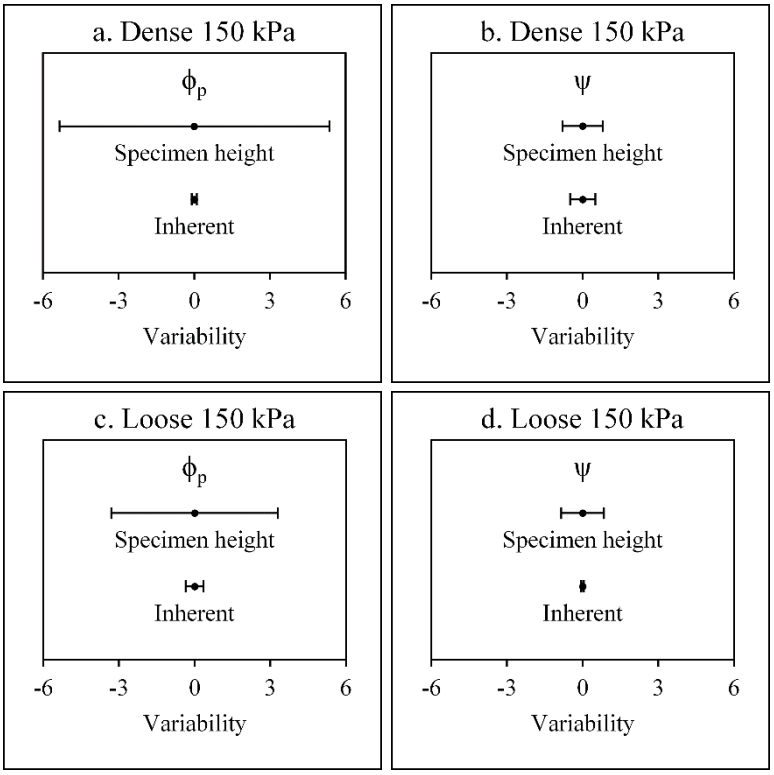


Figure 5.21: Influence of specimen height on measured ϕ_p and ψ values for gravel specimens at 150 kPa

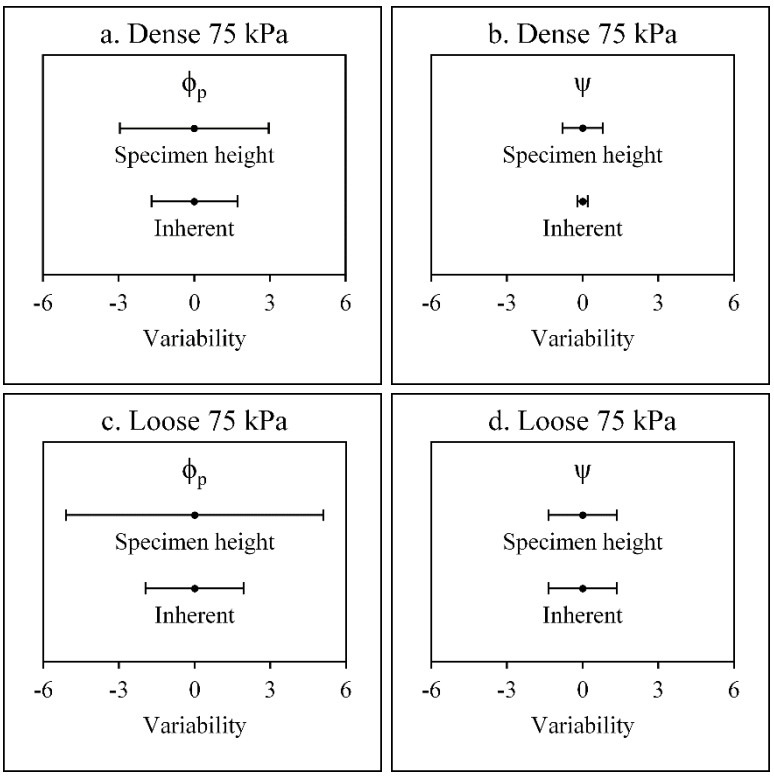


Figure 5.22: Influence of specimen height on measured ϕ_p and ψ values for gravel specimens at 75 kPa

5.4 Summary

Feasibility testing of using soil-salt mixtures to investigate the impact of internal erosion on mechanical behaviour found that modifications would be required to conventional direct shear box (DSB) equipment. These were to facilitate percolation of water through the shear box and to prevent rotation of the top platen. This was achieved by building a frame around a conventional DSB to fix the top-half and house a linear bearing, through which a vertical shaft ran, connected rigidly to the top platen.

A literature review of research into DSB testing equipment suggested that results from the variedSB could be erroneous due to two factors. Firstly, as the vertical force was measured by a load cell above the shear plane, increases in vertical stress due to in-box friction could not be measured. Secondly, the particle size of the gravel tested was relatively large for the given shear box and the specimen height decreased during salt dissolution. This could result in shear band formation being impeded, as the H/D_{max} ratio reduced. Calibration testing found that by utilising latex membranes and silicone grease the measured shear strength of silica sand was close to that anticipated by flow rules. However, this means of lubrication was insufficient to prevent in-box friction effects for the significantly coarser gravel. Measured shear resistance also correlated strongly to specimen height. The measured peak angle of dilation was found to be largely independent of both wall lubrication and specimen height.

As expected from flow rules, a strong relationship between peak dilation angles and friction angles was shown (Figure 5.17 and Figure 5.20). Thus, if an accurate measure of the peak dilation angle is possible, the shear strength of the specimen can be determined. As the main goal of this thesis was to quantify the change in shear strength due to internal erosion, peak dilation angles, which are subject to less test variation compared to friction angles due to boundary conditions necessary to facilitate seepage, can be adequately used to assess this change. As the dilation angle is a measure of that component of soil strength due to particle packing arrangements, and it is this arrangement that changes during internal erosion, the use of dilation angles is further justified in this study.

Chapter 6 Soil-salt mixture preparation considerations

This chapter outlines the development of methods to determine the maximum and minimum densities of gravel-sand and gravel-salt mixtures that were repeatable, minimised particle breakage and segregation, and correctly reproduced the void ratio of coarser fabric of the mixture. This was to establish a more accurate method for using salt as an analogue for sand, taking into account differences between salt and sand particle shape, hardness and particle specific gravity.

6.1 Measuring soil compactness

A soil consists of an assemblage of independent particles; the compactness of the soil influences its mechanical properties. The physical nature of the particles, that is particle size distribution and particle shape, dictates the loosest and densest possible states of the soil mass. The strength of a non-plastic soil will be a maximum at its densest packing and a minimum at its loosest packing, although this becomes less distinct at higher confining stress (Bolton, 1986). Compactness of a soil, or its physical state, can be referenced, therefore, to these limiting states of compactness. Common measures of compactness are: dry density, ρ_d (mass of dry soil per unit volume); porosity, n (ratio of voids volume to total volume); or void ratio e (ratio of void volume to solid volume). The selection of one measure of compactness over another is largely a matter of convenience or personal preference.

For spheres of uniform diameter, the minimum possible void ratio of 0.35 is obtained when the particles are arranged in a tetrahedral packing. Likewise, the maximum void ratio, in which all adjacent particles still touch is 0.91, and is obtained when the particles are arranged in a cubic packing. However, this arrangement is not stable in a gravitational field, which makes the theoretical maximum void ratio impossible to model (Lade et al., 1998). Natural soils are not uniform spheres and so, these limiting values are determined experimentally. Consequently, these are not actual extreme values but rather densest and loosest packings possible for a given set of procedures to produce them. They are termed, therefore, reference void ratios. Procedures used to

determine loosest packing rely on assembling a structure of particles with the maximum possible hindrance to their movement during assembly. On the other hand, densest packing relies on assembling the particles with as little hindrance as possible, so that particles can move about until the closest packing is achieved (Germaine and Germaine, 2009).

Tavenas and La Rochelle (1972) reported more than thirty experimental techniques for creating reference void ratio structures and advocated the adoption of standardised methods proposed by the American Society for Testing and Materials (ASTM). ASTM D4254 describes three methods to determine maximum void ratio: (i) funnel deposition; (ii) tube deposition into a standard mould and; (iii) inverting a soil-filled cylinder. ASTM D4253 describes the vibrating table method for determining minimum void ratio. The practice for this is first to determine maximum void ratio (e_{max}) by funnel deposition of an oven dry specimen into a standard mould. A collar is then fastened to the mould, a 13.8 ± 0.1 kPa surcharge placed on the specimen within the collar, the assembly secured to a vertically vibrating table and vibrated for a standard period, and the minimum void ratio (e_{min}) determined.

Of the three standard ASTM methods for determining e_{max}, the funnel method is reported to result in marginally higher void ratios (Tavenas and La Rochelle, 1972). The only difficulty in carrying out the funnel method in a research setting is the size of the standard mould recommended when limited quantities of material are available. However, special moulds are permitted, provided specimen height is 0.7 to 1.3 times the diameter. The funnel method described in ASTM D4254 was therefore adopted, although some minor variations were incorporated as described below.

Criticisms of the vibrating table method from literature are that many university laboratories do not have vibrating tables (Germaine and Germaine, 2009); particle breakage is possible (Lade et al., 1998); and the stipulation that the method can only be used for soils with less than 15 % passing the 0.075 mm sieve (Cubrinovski and Ishihara, 2002). Although a vibrating table was available for the present study,

excessive particle breakage was observed especially of the gravel-size particles. Vibration amplitude could not be altered and so this precluded any possible optimisation. Lade et al. (1998) proposed an alternative method to determine e_{min}, which is reported to result in minimal particle breakage. This method required spooning material into a 2000 mL graduated cylinder, which is tapped 8 times, twice each on opposite sides, after each three spoons. Such a method was also used by Cubrinovski and Ishihara (2002) for gravels. When implementing this method, it was found that although the mass of material in the cylinder could be determined accurately, volume was difficult to determine accurately due to the resulting uneven surface within the cylinder. To determine volume accurately variations were therefore adopted as outlined below.

6.2 Proposed method for determining reference void ratios

A special mould, as per ASTM D4254, was fabricated for this study, relevant details of which are given in Table 6.1.

Table 6.1: Dimensions of special mould

Item	Value (mL)	Comment
Theoretical volume by direct measurement	516	Diameter = 79.7 mm Height = 103.4 mm
Volume by water filling	519	at 19.5 °C
Average volume	518	

From a given sample, an oven-dried specimen between 0.9 and 1.2 kg was prepared. The mass prepared was roughly 10 % greater than the mass anticipated to fill the mould, based on the expected density. As sandy gravels can segregate during handling, the specimen was riffled into four equal portions. After weighing the empty mould to an accuracy of 0.1 g, the four equal portions were gently poured into a funnel with a 25 mm diameter spout and hose that initially rested at the bottom of the mould. Lifting the funnel gradually in a spiral allowed the material to be deposited with maximum hindrance, to roughly 25 mm above the rim. A straightedge was then used gently to cut off the excess material and a brush used to remove excess grains from outside the mould. The mass of the specimen and mould was then measured,

from which the mass of specimen could be determined and subsequently the minimum dry density. Using the particle specific gravity, G_s, e_{max} was determined.

The specimen used above to determine e_{max} was then riffled into four equal portions. A collar was attached to the mould and material spooned into the mould from an average drop height of 300 mm. Following each (approximately 15 g) lift, the mould was tapped 8 times, twice each on opposite sides, with a rubber mallet. Once all material was rained into the mould, the standard surcharge (13.8 kPa) was lowered into the collar. The mould was tapped, as explained above, to level the surface of the specimen, so that an accurate volume measurement could be made. Following careful removal of the collar and surcharge, a 5.0 mm thick steel plate was lowered into the mould. The distance between the edge of the mould and plate was measured at four points, using a digital depth gauge with a 0.05 mm accuracy. From this, the average height of the specimen and hence specimen volume could be determined. The mass of mould and of specimen was then determined. From these measurements, the maximum dry density could be determined. Using the particle specific gravity, G_s, e_{min} was determined.

The specimen was then mixed with the material left over from the maximum void ratio determination and the procedures repeated. At least three individual determinations of maximum and minimum void ratio were carried out on each sample of soil used in subsequent testing.

6.3 Gravel-sand mixtures

To investigate the fabric changes as the finer fraction increases, different composite gradations were prepared from the adopted sand (S) and gravel (G) gradations (see Chapter 3). Particle size distributions (PSD) of S and G are repeated here (Figure 6.1) along with an example of a composite gradation with a finer fraction F = 15 %. The material used was a non-plastic, residual granite, which was separated into different particle size ranges (Table 6.2) and oven dried. Specimen gradations with increasing finer fraction (F) were prepared by recombining individual masses of the different

separated particle size ranges. These individual masses ranged between 2.00 g and 370.00 g and were measured to the nearest 0.02 g.

Table 6.2: Particle sizes of base material used to form gravel and sand gradations

Material	Grain size ranges (mm)
Gravel	0.710 – 1.18, 1.18 – 2.36, 2.36 – 3.35, 3.35 – 4.75, 4.75 – 6.7
Sand	0.053 – 0.075, 0.075 – 0.105, 0.105 – 0.150, 0.150 – 0.250, 0.250 – 0.425

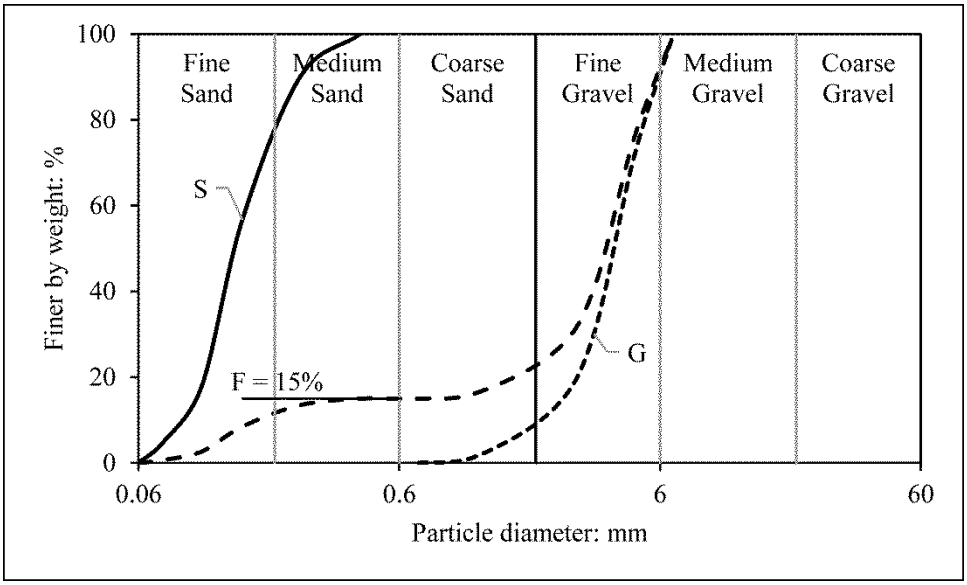


Figure 6.1: Gradations investigated

The small pyknometer method was used in accordance with clause 8.3 of BS1377: Part 2: 1990 to determine G_s. Separate values were determined for sand and gravel constituents (Table 6.3) and were found to be consistent with expected minerals in residual granite. Repeatability was satisfactory as the standard deviations were close to or better than 0.007, which is the expected order of error for G_s (Germaine and Germaine, 2009). For each composite gradation, G_s was interpolated based on the proportions of the components.

Table 6.3: Gravel-sand particle specific gravities

Material	Particle size range (mm)	Particle specific gravity, G_s	
		Average	Standard deviation
G	0.710 – 1.18	2.66	0.008
S	0.105 – 0.150	2.69	0.001

A decrease (Figure 6.2) in both e_{min} and e_{max} of the combined material was observed up to approximately F = 30 % after which both increased. This indicates sand initially

sitting within gravel voids and then the sand holding the gravel apart. Germaine and Germaine (2009) report the error in reference states of compactness to be 0.01 g/cm^3 for maximum density and 0.008 g/cm^3 for minimum density, based on tests on poorly graded sands. Repeatability (Table 6.4) was therefore on average satisfactory, although the standard deviation for a few tests was greater than the values proposed by Germaine and Germaine (2009). Furthermore, it is apparent that the method to determine e_{min} was slightly less repeatable than the method to determine e_{max}. This is attributed to minor variations in mallet tamping.

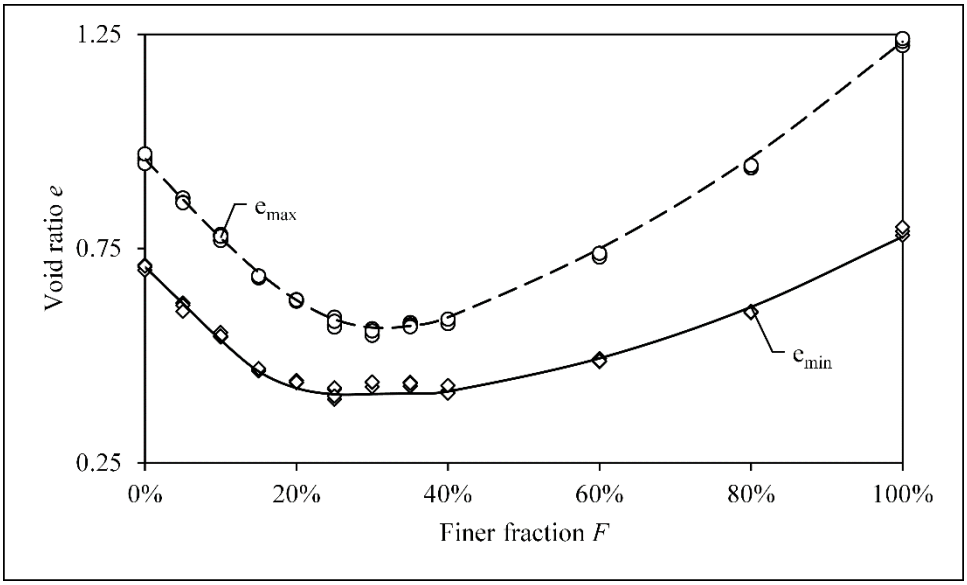


Figure 6.2: Gravel-sand void ratios

Table 6.4: Gravel-sand soils dry density and void ratio errors

State	Standard deviation	
	Dry density (g/cm^3)	Void Ratio
	Average (Range)	Average (Range)
Loosest	0.005 (0.002 – 0.010)	0.006 (0.002 – 0.009)
Densest	0.007 (0.002 – 0.016)	0.006 (0.002 – 0.012)

As e_{min} was determined with a non-standard method, a composite grading with F = 15 % was tested according to an alternative raining method that did not incorporate tapping outlined in Germaine and Germaine (2009). These authors indicated that their method gives comparable results to the vibrating table method. Using this raining method e_{min} was determined as 0.51. However, with the mallet-tamping method proposed herein a slightly denser state was achieved, with e_{min} determined as 0.47. The raining method was therefore not adopted.

6.4 Gravel-salt mixtures

The sodium chloride, used as an analogue for the erodible finer sand, was ordinary table salt, crushed and separated into equivalent particle size ranges (Table 6.5). These separated ranges were recombined to form gravel-salt mixtures in a similar manner to the gravel-sand mixtures. Possible limitations to the use of salt as an analogue, due to differences in shape, hardness and particle specific gravity, are now explored.

Table 6.5: Particle sizes of base material used to form sand-sized salt gradations

Material	Grain size ranges (mm)
Salt	0.053 – 0.075, 0.075 – 0.105, 0.105 – 0.150, 0.150 – 0.250, 0.250 – 0.425

Light microscope images of the various sand and salt size ranges are compared in Figure 6.3. Sand and salt particles are of similar size, angularity and sphericity (Cho et al. (2006) Sphericity values between 0.5 and 0.7 and Roundness values between 0.5 and 0.7). Salt particles are however slightly smoother, a consequence of cleavage planes (preferential planes of weakness) which are absent in the sand particles.

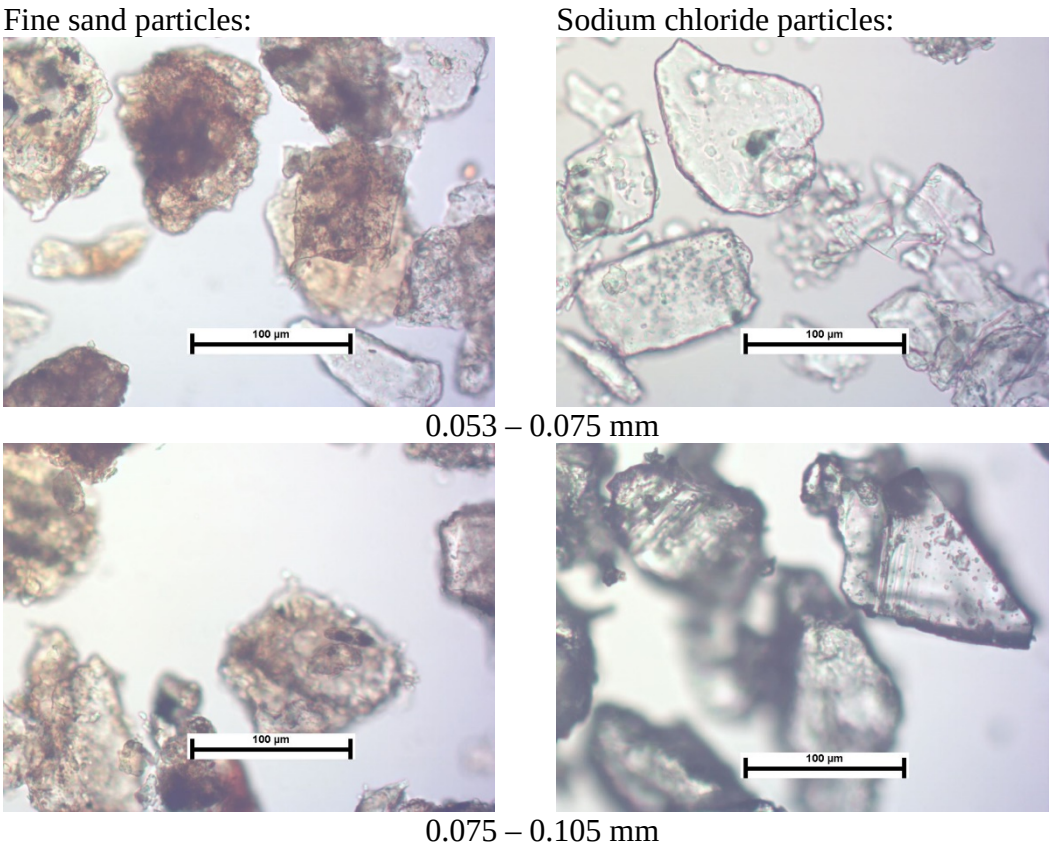


Figure 6.3: Light microscope images of fine sand and salt particles

Fine sand particles: Sodium chloride particles:

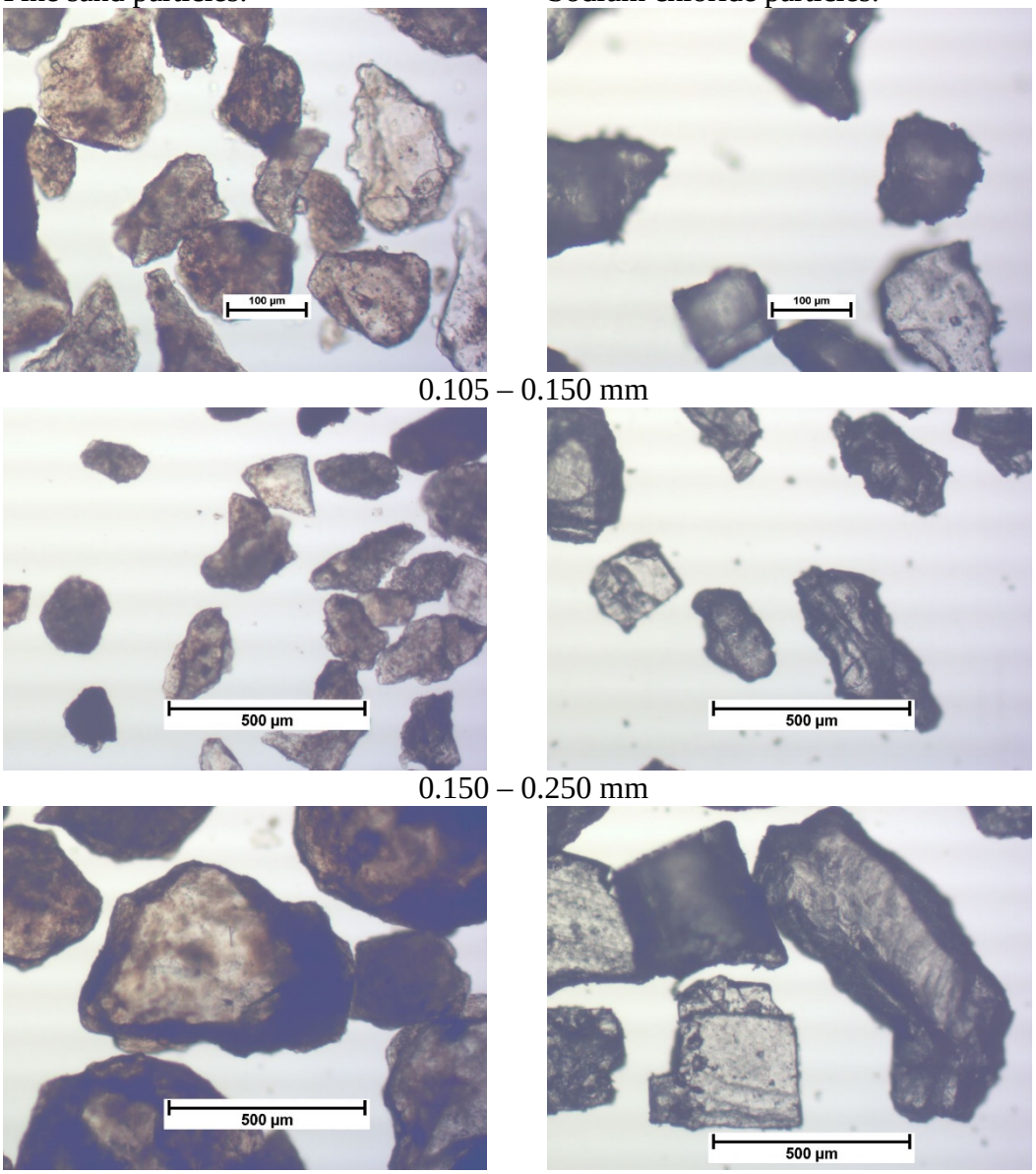


Figure 6.3 (continued): Light microscope images of fine sand and salt particles

Another difference is particle hardness. On the Mohs hardness scale, the minerals making up granite have a hardness of approximately 6, whereas sodium chloride has a hardness of 2.5 (Kehew, 2006). To investigate whether specimen preparation would cause particle breakdown, a sand sample and a salt sample were prepared. Each was then sieved to determine their PSDs. Two more samples were prepared and riffled a number of times to simulate the abrasion that may occur during specimen preparation. These riffled samples were then sieved to determine whether their PSDs had altered. It is clear (Figure 6.4) that specimen preparation has minimal effect on the particle size of the sand. On the other hand, the salt sample (Figure 6.5) undergoes some

particle breakdown, especially during sieving. Percentage passing at 0.06 mm for the sieved specimen was 7 %, for the riffled and sieved sample it was 11 % and for the theoretical sample it was 2 %. As specimen preparation only involved riffling, it can reasonably be expected that the percentage passing at 0.06 mm may change by 4 %. This limited particle crushing is unavoidable. As the shape of the PSD curve does not change significantly and the salt will make up at most 35 % of the final grading, tested composite gradations will change by less than 1 %.

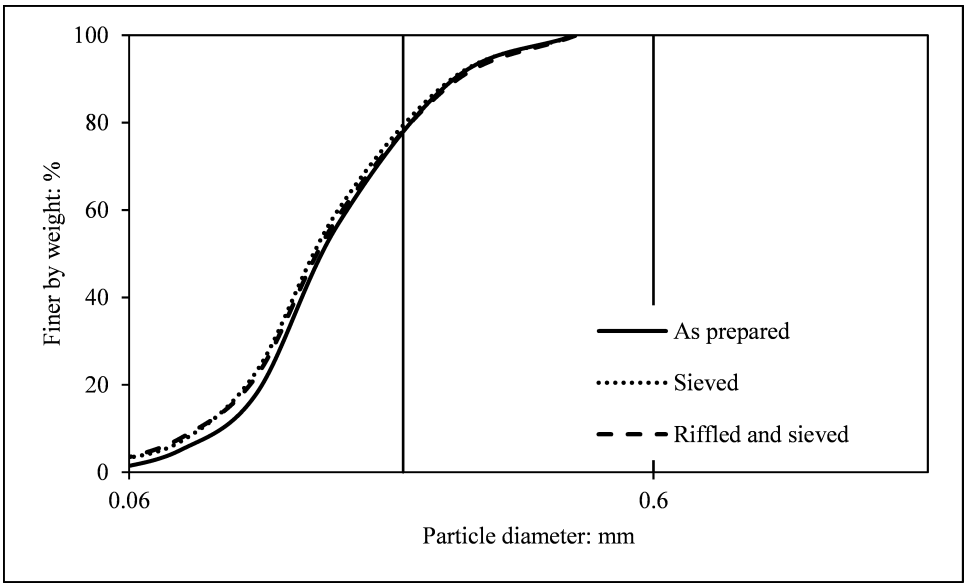


Figure 6.4: Impact of specimen preparation on sand particle sizes

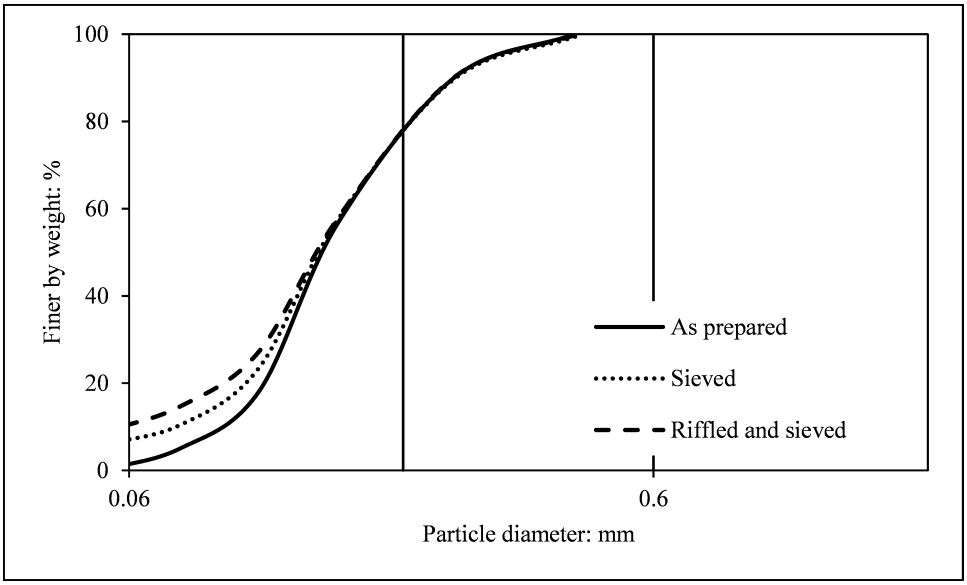


Figure 6.5: Impact of specimen preparation on salt particle sizes

Due to differences in particle specific gravity G_s, the theoretically correct approach would be to replace sand particles with an equivalent volume of salt. However, it was apparent from testing to determine minimum void ratios (densest packing) with increasing F that salt packed more efficiently than sand. Consequently, at a given F, the equivalent void ratio of the coarser particles, e_c ($e_c = (V_t - V_c) / V_c$, where V_t is the total soil volume and V_c is the volume occupied by coarser particles) was higher for the sand-gravel mixes (Figure 6.6). As the fabric change to be investigated is the change in the coarser fabric when finer particles are lost, larger volumes of salt would be required to achieve an equivalent e_c. By comparing the e_c values obtained for the gravel-sand and gravel-salt mixes, it was found that replacing sand with salt by mass achieved equivalent e_c for dense gravel-sand and gravel-salt mixes (Figure 6.7).

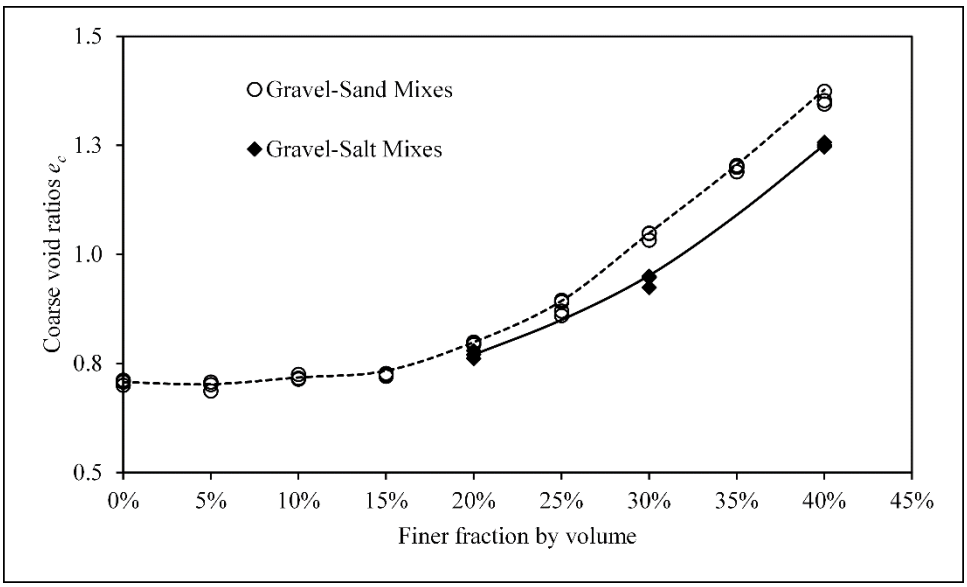


Figure 6.6: Coarse void ratios for dense mixtures prepared by volume

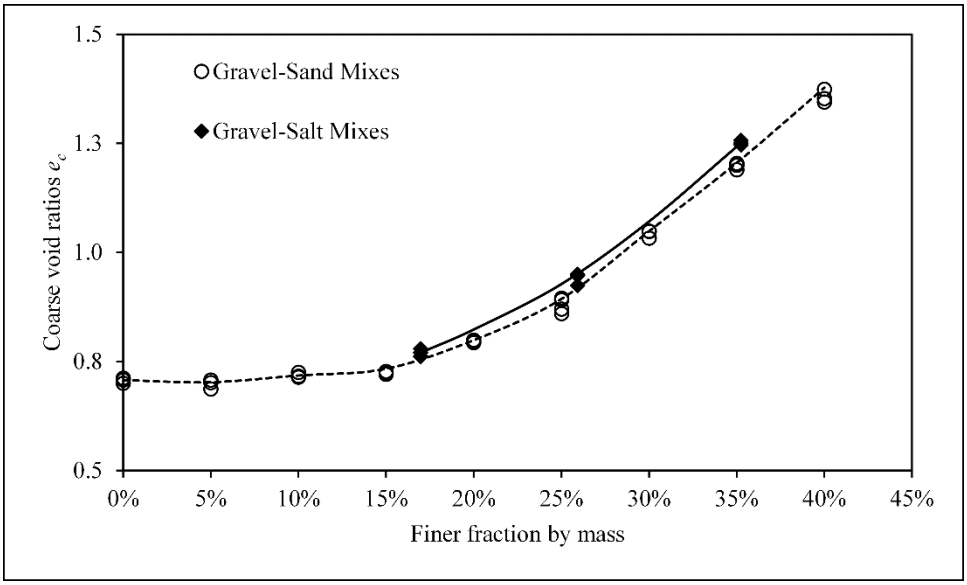


Figure 6.7: Coarse void ratios for dense mixtures prepared by mass

Tests to determine maximum void ratios (loosest packing) found that equivalent gravel-salt mixtures could be obtained by replacing sand on a volume basis (Figure 6.8) rather than on a mass basis (Figure 6.9). For high F values, e_c values were not equivalent, consequently, tests on loose mixtures were kept to F < 30 %.

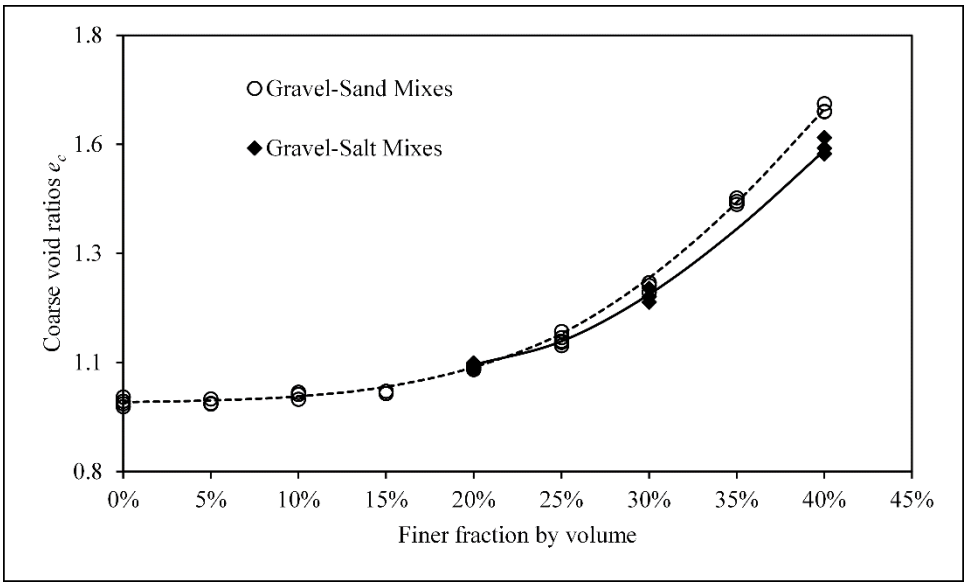


Figure 6.8: Coarse void ratios for loose mixtures prepared by volume

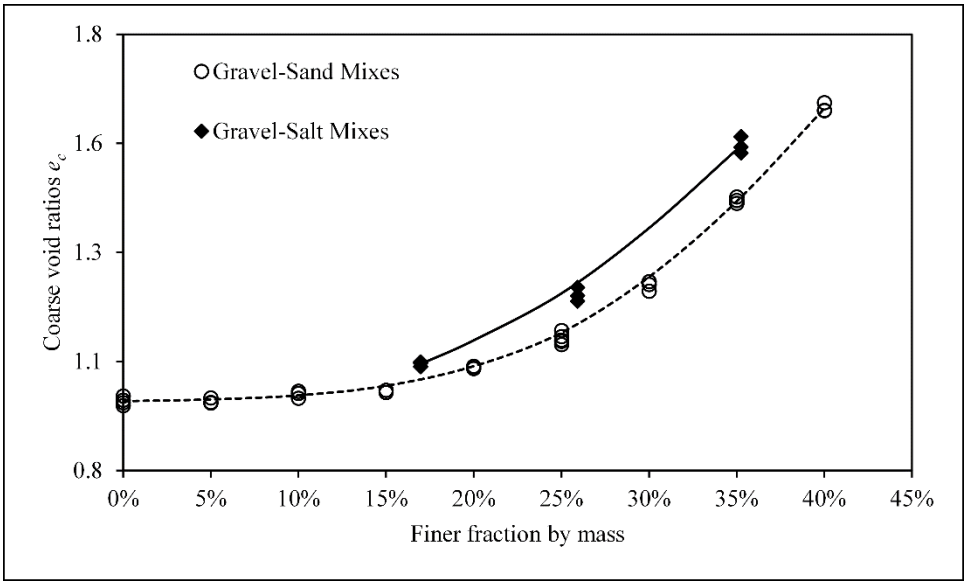


Figure 6.9: Coarse void ratios for loose mixtures prepared by mass

6.5 Summary

A review of methods to determine e_{max} found that the standardised funnel method (ASTM D4254) could be implemented with minor variations. One variation used, which is permitted by the standard, was the use of a smaller mould, due to material availability constraints. The second variation was to riffle the specimen into equal portions that were poured sequentially into the mould, to mitigate potential segregation of gravel-sands.

Lack of access to an adequate vibrating table that would prevent particle breakage, prevented using the standardised vibrating table method (ASTM D4253) for e_{min} determinations. A method proposed by Lade et al. (1998), in which a specimen is incrementally spooned into a graduated glass cylinder and then tapped after each lift, was adopted. To improve accuracy with which volume could be determined, a steel mould of known volume was used. Specimen height was determined by carefully lowering a disk of known height onto the specimen within the mould, then measuring the height between the mould rim and disk to determine the specimen height.

These methods were used to investigate packing behaviour of the adopted gradations. Results showed consistency with methods proposed by other authors and acceptable repeatability.

Preparation considerations due to differences in particle shape, hardness and specific gravity between sand and salt were explored. These differences resulted in different particle packing behaviour, requiring consideration of the fabric change to be modelled. In the case of internal erosion, because the change to be modelled is the change in the coarser fabric as finer particles are lost, replacing fine sand with salt on a mass basis rather than a volume basis was found to reproduce the desired dense fabric changes with varying finer fraction best. However, for loose fabric changes, replacing fine sand on a volume basis was found to reproduce best the desired changes.

Chapter 7 Internal erosion and mechanical behaviour

This chapter presents experimental work using the developed vertical axis restrained internal erosion shear box (variedSB). This device was used to investigate one particular internally unstable gradation to develop a more comprehensive understanding of the effects of internal erosion on mechanical behaviour. After stating the experimental aim, the experimental methodology is outlined. Results from the experimental program are presented followed by analysis. Observations made are then compared to mechanical effects suggested in the literature.

7.1 Experimental aim

The experimental aim was to investigate the validity of the theoretical framework outlined in Chapter 3. This framework suggests that for low finer fractions ($F < F_t$), the loss of finer particles will result in negligible change in mechanical behaviour both when deviatoric stress is low (i.e. predominantly isotropic stress) and when deviatoric stress is high; that is when the soil is close to yielding. On the other hand, for intermediate finer fractions ($F_t < F < F_c$), although finer particle loss may result in small changes in mechanical behaviour under low deviatoric stress (i.e. predominantly isotropic stress), the fabric's ability to resist large deviatoric stresses will be compromised. For high finer fractions ($F > F_c$) finer particles are integral to load transfer and are unlikely lost under normal seepage conditions.

Under one-dimensional, laterally restrained loading, it is therefore expected that loss of finer particles should result in negligible settlement for $F < F_c$. Shearing specimens with $F < F_t$ should show little change in shear strength following finer particle loss. However, for $F > F_t$ the shear strength should decrease following loss of finer particles. Although testing gradations with $F > F_c$ is possible, with the proposed methodology, this is not likely to be a real problem under normal seepage conditions. If loss of finer particles were to occur in such specimens, significant settlement and loss of shear strength should occur.

7.2 Experimental method

7.2.1 Specimen preparation

The validity of the transition (F_t = 15 %) and critical (F_c = 27 %) finer fractions, identified in Chapter 3 for the internally unstable composite gradations of sand (S) and gravel (G), are investigated here. Gradations for S and G are repeated here as Figure 7.1 for ease of reference. The experimental investigation also sought to investigate the question of how much finer particle loss was required to destabilise the fabric. To do this, four different types of specimen were prepared:

1. Specimens with both fine sand (S) and fine gravel (G). This series was used to investigate behaviour without any finer particle loss. These are referred to as *all-sand-fines* specimens.
2. Specimens with fine sand completely replaced with fine sand-sized sodium chloride salt. This series was used to investigate the effect of complete finer particle loss. These are referred to as *all-salt-fines* specimens.
3. Specimens with half of the fine sand replaced with fine sand-sized sodium chloride salt. This series was used to investigate the effect of partial finer particle loss. These are referred to as *half-salt-fines* specimens.
4. Specimens with a quarter of the fine sand replaced with fine sand-sized sodium chloride salt. This series was used to investigate the effect of minor finer particle loss. These are referred to as *quarter-salt-fines* specimens.

For each series, specimens with different finer fractions were prepared, quantified by the percentage of finer particles, F. Kenney and Lau (1985) proposed that finer particles are either lost incrementally from the smallest to the largest erodible particle or evenly from the erodible portion of the gradation. It is more likely that smaller less stressed particles are lost first, followed by larger more stressed particles. However, DEM studies by Scholtès et al. (2010) suggest that the two approaches do not result in substantially different final states. Therefore, for series 3 and 4, the portion of salt added had the same gradation as the sand, modelling particle loss taking place evenly from the entire erodible portion.

Specimens were prepared by combining oven dried base material, by mass, from the various grain size ranges summarised in Table 7.1 for ease of reference from Table 6.2 and Table 6.5. Specimen masses ranged between 600.11 and 856.89 g and were prepared from masses of base material ranging between 1.30 g and 279.20 g (measured to the nearest 0.02 g). Specimens were placed in an oven overnight to ensure no moisture was present; measured moisture contents after drying were in the order of approximately 0.1 %.

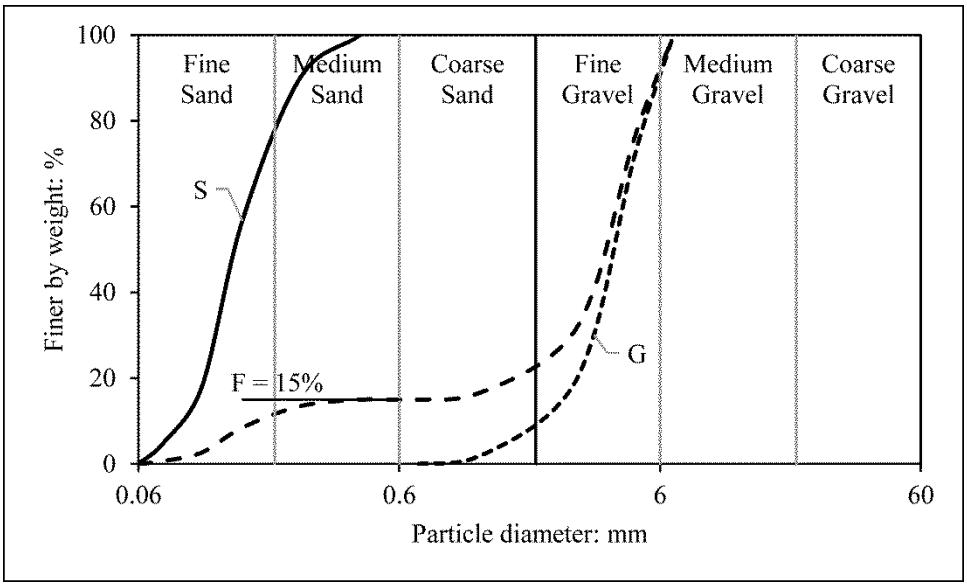


Figure 7.1: Gradations investigated

Table 7.1: Particle sizes of base material

Material	Grain size ranges (mm)
Gravel	0.710 – 1.18, 1.18 – 2.36, 2.36 – 3.35, 3.35 – 4.75, 4.75 – 6.7
Sand	0.053 – 0.075, 0.075 – 0.105, 0.105 – 0.150, 0.150 – 0.250, 0.250 – 0.425
Salt	0.053 – 0.075, 0.075 – 0.105, 0.105 – 0.150, 0.150 – 0.250, 0.250 – 0.425

The variedSB was prepared for testing by placing silicone grease and latex membranes on all inside faces of the two halves of the shear box. The two halves were separated by PTFE (Teflon) spacers and secured with setscrews. A perforated grid plate was placed in the bottom of the shear box, over the recessed drainage channels. The initial mass of bath and shear box was determined to the nearest 0.1 g. Dense specimens were prepared by raining four riffled portions from a height of 300 mm and loose specimens by gently pouring four riffled portions using a funnel with a 25 mm spout and hose. Riffling was necessary to reduce segregation. Once prepared, the mass of bath, shear box and specimen was measured to the nearest 0.1 g. The top

perforated grid plate was placed and seated by hand for loose specimens and with a rubber mallet for dense specimens. A small spirit level was used to ensure the top surface was horizontal. Traditional preparation methods, such as dry pluviation through a nest of sieves or wet tamping, were not possible due to the wide range of particle sizes and the need to prevent premature salt dissolution.

The assembled shear box was then gently placed onto the load frame. The top loading platen was placed and the top half of the shear box secured to the vertical restraining frame. The loading yoke was placed on the loading shaft to seat all the components and the vertical LVDT fitted. Using a sliding calliper, with a 0.1 mm accuracy as a height gauge, the specimen height was determined using the vertical restraining frame as horizontal datum. Subsequent height changes were determined using the LVDT, which had an accuracy of 0.01 mm. A vertical stress of either 74 ± 1.0 kPa or 151 ± 1.9 kPa was then applied. For ease of reference these two stresses are referred to as 75 kPa or 150 kPa respectively. Vertical deflections were monitored until constant, which invariably took less than 2 minutes. From these measurements, the initial void ratio was then determined. Due to difference in packing behaviour between gravel-salt and gravel-sand mixtures, overall void ratio was not found to be a comparable measure of compactness (see Chapter 6). The coarse void ratio (e_c) on the other hand, was found to be a more suitable measure of specimen compactness and is used instead ($e_c = (V_t - V_c) / V_c$, where V_t is total soil volume and V_c is the volume occupied by coarser particles).

An observation-based experimental program was followed rather than testing every possible combination. Specimen constituents, finer fraction, consistency and applied vertical stress, were refined based on observations from preceding tests. The main guiding observations included: measurement variability, whether any change in mechanical behaviour was observed and whether regression could be used to interpolate intermediate values. In total 85 specimens were prepared and tested, as summarised in Table 7.2.

Table 7.2: Summary of internal erosion test specimens

Series	Global consistency	Applied σ_{yy} (kPa)	Successive specimen F (%) and $e_{c,0}$‡	
All-sand-fines	Dense	150	F:	5, 5, **10**, **10**, 15, 15, **20**, **20**, 25, 25, **30**, **30** and 35
			$e_{c,0}$:	0.74, 0.76, **0.74**, **0.72**, 0.75, 0.74, **0.80**, **0.77**, 0.88, 0.88, **1.03**, **1.02** and 1.17
	Dense	75	F:	5, 5, **10**, **10**, 15, 15, **20**, **20**, 25, 25, **30** and **30**
			$e_{c,0}$:	0.73, 0.75, **0.76**, **0.75**, 0.74, 0.76, **0.83**, **0.82**, 0.91, 0.91, **1.03** and **1.04**
	Loose	150	F:	5, 5, **10**, **10**, 15, 15, **20**, **20**, 25, 25, **30** and **30**
			$e_{c,0}$:	0.99, 0.96, **0.98**, **0.99**, 1.00, 1.00, **1.05**, **1.03**, 1.13, 1.13, **1.21** and **1.22**
	Loose	75	F:	5, **15** and 25
			$e_{c,0}$:	0.98, **1.01** and 1.13
All-salt-fines	Dense	150	F:	6, 6, **12**, **12**, 18, 18, **23**, **23**, 29, 29, **34** and **34**
			$e_{c,0}$:	0.75, 0.75, **0.74**, **0.72**, 0.80, 0.77, **0.86**, **0.87**, 0.95, 0.97, **1.13** and **1.14**
	Dense	75	F:	6, 6, **12**, **12**, 18, 18, **23**, **23**, 29, 29, **34** and **34**
			$e_{c,0}$:	0.75, 0.74, **0.77**, **0.76**, 0.79, 0.80, **0.86**, **0.86**, 0.97, 0.98, **1.18** and **1.18**
	Loose	150	F:	5, **10**, 15, **20**, 25 and **30**
			$e_{c,0}$:	0.95, **0.97**, 0.99, **1.04**, 1.12 and **1.17**
	Loose	75	F:	5 and 25
			$e_{c,0}$:	0.96 and 1.11
Half-salt-fines	Dense	150	F:	20, 20, 20, **25**, **25**, 30 and 30
			$e_{c,0}$:	0.80, 0.82, 0.81, **0.89**, **0.88**, 1.02 and 1.01
Quarter-salt-fines	Dense	150	F:	20, 20, **25**, **25**, 30 and 30
			$e_{c,0}$:	0.79, 0.80, **0.88**, **0.88**, 1.01 and 1.01

‡ Bold typeface for ease of reference only

To assess the accuracy of the preparation method, measured $e_{c,0}$ values are plotted in Figure 7.2 against reference values determined in Chapter 6. Compared to D_r = 100 %, the dense preparation method resulted in slightly looser specimens at low F and slightly denser specimens at high F. This increase in density with F can be attributed to compression of finer particles under the larger vertical stress used in the variedSB tests than the 13.8 kPa used in the e_{min} determination. D_r for dense specimens was on average 106 % and ranged between 83 % and 136 %. To assess the repeatability of the preparation method, a third-degree polynomial was plotted through $e_{c,0\ values}$ and standard error in y (S_{ey}) determined. S_{ey} for dense specimens was 0.02 whereas for the reference state standard error was 0.007. The loose preparation method resulted in $e_{c,0}$ closer to the D_r = 0 % reference state, except at high F. This departure at high F can be attributed to compression of finer particles. D_r for the loose specimens was on average 6 % and ranged between -3 % and 43 %. S_{ey} for loose specimens was 0.01 whereas for the reference state standard error was 0.007.

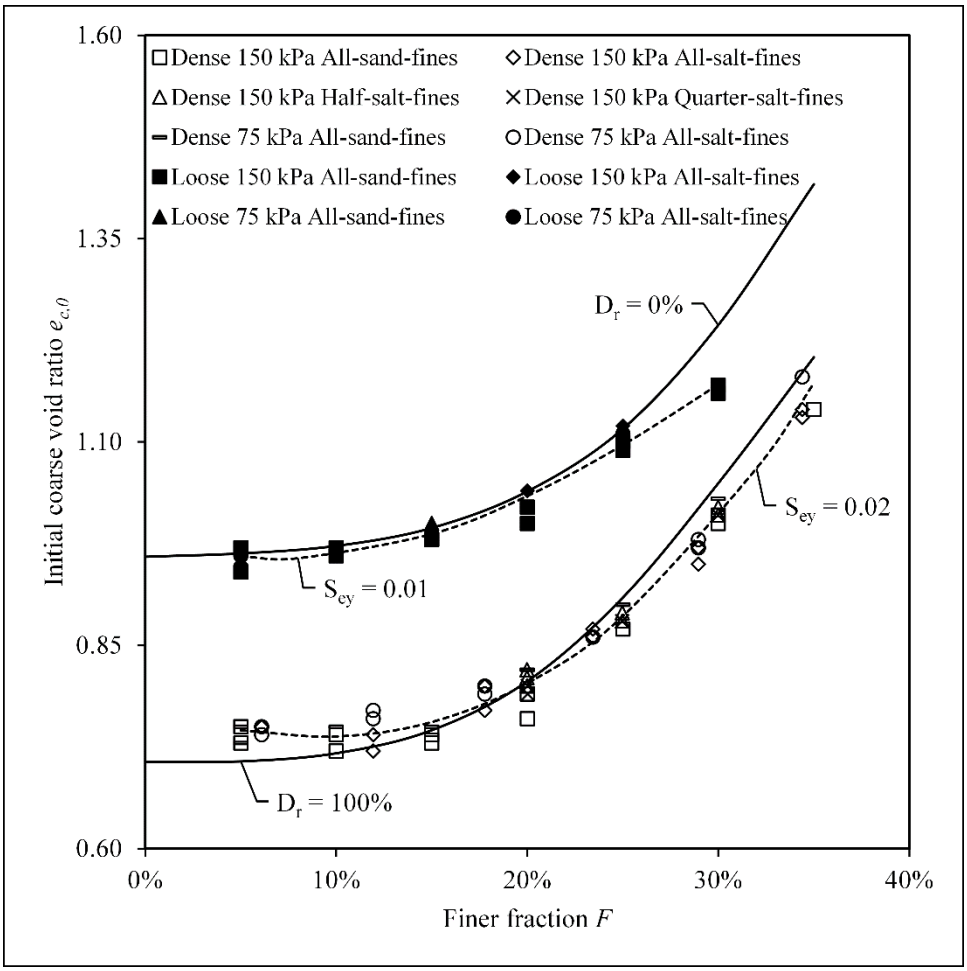


Figure 7.2: Initial coarse void ratio in relation to reference states

It is evident from the scatter in Figure 7.2 that the large particles and small specimen size affected the repeatability and accuracy with which e_c could be determined. The error in e_c can be estimated based on the error in measuring volume and mass with the following equation adapted for direct shear box testing from the Vaid and Sivathayalan (1996) equation for triaxial testing:

$$\Delta e_c = (1 + e_c)\left[\frac{2\Delta L}{L} + \frac{\Delta H}{H} + \frac{\Delta G_s}{G_s} + \frac{\Delta M}{M}\right] \qquad \text{Equation 7.1}$$

where e_c, L, H, G_s and M are the ambient coarse void ratio, specimen length, specimen height, particle specific gravity and mass respectively. Δe_c, ΔL, ΔH, ΔG_s and ΔM are the measurement error in coarse void ratio, specimen length, specimen height, particle specific gravity and mass respectively. It is reasonable to assume that ΔG_s is small, therefore the error due to G_s falls away in Equation 7.1, implying that for a given specimen size, Δe_c depends on errors in measuring length (ΔL), height (ΔH), mass (ΔM) and ambient coarse void ratio (e_c).

The resolution with which specimen length and height could be measured was estimated to be 0.25 and 0.1 mm respectively. This was based on the sliding calliper's accuracy and the variation in thickness of the latex and silicone membranes placed within the shear box. Vaid and Sivathayalan (1996) reported that the resolution with which triaxial specimen circumferences and height can be determined are in the order of 0.5 and 0.01 mm respectively. Mass could be determined with an accuracy of 0.10 g. Vaid and Sivathayalan (1996) reported the same accuracy. For these resolutions, Δe_c is given as a function of ambient e_c in Figure 7.3. This figure shows that the greatest source of error is in determining the specimen length. For comparison, measured Δe_c (that is S_{ey} from Figure 7.2) for dense and loose specimens along with error bars representing the range of ambient e_c (that is the range of measured e_c in Figure 7.2) for dense and loose specimens are shown in Figure 7.3. It is evident that the measured Δe_c are marginally bigger than computed Δe_c for dense specimens, but measured Δe_c are marginally smaller than computed Δe_c for loose specimens. Vaid and Sivathayalan (1996) calculated a similar degree of error for

50 mm diameter triaxial specimens. Although the accuracy with which shear box specimen void ratios were determined was poorer than reference state void ratios, the accuracy was not significantly different to other methods of geotechnical laboratory testing.

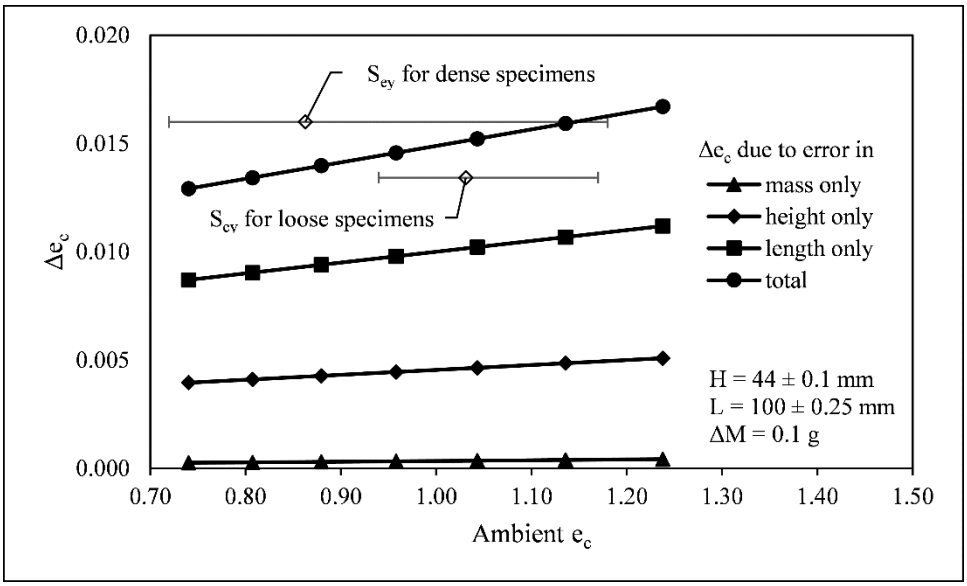


Figure 7.3: Coarse void ratio error due to resolution of volume and mass measurements

The effect of differences in salt and sand hardness on specimen compression during vertical loading was also investigated. Vertical strains during vertical loading, under either 75 or 150 kPa, prior to flooding were calculated for each test. Average and standard deviation of these vertical strains are given in Table 7.3. It is evident that vertical strain was dependent on consistency and applied vertical stress, but largely independent of whether finer particles were salt or sand.

Table 7.3: Vertical strain during vertical loading

Series	Consistency	Applied σ_{yy} (kPa)	Vertical strain	
			Average	Standard deviation
All-sand-fines	Dense	75	0.6%	0.2%
All-salt-fines			0.5%	0.2%
All-sand-fines	Loose		0.5%	0.1%
All-salt-fines			0.6%	0.3%
All-sand-fines	Dense	150	1.6%	0.4%
All-salt-fines			1.2%	0.3%
Half-salt-fines			0.9%	0.3%
Quarter-salt-fines			0.8%	0.2%
All-sand-fines	Loose		3.1%	0.2%
All-salt-fines			3.4%	0.3%

7.2.2 Dissolution under one-dimensional loading

After specimens had been loaded, flow into the specimen was initiated from the bottom of the bath by feeding water through the drainage outlet (Figure 7.4). This was to flush the drainage collection channels and to force air out of the voids. This was continued until flow was observed at the top or sides of the shear box. The bath was then filled from the top. Due to the coarseness of the material, this was considered sufficient to flood the specimen.

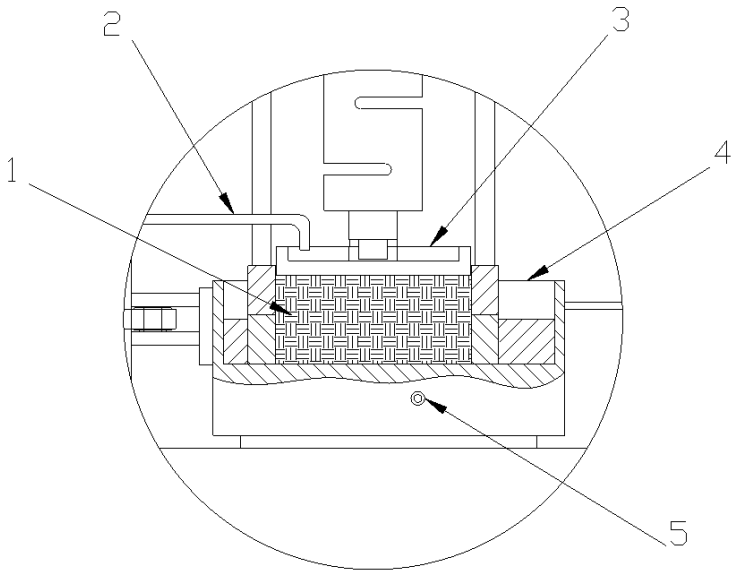


Figure 7.4: Illustration of dissolution process: 1. Specimen; 2. Water supply; 3. Top platen with shallow recess and numerous perforations to facilitate vertical flow into specimen; 4. Bath; 5. Drainage outlet

Water fed onto the top platen could either overflow the top platen into the bath or through the specimen and out of the drainage outlet. The inflow rate was maintained to ensure the bath remained flooded at all times. At regular intervals during dissolution, the time to collect a set volume of water from the drainage outlet was measured. Although the specimen was not sealed off from the bath, a discharge velocity was calculated assuming all flow went through the specimen. For all-salt-fines specimens, this discharge velocity was in the order of 0.003 cm/s. Varying this between 0.001 and 0.01 cm/s was found to have a negligible effect on recorded settlement. For half-salt-fines and quarter-salt-fines specimens, discharge velocities were kept low, in the order of 0.001 cm/s, to reduce any possible migration of fine sand particles.

Salt dissolution was monitored by measuring the conductivity (C) of the seepage in units of Siemens (S) with a Jenway 430 Portable pH/Conductivity meter. For all-salt-fines specimens with small finer fractions, settlement was immediate from the onset of seepage (Figure 7.5a). Whereas, for all-salt-fines specimens with large finer fractions, settlement was initially gradual and then accelerated (Figure 7.5b). Rapid settlement was accompanied by a rapid decrease in conductivity. Seepage was maintained after the rapid drop in conductivity for all-salt-fines specimens until negligible changes in settlement and conductivity were recorded. However, for half-salt-fines and quarter-salt-fines specimens seepage was stopped when the conductivity dropped below 10 mS (the average measured final conductivity was 7.0 mS) to limit possible fine sand migration. This cut-off was chosen as negligible settlement after this point had been observed in prior tests. Furthermore, a salt solution of mass concentration 0.008 g/mL was measured to have a conductivity of 10 mS (Figure 7.6).

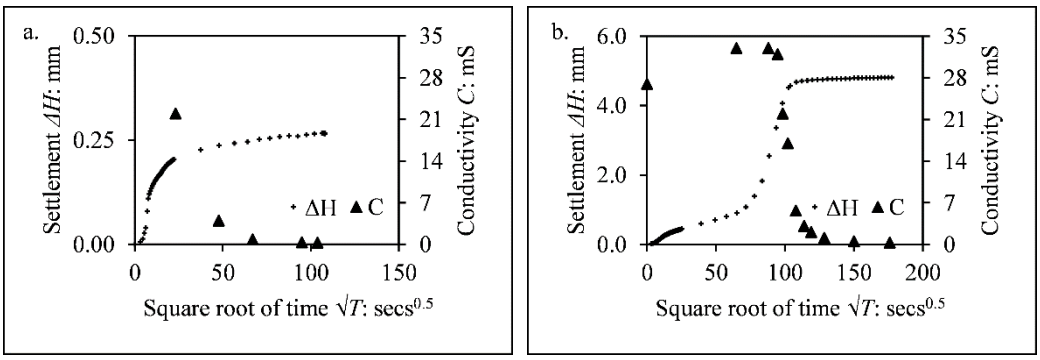


Figure 7.5: Dissolution of all-salt-fines specimens: a. F = 6% and b. F = 34 %

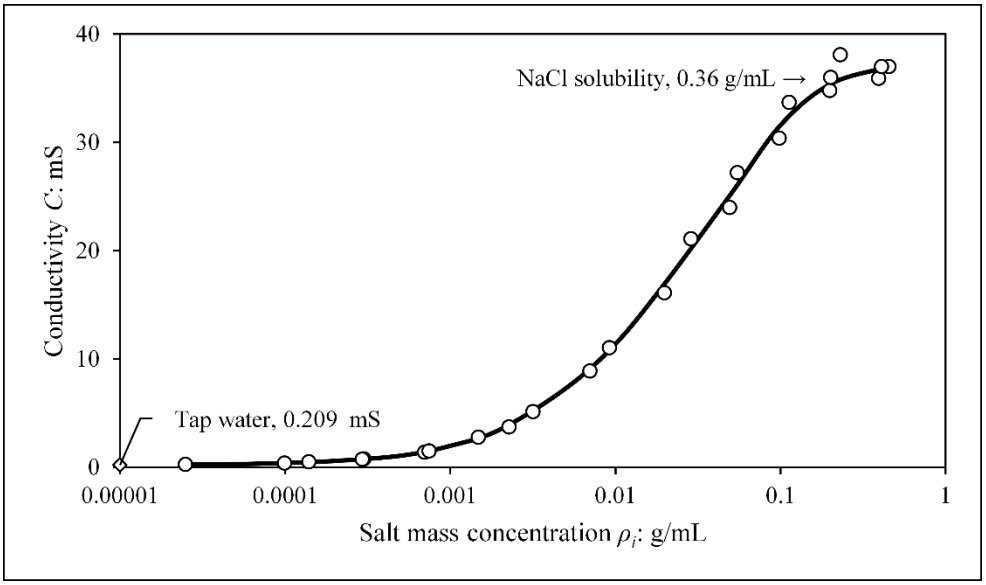


Figure 7.6: Relationship between salt mass concentration and conductivity at 15.4 °C

7.2.3 Shearing

When flooding (in the case of all-sand) or dissolution (in the case of part salt) was complete, the various supply and outflow pipes were removed and the drain blocked to maintain a flooded bath. Specimens were then sheared at a rate of 0.5 mm/min for a shear displacement of 17 mm.

The vertical force was observed to increase during the test, possibly due to the effects of dilation and friction in the loading assembly. For specimens under a vertical stress of 150 kPa the average increase in vertical force was 9 % with a standard deviation of 5 %. Whereas, for specimens under a vertical stress of 75 kPa, the average increase in vertical stress was 6 % with a standard deviation of 5 %. These increases were similar to those seen during calibration testing (see Chapter 5).

Once shearing was complete, the shear box was dismantled and the specimen removed and separated. In all cases, no evidence of undissolved salt was observed. For half-salt-fines and quarter-salt-fines specimens, the shear box was not immediately dismantled; instead, the box was frozen overnight, enabling the specimen to be removed as a solid block (Figure 7.7) and dissected along the shear plane using hot water (Figure 7.8). The two halves were then oven dried and sieved to determine the extent of fine sand migration.



Figure 7.7: Typical frozen specimen showing latex membranes (Specimen No. S1G-F30-D-150-50_50-1)



Figure 7.8: Typical frozen specimen showing sheared halves (Specimen No. S1G-F25-D-150-25_75-1)

Although some particle loss was unavoidable during specimen dismantling, the greatest difficulty was separating the two halves into representative portions. For the half-salt-fines specimens hot water was run over the bottom half until half the specimen had melted into a collecting bowl. Finer particles however, were generally carried away in preference to the coarser particles. This was because the coarser particles remained joined to the frozen portion. Consequently, a greater portion of finer particles accumulated into the melted bottom portion (Figure 7.9a) than may have been the actual case. Such that it would appear that, there was 48 % more finer particles in the bottom half than in the top half.

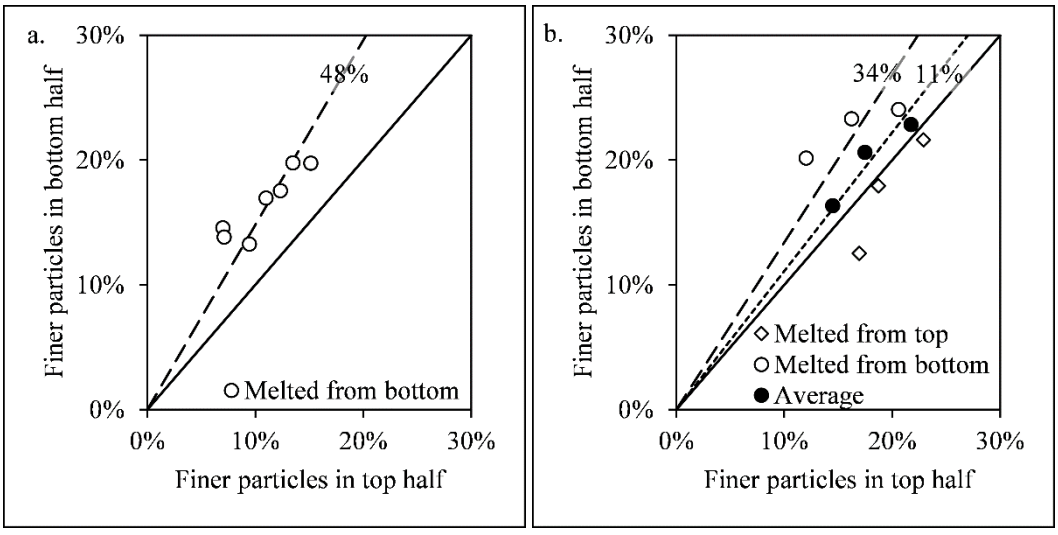


Figure 7.9: Fines migration: a. half-salt-fines specimens, b. quarter-salt fines specimens

For quarter-salt-fines specimens, for each test pair, one specimen was melted from the top and the other from the bottom. In all cases, the portion melted by running water had a greater portion of finer particles. For specimens melted from the bottom it appeared that this portion had 34 % more finer particles, whereas specimens melted from the top had 10 % more finer particles in the melted top half (Figure 7.9b). Averaging these two therefore gives a better indication of finer particle migration. This showed that the bottom half had on average 11 % more finer particles than the top portion. Although one cannot be sure, it is likely that finer particle migration suggested in Figure 7.9a for the half-salt-fines specimens is overestimated.

Finer particle migration is unavoidable however, those finer particles that do migrate are likely not actively involved in load transfer. The uneven distribution of finer particles that results would have affected the settlement and shear results. The extent of this impact is difficult to determine accurately. It is argued that despite these limitations, the experimental approach provided a more realistic analogy to the real mechanism than presented in previous research.

The equipment was then washed and prepared for the next test.

7.3 Results

7.3.1 Dissolution under one-dimensional loading

Table 7.4 gives final coarse void ratio ($e_{c,d}$) following either flooding or dissolution. All raw data is provided in companion files (see Appendix B for details).

Table 7.4: Post flooding and dissolution coarse void ratios

Series	Global consistency	Applied σ_{yy} (kPa)	Successive specimen F (%) and $e_{c,d}$‡	
All-sand-fines	Dense	150	F:	5, 5, **10**, **10**, 15, 15, **20**, **20**, 25, 25, 3**0**, **30** and 35
			$e_{c,d}$:	0.73, 0.75, **0.74**, **0.72**, 0.74, 0.73, **0.79**, **0.76**, 0.87, 0.87, **1.01**, **1.00** and 1.14
	Dense	75	F:	5, 5, **10**, **10**, 15, 15, **20**, **20**, 25, 25, **30** and **30**
			$e_{c,d}$:	0.73, 0.75, **0.75**, **0.75**, 0.74, 0.75, **0.82**, **0.82**, 0.90, 0.90, **1.01**, and **1.03**
	Loose	150	F:	5, 5, **10**, **10**, 15, 15, **20**, **20**, 25, 25, **30** and **30**
			$e_{c,d}$:	0.97, 0.94, **0.96**, **0.97**, 0.98, 0.98, **1.02**, **1.00**, 1.09, 1.10, **1.16** and **1.17**
	Loose	75	F:	5, **15** and 25
			$e_{c,d}$:	0.97, **1.00** and 1.10
All-salt-fines	Dense	150	F:	6, 6, **12**, **12**, 18, 18, **23**, **23**, 29, 29, **34** and **34**
			$e_{c,d}$:	0.74, 0.74, **0.72**, **0.70**, 0.77, 0.74, **0.78**, **0.80**, 0.82, 0.86, **0.89** and **0.91**
	Dense	75	F:	6, 6, **12**, **12**, 18, 18, **23**, **23**, 29, 29, **34** and **34**
			$e_{c,d}$:	0.74, 0.73, **0.75**, **0.75**, 0.78, 0.80, **0.83**, **0.82**, 0.91, 0.90, **0.96** and **0.96**
	Loose	150	F:	5, **10**, 15, **20**, 25 and **30**
			$e_{c,d}$:	0.92, **0.92**, 0.92, **0.93**, 0.96 and **0.94**
	Loose	75	F:	5 and 25
			$e_{c,d}$:	0.94 and 0.97
Half-salt-fines	Dense	150	F:	20, 20, 20, **25**, **25**, 30 and 30
			$e_{c,d}$:	0.78, 0.80, 0.79, **0.85**, **0.85**, 0.91 and 0.90
Quarter-salt-fines	Dense	150	F:	20, 20, **25**, **25**, 30 and 30
			$e_{c,d}$:	0.78, 0.79, **0.85**, **0.85**, 0.93 and 0.94
‡ Bold typeface for ease of reference only				

7.3.2 Shearing

Figure 7.10 shows typical shear behaviour observed for dense specimens under an applied vertical stress of 150 kPa. For small finer fractions (Figure 7.10a), although there is a slight decrease in shear resistance, recorded vertical displacements are essentially equal following complete finer particle loss. For intermediate finer fractions (Figure 7.10b) there is a significant decrease in shear resistance and a slight decrease in vertical displacements following complete finer particle loss. For large finer fractions (Figure 7.10c) there is a significant decrease in both shear resistance and vertical displacements following complete finer particle loss. Comparing Figure 7.10c to Figure 7.10d it is evident that even when half or a quarter of finer particles are lost the shear resistance and vertical displacements decrease. It is apparent that dense specimens that are dilatant due to the presence of finer particles become increasingly less dilatant as finer particles are lost. The change in behaviour becomes more pronounced at higher finer fraction.

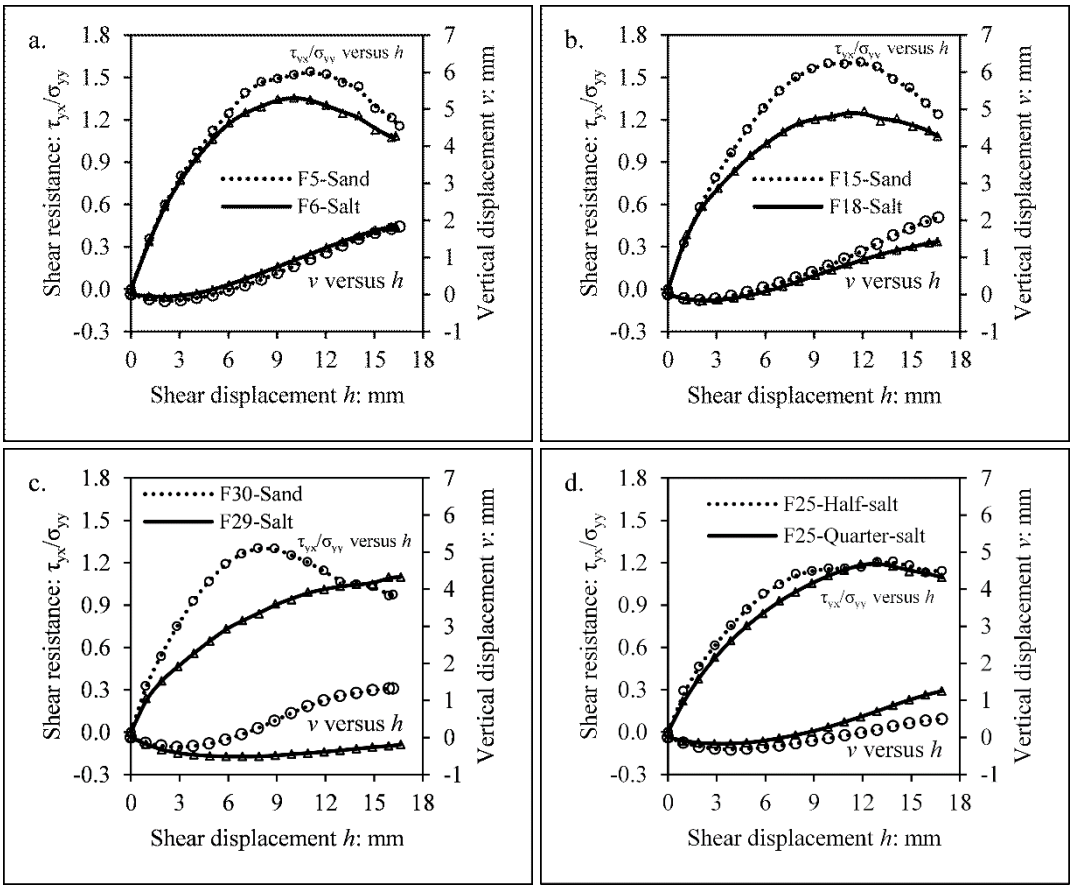


Figure 7.10: Behaviour of dense specimens under an applied vertical stress of 150 kPa: a. small finer fractions, b. intermediate finer fractions, c. large finer fractions and d. intermediate finer fractions with half and quarter finer particle loss

Figure 7.11 shows typical shear behaviour observed for dense specimens under an applied vertical stress of 75 kPa. For small finer fractions (Figure 7.11a) shear resistance does not change and vertical displacements are essentially equal following complete finer particle loss. However, for intermediate finer fractions (Figure 7.11b) both shear resistance and vertical displacements reduce following complete finer particle loss. A similar reduction in dilatancy, as observed for dense specimens under 150 kPa, is evident.

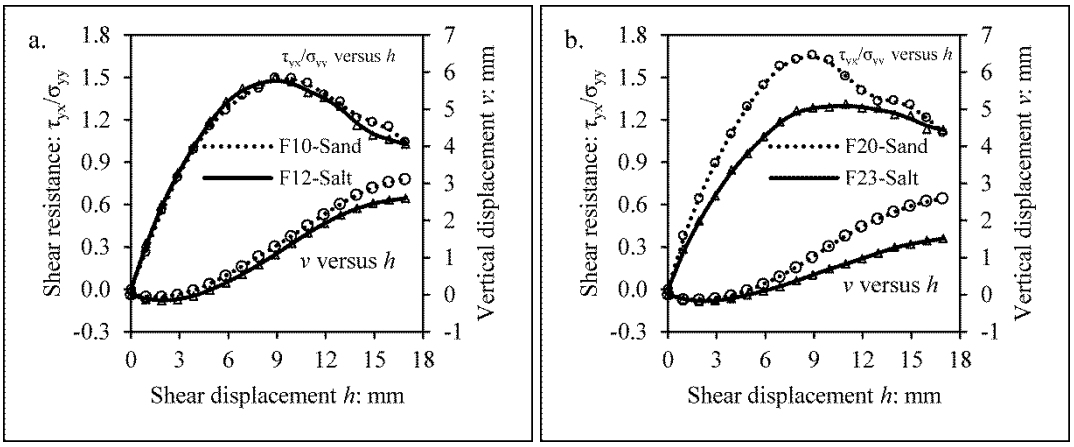


Figure 7.11: Behaviour of dense specimens under an applied vertical stress of 75 kPa: a. small finer fractions and b. intermediate finer fractions

Figure 7.12 shows typical shear behaviour observed for loose specimens under an applied vertical stress of 150 kPa. The loose specimens with sand particles are essentially contractant showing no distinct peak and small vertical displacements. Following complete finer particle loss, although a minor decrease in shear resistance and vertical displacements was recorded, shear resistance does not reduce significantly. Comparing Figure 7.12a to Figure 7.12b shows that this behaviour was not significantly different for small and large finer fractions.

Due to negligible changes in the shear behaviour of loose specimens under an average vertical stress of 150 kPa, only a few tests were done under an average vertical stress of 75 kPa. The aim of these tests was simply to see whether behaviour would be significantly different at lower vertical stresses. It is evident that for both small finer fractions (Figure 7.13a) and large finer fractions (Figure 7.13b) shear behaviour was not significantly different under lower vertical stresses.

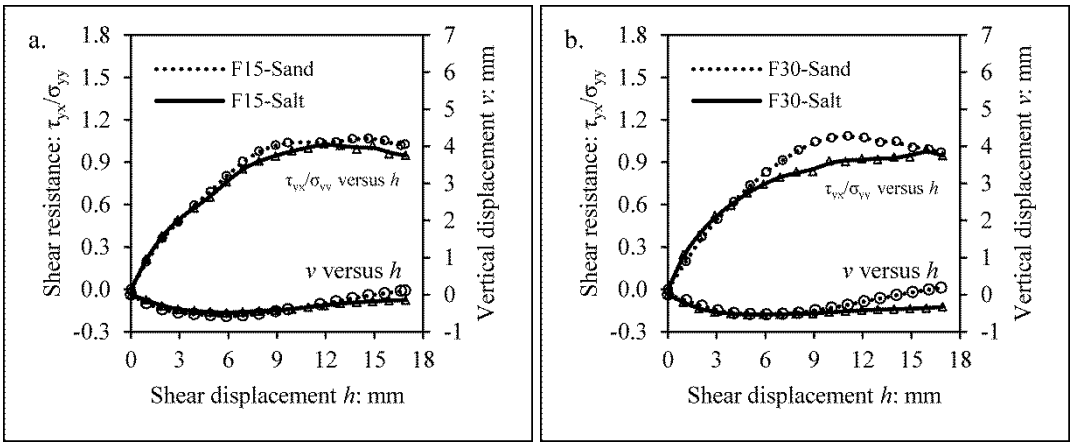


Figure 7.12: Behaviour of loose specimens under an applied vertical stress of 150 kPa: a. small finer fractions and b. large finer fractions

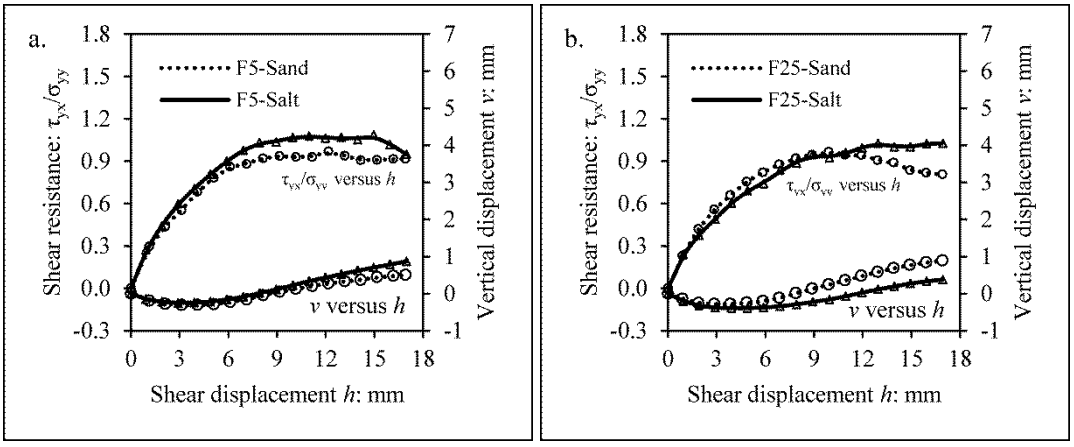


Figure 7.13: Behaviour of loose specimens under an applied vertical stress of 75 kPa: a. small finer fractions and b. large finer fractions

A smoothed line was fitted through the raw data using a spline function algorithm (Klasson, 2008). The peak value of τ_{yx}/σ_{yy} was used to obtain ϕ_p using Equation 5.1. The final values of τ_{yx}/σ_{yy} were used to obtain ϕ_{cv} using Equation 5.1. The spline function algorithm (Klasson, 2008) enables one to calculate the derivatives of the fitted spline. This was used to determine the maximum value of $\delta v/\delta h$ from which ψ was calculated using Equation 5.2. Table 7.5 summarises ϕ_p and ϕ_{cv} values obtained and Table 7.6 summarises ψ obtained for all tests. All raw data is provided in companion files (see Appendix B for details).

Table 7.5: Summary of peak and constant volume friction angles

Series	Global consistency	Applied σ_{yy} (kPa)	Successive specimen F (%), ϕ_p (°) and ϕ_{cv} (°)‡	
All-sand-fines	Dense	150	F:	5, 5, **10**, **10**, 15, 15, **20**, **20**, 25, 25, 3**0**, **30** and 35
			$\phi_{p:}$	56.9, 50.8, **52.9**, **56.1**, 54.4, 58.0, **55.2**, **55.1**, 56.1, 53.9, **53.2**, **54.2** and 52.7
			ϕ_{cv}:	49.3, 48.1, **48.8**, **49.7**, 45.9, 50.9, **46.7**, **44.9**, 48.0, 46.1, **46.3**, **44.2** and 47.2
	Dense	75	F:	5, 5, **10**, **10**, 15, 15, **20**, **20**, 25, 25, **30** and **30**
			$\phi_{p:}$	54.7, 54.9, **56.2**, **56.1**, 56.1, 57.1, **58.7**, **56.9**, 57.4, 55.0, **50.0** and **50.2**
			ϕ_{cv}:	44.2, 46.8, **46.7**, **46.2**, 48.3, 45.7, **48.1**, **45.6**, 45.4, 43.5, **40.2** and **41.3**
	Loose	150	F:	5, 5, **10**, **10**, 15, 15, **20**, **20**, 25, 25, **30** and **30**
			$\phi_{p:}$	46.9, 45.5, **46.5**, **43.0**, 46.8, 47.7, **48.4**, **47.4**, 45.5, 45.5, **45.2** and **47.3**
			ϕ_{cv}:	46.4, 44.5, **45.9**, **42.7**, 46.3, 47.0, **47.9**, **47.2**, 43.3, 44.6, **44.5** and **45.6**
	Loose	75	F:	5, **15** and 25
			$\phi_{p:}$	43.7, **47.7** and 43.7
			ϕ_{cv}:	42.8, **46.7** and 40.8
All-salt-fines	Dense	150	F:	6, 6, **12**, **12**, 18, 18, **23**, **23**, 29, 29, **34** and **34**
			$\phi_{p:}$	53.0, 53.5, **51.1**, **52.3**, 51.2, 52.4, **48.8**, **47.3**, 44.4, 47.5, **40.9** and **43.7**
			ϕ_{cv}:	47.4, 47.3, **45.9**, **46.7**, 47.3, 49.3, **48.5**, **46.8**, 44.7, 47.7, **39.8** and **43.5**
	Dense	75	F:	6, 6, **12**, **12**, 18, 18, **23**, **23**, 29, 29, **34** and **34**
			$\phi_{p:}$	55.3, 55.7, **55.9**, **53.5**, 55.0, 53.1, **52.4**, **49.1**, 50.3, 44.5, **45.0** and **44.3**
			ϕ_{cv}:	44.4, 45.7, **45.8**, **48.4**, 48.3, 45.9, **48.5**, **46.2**, 50.4, 46.1, **44.1** and **43.4**
	Loose	150	F:	5, **10**, 15, **20**, 25 and **30**
			$\phi_{p:}$	45.7, **45.4**, 45.7, **42.0**, 43.9 and **44.2**
			ϕ_{cv}:	44.9, **41.8**, 43.5, **41.9**, 43.3 and **43.4**
	Loose	75	F:	5 and 25
			$\phi_{p:}$	47.0 and 45.8
			ϕ_{cv}:	43.4 and 45.8

‡ Bold typeface for ease of reference only

Table 7.5 (continued): Summary of peak and constant volume friction angles

Series	Global consistency	Applied σ_{yy} (kPa)	Successive specimen F (%), ϕ_p (°) and ϕ_{cv} (°)	
Half-salt-fines	Dense	150	F:	20, 20, 20, **25**, **25**, 30 and 30
			$\phi_{p:}$	51.1, 51.8, 52.3, **49.2**, **50.2**, 44.1 and 46.0
			ϕ_{cv}:	47.8, 47.7, 49.4, **49.0**, **48.8**, 43.2 and 46.0
Quarter-salt-fines	Dense	150	F:	20, 20, **25**, **25**, 30 and 30
			$\phi_{p:}$	52.7, 52.9, **50.0**, **50.4**, 48.5 and 46.5
			ϕ_{cv}:	49.0, 50.1, **47.6**, **47.4**, 45.0 and 46.5

Table 7.6: Summary of dilation angles

Series	Global consistency	Applied σ_{yy} (kPa)	Successive specimen F (%) and ψ (°)	
All-sand-fines	Dense	150	F:	5, 5, **10**, **10**, 15, 15, **20**, **20**, 25, 25, 3**0**, **30** and 35
			ψ:	10.7, 9.2, **12.2**, **11.7**, 14.0, 12.5, **14.5**, **14.1**, 12.1, 13.6, **10.9**, **11.4** and 9.4
	Dense	75	F:	5, 5, **10**, **10**, 15, 15, **20**, **20**, 25, 25, **30** and **30**
			ψ:	17.2, 16.1, **17.1**, **16.4**, 17.0, 18.0, **15.9**, **17.6**, 14.9, 14.3, **12.0** and **11.9**
	Loose	150	F:	5, 5, **10**, **10**, 15, 15, **20**, **20**, 25, 25, **30** and **30**
			ψ:	2.4, 3.0, **3.8**, **3.6**, 4.9, 3.5, **5.1**, **3.8**, 4.6, 5.0, **5.5** and **5.1**
	Loose	75	F:	5, **15** and 25
			ψ:	5.8, **6.0** and 7.0
All-salt-fines	Dense	150	F:	6, 6, **12**, **12**, 18, 18, **23**, **23**, 29, 29, **34** and **34**
			ψ:	10.3, 9.8, **11.7**, **12.2**, 8.7, 8.1, **8.1**, **5.2**, 4.6, 2.4, **2.1** and **1.3**
	Dense	75	F:	6, 6, **12**, **12**, 18, 18, **23**, **23**, 29, 29, **34** and **34**
			ψ:	18.1, 16.8, **16.0**, **13.7**, 14.1, 12.9, **8.9**, **10.5**, 5.0, 6.5, **4.7** and **3.6**
	Loose	150	F:	5, **10**, 15, **20**, 25 and **30**
			ψ:	2.1, **3.2**, 2.9, **2.4**, 2.8 and **1.7**
	Loose	75	F:	5 and 25
			ψ:	6.6 and 5.5
Half-salt-fines	Dense	150	F:	20, 20, 20, **25**, **25**, 30 and 30
			ψ:	9.4, 7.3, 7.0, 5.7, 5.2, 2.4 and 3.4
Quarter-salt-fines	Dense	150	F:	20, 20, **25**, **25**, 30 and 30
			ψ:	8.3, 10.1, **8.8**, **7.7**, 6.6 and 4.4

Thermann et al. (2006) investigated the influence of laboratory assistant, displacement rate, specimen diameter and test apparatus on the repeatability of direct shear box testing. Of relevance to this thesis is the variability due to laboratory assistant (specimen preparation) as all other factors were kept constant. In the Thermann et al. (2006) study, two laboratory assistants carried out 5 tests at 5 vertical stresses, determining five friction angles. The absolute difference between the five friction angles was 10 ° and 5 ° for each assistant, or standard deviations of 1.7 and 0.8 ° respectively. However, when each assistant's five friction angles were averaged, the absolute difference between the two means was 1.97 °. Friction angles in this thesis were calculated based on single direct shear tests assuming the cohesion intercept was zero. This made investigating the error even more vital, as friction angles were not based on averages, which result in less error, but on single values. In order to assess repeatability in the current study 36 paired-tests were done. The absolute difference between ϕ_p, ϕ_{cv} and ψ values obtained in each paired-test was calculated (Figure 7.14). The average absolute difference between ϕ_p and ϕ_{cv} values was 1.7 and 1.8 ° respectively. This level of error is similar to that reported by Thermann et al. (2006) when average values are compared. Less guidance is available for error in ψ values. However, in this case, the average absolute difference in ψ values was 1.1 °. Although the average absolute errors are similar for the three measures of shear resistance, it is apparent, from the lower scatter, that ψ values showed better repeatability.

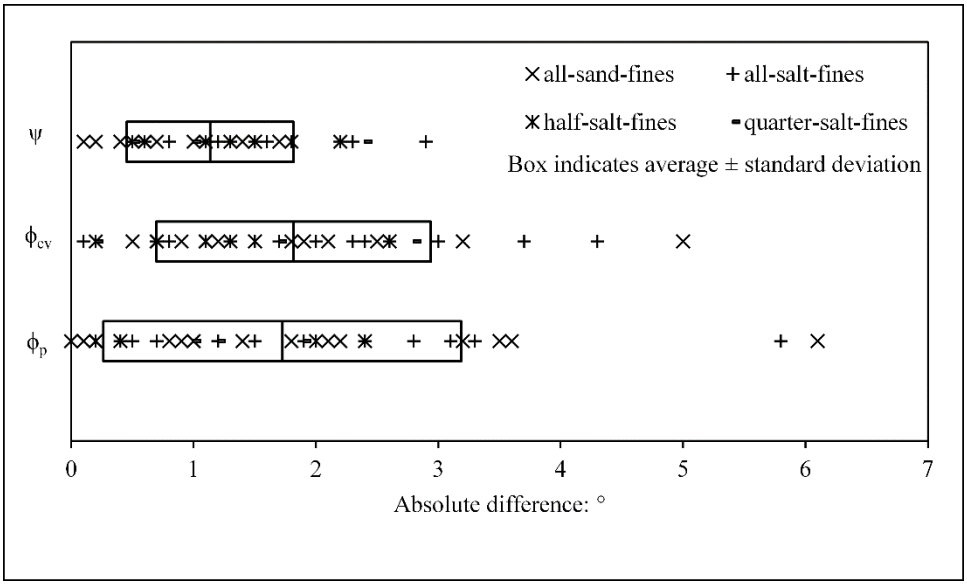


Figure 7.14: Absolute difference between values determined from paired tests

The better repeatability in ψ is in line with conclusions made in Chapter 5 and suggests that comparison of shear strength should be based predominantly on ψ rather than ϕ_p or ϕ_{cv}. However, this requires that ϕ_{cv} remain constant irrespective of F. Chang et al. (2014) suggested that as a soil becomes coarser as finer particles are lost ϕ_{cv} increases. ϕ_{cv} values from the present study are plotted against F in Figure 7.15. The large scatter in ϕ_{cv} values is due to limited horizontal displacement, such that constant volume conditions could not be reached in all cases, and in-box friction. However, F did not appear to affect ϕ_{cv} with the probability of no trend (zero slope) being 0.7.

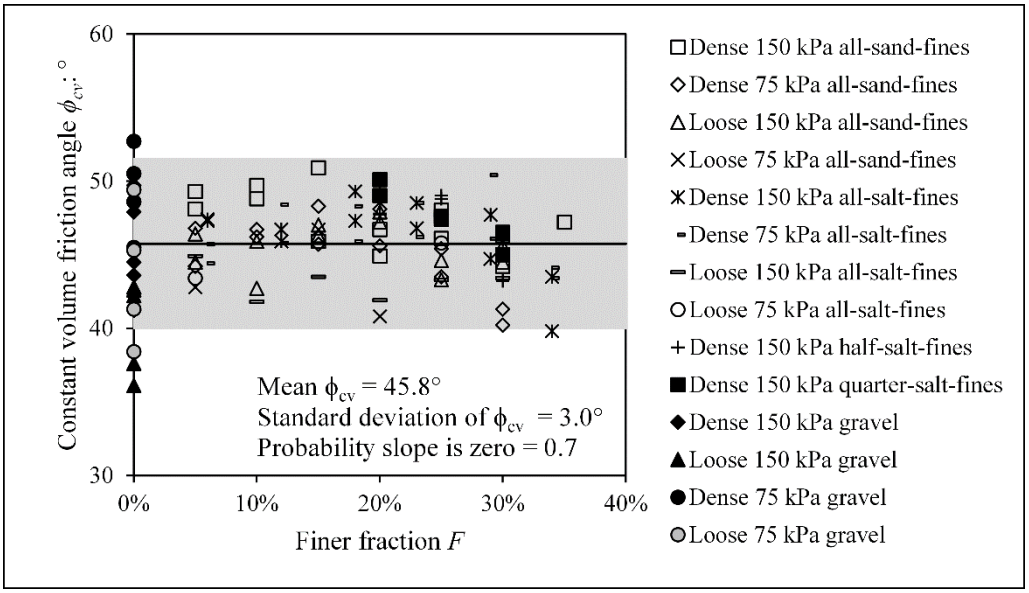


Figure 7.15: Influence of finer fraction on constant volume friction angle

The average ϕ_{cv} value for the entire data set is indicated in Figure 7.15 along with a shaded region indicating the 95 % prediction interval. The average ϕ_{cv} for dense specimens was 46.7 ° (standard deviation 2.5 °) and the average for loose specimens was 43.7 ° (standard deviation 2.9 °). These ϕ_{cv} values are higher than typical values of 37 ° for feldspathic sands (Bolton, 1986) such as the granitic material used in this study. Estimating ϕ_{cv} from the angle of a continuously falling slope in a rotating cylinder (Atkinson, 2007) suggested that it was in fact between 37 and 39 °. The reason the indicated ϕ_{cv} are high is due to the effects of in-box friction, which applies an additional normal load on the shear plane that is not measured by the load cell above the shear box. This additional unmeasured normal load increases with density, hence the different measured ϕ_{cv} for dense and loose specimens. Limited shear displacement also meant constant volume conditions were not fully reached.

Basing the interpretation of shear strength on ψ values also requires that flow rules apply. Plotting ϕ_p versus ψ (Figure 7.16) shows general agreement with the flow rule (Equation 5.8) proposed by Bolton (1986), although the slope is steeper at 0.9 and there is considerable scatter. The intercept of the best fit suggests ϕ_{cv} was 42.0 °. This value is also higher than obtained from the angle of a continuously falling slope in a rotating cylinder (37 – 39 °) for the same reasons outlined above.

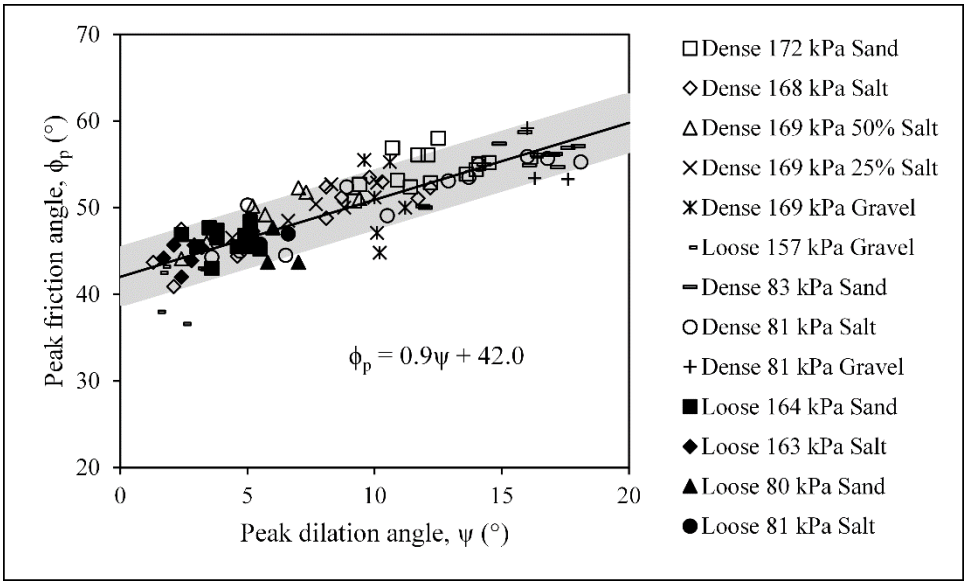


Figure 7.16: Influence of specimen density and finer fraction on flow rules

Because of the observations outlined above that ψ showed greater repeatability, that ϕ_{cv} values were independent of finer fraction and that results showed general agreement with flow rules, comparisons of shear strengths was based on ψ rather than ϕ_{cv} and ϕ_p.

7.4 Discussion of results

7.4.1 Dissolution under one-dimensional loading

Results from tests on dense specimens under a vertical stress of 150 kPa are presented (Figure 7.17). Figure 7.17a shows flooded coarse and global void ratios for all-sand-fines specimens with best fit curves A and B. Up to F = 15 % (F_t) packing behaviour was close to that of a binary mixture, with e_c marginally higher than $e_{c\ min}$ but remaining constant. As F increases, e_c increases and exceeds $e_{c\ max}$ at F = 27 % (F_c).

Figure 7.17b illustrates pre and post finer particle loss coarse void ratios for all-salt-fines specimens (i.e. initial and then dissolved e_c). Sterpi (2003) suggested that the volume change caused by finer particle loss could be quantified by either assuming: (i) total volume remains constant; (ii) global void volume remains constant; or (iii) global void ratio remains constant. If the effect of finer particle loss is that the total volume (V_t) remains constant, then e_c would not change and would remain along line A. If the effect of finer particle loss is that the overall void volume (V_v) remains constant, the values of e_c would decrease to lie along line C (see Appendix C.2 for phase relationship derivations). If the effect of finer particle loss is that the global void ratio (e) remains constant, the values of e_c would decreases still more to lie along line B. The actual volume changes are illustrated by the open symbols and lie along line D. For $F < F_t$ the volume changes were negligible but above F_t some volume change took place. As lines B and C lie below $e_{c\,min,}$ they are impossible states of compactness and as expected, such large volume changes did not take place.

Figure 7.17c illustrates pre and post finer particle loss coarse void ratios for half-salt-fines specimens. As expected, less settlement took place when only half of the finer particles were lost, with e_c remaining essentially unchanged (remaining along line A) for $F_t < F < F_c$. Similar settlements were recorded when a quarter of the finer particles were lost (Figure 7.17d). Results for half-salt-fines and quarter-salt-fines, being intermediate between all-sand-fines and all-salt-fines results, shows that the uneven distribution of finer particles observed following testing did not affect settlement behaviour significantly.

The smaller settlements when only a half or a quarter of finer particles were lost for $F_t < F < F_c$, suggests that not all finer particles are lost in these fabrics as some finer particles are load bearing and therefore stabilised. As F increases above F_t, finer particles hinder the coarser particles from moving into their densest arrangement. The finer particles that hinder the coarser particles must therefore be loaded. The largest volume change was recorded for $F > F_c$ in all cases, reflecting the increased load on finer particles as F increases.

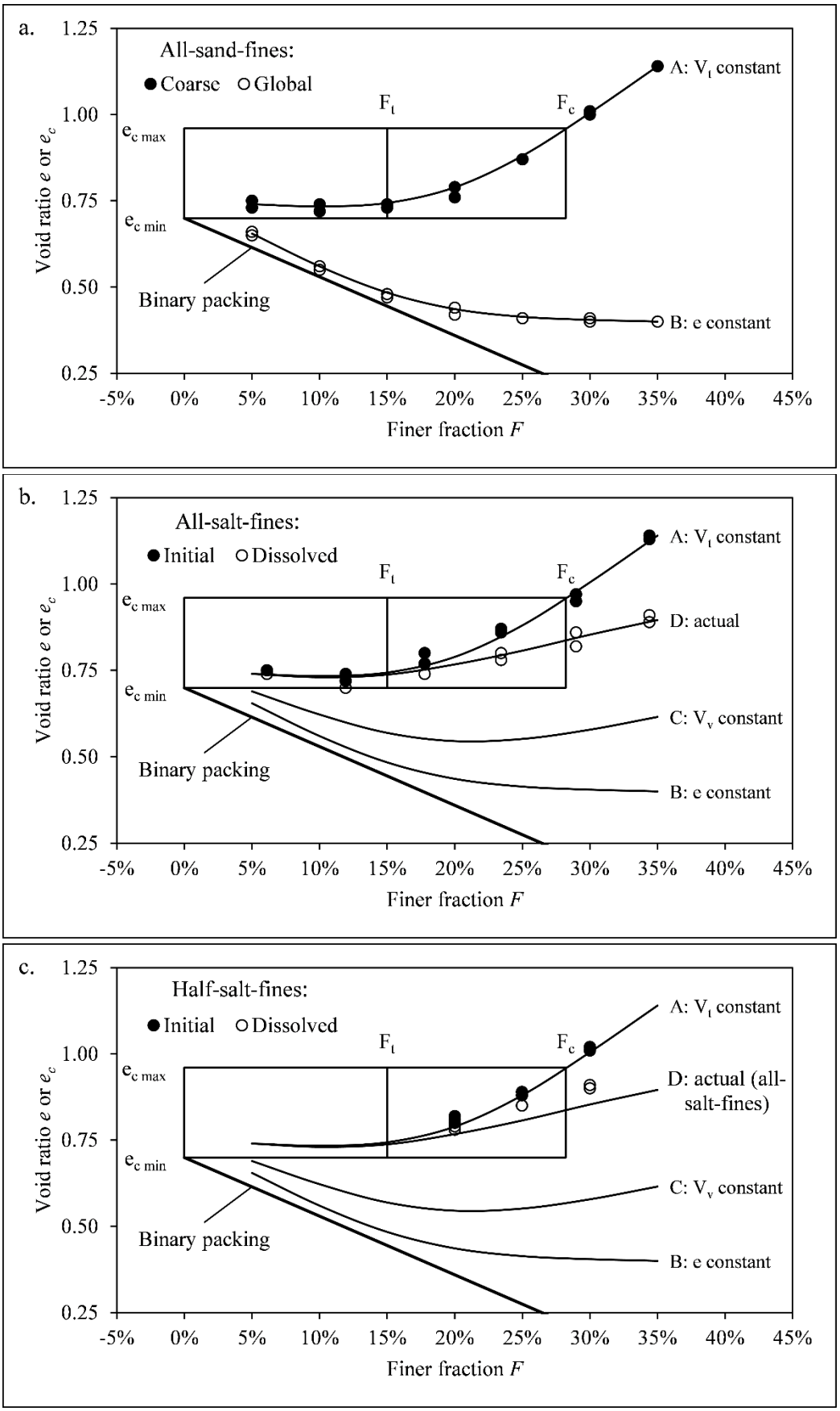


Figure 7.17: Changes in void ratios for dense specimens under 150 kPa vertical stress, a. all-sand-fines, b. all-salt-fines, c. half-salt-fines and d. quarter-salt-fines.

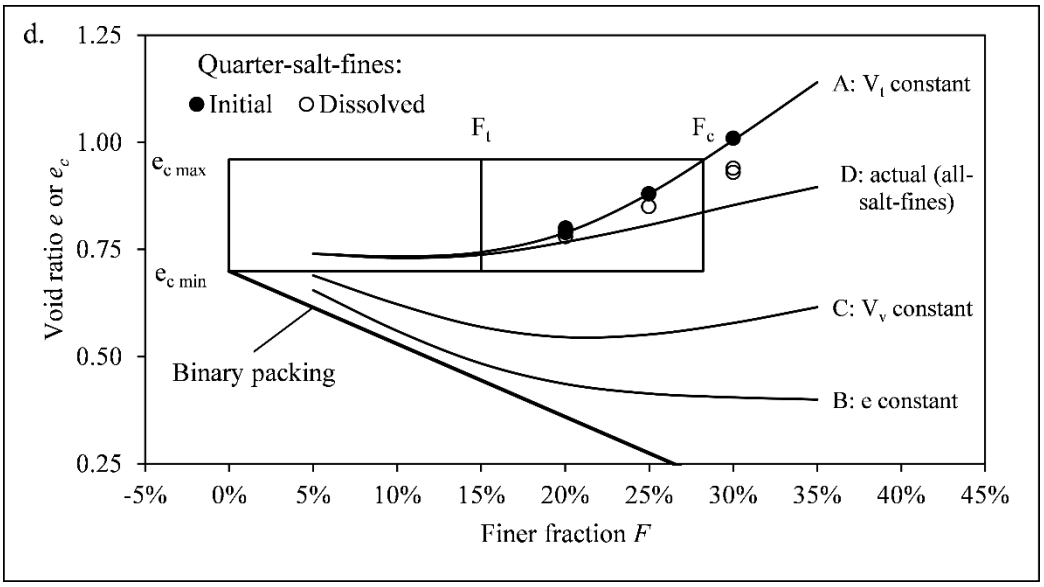


Figure 7.17 (continued): Changes in void ratios for dense specimens under 150 kPa vertical stress, a. all-sand-fines, b. all-salt-fines, c. half-salt-fines and d. quarter-salt-fines

Results from the various tests on dense specimens under a vertical stress of 75 kPa are presented in Figure 7.18. Figure 7.18a shows that flooded global and coarse void ratios for all-sand-fines specimens were similar to those recorded for dense specimens under a vertical stress of 150 kPa (Figure 7.17a). Figure 7.18b illustrates pre and post finer particle loss coarse void ratios for all-salt-fines specimens (i.e. initial and then dissolved e_c). Line A represents the total volume remaining constant, line B the global void volume remaining constant and line C the global void ratio remaining constant. Volume changes were similar to those observed for dense specimens under a vertical stress of 150 kPa (Figure 7.17b).

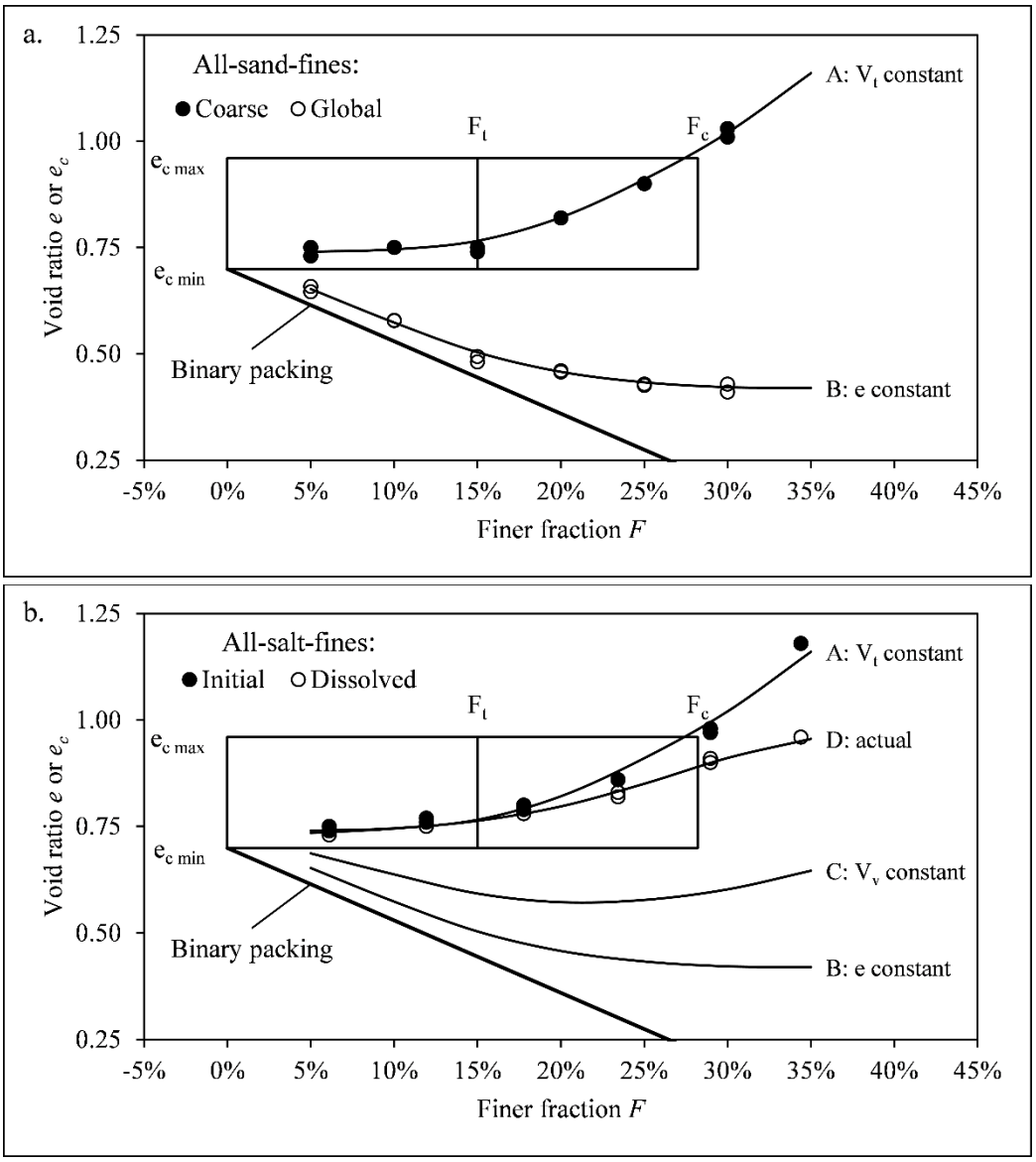


Figure 7.18: Changes in void ratios for dense specimens under 75 kPa vertical stress, a. all-sand-fines and b. all-salt-fines

Results from various tests on loose specimens under a vertical stress of 150 kPa are presented in Figure 7.19. Figure 7.19a illustrates flooded coarse and global void ratios for all-sand-fines specimens along with best fit curves A and B. Up to F = 15 % packing behaviour was equal to that of a binary mixture, with e_c remaining constant at $e_{c\,max}$. As F increases, e_c increases and exceeds $e_{c\,max}$. Figure 7.19b illustrates pre and post finer particle loss coarse void ratios for all-salt-fines specimens (i.e. initial and then dissolved e_c). Lines A, B and C represent the various potential volume changes outlined above. Despite portions of line B and C laying above $e_{c\,min}$, that is representing physically admissible volume changes, smaller volume changes than required to reach these states were recorded following finer particle loss. As expected,

all post finer particle loss void ratios fell below $e_{c\ max}$, as this represents the loosest stable packing of the remaining coarse material.

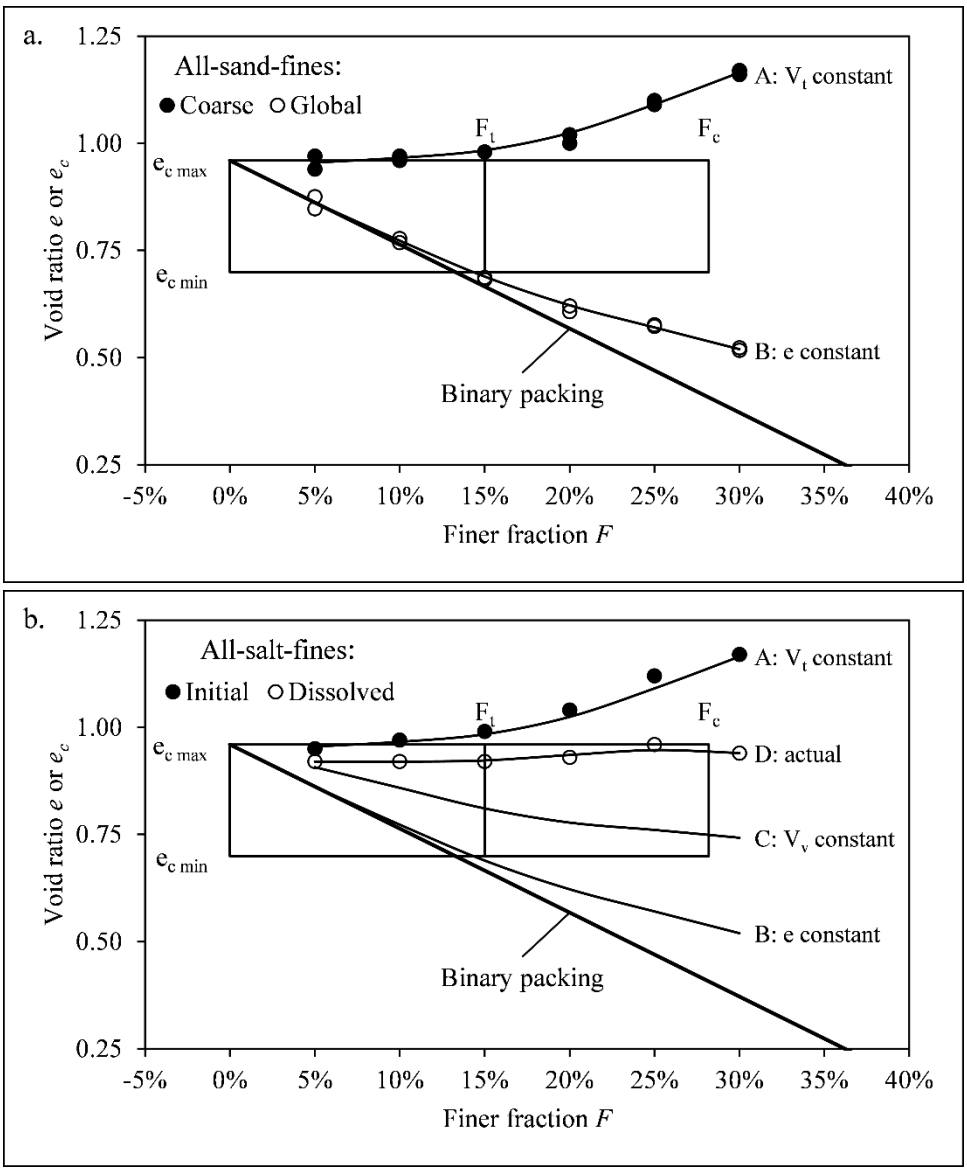


Figure 7.19: Changes in void ratios for loose specimens under 150 kPa vertical stress, a. all-sand-fines and b. all-salt-fines

Results from tests on loose specimens under a vertical stress of 75 kPa are presented in Figure 7.20, in a similar manner as those at 150 kPa (Figure 7.19). Although fewer tests were done at 75 kPa, it is, evident that behaviour is similar to loose specimens tested under a vertical stress of 150 kPa.

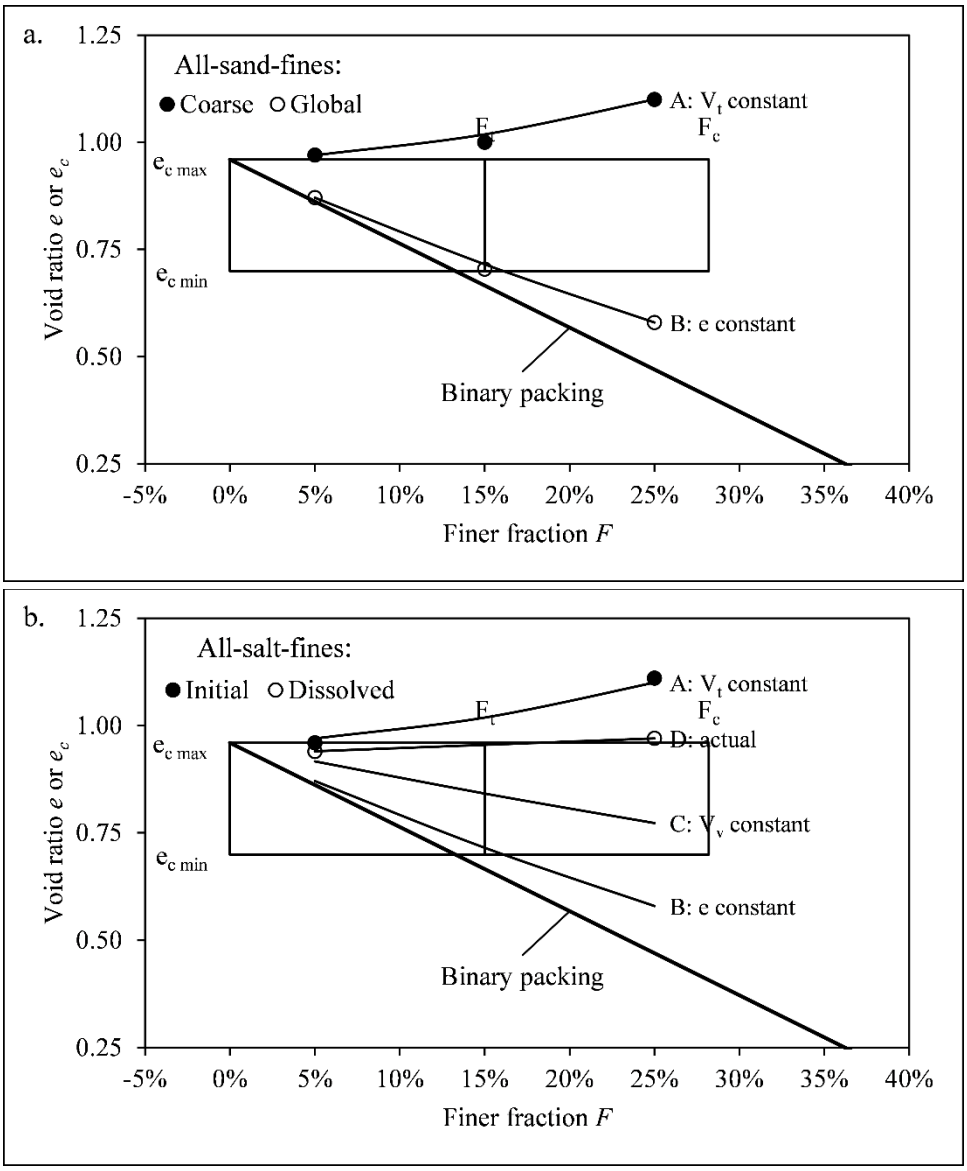


Figure 7.20: Changes in void ratios for loose specimens under 75 kPa vertical stress, a. all-sand-fines and b. all-salt-fines

Based on the post finer particle loss e_c, presented above for dense and loose tests under each vertical stress, it is possible to define settlement envelopes (Figure 7.21). On Figure 7.21 the solid lines show the initial values of e_c for the dense and loose specimens. If the effect of suffusion is that the total volume remains constant, then e_c will be the same after finer particle loss. If the effect of suffusion is that the overall void volume remains constant, the values of e_c would decrease to the chain dotted lines. If the effect of suffusion is that overall void ratio remains constant, the values of e_c would decrease still more, lines showing the results of this assumption are not shown in Figure 7.21. The actual measured values of e_c after finer particle loss are shown by the two pairs of dotted and dashed lines; dotted lines for tests at 150 kPa

and dashed lines for tests at 75 kPa. The upper line of each pair showing the boundary for loose specimens and the lower line of each pair showing the boundary for dense specimens. Soils at intermediate D_r will likely settle to e_c between these boundaries, with higher e_c obtained for lower D_r. It is evident that at higher vertical stresses, both the upper and lower boundaries move down. This is to be expected, as higher stresses will induce greater settlements. Of the assumptions proposed by Sterpi (2003), that of constant total volume fits the experimental envelopes best. However, the coarser particles have limiting packings (i.e. $e_{c\,max}$ and $e_{c\,min}$) and e_c after settlement did not go above or below these boundaries.

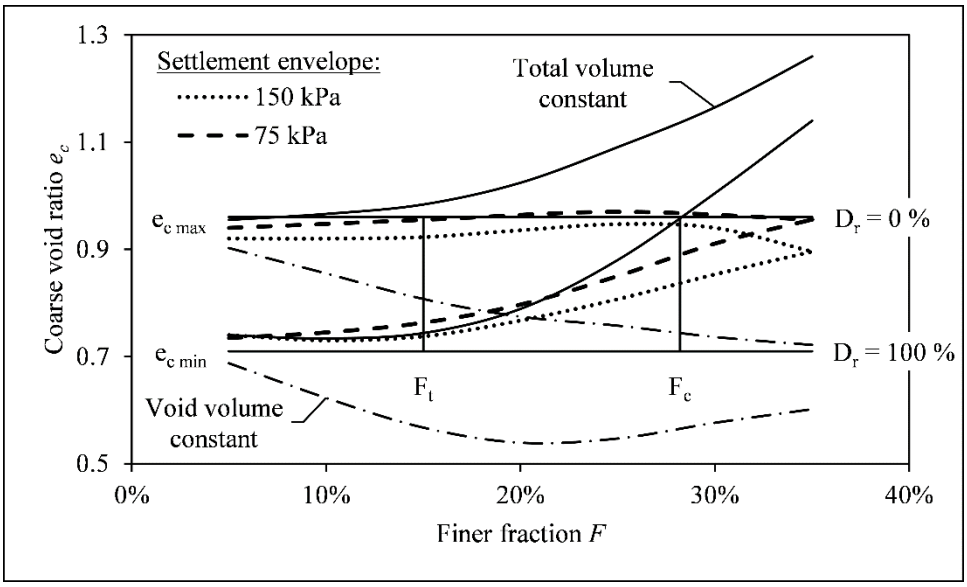


Figure 7.21: Settlement envelopes of internally unstable soils

Figure 7.22 plots flooded or dissolved e_c against initial e_c after load application but prior to wetting. Also included are lines indicating the relative density of the coarser particles ($D_{r,ec}$). To quantify settlement that took place during flooding or dissolution under one-dimensional loading, settlement potential (SP) contours are indicated. These were calculated from Equation 7.2:

$$SP = \frac{e_{c,0} - e_{c,d}}{1 + e_{c,0}} \qquad \text{Equation 7.2}$$

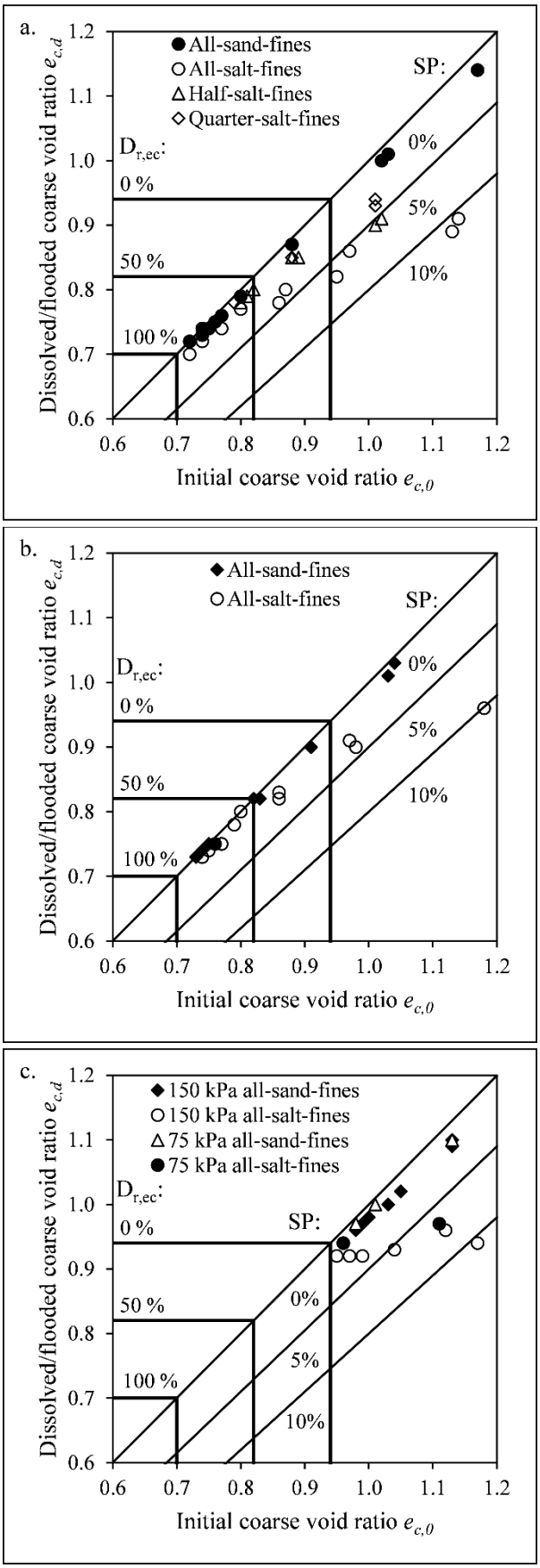


Figure 7.22: Change in coarse void ratios due to finer particle loss: a. Dense specimens at 150 kPa; b. Dense specimens at 75 kPa; and c. All loose specimens

As expected, for all-sand-fines specimens, at all consistencies and applied stress, e_c did not change significantly due to flooding (Figure 7.22). Although at high initial e_c some settlement did take place during flooding. These specimens had significant portions of finer particles and these likely rearranged during flooding resulting in the observed settlement. SP ranged between 0 and 1.4 % for dense specimens and between 0.5 and 2.3 % for loose specimens.

Figure 7.22a shows results from all dense specimens under a vertical stress of 150 kPa. For all-salt-fines specimens, e_c did not change significantly for specimens with $D_{r,ec}$ between 50 and 100 %. SP ranged between 1 and 2 %, similar ranges of values were recorded for all-sand-fines specimens. This suggests that the additional settlement due to finer particle loss was negligible. However, for $D_{r,ec} < 50$ % increasing settlement was observed reflecting the larger role finer particles play in supporting coarser particles. The average SP value for these specimens was 4 %. As expected, less settlement took place for half-salt-fines and quarter-salt-fines as only a portion of the finer particles were lost with SP values ranging between 2 and 5 %. Figure 7.22b shows the behaviour of dense specimens under a vertical stress of 75 kPa was similar to that under 150 kPa, although slightly less settlement occurred under the lower vertical stress.

Figure 7.22c illustrates settlement that occurred for loose specimens at both 150 and 75 kPa. All post finer particle loss e_c were essentially at $D_{r,ec} \approx 0$ %, as this represented the loosest stable arrangement of the coarser particles.

It is somewhat misleading to discuss the dissolution behaviour under one-dimensional settlement using e_c, as it appears that in all cases the void ratio gets smaller. However, prior to finer particle loss the global void ratio (e), is smaller than coarse void ratio (e_c), due to the presence of finer particles. Figure 7.23 shows initial e (all-sand-fines specimens in which no finer particle loss took place) and e after finer particle loss (all-salt-fines, half-salt-fines and quarter-salt-fines specimens in which 100, 50 and 25 % of the finer fraction was lost). In the case of 100 % finer particle loss, e will become equal to e_c. Thus, during finer particle loss, although e_c decreases slightly, e increases substantially and it is this global change in fabric that will control shear strength.

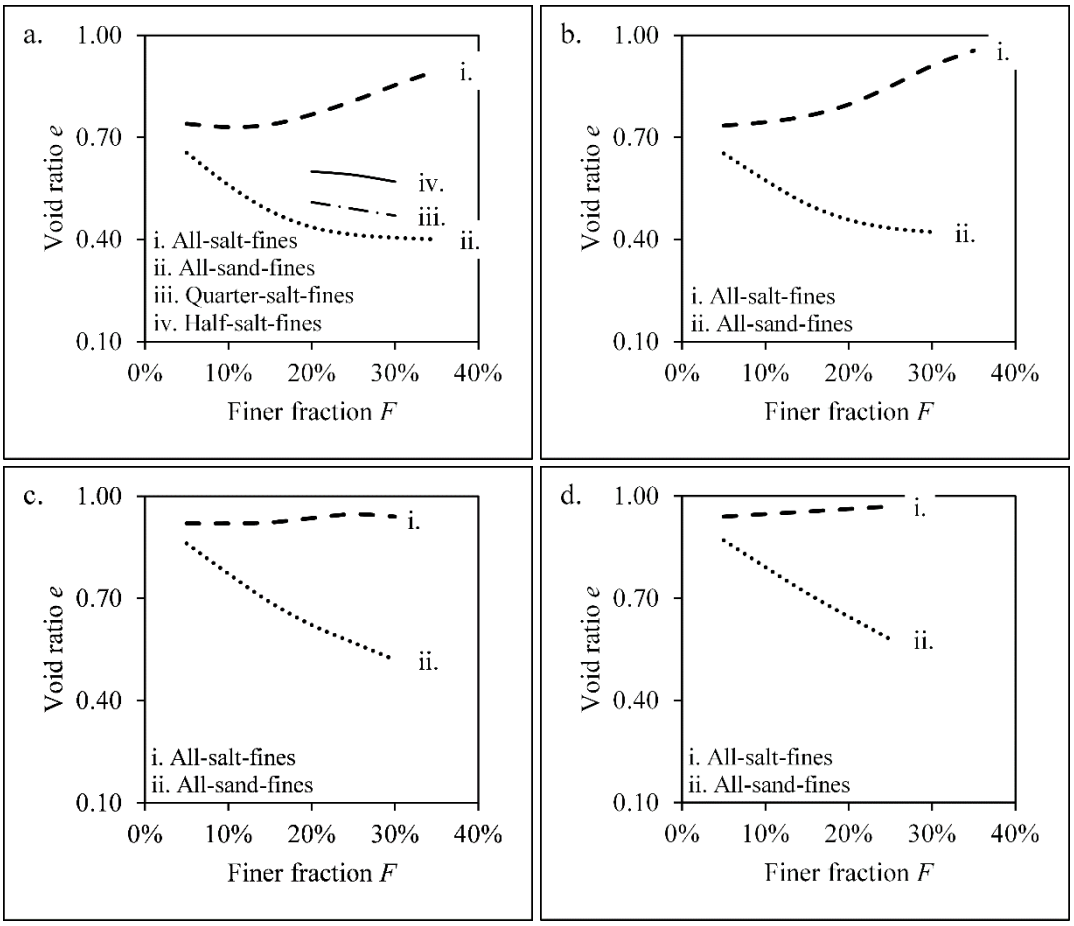


Figure 7.23: Summary of settlement behaviour for different percentages of finer particle loss, a. Dense specimens at 150 kPa vertical stress, b. Dense specimens at 75 kPa vertical stress, c. Loose specimens at 150 kPa vertical stress and c. Loose specimens at 75 kPa

7.4.2 Shearing

Change in shear behaviour with increasing finer fraction

Figure 7.24 shows measured ψ with increasing F for: (i) all-sand-fines specimens in which no finer particles were lost, (ii) all-salt-fines specimens in which all finer particles were lost, (iii) half-salt-fines specimens in which 50 % of finer particles were lost and (iv) quarter-salt-fines specimens in which 25 % of finer particles were lost. Prior to dissolution, specimens were dense and shearing was under an initial vertical stress of 150 kPa. Also included in this figure are ψ measured for dense and loose specimens of the coarser fabric only (i.e. F = 0 %). Third-degree polynomial regression curves are plotted through the all-sand-fines and all-salt-fines data and shaded areas indicate 95 % prediction intervals.

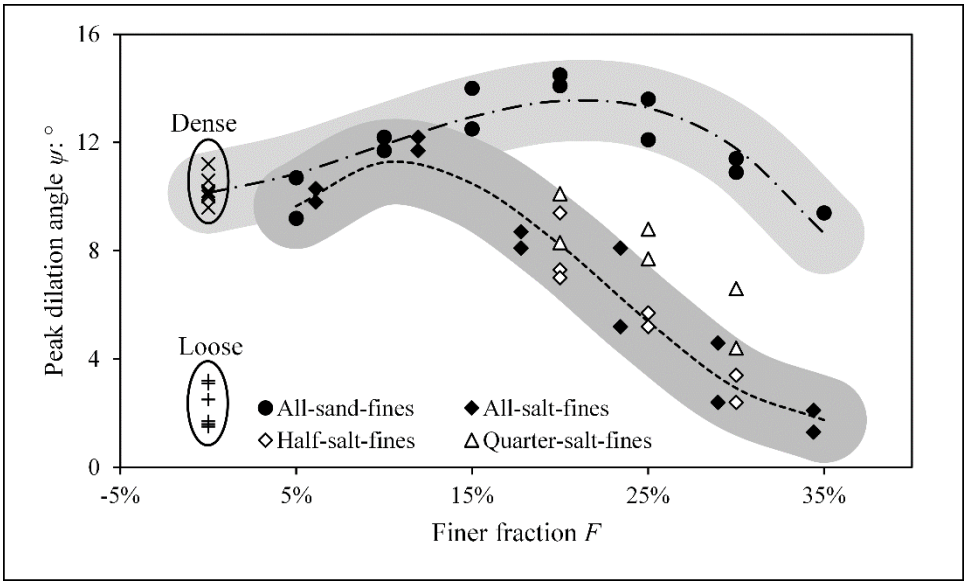


Figure 7.24: Shear behaviour of dense specimens under an initial vertical stress of 150 kPa with different finer fractions and finer particle loss

Considering all-sand-fines specimens (Figure 7.24), it is evident that finer particles increase shear strength up to a point, after which additional finer particles appear to decrease shear strength. Considering all-salt-fines specimens (Figure 7.24), no significant weakening of shear strength is observed for F < 15%, on the contrary a slight increase is observed. With F > 15 % shear strength is observed to decrease significantly, with measured ψ reducing to similar values as the coarser fabric in a loose state as F increases. The reduction in ψ caused by finer particle loss ranges from a few degrees to 9 °.

A similar weakening in shear strength is observed in half-salt-fines and quarter-salt-fines specimens (Figure 7.24). Some of the quarter-salt-fines specimens exhibited a similar reduction in shear strength, although on average, the reduction was not as large as for all-salt-fines and half-salt-fines specimens. Results for half-salt-fines and quarter-salt-fines, being intermediate between all-sand-fines and all-salt-fines results, shows that the uneven distribution of finer particles observed following testing did not affect shear behaviour significantly. Overall, this shows that it is not necessary for all finer particles to be lost to reduce the available shear strength. Rather a metastable fabric is likely to develop where finer particles sit between coarser particles with locally enlarged voids due to finer particle loss.

Figure 7.25 shows measured ψ with increasing F, for the same conditions as Figure 7.24 except that shearing was under an initial vertical stress of 75 kPa. Considering the all-sand-fines specimens, in which no finer particle loss took place, finer particles do not significantly increase shear strength, as was apparent for tests under the larger vertical stress. Nevertheless, additional finer particles do decrease the shear strength following particle loss in a similar manner. Another difference is that ψ values are larger under the lower vertical stress. The weakening caused by finer particle loss is similar to that in Figure 7.24 but the reduction in ψ is not as large as for the tests under an initial vertical stress of 150 kPa and ranges from a few degrees to 5 °.

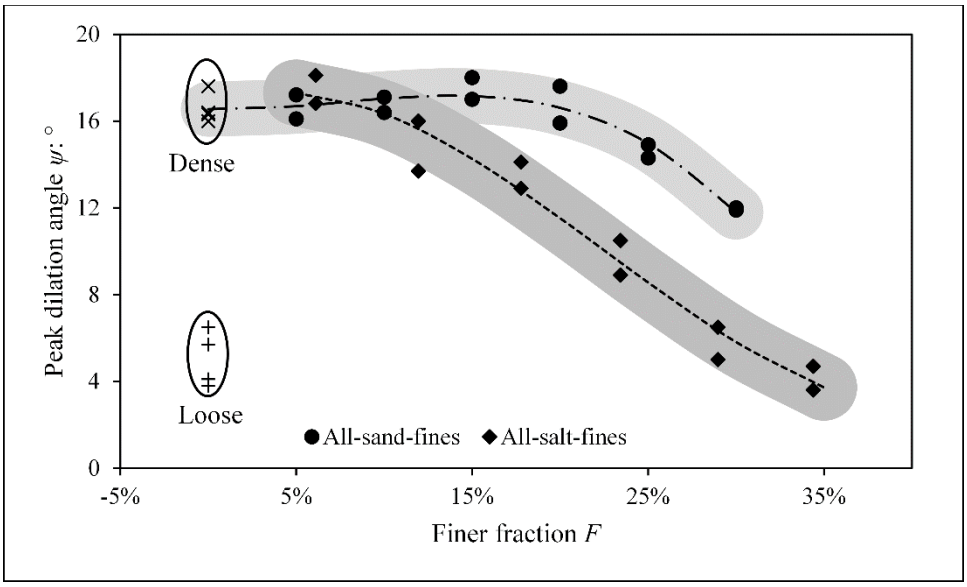


Figure 7.25: Shear behaviour of dense specimens under an initial vertical stress of 75 kPa with different finer fractions and finer particle loss

Figure 7.26 shows measured ψ with increasing F, for the same conditions as Figure 7.24 except that all specimens were initially loose. Sufficient data was only available to determine 95 % prediction intervals for the all-sand-fines specimens. However, a similar prediction interval is assumed and drawn to illustrate the scatter in all-salt-fines data. For the all-sand-fines specimens, finer particles marginally increase strength. As these specimens are loose, the strength is significantly less than measured for dense specimens. A marginal weakening of shear strength is observed for salt specimens with F > 15 %, with strength being similar to that of the coarser fabric in a loose state. These results suggest that, for loose specimens, finer particles add some strength to the "flow" fabric that develops at the critical state (Murthy et al., 2007).

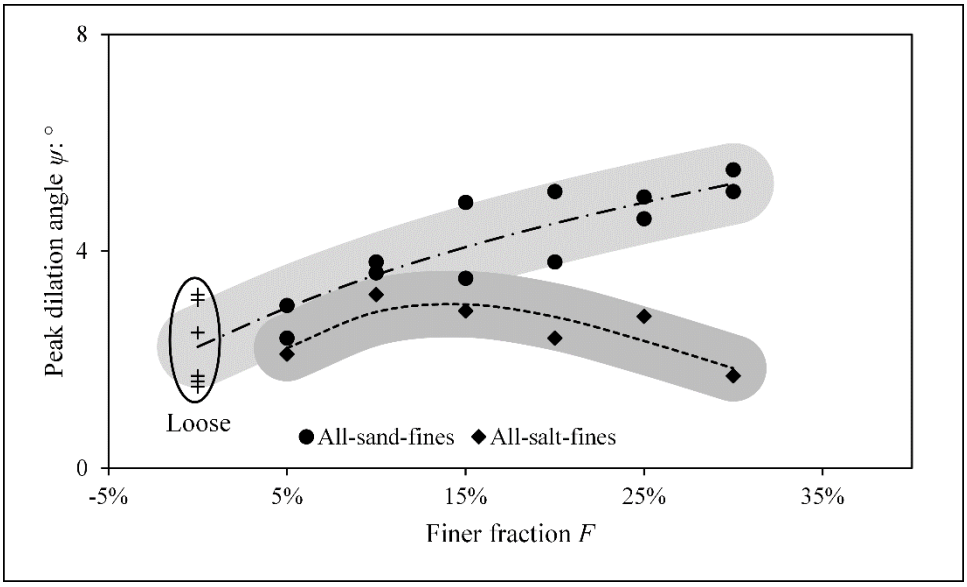


Figure 7.26: Shear behaviour of loose specimens under an initial vertical stress of 150 kPa with different finer fractions and finer particle loss

For the limited tests carried out on loose specimens under an initial vertical stress of 75 kPa (Figure 7.27), measured behaviour was not significantly different to that described in the preceding paragraph. The main difference being that ψ values were marginally higher due to the lower vertical stress. As no significant change in shear strength for loose specimens under either vertical stress value was noted, no further analysis of these results is presented.

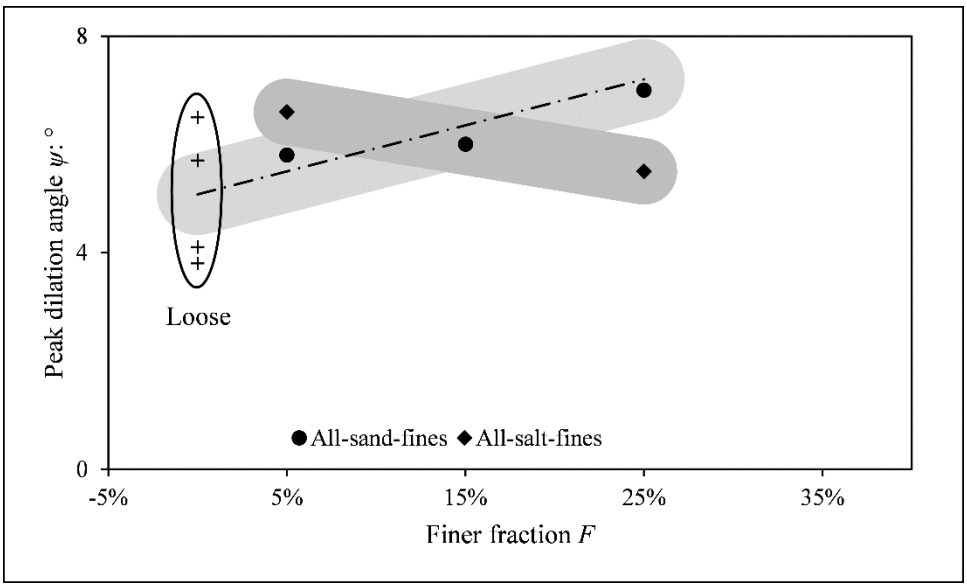


Figure 7.27: Shear behaviour of loose specimens under an initial vertical stress of 75 kPa with different finer fractions and finer particle loss

Change in shear behaviour with coarse void ratio

Figure 7.28 plots ψ against the relative density of the coarser particles ($D_{r,ec}$) for: (i) all-sand-fines specimens in which no fines were lost, (ii) all-salt-fines specimens in which all finer particles were lost, (iii) half-salt-fines specimens in which 50 % of finer particles were lost and (iv) quarter-salt-fines specimens in which 25 % of finer particles were lost. Specimens were initially dense and shearing was under an initial vertical stress of 150 kPa. As e_c was in some cases greater than its value when coarser particles alone were in their loosest state due to the presence of finer particles, $D_{r,ec}$ values less than 0 % were set to 0 %. Superimposed on the data are contours for F_t = 15 % and F_c = 27 %.

Considering first the all-salt-fines specimens, the measured strength is directly proportional to $D_{r,ec}$ (Figure 7.28). This is to be expected as with all finer particles lost $D_{r,ec}$ is a measure of global relative density. Considering the all-sand-fines, half-salt-fines and quarter-salt-fines specimens, strength steadily increases as a larger portion of coarse voids are filled with finer particles. Thus, although the coarser particles are in a state looser than the maximum density that they could be alone, finer particles provide reinforcing. Therefore, when $F_t < F < F_c$ finer particles form part of the load bearing fabric when developing peak strength (i.e. resisting deviatoric stresses), with the role of finer particles increasing as F increases. For $F < F_t$ the measured shear

behaviour is largely unaffected by the removal of finer particles, with the shear strength of specimens with and without finer particles being similar.

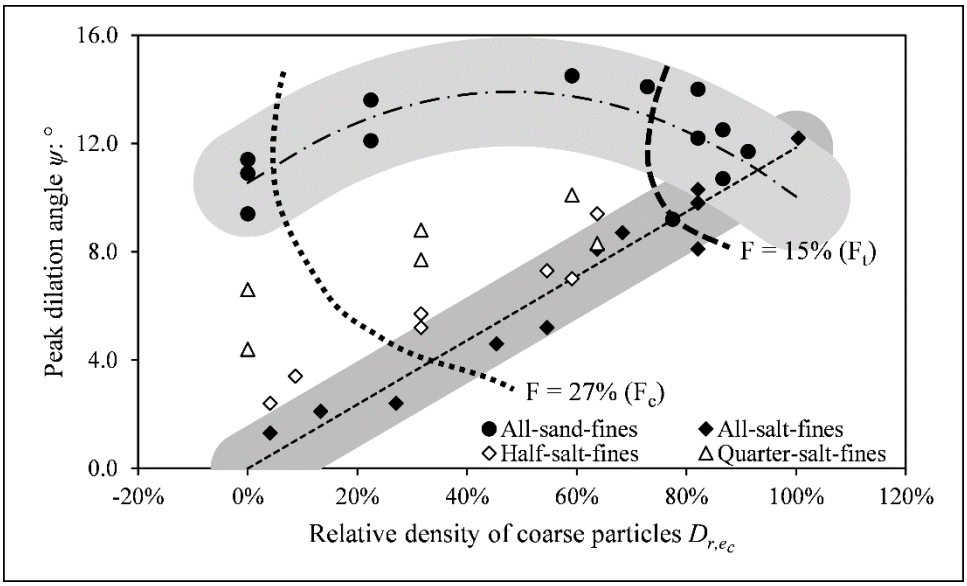


Figure 7.28: Shear behaviour of dense specimens under an initial vertical stress of 150 kPa in relation to coarse void ratio

Figure 7.29 plots ψ against $D_{r,ec}$ for the same conditions in Figure 7.28 except that shearing was under an initial vertical stress of 75 kPa. It is clear that behaviour is similar to that described above for specimens under the larger vertical stress. It is, therefore, evident that finer particles play a similar role in developing peak strength (i.e. resisting deviatoric stresses) for $F_t < F < F_c$.

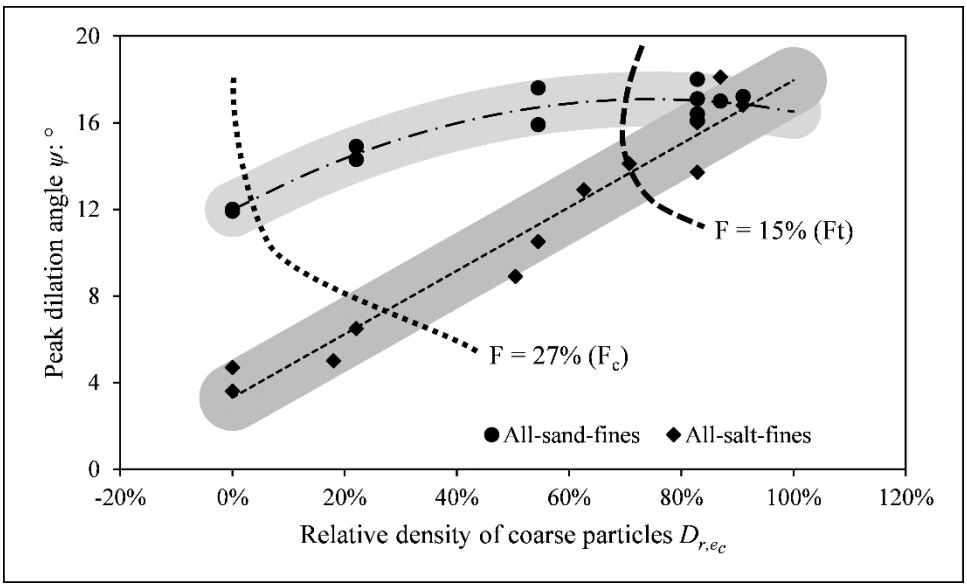


Figure 7.29: Shear behaviour of dense specimens under an initial vertical stress of 75 kPa in relation to coarse void ratio

Change in shear behaviour with global void ratio

From the above discussions, it is apparent that the change in behaviour is both a function of how the coarse void ratio changes and how much of this void space is filled with finer particles. A measure of the combination of these two is the global void ratio (e). When e is referenced to its limiting values as relative density (D_r), soil shear strength is observed to increases with an increase in D_r. This is indeed the case under both high vertical stress (Figure 7.30) and low vertical stress (Figure 7.31). D_r indicated is based on the void ratio following either flooding or dissolution of salt. As reference void ratios (e_{min} and e_{max}) were determined on dry samples, some tested specimens had marginally lower void ratios due to flooding, D_r values greater than 100 % were therefore set to 100 %. It is evident that at higher vertical stress, dilation is suppressed, particularly at low D_r; this is consistent with expected behaviour (Bolton, 1986).

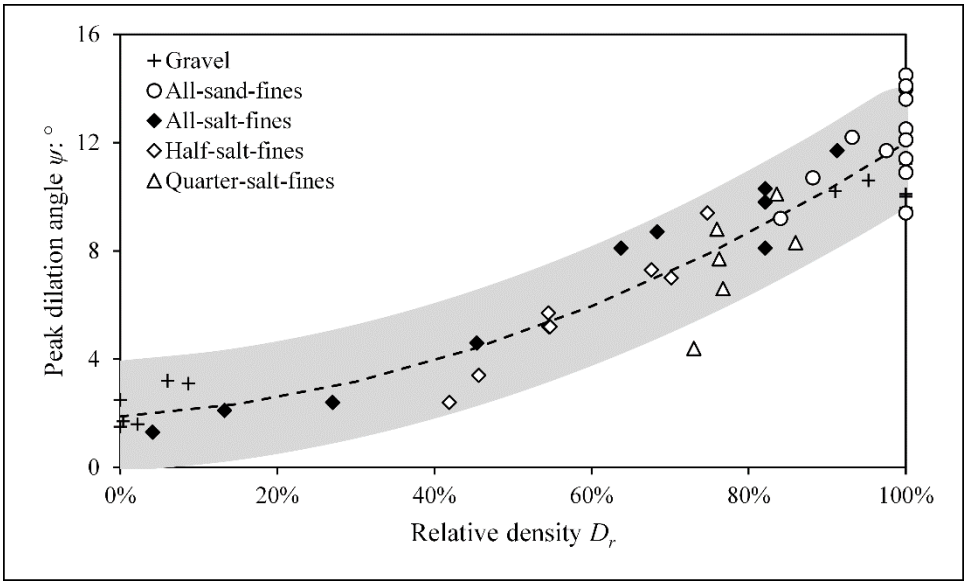


Figure 7.30: Shear behaviour of dense specimens under an initial vertical stress of 150 kPa in relation to global relative density

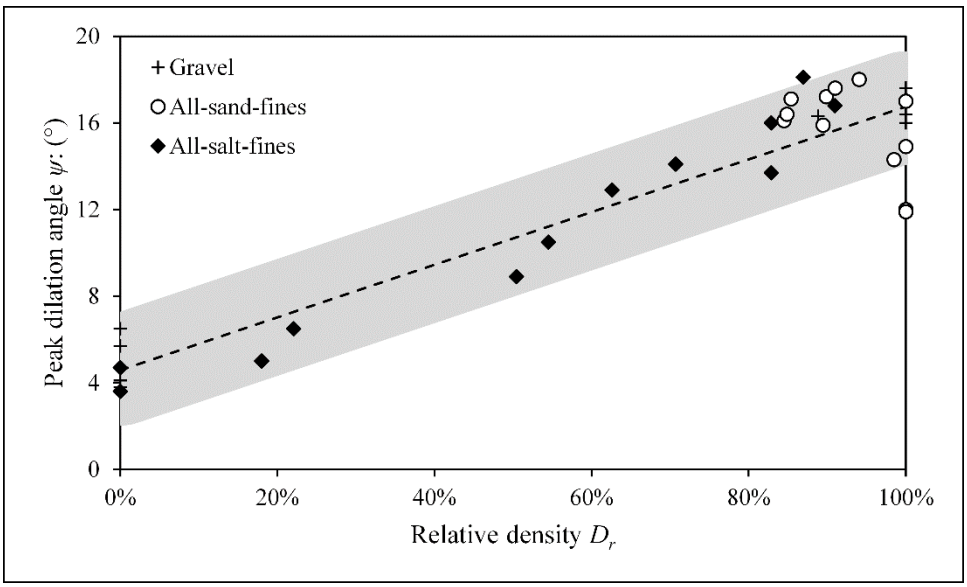


Figure 7.31: Shear behaviour of dense specimens under an initial vertical stress of 75 kPa in relation to global relative density

7.5 Observed changes of mechanical behaviour compared to changes described in literature

Sterpi (2003) suggested that finer particle loss results in an increase in density in some cases. In contrast, in the present study, in no cases did the global density increase. Instead global density decreased as global volume did not decrease in proportion to the quantity of finer particles lost. To investigate the change in strength, Sterpi (2003) reconstituted specimens with different finer fractions and initial relative densities and stated that, "partial or total removal of the fine particles produces, in general, an increase of stiffness and shear strength, for both cases of constant ([D_r =]70%) and reduced ([D_r =]30%) relative densities. Only one case is reported of negligible variation of stiffness and slight loss of shear resistance, that is the case of partial erosion (μ_e [fraction of finer particles lost] = 0.1) associated with a reduction of relative density (D_r = 30%)." In contrast to these findings, in the present study no increase in shear resistance following partial or total removal of finer particles was observed (when considering dilation angles). Although stiffness could not be explicitly measured in the variedSB, the slope of τ_{yx}/σ_{yy} versus shear displacement (h) decreased in all instances following finer particle loss. This reduction in slope is an indication of a reduction in stiffness (Noonan and Nixon, 1972). These clear differences highlight the difficulty of trying to model fabric changes by reconstituting specimens.

Chang et al. (2014), by subjecting specimens to suffusion in a triaxial cell, showed that a global increase in void ratio occurs. Following finer particle loss of 2.5 – 6.8 % (measured as a fraction of total mass) peak friction angles were observed to reduce by between 1.1 – 5.9 °. The soil studied by Chang et al. (2014) was a 65:35 mixture of a 1.18 – 5.0 mm gravel and 0.09 – 0.15 mm sand. Observations in the present study suggest that the finer particles in the Chang et al. (2014) grading are loaded, as they constitute a significant fraction of the grading (i.e. F = 35 %). This is reflected in the change in shear behaviour reported by Chang et al. (2014) following a small loss of finer particles. Although their findings are in agreement with observations made in the present study, the change in shear behaviour, after such a small loss of finer particles, may be more a consequence of the void ratio increasing due to particle rearrangement under the large hydraulic gradients used, rather than due to finer particle loss.

Ouyang and Takahashi (2015), using a triaxial setup adapted to allow high pressure seepage, showed that the coarse void ratio remains relatively unchanged for F = 15 and 25 % but changed significantly for F = 35 %. Whilst otherwise in agreement with the results presented in this study, Ouyang and Takahashi (2015) suggested that peak and residual strengths were greater for specimens after being subjected to internal erosion. They suggested that coarser particles underwent rearrangement during seepage which may be the reason for their observations differing to those reported in this thesis.

Muir Wood et al. (2010) using DEM and continuum modelling showed that an initially dilatant soil could become contractant, as finer particles are lost. Both approaches showed that this change in shear behaviour occurred following finer particle losses of less than 5 % (measured as a fraction of total mass). Gradations investigated with DEM had a ratio of maximum to minimum particle size ranging between 2 and 20. In contrast, the gradation investigated in the present study had a ratio of maximum to minimum particle size of 126, which is more representative of internally unstable soils. The finer particles were therefore significantly smaller than the coarser particles in the present study than in the Muir Wood et al. (2010) study. Consequently, a greater quantity of finer particles could be lost with no significant

change in shear strength in the present study than in the Muir Wood et al. (2010) study. The volume changes accompanying finer particle loss in the Muir Wood et al. (2010) continuum model were optimised using their DEM study and so the continuum model predicted similar changes in shear behaviour after minor finer particle loss.

Scholtès et al. (2010) also showed, using DEM and continuum modelling, that an initially dilatant soil could become contractant, as finer particles are lost. Both approaches showed a change in shear behaviour following less than 5 % finer particle loss (measured as a fraction of total mass). The change in shear behaviour following this small loss of finer particles is likely because the Scholtès et al. (2010) study assumed a gradation with a ratio of maximum to minimum particle size of 7.5. The continuum model developed by Scholtès et al. (2010) did not take into account the actual size of finer particles lost and assumed all particles equally participate in load transfer. Consequently, only a small loss of particles destabilised the material.

It is likely that if wider gradations, as considered in the present study, are simulated with DEM, changes in shear strength would only be observed following greater finer particle loss. However, as particles become smaller, more particles are required per unit volume and this increases the computational capacity required. At this stage the required computer technology does not seem to be readily available to consider such realistic gradations (Shire et al., 2014).

Fannin and Slangen (2014) proposed that the term suffusion should be used when finer particle loss has no effect on mechanical behaviour and the term suffosion used when mechanical behaviour is impacted. Moffat et al. (2011) suggested that initially at low hydraulic gradients, suffusion takes place developing into suffosion as the hydraulic gradient increases. The findings of the current study suggest that the occurrence of suffusion or suffosion also depends on soil fabric. This is because: (i) for soils with small finer fractions ($F < F_t$), mechanical behaviour is unaffected (i.e. suffusion) and; (ii) for intermediate finer fractions ($F_t < F < F_c$), mechanical behaviour is affected (i.e. suffosion). Admittedly, hydraulic gradients could increase until

heaving takes place, but this would no longer be a movement of finer particles but the entire mass. Such heaving would result in a significant change in mechanical behaviour.

7.6 Conceptual critical state framework for suffusion and suffosion

Due to the ill-defined shearing mechanics in direct shear box testing, only generalised observations regarding continuum modelling can be made. Muir Wood et al. (2010) proposed that particle loss could be interpreted within the critical state soil mechanics framework. Key to this framework is the state parameter which is the vertical distance from the critical state line in specific volume ($\upsilon = 1 + e$) and log effective stress ($\log \sigma'$) space (Been and Jefferies, 1985). The critical state line (CSL) defines a locus of points at which indefinite shearing can occur at constant stress and constant volume. If a granular soil's specific volume, at a given effective stress (p'), plots below the CSL, it will dilate when sheared, and if it plots above, it will contract. A positive state parameter indicates states above the CSL and negative values states below the CSL.

It is suggested that to model the mechanical effects of internal erosion, two CSLs need to be defined: one for the global fabric and one for the coarser fabric that is left behind after erosion. Due to the narrowing of the grading that takes place during finer particle loss, e_{min} and e_{max} will increase (Biarez and Hicher, 1994), causing the CSL to rise (Cho et al., 2006, Chen et al., 2016). These two CSLs are illustrated on the left-hand side of Figure 7.32. Conversely, the global CSL is likely to fall slightly as the finer fraction increases, but for clarity this effect is ignored and the same global CSL is shown across Figure 7.32 for all F values. Considering dense soils (i.e. $D_r \sim 100$ %) with $F < F_t$, both global and coarser fabrics will be on the negative side of their respective CSL. As with the global fabric, the coarser fabric will have two limiting specific volumes ($\widehat{\upsilon_p}$ and $\widecheck{\upsilon_p}$) corresponding to maximum and minimum e_c. These will limit possible states and are likely dependent on stress level (Verdugo and Ishihara, 1996). For dense soils with $F < F_t$ both the global and coarser fabrics will be at their limiting specific volumes. Consequently, the increase in specific volume (up arrow in

Figure 7.32) due to finer particle loss is compensated for by the rise in CSL and shear behaviour is largely unaffected.

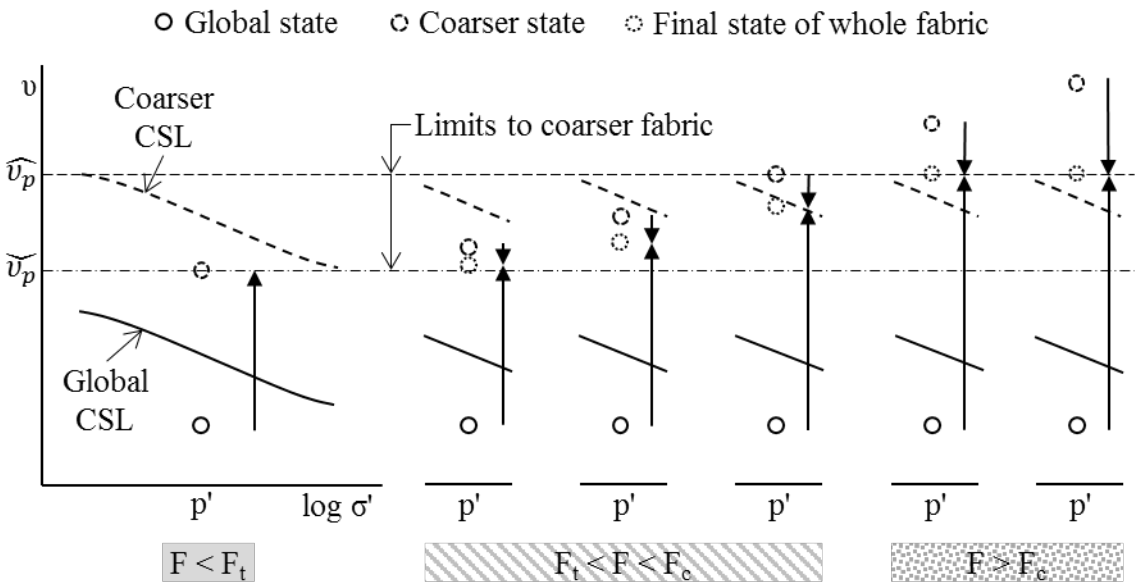


Figure 7.32: Conceptual framework for strength behaviour during internal erosion (relative positions are exaggerated for clarity)

Prior to finer particle loss, for dense soils (i.e. D_r ~ 100 %) in the range $F_t < F < F_c$ the state parameter for the coarser fabric will be less negative and then become positive with increasing F (left to right in the middle part of Figure 7.32), although the global state parameter remains negative. During finer particle loss, some contraction of the coarser fabric may occur (down arrows in Figure 7.32). This may be limited in reality, as finer particles carrying load will not be eroded and global volume will not change. Partial loss of the finer fabric will influence the position of the resulting CSL, which will then lie somewhere between the global and coarse CSLs shown in Figure 7.32. Findings in the present study suggest that the majority of the erodible particles can be lost with small global volume change, suggesting the effect on the CSL of partial finer particle loss can be ignored. This means that the coarser fabric state parameter remains essentially unchanged during erosion. Consequently, the increases in specific volume due to finer particle loss (up arrows in Figure 7.32) are not compensated for by a rise in CSL and shear strength reduces.

For dense soils (i.e. D_r ~ 100 %) with $F > F_c$, the specific volume of the coarser fabric will be above $\widehat{\upsilon_p}$. Although this means that the finer fabric is integral to load transfer

and not erodible, results from this thesis show that the coarser fabric collapses to $\widehat{v_p}$. This state then dictates the weak shear strength.

For loose soils (i.e. D_r ~ 0 %), both the global and coarser fabrics will lie above their respective CSL. Removal of finer fabric results in collapse of the coarser fabric to $\widehat{v_p}$. Shear strength is weak regardless of whether finer particle loss takes place. For soils at intermediate consistencies, it is suggested that the coarser fabric will remain largely unchanged during finer particle loss, provided its specific volume lies between $\widehat{v_p}$ and $\widetilde{v_p}$ and the shear strength will be dependent on the ensuing state parameter. Assuming that the coarser fabric does not collapse is in any case conservative, as any collapse in the coarser fabric due to finer particle loss that would result in a decrease in the coarser fabrics state parameter, is ignored.

Chapter 8 Conclusions and recommendations

8.1 Conclusions

A critical review of literature relating to internal erosion, in particular suffusion, which is the loss of finer particles from a soil mass under the action of seepage, showed considerable research into geometric and hydromechanical criteria. However, understanding the mechanical effects of internal erosion is still a developing area of geotechnical research. The objective of this thesis was, therefore, to explore via experimentation the volume and shear strength changes due suffusion. As shown in the main text, prior attempts using reconstituted specimens and triaxial specimens subjected to seepage have been unable to recreate fabric changes adequately. Using sodium chloride salt as an analogue for erodible finer particles was found to be a more accurate means to observe the effects of these fabric changes.

The main benefit of this approach was that a controlled quantity of finer particles could be lost, under representative hydromechanical conditions, within realistic experimental time scales. Although simple in concept, differences in particle shape, hardness and particle specific gravity required investigation to establish an optimum method of using salt as an analogue. A two-fold approach to this investigation was necessary: (i) to determine the fabric change to be investigated and; (ii) to determine how salt could be used to produce it.

Internally unstable soils are characterised by coarser and finer fabrics made up of non-erodible and erodible particles respectively. When the finer particles make up a small portion of the soil, the coarser particles remain at essentially their densest fabric. Above a certain transition finer fraction (F_t), coarser particles are increasingly hindered by finer particles from attaining their densest packing until their limiting fabric is reached, at a higher critical finer fraction (F_c). Thus, the fabric change to be investigated is how this coarser fabric changes, as finer particles are lost. Due to the physical difference in their grains' properties, replacing sand on a mass basis with salt

was found to create initially dense fabrics (D_r ~ 100 %). Whereas replacing sand on a volume basis with salt was found to create initially loose fabrics (D_r ~ 0 %) better.

To investigate the mechanical effects of finer particle loss, the vertical axis restrained internal erosion direct shear box (variedSB) was constructed. This device allowed settlement during finer particle loss (i.e. salt dissolution) under one-dimensional loading and change in shear resistance after finer particle loss to be quantified. Although this device had limitations due to vertical forces being measured above the shear plane and the size of the shear box relative to grain size, measured dilation angles allowed changes in shear strength to be accurately compared.

A significant finding of this study is that for an internally unstable soil, mechanical behaviour can be largely unaffected if the portion of erodible finer particles is less than $F_{t,}$ which was approximately 15 % for the gravel-sand soil investigated. For dense (D_r ~ 100 %) specimens, settlement due to flooding and dissolution were the same, although for loose specimens (D_r ~ 0 %) dissolution resulted in marginally more settlement. For dense specimens, total volume remained essentially constant during finer particle loss, both under a vertical stress of 75 and 150 kPa. As a result, the void ratio of the soil increased. Despite this, shear strength was unaffected, with similar dilation angles recorded for specimens with finer particles present and following finer particle loss.

The reason for this behaviour is that for low finer fractions ($F < F_t$) the non-erodible coarser particles remain at the same effective void ratio. Finer erodible particles only partially fill the voids between the coarser particles. Consequently, D_r after finer particle loss is the same as initial D_r, as the narrowing of the gradation results in e_{min} and e_{max} increasing. From a critical state soil mechanics point of view, although the specific volume increases due to finer particle loss, the position of the critical state line rises and the state parameter before and after finer particle loss remains essentially unchanged.

Thus, for soils with a small finer fraction ($F < F_t$), the effect of internal erosion on mechanical behaviour is likely negligible. However, if such a material were used as a critical filter, its continued function could be jeopardised, potentially leading to additional mechanisms of internal erosion. This is because the material will become coarser and therefore potentially unable to retain base material. In addition, its hydraulic conductivity will increase.

For soils with erodible finer fraction between F_t and F_c, mechanical behaviour was changed by finer particle loss. F_c was approximately 27 % for the gravel-sand soil investigated. For dense (D_r ~ 100 %) specimens, settlement due to dissolution became greater than that due to flooding as F increased. For loose (D_r ~ 0 %) specimens, settlement due to dissolution was significantly greater than that due to flooding. Settlement under a vertical stress of 75 kPa was less than settlement under a vertical stress of 150 kPa. Dense (D_r ~ 100 %) specimens in which 25 and 50 % of finer particles were dissolved under a vertical stress of 150 kPa showed similar settlement to that due to flooding alone. It is, therefore, likely that not all finer particles are lost due to seepage at F close to F_c, as they are increasingly part of the load bearing fabric. It was evident that the coarser fabric does not collapse significantly due to finer particle loss, and its effective void ratio does not change. Consequently, the global void ratio increases.

Due to this increase in global void ratio, shearing initially dense (D_r ~ 100 %) specimens following finer particle loss showed a loss of shear strength, which increased as F approached F_c. For $F \geq F_c$, the resulting shear strength was that of the coarser fabric in a loose (D_r ~ 0 %) state. A greater loss of strength was observed under a vertical stress of 150 kPa compared to 75 kPa. This was because dilation was suppressed at the higher vertical stress. A similar loss of shear strength was observed following dissolution of dense (D_r ~ 100 %) specimens in which 25 and 50 % of finer particles were dissolved under a vertical stress of 150 kPa. This shows that even minor finer particle loss can significantly destabilise the soil. Shearing initially loose (D_r ~ 0 %) specimens following finer particle loss showed no substantial change in shear strength, both under a vertical stress of 150 and 75 kPa.

The reason for the changing shear strength as finer particles are lost when $F_t < F < F_c$ is that as F increases from F_t to F_c, the effective void ratio of the coarser fabric increases from its minimum void ratio to its maximum void ratio. As the coarser particles are at a packing tighter than their loosest packing (i.e. maximum e_c), they can remain in a relatively stable arrangement even if all finer particles are removed. Finer particle loss, therefore, results in a negligible collapse of the coarser fabric. This is not to say finer particles play no role, as some settlement was observed when F approached F_c, however their role is minor as evidenced by the negligible settlement recorded following 50 % finer particle loss. So although an initially dense soil (D_r ~ 100 %) with $F = F_t$ can remain dense following finer particle loss, a dense soil with $F = F_c$ will become loose (D_r ~ 0 %) following finer particle loss. This is because the void ratio of the coarser fabric does not change and so its void ratio relative to its limiting values does not change. Measured dilation angles showed this change from dense to loose behaviour following dissolution as F increased from F_t to F_c.

From a critical state soil mechanics point of view, the state parameter of the coarser fabric essentially does not change due to finer particle loss. For a soil at its minimum specific volume, with an erodible finer fraction of F_t, the coarser fabric will also be at its minimum specific volume. As F increases to F_c, although the soil remains at its minimum specific volume, the coarser fabric moves to its maximum specific volume. Therefore, the state parameter of the coarser fabric goes from being negative at F_t to positive at F_c. As the state parameter of the coarser fabric essentially does not change due to finer particle loss, the soil will become increasingly contractant, as the portion of finer particles increases and is lost.

The fact that the loss of finer particles when $F_t < F < F_c$ reduces peak shear strength, shows that finer particles are required as part of the load bearing fabric when resisting deviatoric stresses. The loss of finer particles from such fabrics, resisting deviatoric stresses, would therefore have an immediate impact on mechanical behaviour. Those finer particles forming part of the load bearing fabric would however be less susceptible to loss. It is suggested that when $F_t < F < F_c$, finer particle loss is more likely to take place in zones in which shear distortions are low.

For soils with erodible finer fraction above F_c, finer particle loss simulated by dissolution of salt resulted in large settlements and reductions in strength. This reflects the integral part the finer particles play in load transfer; finer particles in such soils are therefore unlikely at risk of suffusion. This does not rule out other forms of internal erosion, due to extreme hydromechanical conditions.

It has been suggested in the literature that suffusion is particle loss accompanied by no change in mechanical behaviour, whereas suffosion is accompanied by a change in mechanical behaviour. It has further been suggested that suffusion develops into suffosion as hydraulic gradient increases. Based on the observations in the present work it is argued that suffusion and suffosion are more dependent on soil fabric than hydromechanical conditions. The findings suggest that some soils exhibit suffusion ($F < F_t$) while others exhibit suffosion ($F_t < F < F_c$), depending on the quantity of erodible particles. Undoubtedly, hydromechanical conditions do play a part; however, it is argued that soil fabric also plays a key role.

This research also sought to investigate how F_t and F_c differ for other soils. Three different approaches were used: (i) a Monte Carlo simulation of packing behaviour; (ii) a review of studies on soil packing behaviour and; (iii) experimentally. Defining F_t as the point at which the coarser fabric is no longer at its minimum void ratio, and F_c as the point at which the coarser fabric is at its maximum void ratio. A Monte Carlo simulation of packing behaviour of coarser particles as F increases, assuming F_t varies between 10 and 20 %, suggested that F_c is on average 26 %, with a standard uncertainty of ±3 % and a maximum uncertainty of ±8 %.

A database of eleven soil packing behaviour studies, in which twenty-one composite gradations were investigated, was compiled. Internal filter ratios (D_{15c}/D_{85f}) for the twenty-one composite gradations ranged between 1.9 and 51. From these studies, the change in relative density of the coarser particles with finer fraction was determined. For each composite gradation, F_t was determined by assuming the coarser fabric remained essentially at its densest fabric up to $D_{r,ec}$ = 90 %. F_c was determined by

assuming the coarser fabric reached its loosest packing at $D_{r,ec}$ = -10 %. This showed that at D_{15c}/D_{85f} > 4, F_t increased rapidly from 5 % to 17 % and F_c increased slower from 22 % to 33 %.

The experimental approach used a suffusion oedometer and punch (SOAP) device. This device enabled settlement to be monitored during salt dissolution and the strength of the resulting fabric to be determined via a punch test. The device's large diameter allowed soil mixtures with D_{15c}/D_{85f} ranging between 1.8 and 46 to be tested. Results from these tests validated the F_t boundary from the packing behaviour studies but suggested the F_c boundary may be lower. Results from these tests are presented in a chart that can be used to assess the potential mechanical impact of internal erosion for a particular internally unstable soil based on its gradation.

8.2 Recommendations for future work

Future research should look to develop the variedSB so that vertical forces can be measured below the shear plane and a larger shear box used to reduce grain size effects. Additional gradations can then be investigated to ascertain whether observations made in this thesis can be applied to a wider range of soils. A better understanding of the mechanical effects could also be obtained by adapting triaxial-type equipment to facilitate percolation and salt dissolution. Such an approach could develop the understanding of finer particle loss at different stress states, the effect on both small and large strain stiffness, and analysis carried out within the framework of critical state soil mechanics.

References

Where original publications could not be found, dates are indicated as circa (i.e. c1856) and the referring article cited.

ÅBERG, B. 1993. Washout of grains from filtered sand and gravel materials. *Journal of Geotechnical and Geoenvironmental Engineering,* 119**,** 36-53.

ANG, A. H.-S. & TANG, W. H. 2007. *Probability concepts in engineering : emphasis on applications in civil & environmental engineering* New York, Wiley.

ARMSTRONG, E. L. 1977. Selection of the type of dam. *In:* GOLZE, A. R. (ed.) *Handbook of dam engineering.* New York: Van Norstrand Reinhold Company.

ARTHUR, J. R. F. & DUNSTAN, T. 1988. Discussion: Sixth Géotechnique symposium in print. The engineering application of direct and simple shear testing. . *Géotechnique,* 38**,** 651-652.

ATKINSON, J. H. 2007. *The mechanics of soils and foundations,* Oxon, Taylor & Francis.

BEEN, K. & JEFFERIES, M. G. 1985. A state parameter for sands. *Géotechnique,* 35**,** 99-112.

BENDAHMANE, F., MAROT, D. & ALEXIS, A. 2008. Experimental parametric study of suffusion and backward erosion. *Journal of Geotechnical and Geoenvironmental Engineering,* 134**,** 57-67.

BENDAHMANE, F., MAROT, D., ROSQUOËT, F. & ALEXIS, A. 2006. Characterization of internal erosion in sand kaolin soils: Experimental study. *Revue européenne de génie civil,* 10**,** 505-520.

BEZUIJEN, A. & STEEDMAN, R. S. Scaling of hydraulic processes. 7th Intl. Conf. on Physical Modelling in Geotechnics (ICPMG 2010), 28 Jun - 1 Jul 2010 Zurich, Switzerland. CRC Press, 93-98.

BIAREZ, J. & HICHER, P.-Y. 1994. *Elementary mechanics of soil behaviour: saturated remoulded soils,* Rotterdam, AA Balkema.

BLIGHT, G. E. 1958. *The investigation of filter sands and the establishment of a criterion for the condition that a sand is a filter in itself.* MSc, University of the Witwatersrand.

BOLTON, M. D. 1986. The strength and dilatancy of sands. *Géotechnique,* 36**,** 65-78.

BONELLI, S. & MAROT, D. 2011. Micromechanical modeling of internal erosion. *European Journal of Environmental and Civil Engineering,* 15**,** 1207-1224.

BRIDLE, R. 2014. Using the ICOLD Bulletin to investigate some internal erosion incidents in embankment dams. *In:* CHENG, L., DRAPER, S. & AN, H. (eds.) *Scour and Erosion.* Perth, Australia: Taylor & Francis Group.

BROWN, A. & BRUGGEMANN, D. 2002. Arminou Dam, Cyprus, and construction joints in diaphragm cut-off walls. *Géotechnique,* 52**,** 3-13.

BURENKOVA, V. V. Assessment of suffusion in non-cohesive and graded soils. Filters in Geotechnical and Hydarulic Engineering, 1993 Karlsruhe, Germany. 357-360.

BURLAND, J. B. 2008. Reflections on Victor de Mello, friend, engineer and philosopher. *Soils and Rocks,* 31**,** 111-123.

CASAGRANDE, A. 1948. Classification and identification of soils. *Transactions of the American Society of Civil Engineers,* 113**,** 901-930.
CEDERGREN, H. R. 1977. *Seepage, drainage, and flow nets,* New York, John Wiley & Sons.
CERATO, A. B. & LUTENEGGER, A. J. 2006. Specimen size and scale effects of direct shear box tests of sands. *Geotechnical Testing Journal,* 29**,** 507.
CHANG, D. S. & ZHANG, L. M. 2012. Critical hydraulic gradients of internal erosion under complex stress states. *Journal of Geotechnical and Geoenvironmental Engineering,* 139**,** 1454-1467.
CHANG, D. S. & ZHANG, L. M. 2013. Extended internal stability criteria for soils under seepage. *Soils and Foundations,* 53**,** 569-583.
CHANG, D. S., ZHANG, L. M. & CHEUK, J. 2014. Mechanical consequences of internal soil erosion. *Transactions Hong Kong Institution of Engineers,* 21**,** 198-208.
CHAPIUS, R. P. 1992. Similiarity of internal stability criteria for granular soils. *Canadian Geotechnical Journal,* 29**,** 711-713.
CHAPUIS, R. P., CONTANT, A. & BAASS, K. A. 1996. Migration of fines in 0-20 mm crushed base during placement, compaction, and seepage under laboratory conditions. *Canadian Geotechnical Journal,* 33**,** 168-176.
CHEN, C., ZHANG, L. & CHANG, D. 2016. Stress-strain behavior of granular soils subjected to internal erosion. *Journal of Geotechnical and Geoenvironmental Engineering*.
CHO, G.-C., DODDS, J. & SANTAMARINA, J. C. 2006. Particle shape effects on packing density, stiffness, and strength: natural and crushed sands. *Journal of Geotechnical and Geoenvironmental Engineering,* 132**,** 591-602.
CIVIDINI, A. & GIODA, G. 2004. Finite-element approach to the erosion and transport of fine particles in granular soils. *International Journal of Geomechanics,* 4**,** 191-198.
CUBRINOVSKI, M. & ISHIHARA, K. 2002. Maximum and minimum void ratio characteristics of sands. *Soils and Foundations,* 42**,** 65-78.
CYRIL, G., YVES-HENRI, F., RÉMI, B. & CHIA-CHUN, H. 2009. Contact erosion at the interface between granular coarse soil and various base soils under tangential flow condition. *Journal of Geotechnical and Geoenvironmental Engineering*.
DALLO, Y. A. H., WANG, Y. & AHMED, O. Y. 2013. Assessment of the internal stability of granular soils against suffusion. *European Journal of Environmental and Civil Engineering,* 17**,** 219-230.
DAVIS, E. H. 1968. Theories of plasticity and the failure of soil masses. *Soil mechanics: Selected topics***,** 341-380.
DE MELLO, V. F. B. Some lessons from unsuspected, real and fictious problems in earth dam engineering in Brazil. 6th Regional Soil Mechanics and Foundation Engineering Conference for Africa, 1975 Durban, South Africa. Rotterdam: AA Balkema, 285-297.
DEN ADEL, H., BAKKER, K. J. & KLEIN BRETELER, K. A. Internal instability of minestone. International symposium on modelling soil-water-structure interactions, 1988. Rotterdam: Balkema, 225-231.
ESKIŞAR, T., OTANI, J. & HIRONAKA, J. 2012. Visualization of soil arching on reinforced embankment with rigid pile foundation using X-ray CT. *Geotextiles and Geomembranes,* 32**,** 44-54.

EVANS, M. & ZHOU, S. 1995. Liquefaction behavior of sand-gravel composites. *Journal of Geotechnical Engineering,* 121**,** 287-298.

FANNIN, R. J. 2008. Karl Terzaghi: from theory to practice in geotechnical filter design. *Journal of Geotechnical and Geoenvironmental Engineering,* 134**,** 267-276.

FANNIN, R. J. & SLANGEN, P. 2014. On the distinct phenomena of suffusion and suffosion. *Géotechnique Letters,* 4**,** 289-294.

FELL, R. & FRY, J. J. 2007. *The state of the art of assessing the likelihood of internal erosion of embankment dams, water retaining structures and their foundations,* Taylor & Francis.

FELL, R., WAN, C. F., CYGANIEWICZ, J. & FOSTER, M. 2003. Time for development of internal erosion and piping in embankment dams. *Journal of Geotechnical and Geoenvironmental Engineering,* 129**,** 307-314.

FENTON, G. A. & GRIFFITHS, D. 1996. Statistics of free surface flow through stochastic earth dam. *Journal of Geotechnical Engineering,* 122**,** 427-436.

FENTON, G. A. & GRIFFITHS, D. V. 1997. Extreme hydraulic gradient statistics in stochastic earth dam. *Journal of Geotechnical and Geoenvironmental Engineering,* 123**,** 995-1000.

FOSTER, M. & FELL, R. 2001. Assessing embankment dam filters that do not satisfy design criteria. *Journal of Geotechnical and Geoenvironmental Engineering,* 127**,** 398-407.

FOSTER, M., FELL, R. & SPANNAGLE, M. 2000a. A method for assessing the relative likelihood of failure of embankment dams by piping. *Canadian Geotechnical Journal,* 37**,** 1025-1061.

FOSTER, M., FELL, R. & SPANNAGLE, M. 2000b. The statistics of embankment dam failures and accidents. *Canadian Geotechnical Journal,* 37**,** 1000-1024.

FOSTER, M., FELL, R. & SPANNAGLE, M. 2002. A method for assessing the relative likelihood of failure of embankment dams by piping: reply. *Canadian Geotechnical Journal,* 39**,** 497-500.

FREEZE, R. A. 1994. Henry Darcy and the fountains of Dijon. *Groundwater,* 32**,** 23-30.

FUJISAWA, K., MURAKAMI, A. & NISHIMURA, S. 2010. Numerical analysis of the erosion and the transport of fine particles within soils leading to the piping phenomenon. *Soils and Foundations,* 50**,** 471-482.

GARNER, S. J. & FANNIN, R. J. 2010. Understanding internal erosion: a decade of research following a sinkhole event. *Hydropower and Dams,* 17**,** 93-98.

GARNER, S. J. & SOBKOWICZ, J. C. Internal instability in gap-graded cores and filters. Canadian Dam Association Annual Conference, 2002 Victoria, B.C.

GEO-SLOPE 2007. SIGMA/W A software package for stress deformation modelling, Ver. 7. Calgary, Alberta: GEO-SLOPE International.

GERMAINE, J. T. & GERMAINE, A. V. 2009. *Geotechnical laboratory measurement for engineers,* New Jersey, John Wiley & Sons.

GRIFFITHS, D. & LANE, P. 1999. Slope stability analysis by finite elements. *Géotechnique,* 49**,** 387-403.

GUO, P. 2008. Modified direct shear test for anisotropic strength of sand. *Journal of Geotechnical and Geoenvironmental Engineering,* 134**,** 1311-1318.

HALL, S. A., BORNERT, M., DESRUES, J., PANNIER, Y., LENOIR, N., VIGGIANI, G. & BÉSUELLE, P. 2010. Discrete and continuum analysis of localised deformation in sand using X-ray μCT and volumetric digital image correlation. *Géotechnique,* 60**,** 315-322.

HAMIDI, A., ALIZADEH, M. & SOLEIMANI, S. M. 2009. Effect of particle crushing on shear strength and dilation characteristics of sand-gravel mixtures. *International Journal of Civil Engineering,* 7**,** 61-72.

HICHER, P.-Y. 2013. Modelling the impact of particle removal on granular material behaviour. *Géotechnique,* 63**,** 118-128.

HOLTZ, R. D. & KOVACS, W. D. 1981. *An introduction to geotechnical engineering,* New Jersey, Prentice Hall.

HONJO, Y., HAQUE, M. A. & TSAI, K. A. Self-filtration behaviour of broadly and gap graded cohesionless soils. *In:* LAFLEUR, J. & ROLLIN, A. L., eds. Geofilters '96, 1996 Montreal, QC. Richmond, BC: BiTech Publishers, 227-236.

HOULSBY, G. T. 1991. *How the dilatancy of soils affects their behaviour*, University of Oxford, Department of Engineering Science.

ICOLD 1986. *Bulletin 53 Static anaylsis of embankment dams,* Paris, International Commision on Large Dams (ICOLD).

ICOLD 2014. *Bulletin 164 Internal erosion of exisiting dams, levees and dikes, and their foundations.,* Paris, International Commision on Large Dams (ICOLD).

INDRARATNA, B., NGUYEN, V. T. & RUJIKIATKAMJORN, C. 2011. Assessing the potential of internal erosion and suffusion of granular soils. *Journal of Geotechnical and Geoenvironmental Engineering,* 137**,** 550-554.

INDRARATNA, B. & RADAMPOLA, S. 2002. Analysis of critical hydraulic gradient for particle movement in filtration. *Journal of Geotechnical and Geoenvironmental Engineering,* 128**,** 347-350.

ISTOMINA, V. S. 1957. *Filtration stability of soils,* Moscow, Leningrad, Goskomizdat.

JANSEN, R. B. 1988. *Advanced dam engineering: For design, construction, and rehabilitation,* New York, Van Norstrand Reinhold Company.

JEWELL, R. A. 1989. Direct shear tests on sand. *Géotechnique,* 39**,** 309-322.

JEWELL, R. A. & WROTH, C. P. 1987. Direct shear tests on reinforced sand. *Géotechnique,* 37**,** 53-68.

KAKUTURU, S. & REDDI, L. N. 2006. Mechanistic model for self-healing of core cracks in earth dams. *Journal of Geotechnical and Geoenvironmental Engineering,* 132**,** 890-901.

KE, L. & TAKAHASHI, A. 2012. Influence of internal erosion on deformation and strength of gap-graded non-cohesive soil. *6th Intl. Conf. on Scour and Erosion (ICSE-6).* Paris, France.

KEHEW, A. E. 2006. *Geology for engineers & environmental scientists,* New Jersey, Pearson Prentice Hall.

KENNEY, T. C. & LAU, D. 1985. Internal stability of granular filters. *Canadian Geotechnical Journal,* 22**,** 215-225.

KENNEY, T. C. & LAU, D. 1986. Internal stability of granular filters: Reply. *Canadian Geotechnical Journal,* 23**,** 420-423.

KENNEY, T. C., LAU, D. & OFOEGBU, G. I. 1984. Permeability of compacted granular materials. *Canadian Geotechnical Journal,* 21**,** 726-729.

KEZDI, A. 1969. *Increase of protective capacity of flood control dikes.,* Budapest, Hungary, Department of Geotechnique, Technical University.

KEZDI, A. 1979. *Soil physics selcted topcs,* Amsterdam, Elsevier.

KLASSON, K. T. 2008. Construction of spline functions in spreadsheets to smooth experimental data. *Advances in Engineering Software,* 39**,** 422-429.

KOVÁCS, G. 1981. *Seepage hydraulics,* Amsterdam, Elsevier.

KUMARA, J. & HAYANO, K. Evaulation of defomration charactersitcis of fouled ballast by a 3-D discerete element method. *In:* CUI, Y.-J., EMERIAULT, F., CUIRA, F., GHABEZLOO, S., PEREIRA, J.-M., REBOUL, M., RAVEL, H. & TANG, A. M., eds. 5th International Young Geotechnical Engineers' Conference, 2013 Paris, France. IOS Press, 257-260.

LADE, P. V., LIGGIO, C. D. & YAMAMURO, J. A. 1998. Effects of non-plastic fines on minimum and maximum void ratios of sand. *Geotechnical Testing Journal,* 21**,** 336-347.

LADE, P. V. & YAMAMURO, J. A. 1997. Effects of nonplastic fines on static liquefaction of sands. *Canadian Geotechnical Journal,* 34**,** 918-928.

LAFLEUR, J., MLYNAREK, J. & ROLLIN, A. L. 1989. Filtration of broadly graded cohesionless soils. *Journal of Geotechnical Engineering,* 115**,** 1747-1768.

LANGROUDI, M. F., SOROUSH, A. & SHOURIJEH, P. T. 2015. A comparison of micromechanical assessments with internal stability/instability criteria for soils. *Powder Technology,* 276**,** 66-79.

LEHANE, B. M. & LIU, Q. B. 2013. Measurement of shearing characteristics of granular materials at low stress levels in a shear box. *Geotechnical & Geological Engineering,* 31**,** 329-336.

LI, M. 2008. *Seepage induced instability in widely graded soils.* PhD, The University of British Columbia.

LI, M. & FANNIN, R. J. 2008. Comparison of two criteria for internal stability of granular soil. *Canadian Geotechnical Journal,* 45**,** 1303-1309.

LI, M. & FANNIN, R. J. 2012. A theoretical envelope for internal instability of cohesionless soil. *Géotechnique,* 62**,** 77-80.

LI, M., FANNIN, R. J. & GARNER, S. J. Application of a new criterion for assessing the susceptibility to internal erosion. Canadian Dam Association Annual Conference, 3-8 Oct 2009 Whistler, BC, Canada.

LINGS, M. L. & DIETZ, M. S. 2004. An improved direct shear apparatus for sand. *Géotechnique,* 54**,** 245-256.

LIU, S. H., SUN, D. & MATSUOKA, H. 2005. On the interface friction in direct shear test. *Computers and Geotechnics,* 32**,** 317-325.

MAROT, D., LE, V. D., GARNIER, J., THOREL, L. & AUDRAIN, P. 2012. Study of scale effect in an internal erosion mechanism: centrifuge model and energy analysis. *European Journal of Environmental and Civil Engineering,* 16**,** 1-19.

MATTHEWS, M. C. 1988. The engineering application of direct and simple shear testing. *Ground Engineering,* 21**,** 13-21.

MAYNE, P. W. Updating our geotechnical curricula via a balanced approach of in-situ, laboratory, and geophysical testing of soil. 61st Annual Geotechnical Conference, 2013. 65-86.

MCDOUGALL, J. R., KELLY, D. & BARRETO, D. 2013. Particle loss and volume change on dissolution: experimental results and analysis of particle size and amount effects. *ACTA Geotechnica,* 8**,** 619-627.

MEYER, W., SCHUSTER, R. L. & SABOL, M. A. 1994. Potential for seepage erosion of landslide dam. *Journal of Geotechnical Engineering,* 120**,** 1211-1229.

MILLIGAN, V. 1986. Internal stability of granular filters: Discussion. *Canadian Geotechnical Journal,* 23**,** 414-418.

MOFFAT, R. & FANNIN, R. J. 2011. A hydromechanical relation governing internal stability of cohesionless soil. *Canadian Geotechnical Journal,* 48**,** 413-424.

MOFFAT, R., FANNIN, R. J. & GARNER, S. J. 2011. Spatial and temporal progression of internal erosion in cohesionless soil. *Canadian Geotechnical Journal,* 48**,** 399-412.

MOFFAT, R. & HERRERA, P. 2014. Hydromechanical model for internal erosion and its relationship with the stress transmitted by the finer soil fraction. *ACTA Geotechnica***,** 1-8.

MOLENKAMP, F., CALLE, E. O. F., HEUSDENS, J. J. & KOENDERS, M. A. Cyclic filter tests in a triaxial cell. 7th European Conference on Soil Mechanics and Foundation Engineering, 1979 Brighton. 97-101.

MUIR WOOD, D., MAEDA, K. & NUKUDANI, E. 2010. Modelling mechanical consequences of erosion. *Géotechnique,* 60**,** 447-457.

MURTHY, T. G., LOUKIDIS, D., CARRARO, J. A. H., PREZZI, M. & SALGADO, R. 2007. Undrained monotonic response of clean and silty sands. *Géotechnique,* 57**,** 273-288.

NOONAN, D. K. J. & NIXON, J. F. 1972. The determination of Young's modulus from the direct shear test. *Canadian Geotechnical Journal,* 9**,** 504-507.

OUYANG, M. & TAKAHASHI, A. 2015. Influence of initial fines content on fabric of soils subjected to internal erosion. *Canadian Geotechnical Journal,* 53**,** 299-313.

POTTS, D. M., DOUNIAS, G. T. & VAUGHAN, P. R. 1987. Finite element analysis of the direct shear box test. *Géotechnique,* 37**,** 11-23.

POULOS, S. J. 1971. *The stress-strain curves of soils,* Winchester, Mass., Geotechnical Engineers, Inc.

POWRIE, W. 2014. *Soil Mechanics: Concepts and Applications,* Boca Raton, CRC Press.

RAHMAN, M. M. & LO, S. R. 2008. The prediction of equivalent granular steady state line of loose sand with fines. *Geomechanics and Geoengineering: An International Journal,* 3**,** 179-190.

RAHMAN, M. M. & LO, S. R. 2014. Undrained Behavior of Sand-Fines Mixtures and Their State Parameter. *Journal of Geotechnical and Geoenvironmental Engineering,* 140**,** 04014036.

RECHENMACHER, A., ABEDI, S. & CHUPIN, O. 2010. Evolution of force chains in shear bands in sands. *Géotechnique,* 60**,** 343-351.

RICHARDS, K. S. & REDDY, K. R. 2007. Critical appraisal of piping phenomena in earth dams. *Bulletin of Engineering Geology and the Environment,* 66**,** 381-402.

RÖNNQVIST, H. 2009. Long-term behaviour of internal erosion afflicted dams comprising broadly graded soils. *Dam Engineering,* 20**,** 149-197.

RÖNNQVIST, H. 2015. *On the Assessment of Internal Erosion of Dam Cores of Glacial Till.* PhD, Luleå University of Technology.

RÖNNQVIST, H., FANNIN, R. J. & VIKLANDER, P. 2014. On the use of empirical methods for assessment of filters in embankment dams. *Géotechnique Letters,* 4**,** 272-282.

RÖNNQVIST, H. & VIKLANDER, P. 2014. Extending the Kenney–Lau method to dam core soils of glacial till. *Geotechnical Research,* 1**,** 73-87.

ROWE, P. W. 1962. The stress-dilatancy relation for static equilibrium of an assembly of particles in contact. *Proceedings of the Royal Society of London A: Mathematical, Physical and Engineering Sciences,* 269**,** 500-527.

SADREKARIMI, A. & OLSON, S. M. 2011. Critical state friction angle of sands. *Géotechnique,* 61**,** 771-783.

SALGADO, R., BANDINI, P. & KARIM, A. 2000. Shear strength and stiffness of silty sand. *Journal of Geotechnical and Geoenvironmental Engineering,* 126**,** 451-462.
SANTAMARINA, J. C. & CHO, G. C. 2001. Determination of critical state parameters in sandy soils-simple procedure. *Geotechnical Testing Journal,* 24**,** 185-192.
SCHANZ, T. & VERMEER, P. A. 1996. Angles of friction and dilatancy of sand. *Géotechnique,* 46**,** 145-152.
SCHOLTÈS, L., HICHER, P.-Y. & SIBILLE, L. 2010. Multiscale approaches to describe mechanical responses induced by particle removal in granular materials. *Comptes Rendus Mécanique,* 338**,** 627-638.
SHERARD, J. L. Sinkholes in dams of coarse, broadly graded soils. 13th International Conference on Large Dams, 1979 New Dehli, India. 25-35.
SHERARD, J. L. & DUNNIGAN, L. P. 1986. Internal stability of granular filters: Discussion. *Canadian Geotechnical Journal,* 23**,** 418-420.
SHERARD, J. L. & DUNNIGAN, L. P. 1989. Critical filters for impervious soils. *Journal of Geotechnical Engineering,* 115**,** 927-947.
SHIBUYA, S., MITACHI, T. & TAMATE, S. 1997. Interpretation of direct shear box testing of sands as quasi-simple shear. *Géotechnique,* 47**,** 769-790.
SHIN, H. & SANTAMARINA, J. C. 2009. Mineral dissolution and the evolution of k0. *Journal of Geotechnical and Geoenvironmental Engineering,* 135**,** 1141-1147.
SHIRE, T. & O'SULLIVAN, C. 2016. Constriction size distributions of granular filters: a numerical study. *Géotechnique,* 66**,** 826-839.
SHIRE, T., O'SULLIVAN, C., HANLEY, K. J. & FANNIN, R. J. 2014. Fabric and effective stress distribution in internally unstable soils. *Journal of Geotechnical and Geoenvironmental Engineering,* 140.
SHWIYHAT, N. & XIAO, M. Effect of suffusion on mechanical characteristics of sand. *In:* BURNS, S. E., BHATIA, S. K., AVILA, C. M. & HUNT, B. E., eds. 5th International Conference on Scour and Erosion (ICSE-5), 2010 San Francisco, California, United States. ASCE, 378-386.
SIMONI, A. & HOULSBY, G. T. 2006. The direct shear strength and dilatancy of sand–gravel mixtures. *Geotechnical & Geological Engineering,* 24**,** 523-549.
SKEMPTON, A. W. 1949. Alexandre Collin. *Géotechnique,* 1**,** 215-222.
SKEMPTON, A. W. & BISHOP, A. W. 1950. The measurement of the shear strength of soils. *Géotechnique,* 2**,** 90-108.
SKEMPTON, A. W. & BROGAN, J. M. 1994. Experiments on piping in sandy gravels. *Géotechnique,* 44**,** 449-460.
SMITH, N. 1971. *A history of dams,* London, Peter Davies.
STERPI, D. 2003. Effects of the erosion and transport of fine particles due to seepage flow. *International Journal of Geomechanics,* 3**,** 111-122.
TAVENAS, F. & LA ROCHELLE, P. 1972. Accuracy of relative density measurements. *Géotechnique,* 22**,** 549-562.
TAYLOR, D. W. 1948. *Fundamentals of soil mechancis,* New York, Wiley.
TERZAGHI, K. 1925. *Erdbaumechanik,* Vienna, Deuticke.
THERMANN, K., GAU, C. & TIEDEMANN, J. 2006. Shear strength parameters from direct shear tests–influencing factors and their significance. *IAEG2006.* Nottinham, United Kingdom.

THEVANAYAGAM, S., SHENTHAN, T., MOHAN, S. & LIANG, J. 2002. Undrained fragility of clean sands, silty sands, and sandy silts. *Journal of Geotechnical and Geoenvironmental Engineering,* 128**,** 849-859.

TO, H. D., SCHEUERMANN, A. & GALINDO-TORRES, S. A. 2016. Probability of transportation of loose particles in suffusion assessment by self-filtration criteria. *Journal of Geotechnical and Geoenvironmental Engineering,* 142**,** 04015078.

TORRANCE, J. K., ELLIOT, T., MARTIN, R. & HECK, R. J. 2008. X-ray computed tomography of frozen soil. *Cold Regions Sci. and Tech.,* 53**,** 75-82.

USACE 1953. Filter experiments and design criteria. Vicksburg, MS: Waterways experiment station: Unites States Army Corps of Engineers.

USBR-USACE 2015. Best Practices in Dam and Levee Safety Risk Analysis. *In:* ENGINEERS, U. S. B. O. R.-U. S. A. C. O. (ed.).

VAID, Y. P. & SIVATHAYALAN, S. 1996. Errors in estimates of void ratio of laboratory sand specimens. *Canadian Geotechnical Journal,* 33**,** 1017-1020.

VALLEJO, L. E. 2001. Interpretation of the limits in shear strength in binary granular mixtures. *Canadian Geotechnical Journal,* 38**,** 1097-1104.

VALLEJO, L. E. & MAWBY, R. 2000. Porosity influence on the shear strength of granular material–clay mixtures. *Engineering Geology,* 58**,** 125-136.

VAN BEEK, V. M., BEZUIJEN, A., SELLMEIJER, J. B. & BARENDS, F. B. J. 2014. Initiation of backward erosion piping in uniform sands. *Géotechnique,* 64**,** 927-941.

VASIL'EVA, A. A., MIKHEEV, V. V. & LOBANOVA, G. L. 1971. How the strength properties of gravel soils depend on the type and state of the sand filling the pores. *Soil Mech Found Eng,* 8**,** 167-171.

VERDUGO, R. & ISHIHARA, K. 1996. The steady state of sandy soils. *Soils and Foundations,* 36**,** 81-91.

VERVECKAITE, N., AMSIEJUS, J. & STRAGYS, V. 2007. Stress-strain analysis in the soil sample during laboratory testing. *Journal of Civil Engineering and Management,* 13**,** 63-70.

VORSTER, T. E. B., SOGA, K., MAIR, R. J., BENNETT, P. J., KLAR, A. & CHOY, C. K. 2006. The use of fibre optic sensors to monitor pipeline response to tunnelling. *GeoCongress 2006: Geotechnical Engineering in the Information Technology Age,* 2006**,** 33-33.

WAN, C. F. & FELL, R. 2004. Experimental investigation of internal instability of soils in embankment dams and their foundations. Sydney: School of Civil and Environmental Engineering, The University of New South Wales.

WAN, C. F. & FELL, R. 2008. Assessing the potential of internal instability and suffusion in embankment dams and their foundations. *Journal of Geotechnical and Geoenvironmental Engineering,* 134**,** 401-407.

WANG, J. & GUTIERREZ, M. 2010. Discrete element simulations of direct shear specimen scale effects. *Géotechnique,* 60**,** 395-409.

WHITE, D. J., TAKE, W. A. & BOLTON, M. D. 2003. Soil deformation measurement using particle image velocimetry (PIV) and photogrammetry. *Géotechnique,* 53**,** 619-631.

WITTMANN, L. Phenomena and parameters of two-component-soil. IAHR Symposium on the effects of flow through porous media, 1978 Thessaloniki, Greece. 68-80.

YAMAMURO, J. & COVERT, K. 2001. Monotonic and cyclic liquefaction of very loose sands with high silt content. *Journal of Geotechnical and Geoenvironmental Engineering,* 127**,** 314-324.
YANG, J., WEI, L. M. & DAI, B. B. 2015. State variables for silty sands: Global void ratio or skeleton void ratio? *Soils and Foundations,* 55**,** 99-111.
YANG, S. L., GRANDE, L. & SANDVEN, R. 2006. Steady-state lines of sand–silt mixtures. *Canadian Geotechnical Journal,* 43**,** 1213-1219.
YILMAZ, Y. 2009. A study on the limit void ratio characteristics of medium to fine mixed graded sands. *Engineering Geology,* 104**,** 290-294.
YONG, R. W. & WARKENTIN, B. P. 1975. *Soil properties and behaviour,* Amsterdam, Elsevier Scientific.
ZHANG, L. & DU, J. 1997. Effects of abutment slopes on the performance of high rockfill dams. *Canadian Geotechnical Journal,* 34**,** 489-497.
ZHANG, L. M. & CHEN, Q. 2006. Seepage failure mechanism of the Gouhou rockfill dam during reservoir water infiltration. *Soils and Foundations,* 46**,** 557-568.
ZOU, Y.-H., CHEN, Q. & HE, C.-R. 2013. A new large-scale plane-strain permeameter for gravelly clay soil under stresses. *KSCE Journal of Civil Engineering,* 17**,** 681-690.

Appendix A Distinguishing between "fines content" and "finer fraction"

Some confusion exist in the literature as to the correct term for the portion of a gradation that is lost due to internal erosion (Table A.1). Within the geotechnical literature, studies on the role of various particle size ranges in a soil's mechanical behaviour are legion. One particular area of research is the role of fines content in the liquefaction potential of sands (e.g. Thevanayagam et al. (2002); Rahman and Lo (2008)). Generally, in such studies "fines content" is defined as the percentage of particles smaller than 0.075 mm (ASTM D2487) or alternatively 0.063 mm (BS1377-2). The choice of division is largely a matter of preference and highlights the arbitrary nature of the division (Casagrande, 1948). However, to avoid confusion with previous research the term "finer fraction" is used in this thesis to define potentially erodible particles. "Finer" is used over "fine" as the latter implies a precise delineation, when in fact the delineation is unlikely to be ever precisely defined. Terms such as "fines", "small", "loose" or "suffusive" have been used to a lesser extent in this context. They are not used here as they may introduce ambiguity.

Table A.1 Summary of terms used to describe lost particles

Author	Description (Italic emphasis added)
(USACE, 1953)	"…movement of *fines*…"
(Blight, 1958)	"…the *fine particles* rapidly washed out leaving a skeleton of coarser grains…"
(Wittmann, 1978)	"…the *finer particles* drawn away by the seeping water."
(Kezdi, 1979)	"Suffusion is a phenomenon where water, while seeping through the pores, carries along the *fine particles* without destroying the soil structure"
(Molenkamp et al., 1979)	"…migration of *finer material*…"
(Sherard, 1979)	"…the *soil fines* are eroded selectively…" "…*fine material* eroded…"
(Kovács, 1981)	"Redistribution of *fine grains* within the layer…"
(Kenney and Lau, 1985)	"…the transport of *small particles* from a soil…"
(den Adel et al., 1988)	"…the *small grains* can easily be washed out…"
(Lafleur et al., 1989)	"An internally unstable soil must be composed of a primary fabric of coarse particles in contact with each other, constituting a porous medium which permits *fine particles* to move freely within the resulting structure."

(Åberg, 1993)	"…washout of *small grains* from broadly graded base materials"
(Burenkova, 1993)	"…*fine particles* are transported in the soil structure…" "…transportation of *fine fractions* out of the soil…"
(Meyer et al., 1994)	"…the process whereby *fine particles* are moved locally into a coarser layer."
(Skempton and Brogan, 1994)	"the *sand* can migrate within the interstices of a framework or primary fabric predominantly formed of the gravel particles, and can be washed out" "the *fines* in a gap-graded material do not fill the voids in the coarse component"
(Chapuis et al., 1996)	"…migration of *fine particles* of a soil within its own pore space."
(Honjo et al., 1996)	"...the *finer* base particles pass through the filter but the coarse particles are caught…"
(Garner and Sobkowicz, 2002)	"…movement of the *fine fraction* within the skeleton of a dispersed, potentially unstable coarse fraction…" "…redistribution of *fine grains* within a stable densely packed skeleton…"
(Sterpi, 2003)	"erosion and transport of *fine particles*"
(Cividini and Gioda, 2004)	"…erosion of the *fine fraction* of the granular soil."
(Fell and Fry, 2007)	"…selective erosion of *fine particles* from the matrix of coarser particles…"
(Richards and Reddy, 2007)	"Gradual loss of *finer matrix materials* in a soil supported by a coarser grained skeleton is termed suffusion…"
(Bendahmane et al., 2008)	"In suffusion, the process is similar, but the coarse particles form a matrix and erosion is only of the *finer particles* in the pore space between the larger particles."
(Li and Fannin, 2008)	"Cohesionless soils under the influence of steady seepage flow can exhibit a behaviour in which grains of the *finer fraction* migrate through the interstices of the matrix formed by the coarser fraction."
(Wan and Fell, 2008)	"Suffusion is the process by which *finer soil particles* are moved through constrictions between larger soil particles by seepage forces."
(Fujisawa et al., 2010)	"Internal erosion is the detachment of *fine particles* from the soil fabric due to the seepage flow and the transport of these particles out of the soil mass"
(Muir Wood et al., 2010)	"The process of internal erosion of *fine particles* from a soil…" "…possibility of erosion of the *smaller particles* within the soil—suffusion—leading to a narrowing of the grading."
(Scholtès et al., 2010)	"When submitted to internal flow, *some particles* tend to be removed from the initial granular material, leading to drastic changes in the microstructure."
(Shwiyhat and Xiao, 2010)	"…suffusion, which is the migration of *fine soil* particles within a coarser soil matrix, or soil skeleton."
(Bonelli and Marot, 2011)	"Suffusion (or suffosion) is an internal erosion process by which *finer soil particles* are detached from the solid matrix and transported through pore constrictions by seepage flow."

(Indraratna et al., 2011)	"Suffusion is a process where water, while seeping thorough (sic) a granular material, dislodges the *fine particles* without destroying the soil structure."
(Moffat and Fannin, 2011)	"…the phenomenon of internal stability results from a loss of *small particles*…"
(Moffat et al., 2011)	"…the *finer fraction* of an internally unstable soil moves within the coarser fraction…"
(Ke and Takahashi, 2012)	"…phenomenon that *small grains* are washed out through the voids between the coarse grains by seepage flow leaving the soil skeleton."
(Marot et al., 2012)	"The *fine particles* are detached and transported through a skeleton constituted by coarser grains."
(Chang and Zhang, 2013)	"Internal stability refers to the ability for the coarse fraction of a soil to prevent the loss of its *fine fraction* due to seepage flow."
(Hicher, 2013)	"…the extraction of *fine particles* from a solid matrix"
(Dallo et al., 2013)	"The internal stability against suffusion of granular soils and filter which have a primary coarser skeleton and loose *finer particles*…"
(Fannin and Slangen, 2014)	"There appears to be consensus in the literature that internal instability is a phenomenon whereby *fine particles* are transported from a non-plastic soil by seepage flow"
(ICOLD, 2014)	"The *small particles* of soil are transported by the seepage flow through the pores of the coarser particles." "…the *finer fraction* is eroded leaving the coarse matrix of the soil"
(Moffat and Herrera, 2014)	"…internally unstable soils … may produce internal erosion or movement of the *finer soil fraction*."
(Rönnqvist et al., 2014)	"…a potential for seepage-induced internal instability, wherein its *finer fraction* washes through the constrictions of its coarser fraction."
(Shire et al., 2014)	"A key mechanism enabling internal instability is the formation of a stress-transmitting matrix dominated by the coarse particles, which leaves the *finer particles* under lower effective stress." "…reduction in stress within the *finer fraction*…" "Internal instability is a form of internal erosion that occurs … when the coarse fraction of the soil is unable to prevent the erosion of the *fine fraction* under the action of seepage."
(Bridle, 2014)	"Suffusion occurs when *fine particles* are driven through the pore spaces in the coarse matrix of a gap-graded soil." "…*suffusive fines*…"
(To et al., 2016)	"In terms of stress transfer, soil particles can be classified into two fractions: *loose particles* and primary fabric"

Appendix B Raw data

All raw data obtained during this study is provided on the accompanying digital compact disc. Table B.1 gives references to the various files used to compile figures and tables in this thesis.

Table B.1 File reference for figures and tables contained in this thesis

Figure or Table	File Reference
Figure 2.1	\\Power point\Image Maker.pptx
Figure 2.2	\\Power point\Image Maker.pptx
Figure 2.3	\\Power point\Image Maker.pptx
Figure 2.4	\\Power point\Image Maker.pptx
Figure 3.1	\\Power point\Image Maker.pptx
Figure 3.2	\\Excel\Other\Chang and Zhang - Criteria (2013).xlsx
Figure 3.3	\\Excel\Other\Chang and Zhang - Criteria (2013).xlsx
Figure 3.4	\\Excel\Other\Specific Gravity and Reference Void Ratios.xlsx
Figure 3.5	\\Excel\Other\Specific Gravity and Reference Void Ratios.xlsx
Figure 3.6	\\Excel\Other\Specific Gravity and Reference Void Ratios.xlsx
Figure 3.7	\\Excel\Other\Specific Gravity and Reference Void Ratios.xlsx
Figure 3.8	\\Excel\Other\Specific Gravity and Reference Void Ratios.xlsx
Figure 3.9	\\Excel\Other\Ft and Fc From Papers.xlsx
Figure 3.10	\\Excel\Other\Ft and Fc From Papers.xlsx
Figure 3.11	\\Excel\Other\Specific Gravity and Reference Void Ratios.xlsx
Figure 3.12	\\Excel\Other\Ft and Fc From Papers.xlsx
Figure 3.13	\\Excel\Other\Ft and Fc From Papers.xlsx
Figure 3.14	\\Excel\Other\Ft and Fc From Papers.xlsx
Figure 4.1	\\Images\Chapter 4\Aggregate.JPG \\Images\Chapter 4\Pebbles.JPG
Figure 4.2	\\Images\Chapter 4\VC Salt.JPG \\Images\Chapter 4\VF Salt.JPG \\Images\Chapter 4\C Salt.JPG \\Images\Chapter 4\F Salt.JPG
Figure 4.3	\\Excel\Other\Specific Gravity and Reference Void Ratios.xlsx
Figure 4.4	\\Excel\Other\Specific Gravity and Reference Void Ratios.xlsx
Figure 4.5	\\Excel\Other\Specific Gravity and Reference Void Ratios.xlsx
Figure 4.6	\\Images\Chapter 4\Pebble proctor crushing.jpg
Figure 4.7	\\Images\Chapter 4\Vibrating table.JPG
Figure 4.8	\\Excel\Other\Specific Gravity and Reference Void Ratios.xlsx
Figure 4.9	\\Excel\Other\Specific Gravity and Reference Void Ratios.xlsx
Figure 4.10	\\Excel\Other\Specific Gravity and Reference Void Ratios.xlsx
Figure 4.11	\\Excel\Other\Specific Gravity and Reference Void Ratios.xlsx
Figure 4.12	\\Cad\SOAP device.dwg

Figure or Table	File Reference
Figure 4.13	\\Cad\SOAP device.dwg
Figure 4.14	\\Excel\Other\Numerical.xlsx
Figure 4.15	\\Cad\SOAP device.dwg
Figure 4.16	\\Excel\Other\Numerical.xlsx
Figure 4.17	\\Excel\Other\Extended Mechanical Criteria.xlsx
Figure 4.18	\\Excel\Other\Extended Mechanical Criteria.xlsx
Figure 4.19	\\Excel\Other\Extended Mechanical Criteria.xlsx
Figure 4.20	\\Excel\Other\Extended Mechanical Criteria.xlsx
Figure 4.21	\\Images\Chapter 4\Pebble crushing.jpg
Figure 4.22	\\Excel\Other\Extended Mechanical Criteria.xlsx
Figure 4.23	\\Excel\Other\EMC Graphs.xlsx
Figure 4.24	\\Excel\Other\EMC Graphs.xlsx
Figure 4.25	\\Excel\Other\EMC Graphs.xlsx
Figure 4.26	\\Excel\Other\EMC Graphs.xlsx
Figure 4.27	\\Excel\Other\EMC Graphs.xlsx
Figure 4.28	\\Excel\Other\EMC Graphs.xlsx
Figure 4.29	\\Excel\Other\EMC Graphs.xlsx
Figure 4.30	\\Excel\Other\EMC Graphs.xlsx
Figure 5.1	\\Cad\Shear Box.dwg
Figure 5.2	\\Images\Chapter 5\Conventional DSB.png
Figure 5.3	\\Cad\Shear Box.dwg
Figure 5.4	\\Cad\Shear Box.dwg
Figure 5.5	\\Images\Chapter 5\Laboratory setup.png
Figure 5.6	\\Excel\Other\Specific Gravity and Reference Void Ratios.xlsx
Figure 5.7	\\Images\Chapter 5\Particle Images
Figure 5.8	\\Images\Chapter 5\Particle Images
Figure 5.9	\\Excel\Level 2\C - 150 - NA - Analysis.xlsx
Figure 5.10	\\Excel\Level 2\C - 150 - NA - Analysis.xlsx
Figure 5.11	\\Excel\Level 2\C - 150 - NA - Analysis.xlsx
Figure 5.12	\\Excel\Level 2\G - 150&75 - NA - Analysis.xlsx
Figure 5.13	\\Excel\Level 2\G - 150&75 - NA - Analysis.xlsx
Figure 5.14	\\Excel\Level 2\G - 150&75 - NA - Analysis.xlsx
Figure 5.15	\\Excel\Level 2\C - 150 - NA - Analysis.xlsx
Figure 5.16	\\Excel\Level 2\G - 150&75 - NA - Analysis.xlsx
Figure 5.17	\\Excel\Level 2\C - 150 - NA - Analysis.xlsx
Figure 5.18	\\Excel\Level 3\ Calibration Testing Tornado Plots.xlsx
Figure 5.19	\\Excel\Level 2\G - 150&75 - NA - Analysis.xlsx
Figure 5.20	\\Excel\Level 2\G - 150&75 - NA - Analysis.xlsx
Figure 5.21	\\Excel\Level 3\ Calibration Testing Tornado Plots.xlsx
Figure 5.22	\\Excel\Level 3\ Calibration Testing Tornado Plots.xlsx
Figure 6.1	\\Excel\Other\Specific Gravity and Reference Void Ratios.xlsx
Figure 6.2	\\Excel\Other\Specific Gravity and Reference Void Ratios.xlsx
Figure 6.3	\\Images\Chapter 6\Particle Images

Figure or Table	File Reference
Figure 6.4	\\Excel\Other\Specific Gravity and Reference Void Ratios.xlsx
Figure 6.5	\\Excel\Other\Specific Gravity and Reference Void Ratios.xlsx
Figure 6.6	\\Excel\Other\Specific Gravity and Reference Void Ratios.xlsx
Figure 6.7	\\Excel\Other\Specific Gravity and Reference Void Ratios.xlsx
Figure 6.8	\\Excel\Other\Specific Gravity and Reference Void Ratios.xlsx
Figure 6.9	\\Excel\Other\Specific Gravity and Reference Void Ratios.xlsx
Figure 7.1	\\Excel\Other\Specific Gravity and Reference Void Ratios.xlsx
Figure 7.2	\\Excel\Level 3\Initial void ratios.xlsx
Figure 7.3	\\Excel\Level 3\Initial void ratios.xlsx
Figure 7.4	\\Cad\Shear Box.dwg
Figure 7.5	\\Excel\Other\Salt Dissolution.xlsx
Figure 7.6	\\Excel\Other\Salt Dissolution.xlsx
Figure 7.7	\\Images\Chapter 7\Frozen blocks.jpg
Figure 7.8	\\Images\Chapter 6\Sheared halves.jpg
Figure 7.9	\\Excel\Level 3\Fines migration.xlsx
Figure 7.10	\\Excel\Level 3\Shear Curves.xlsx
Figure 7.11	\\Excel\Level 3\Shear Curves.xlsx
Figure 7.12	\\Excel\Level 3\Shear Curves.xlsx
Figure 7.13	\\Excel\Level 3\Shear Curves.xlsx
Figure 7.14	\\Excel\Level 3\Error in angles.xlsx
Figure 7.15	\\Excel\Level 3\Shear Curves.xlsx
Figure 7.16	\\Excel\Level 3\Shear Curves.xlsx
Figure 7.17	\\Excel\Level 3\1-D Behaviour.xlsx
Figure 7.18	\\Excel\Level 3\1-D Behaviour.xlsx
Figure 7.19	\\Excel\Level 3\1-D Behaviour.xlsx
Figure 7.20	\\Excel\Level 3\1-D Behaviour.xlsx
Figure 7.21	\\Excel\Level 3\1-D Behaviour - 2.xlsx
Figure 7.22	\\Excel\Level 3\1-D Behaviour.xlsx
Figure 7.23	\\Excel\Level 3\1-D Behaviour - 2.xlsx
Figure 7.24	\\Excel\Level 3\Shear Curves.xlsx
Figure 7.25	\\Excel\Level 3\Shear Curves.xlsx
Figure 7.26	\\Excel\Level 3\Shear Curves.xlsx
Figure 7.27	\\Excel\Level 3\Shear Curves.xlsx
Figure 7.28	\\Excel\Level 3\Shear Curves.xlsx
Figure 7.29	\\Excel\Level 3\Shear Curves.xlsx
Figure 7.30	\\Excel\Level 3\Shear Curves.xlsx
Figure 7.31	\\Excel\Level 3\Shear Curves.xlsx
Figure 7.32	\\Power point\Image Maker.pptx
Table 2.1	Various references as indicated in table
Table 3.1	\\Excel\Other\Specific Gravity and Reference Void Ratios.xlsx
Table 3.2	\\Excel\Other\Specific Gravity and Reference Void Ratios.xlsx
Table 3.3	\\Excel\Other\Ft and Fc From Papers.xlsx
Table 4.1	\\Excel\Other\Specific Gravity and Reference Void Ratios.xlsx

Figure or Table	File Reference
Table 4.2	\\Excel\Other\Specific Gravity and Reference Void Ratios.xlsx
Table 4.3	No digital reference
Table 4.4	No digital reference
Table 4.5	No digital reference
Table 4.6	\\Excel\Other\Extended Mechanical Criteria.xlsx
Table 4.7	\\Excel\Other\Extended Mechanical Criteria.xlsx
Table 4.8	\\Excel\Other\Extended Mechanical Criteria.xlsx
Table 5.1	\\Cad\Shear Box.dwg
Table 5.2	Various references as indicated in table
Table 5.3	Various references as indicated in table
Table 5.4	\\Excel\Other\Specific Gravity and Reference Void Ratios.xlsx
Table 5.5	\\Excel\Level 2\C - 150 - NA - Analysis.xlsx
Table 5.6	\\Excel\Level 2\G - 150&75 - NA - Analysis.xlsx
Table 5.7	\\Excel\Level 2\C - 150 - NA - Analysis.xlsx
Table 5.8	\\Excel\Level 2\G - 150&75 - NA - Analysis.xlsx
Table 5.9	\\Excel\Level 2\G - 150&75 - NA - Analysis.xlsx
Table 5.10	\\Excel\Level 2\G - 150&75 - NA - Analysis.xlsx
Table 5.11	\\Excel\Level 2\G - 150&75 - NA - Analysis.xlsx
Table 6.1	No digital reference
Table 6.2	No digital reference
Table 6.3	\\Excel\Other\Specific Gravity and Reference Void Ratios.xlsx
Table 6.4	\\Excel\Other\Specific Gravity and Reference Void Ratios.xlsx
Table 6.5	No digital reference
Table 7.1	No digital reference
Table 7.2	\\Excel\Level 2\S1G – XXX – XXX – Analysis.xlsx
Table 7.3	\\Excel\Level 3\Initial void ratios.xlsx
Table 7.4	\\Excel\Level 2\S1G – XXX – XXX – Analysis.xlsx
Table 7.5	\\Excel\Level 2\S1G – XXX – XXX – Analysis.xlsx
Table 7.6	\\Excel\Level 2\S1G – XXX – XXX – Analysis.xlsx

Table B.2 details the naming convention of files contained within the folder \\Excel\Level 1\. These files contain the raw data from the variedSB tests.

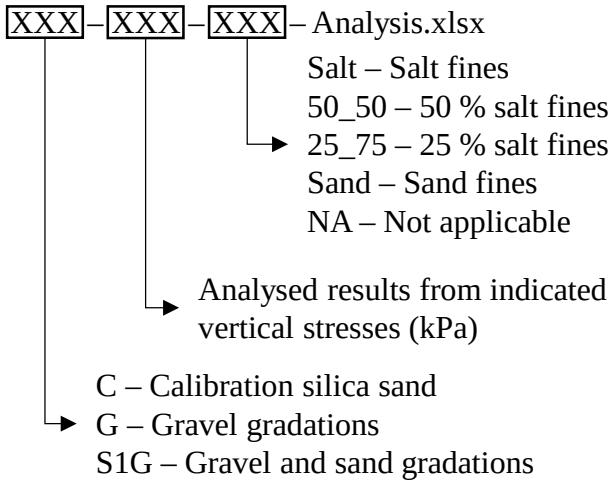
Table B.2: Level 1 files

Test series	File naming convention
Silica sand	C – XXX – 150 – X .xlsx X: Test number XXX: No – No lubrication; V – Petroleum jelly; SL – Silicone and latex C – Calibration with silica sand 150 – Applied vertical stress (kPa)
Gravel	G – X – XXX – X .xlsx X: Test number XXX: 75 – Applied vertical stress (kPa); 150 – Applied vertical stress (kPa) X: L – Loose; D – Dense G – Gravel
Gravel and sand at 150 kPa applied vertical stress	S1G – FXX – X – X .xlsx X: Test number X: L – Loose; D – Dense XX: Fines percentage S1G – Gravel and sand gradations

Test series	File naming convention
Gravel and sand at 75 kPa applied vertical stress	S1G – F[XX] – [X] –75 – [X].xlsx Test number L – Loose D – Dense Fines percentage S1G – Gravel and sand gradations 75 – Applied vertical stress (kPa)
Gravel and all salt fines at 150 kPa applied vertical stress	S1G – F[XX] – [X] – Salt – [X].xlsx Test number L – Loose D – Dense Fines percentage S1G – Gravel and sand gradations Salt – All salt fines
Gravel and all salt fines at 75 kPa applied vertical stress	S1G – F[XX] – [X] – Salt – 75 – [X].xlsx Test number L – Loose D – Dense Fines percentage S1G – Gravel and sand gradations Salt – All salt fines 75 – Applied vertical stress (kPa)
Gravel and partial or minor salt fines at 150 kPa applied vertical stress	S1G – F[XX] – D – [XX_XX] – [X].xlsx Test number 50_50 – 50 % salt fines 25_75 – 25 % salt fines Fines percentage S1G – Gravel and sand gradations D – Dense

Table B.3 details the naming convention of files contained within the folder \\Excel\Level 2\. Raw data from the variedSB tests was analysed in these files.

Table B.3 Level 2 files

Analysis	File naming convention
Analysis of silica sand, gravel, gravel and sand, and gravel and salt data	

Appendix C Phase relationship derivations

C.1 Derivation of Equation 3.1 (Wan and Fell, 2004)

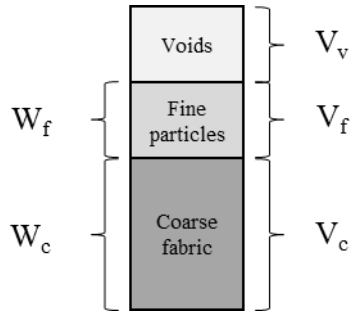


Figure C.1 Phase diagram showing relationships between coarser and finer fabrics

where V_v is volume of voids, V_f is volume of finer particles, V_c is volume of coarser particles, W_f is weight of finer particles W_c is weight of coarser particles, F is weight fraction of the finer particles ($W_f/(W_c+W_f)$), F_c is the critical finer fraction (maximum finer fraction where voids between coarser particles are only partially filled), e_c is void ratio of the coarser fabric and e_f is void ratio of the finer fabric.

The void ratio (e_c) of the coarser fabric, assuming all finer particles are voids:

$$e_c = \frac{V_v+V_f}{V_c} \quad \text{or} \quad V_f = e_c V_c - V_v \qquad \text{C.1.1}$$

The void ratio (e_f) of the finer fabric packed within the voids of the coarser fabric is given by:

$$e_f = \frac{V_v}{V_f} \quad \text{or} \quad V_v = e_f V_f \qquad \text{C.1.2}$$

Substituting C.1.2 into C.1.1 gives:

$$V_f = e_c V_c - e_f V_f \quad \text{or} \quad V_f(1+e_f) = e_c V_c \qquad \text{C.1.3}$$

Dividing both sides of C.1.3 by (V_f + V_c) gives:

$$\frac{V_f}{V_f+V_c}(1+e_f) = \frac{V_c}{V_f+V_c}e_c \qquad \text{C.1.4}$$

If the finer and coarser particles have similar particle specific gravities, the volume ratios can be replaced with weight ratios, and C.1.4 can be replaced by:

$$\frac{W_f}{W_f+W_c}(1+e_f) = \frac{W_c}{w_f+W_c}e_c \qquad \text{or simply}$$

$$F\left(1+e_f\right) = (1-F)e_c \qquad \text{C.1.5}$$

At the critical finer fraction F, becomes F_c and rearranging the terms in C.1.5 gives:

$$F = F_c = \frac{e_c}{1+e_c+e_f} \qquad \text{C.1.6 (Equation 3.1)}$$

C.2 Derivation of Equation C.2

Derivation of Equation C.2 to determine coarse void ratio after finer particle loss assuming the global void volume remains constant:

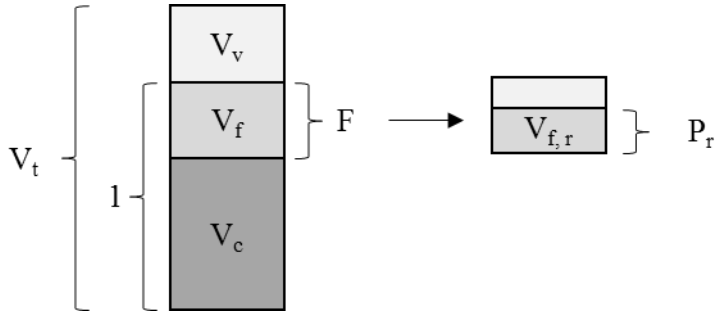


Figure C.2: Phase diagram showing relationships between coarser and finer fabrics

where V_t is total volume, $V_{f,r}$ is volume of fine particles remaining, V_v is volume of voids, F is percentage finer particles, V_f is volume of finer particles, P_r is percentage finer particles remaining and V_c is volume of coarser particles

Definition of percentage fine particles, F:

$$F = \frac{V_f}{V_f + V_c} \qquad \text{C.2.1}$$

Definition of fine particles remaining, P_r:

$$P_r = \frac{V_{f,r}}{V_f} \qquad \text{C.2.2}$$

Definition of global void ratio, e:

$$e = \frac{V_v}{V_c + V_f} \qquad \text{C.2.3}$$

Definition of coarse void ratio prior to dissolution, $e_{c,0}$:

$$e_{c,0} = \frac{V_v + V_f}{V_c} \qquad \text{C.2.4}$$

Definition of coarse void ratio after dissolution, $e_{c,d}$ assuming V_v remains constant:

$$e_{c,vvc} = \frac{V_v + V_f \cdot P_r}{V_c} \qquad \text{C.2.5}$$

Given that, $V_f + V_c = 1$, C.2.1 becomes:

$$V_f = F \qquad \text{C.2.6}$$

and,
$$V_c = 1 - F \qquad \text{C.2.7}$$

Substituting, C.2.6 and C.2.7 into C.2.4 gives:

$$V_v = e_{c,0}(1 - F) - F \qquad \text{C.2.8}$$

Substituting C.2.6, C.2.7 and C.2.8 into C.2.5 gives:

$$e_{c,vvc} = \frac{e_{c,0}(1-F) - F + FP_r}{1 - F} \qquad \text{C.2.7 (Equation C.2)}$$

C.3 Settlement potential derivations

Settlement Potential (SP) is defined as the strain that takes place during flooding and salt dissolution (Equation 4.1 in the main text):

$$SP = \frac{\Delta H}{H_0} \qquad \text{C.3.1}$$

where ΔH is the settlement and H_0 is the initial height. This expressed in terms of coarse void ratios is (given as Equation 7.2 in the main text):

$$SP = \frac{e_{c,0} - e_{c,d}}{1 + e_{c,0}} \qquad \text{C.3.2}$$

where $e_{c,0}$ is the initial coarse void ratio and $e_{c,d}$ is the dissolved or flooded coarse void ratio. Given that:

$$e = \frac{G_s}{\rho} - 1 \qquad \text{C.3.3}$$

C.3.2 can also be expressed in terms of coarser particle density as:

$$SP = 1 - \frac{\rho_{c,0}}{\rho_{c,d}} \qquad \text{C.3.4}$$

where $\rho_{c,0}$ is the initial coarser particle dry density and $\rho_{c,d}$ is the dissolved coarser particle dry density. Dry densities and void ratios can be scaled by their limiting values and expressed as relative densities (D_r):

$$D_r = \left[\frac{\rho_d - \rho_{d,min}}{\rho_{d,max} - \rho_{d,min}}\right]\left[\frac{\rho_{d,max}}{\rho_d}\right] \qquad \text{C.3.5}$$

where ρ_d is the dry density in question, $\rho_{d,min}$ is the minimum dry density and $\rho_{d,max}$ is the maximum dry density. $\rho_{c,0}$ and $\rho_{c,d}$ can be expressed in terms of D_r and substituted into C.3.4 to give:

$$SP = 1 - \left[\frac{\rho_{d,max} - D_{r,ec,d}(\rho_{d,max} - \rho_{d,min})}{\rho_{d,max} - D_{r,ec,0}(\rho_{d,max} - \rho_{d,min})}\right] \qquad \text{C.3.6}$$

where $D_{r,ec,0}$ is the initial relative density of the coarser particles and $D_{r,ec,d}$ is the dissolved relative density of the coarser particles. Rearranging and making $D_{r,ec,d}$ the subject gives (Equation 4.2 in the main text):

$$D_{r,ec,d} = D_{r,ec,0}(1 - SP) + \frac{SP\rho_{d,max}}{\rho_{d,max} - \rho_{d,min}} \qquad \text{C.3.7}$$

alternatively, making, $D_{r,ec,0}$ the subject of the formula:

$$D_{r,ec,0} = \frac{D_{r,ec,d}}{(1 - SP)} - \frac{SP\rho_{d,max}}{(\rho_{d,max} - \rho_{d,min})(1 - SP)} \qquad \text{C.3.8}$$

Equation C.3.7 defines a straight-line relationship between $D_{r,ec,0}$ and $D_{r,ec,d}$. The slope is independent of the reference densities but the intercept is dependent on these densities. The straight line relationship between $D_{r,ec,0}$ and $D_{r,ec,d}$ is therefore dependent on material. To explore whether the difference is significant, values of $D_{r,ec,d}$ for rounded pebble and angular aggregate soils, explored in Chapter 4, for various SP values, were calculated and compared (Figure C.1). The similarity between the values of $D_{r,ec,d}$ decreases with increasing SP, with the ratio between the pebble and aggregate $D_{r,ec,d}$ values at SP = 5 % being 0.96. As this difference is minor using the average of the rounded pebble and angular aggregate $D_{r,ec,d}$ values will not result in any significant difference.

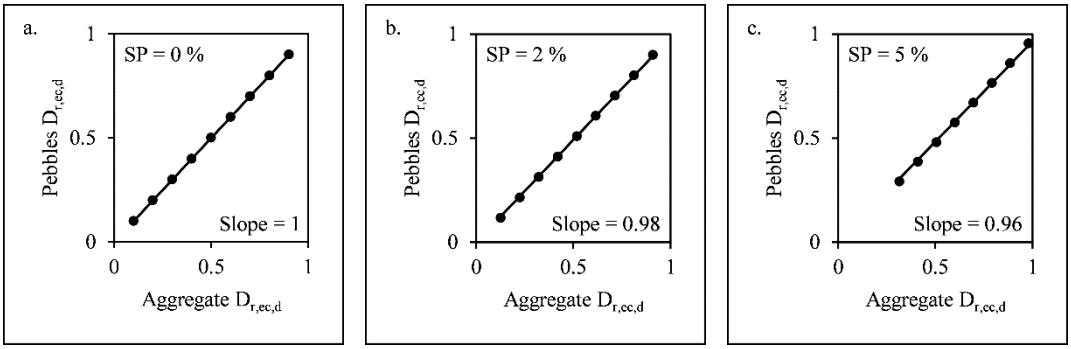


Figure C.1: Comparison of rounded pebble and angular aggregate $D_{r,ec,d}$ for different SP